
Late Triassic to Early Jurassic Plutonism in south Chile (34°-37°S): Its significance for the geodynamic evolution in the transition from Gondwana to Andean orogeny

vorgelegt von
Dipl.-Geol. Paulina S. Vásquez Illanes
Geboren am 05.08.1975 in Puerto Varas, Chile

*von der Fakultät VI-Planen Bauen Umwelt
der Technischen Universität Berlin
zur Erlangung des akademischen Grades*

*Doktorin der Naturwissenschaften
-Dr. rer. Nat.-*

genehmigte Dissertation

Promotionsausschuss:

Vorsitzender: Prof. Dr. rer. nat. Wilhelm Dominik

Berichter: Prof. Dr. rer. nat. Gerhard Franz

Berichter: Prof. Dr. rer. nat. Johannes Glodny

Berichter: Prof. Dr. rer. nat. Rolf L. Romer

Tag der wissenschaftlichen Aussprache: 9. Mai 2008

**Berlin 2008
D 83**

Promotionsausschuss:

Vorsitzender: Prof. Dr. rer. nat. Wilhelm Dominik

Betreuer und Erstgutachter: Prof. Dr. rer. nat. Gerhard Franz

Gutachter: Prof. Dr. rer. nat. Johannes Glodny

Gutachter: Prof. Dr. rer. nat. Rolf L. Romer

Datum der Disputation: 9. Mai 2008

*A mis padres
Mariela y Nelson*

Table of Contents

Prefaces

Abstract.....	i
Zusammenfassung.....	iii
Resumen.....	v
Acknowledgements.....	vii

1. Introduction.....	1
-----------------------------	----------

2. Early Mesozoic granitoids of the Cordillera de la Costa (34-37°S), Chile: Constraints of the onset of Andean Orogeny.....	5
2.1 Introduction.....	5
2.2 Tectonic evolution	6
2.2.1 Gondwana orogeny and Late Paleozoic-Early Mesozoic convergence.....	7
2.2.2 Change to extensional strike slip tectonics.....	7
2.2.3 Onset of the Andean Subduction.....	8
2.3. Results - Characterization of the Early Mesozoic plutonic rocks (34°-37°S): Geology, major, trace element and isotope geochemistry.....	9
2.3.1 La Estrella Granite (~34°15'S).....	15
2.3.2 Pichilemu Granite (34°30'S).....	18
2.3.3 Montecillos Intrusive Rocks (~35°S).....	19
2.3.4 Constitución Granite (~35°S).....	20
2.3.5 Cobquecura Pluton (~36°S).....	22
2.3.6 Cerros del Hualve Pluton (~36°S).....	22
2.3.7 Hualpen Stock (~37°S).....	23
2.4. Age data: Methods, samples, and result.....	23
2.5 Discussion.....	27
2.5.1 Timing of magmatic pulses	27
2.5.2 Changing contribution of the magmatic sources from ~225 to ~150 Ma	28
2.5.3 Possible tectonic setting.....	32
2.6. Summary and conclusions.....	35

3. The Triassic Cobquecura Pluton (Central Chile): an example of a fayalite granite bearing A-Type intrusive massif at a continental margin.....	37
3.1 Introduction.....	37
3.2 Geological setting and petrography.....	38
3.2.1 The Cobquecura Pluton.....	40
3.3 Analytical techniques.....	46
3.4 Whole-rock geochemistry.....	46
3.5 Mineral Chemistry.....	51
3.5.1 Olivine.....	51
3.5.2 Pyroxene.....	52
3.5.3 Amphibole.....	55
3.5.4 Biotite.....	57
3.5.5 Feldspar.....	58
3.5.6 Ilmenite-titanomagnetite.....	59
3.6 Discussion.....	61
3.6.1 Crystallization and emplacement conditions.....	61

3.6.2 Magmatic Evolution.....	62
3.6.3 Tectonic environment of the Cobquecura Pluton.....	63
3.6.4 Comparison with other Late Triassic-Early Jurassic bodies in the Cordillera de la Costa.....	65

4. Origin of fayalite granitoids: new insights from metapelitic xenoliths.....	67
4.1 Introduction.....	67
4.2 Geological setting and petrography.....	68
4.2.1 The Cobquecura Pluton (~36°S, ~72°45'W).....	70
4.2.2 Country rocks.....	72
4.2.3 Characteristics of the xenoliths in the Cobquecura Pluton.....	72
4.3 Geochemical characteristics.....	79
4.4.1 Intrusive rocks.....	79
4.4.2 Metamorphic basement and xenoliths.....	80
4.4 Pb, Nd and Sr isotopic composition.....	86
4.5.1 Intrusive rocks.....	89
4.5.2 Metamorphic basement and xenoliths.....	90
4.5 Discussion.....	90
4.5.1 Nature of the continental crust.....	90
4.5.2 Mantle-derived melts and crustal influence.....	92
4.5.3 Petrogenesis of the Cobquecura Pluton.....	93
4.5.4 Comparison with other fayalite-granitoids worldwide.....	97
4.6 Concluding remarks.....	98

5. Conclusions.....	99
----------------------------	-----------

6. References	103
----------------------------	------------

Liste of Figures

Figure 1.1: Geological map of the Coast of Central Chile (34°- 37°S) with an inset that shows the main geotectonic framework of the Andean continental margin.....	2
Figure 2.1: Geological sketch maps of Chile showing the distribution of outcrops of the metamorphic complexes.....	8
Figure 2.2: Distribution of Triassic-Jurassic intrusive rocks in the Cordillera de la Costa (34°-37°S).....	10
Figure 2.3: Classification diagrams of Triassic and Jurassic intrusive rocks in the Cordillera de la Costa (33°S-37°S).....	15
Figure 2.4: Selected trace element patterns of Triassic and Jurassic igneous rocks (33°S-37°S) normalized to primitive-mantle.....	17
Figure 2.5: REE pattern of Triassic and Jurassic intrusive rocks in the Cordillera de la Costa	18
Figure 2.6: ϵNd vs. initial Sr isotopic compositions of the Triassic-Jurassic intrusives.....	19
Figure 2.7: Trace element vs. trace element after age group of Triassic and Jurassic intrusive rocks in the Cordillera de la Costa (33°S-37°S).....	20
Figure 2.8: Initial Pb isotopic compositions of Triassic and Jurassic magmatic rocks of the Cordillera de la Costa (37-34°S).....	21
Figure 2.9: Results of LA-ICP-MS U-Pb age determinations on zircon from the Cordillera de la Costa (34°S-37°S).....	25
Figure 2.10: Ce + Zr + Nb + Y vs. 10,000Ga/Al discrimination diagrams for granitic rocks.....	33
Figure 3.1: Distribution of late Triassic early Jurassic magmatism in the Cordillera de la Costa (34°-37°S) with a Geological sketch map of the Cobquecura Pluton and sample location.....	40
Figure 3.2: Microphotographs of textures and minerals from the Cobquecura Pluton.....	41
Figure 3.3: Petrographic structures in the Cobquecura Pluton (La Iglesia de la Piedra area)..	43
Figure 3.4: Variation of the A/CNK-index ($\text{Al}_2\text{O}_3/\text{CaO}+\text{Na}_2\text{O}+\text{K}_2\text{O}$) molar) and alkali-content with SiO_2 -content for the intrusive rocks of the Cobquecura Pluton.....	47
Figure 3.5: Variation diagrams of major elements content vs. SiO_2 wt.%	48
Figure 3.6: Variation diagrams of trace element content Zr, V and Cr (ppm) vs. SiO_2 (wt.%).....	49
Figure 3.7: Quadrilateral components of pyroxene compared with olivine and biotite from gabbros and fayalite-granodiorite.....	53
Figure 3.8: Diagrams of element content in mineral vs. element content in the whole rock...	53
Figure 3.9: MnO, TiO_2 and Al_2O_3 vs. X_{Mg} in olivine, clinopyroxene, amphibole and biotite..	54
Figure 3.10: Composition of calcic amphiboles from the Cobquecura Pluton.....	56
Figure 3.11: Zr vs. 10,000×Ga/Al discrimination diagrams for granitic rocks.....	64
Figure 3.12: Non-quadrilateral components Ti, Cr and Na for clinopyroxene from gabbroic rocks in the Cobquecura Pluton.....	65
Figure 4.1: Distribution of late Triassic-early Jurassic magmatism in the Cordillera de la Costa (29°-37°S) and geological sketch map of the Cobquecura Pluton with sample locations.....	69
Figure 4.2: Detailed sketch map from Punta Iglesia de la Piedra and “La Iglesia de la Piedra Profil.....	71
Figure 4.3: Image and drawing of the different types of xenoliths included in the Cobquecura Pluton.....	75
Figure 4.4: Microphotographs of textures and minerals of Cobquecura Pluton xenoliths.....	76
Figure 4.5: LA-ICP-MS U-Pb age determinations on zircon from leucosome of a low-leucosome restitic xenolith (LLRX).....	79
Figure 4.6: Chondrite-normalized REE pattern of Cobquecura Pluton and environs.....	81
Figure 4.7: Primitive mantle-normalized trace element diagrams of Cobquecura Pluton and environs.....	84

Figure 4.8: Variation diagrams of trace element concentrations vs. SiO ₂ and trace element in the Cobquecura intrusive suite.....	85
Figure 4.9: ϵNd_i and $^{87}\text{Sr}/^{86}\text{Sr}_i$ isotopic compositions from the Cobquecura Pluton and related rocks.....	86
Figure 4.10: Initial Pb isotopic composition of the Cobquecura Pluton.....	89
Figure 4.11: Sr-Nd initial isotopic ratios vs. SiO ₂ and La _N /Yb _N ratios.....	91

Liste of Tables

Table 2.1: Summary of characteristics of plutonic rocks of late Triassic-early Jurassic age of the Coastal Cordillera of central Chile.....	12
Table 2.2: Geochemical data of the Triassic-Jurassic intrusive of the Cordillera de la Costa, Chile (34°-37°S).....	13
Table 2.3: Nd, Sr and Pb isotope data of the Triassic-Jurassic intrusive of the Cordillera de la Costa, Chile (34°-37°S).....	16
Table 2.4: Isotopic ages of intrusive rocks from the early Mesozoic rocks of the Cordillera de la Costa, 34-37°S, Chile.....	26
Table 3.1: Petrographic characteristics of the plutonic rocks and dikes of the Cobquecura Pluton.....	44
Table 3.2: Whole-rock geochemical analyses of the Cobquecura Pluton	50
Table 3.3: Representative olivine analyses from rocks of the Cobquecura Pluton.....	51
Table 3.4: Representative pyroxene analyses from rocks of the Cobquecura Pluton.....	55
Table 3.5: Representative amphibole analyses from rocks of the Cobquecura Pluton.....	57
Table 3.6: Representative biotite analyses from rocks of the Cobquecura Pluton.....	58
Table 3.7: Representative ilmenite analyses from rocks of the Cobquecura Pluton.....	59
Table 3.8: Resume of the mineral chemistry characteristic of the plutonic rocks of the Cobquecura Pluton.....	60
Table 4.1: Petrographic characteristics of the different xenoliths included in the Cobquecura Pluton, Cordillera de la Costa, Chile (~36°S, 72°45'W).....	74
Table 4.2: U, Th and Pb isotope analyses for zircon from a low leucosome restitic xenolith.....	77
Table 4.3: Major and trace elements and composition of granitoids, xenoliths and country rocks from the Cobquecura Pluton, Cordillera de la Costa, Chile.....	82
Table 4.4: Whole-rock Sr, Nd and Pb isotope data of granitoids, xenoliths and of country rocks from Cobquecura Pluton at the Cordillera de la Costa, Chile (~36°S).....	87

Liste of Appendix

Appendix A: U-Pb data for Early Mesozoic rocks of the Cordillera de la Costa (34-37°S).....	119
Appendix B: K/Ar ages of intrusive rocks from Cerros del Hualve.....	127
Appendix C: Sample preparation and analytical techniques.....	131
Appendix D: Detailed petrography of the Cobquecura Pluton.....	137

Abstract

The South American margin is a long-lived active margin since the Late Carboniferous (>300 Ma). Two tectonomagmatic stages have been documented for this time at the margin: The Late Paleozoic and the Andean Orogeny (Late Triassic-Recent). The transition between these two orogenic cycles during the emplacement of the Early Mesozoic granitoids of Chile is the subject of this work. The study area lies in the Cordillera de la Costa southern Chile (34 - 37°S). A geodynamic model is proposed based on petrologic-geochemical characteristics of the Early Mesozoic rocks.

New age determinations group the magmatic activity into three pulses: Late Triassic granitic magmatism at 225 - 220 Ma (Hualpen Stock and Constitución Granite), Late Triassic bimodal magmatism at 210 - 197 Ma (Cobquecura Pluton, La Estrella Granite and Pichilemu Granite), and Middle Jurassic mafic magmatism von 175 - 150 Ma (Cerro del Hualve Intrusives and Montecillos Intrusives). These magmatic groups display distinct characteristics and crystallization conditions (remarkably low f_{O_2} and low a_{H_2O} of the 210 - 197 Ma magmatism).

The 225 - 220 Ma and 210 - 197 Ma intrusives are spatially related to NW-SE to N-S striking lineaments. This direction coincides with the orientation of major Permian-Jurassic structures along the Chilean margin. The whole Early Mesozoic magmatism displays geochemical characteristics of subduction-related magmas (Nb-Ta trough and positive Pb anomalies), contemporaneous with an accretionary wedge. Surprisingly, however, the magmatism at 210 - 197 Ma shows geochemical and mineralogical features of an extensional setting, particularly the La Estrella Granite (arfvedsonite granite) and the Cobquecura Pluton (fayalite granitoids).

The Cobquecura Pluton consists of comagmatic gabbroic and (fayalite) granitoid rocks. Occurrences of fayalite-granitoids are only scarcely documented worldwide and are related to an extensional and not to a subduction setting until now. Their petrogenesis is controversially discussed. Fayalite granitoids are generally thought to have crystallized from H_2O -poor and reduced magmas with an f_{O_2} even lower than the fayalite-magnetite-quartz buffer. The major and trace element behavior of the Cobquecura Pluton of Chile moreover shows that the fayalite granites are a product of open-system fractional crystallization from the comagmatic mafic magmas of this suite. The mafic source is similar in composition to the regional subarc-subcontinental mantle. The fayalite granitoids exhibit Sr-Nd isotopic compositions that differ from both the mantle and the known crustal sources of the regional Paleozoic Basement.

In both, gabbros and fayalite granitoids Fe-rich restitic xenoliths (spinel-cordierite-quartz-plagioclase) were discovered, that were probably derived from a deeper (middle or lower) crust than the upper crust exposed at the current surface. Similar geochemical characteristics and Pb-isotopic signatures of the restitic xenoliths and the fayalite granitoids point to an assimilation of Fe-rich deeper continental crust as an important process in fayalite granitoid petrogenesis, a process that has not gained much attention in the fayalite granitoid literature. Furthermore, the magmatic rocks emplaced at 210 - 197 Ma show an unequivocal evidence for a major contribution of a mantle source than older magmatic suites. The Fe-rich mineralogy and the crystallization conditions displayed by the La Estrella Granite and the Cobquecura Pluton are rather uncommon for the Phanerozoic and have been more frequently been reported for anorogenic Proterozoic rocks. In clear contrast, geological and geochemical characteristics of the Chilean continental margin, unambiguously demonstrate that a subduction regime occurred contemporaneously with the emplacement of the investigated magmatic suite.

The magmatism at 225 - 220 Ma and at 175 - 150 have sources similar to that of the North Patagonian Batholith, which is an example for subduction-related cordilleran magmatism. A possible scenario for the transition between the Late Paleozoic and the Andean orogeny is a suprasubduction setting, with an initial phase preceded by oblique subduction that could have generated the extensional NW-SE trending structures followed by steepening of the slab. The steepening of the slab favors melting of the subcontinental mantle and the Triassic-Jurassic subduction geometry could have allowed the emplacement of magmas with an extensional signature and enhanced contributions from mantle sources. These features suggest that the onset of the Andean Orogeny was due to a reconfiguration of the convergence conditions during continuous subduction from the Paleozoic onwards.

Zusammenfassung

Der südamerikanische Kontinentalrand ist ein aktiver Kontinentalrand seit dem Spät Carboniferous. Für diesen Zeitraum (>300 Ma) werden zwei wesentliche tektonomagmatische Phasen postuliert, die spätpaläozoische und die andine Orogenese (Späte Trias-Rezent). Der Übergang zwischen diesen beiden orogenen Zyklen während des frühen Mesozoikums ist Gegenstand der Dissertation. Das Arbeitsgebiet liegt in der Cordillera de la Costa, Südchile (34°S - 37°S). Mit Hilfe petrologisch-geochemischer Methoden wurden Gesteine charakterisiert und ein geodynamisches Modell für den kritischen Zeitraum aufgestellt.

Die Altersbestimmungen unterteilen die magmatische Aktivität in drei frühmesozoische Ereignisse: spätriassischer granitischer Magmatismus von ca. 225 - 220 Ma (Hualpen Stock und Constitución Granit), spätriassischer bimodaler Magmatismus von 210 - 197 Ma (Cobquecura Pluton, La Estrella Granit und Pichilemu Granit) und mittelmajassischer mafischer Magmatismus von ca. 175 - 150 Ma (Cerros del Hualve Intrusion und Montecillos Intrusion). Die drei Gruppen zeigen unterschiedliche Charakteristika und Kristallisationsbedingungen, insbesondere niedrige f_{O_2} und a_{H_2O} des 210 - 197 Ma Magmatismus.

Die Intrusionen von 225 - 220 Ma und 210 - 197 Ma sind an NW-SE bis N-S streichende Lineamente gebunden. Diese fallen mit der Richtung der permisch-jurassischen Hauptstrukturen zusammen, die am gesamten chilenischen Kontinentalrand auftreten. Der frühmesozoische Magmatismus zeigt geochemische Charakteristika subduktionsbezogener Magmen (Nb-Ta Trog, positive Pb Anomalie); zeitgleich tritt ein Akkretionskeil auf. Die 210 - 197 Ma-Plutone zeigen zusätzlich typische geochemisch-mineralogische Merkmale eines Extensions-Regimes, insbesondere der La Estrella Arfvedsonit-Granit und der Fayalit-führende Cobquecura-Pluton.

Der Cobquecura-Pluton setzt sich aus komagmatisch intrudierten Gabbros und Fayalit-Granitoiden zusammen. Fayalit-Granitoide werden als extensionsbezogene Schmelzen und somit als nicht subduktionsbezogen interpretiert. Ihre Petrogenese ist umstritten. Fayalit-Granitoide gelten als Differentiate von H_2O -armen Magmen mit einem f_{O_2} unterhalb des Fayalit-Magnetit-Quarz Puffers. Das Verhalten der Haupt- und Spurenelemente der Fayalit-Granitoide (Chile) zeigt, dass sie Produkte der fraktionierten Kristallisation gabbroider Magmen in einem offenen System darstellen. Die mafische Quelle ist ähnlich der des regionalen subkontinentalen Mantels. Die Sr-Nd Isotopensignaturen unterscheiden sich von den bekannten Mantel- und Krustenquellen des regionalen paläozoischen Grundgebirges.

Sowohl Gabbros als auch die Fayalit-Granitoide enthalten Fe-reiche restitische Xenolithe (Spinell-Cordierit-Quarz-Plagioklas), die aus einem anderen Niveau (mittlere oder untere Kruste) als die Rahmengesteine stammen. Vergleichbare geochemische Charakteristika und Pb-Isotopensignatur der restitischen Xenolithe und der Fayalit-Granitoide weisen auf eine enge genetische Verbindung hin. Die daraus zu schließende Assimilation Fe-reicher Kruste als ein wichtiger Prozess in der Petrogenese der Fayalit-Granitoide hat in der Literatur kaum Beachtung gefunden. Weiterhin deuten die Isotopensignaturen auf einen größeren Einfluss der Mantelquelle als in den älteren Magmatiten hin. Die Fe-reiche Mineralogie und die Kristallisationsbedingungen des La Estrella Granits und des Cobquecura Plutons sind ungewöhnlich für das Phanerozoikum, jedoch häufig in proterozoischen anorogenen Gesteinen. Die geochemischen Signaturen und geologischen Charakteristika dieser Granitoide des chilenischen Kontinentalrandes beweisen jedoch, dass zeitgleich ein Subduktionsregime auftrat.

Der Magmatismus von 225 - 220 Ma und 175 - 150 hat eine ähnliche Quelle wie der nordpatagonische Batolith, ein Beispiel für subduktionsbezogenen Kordillerenmagmatismus. Ein mögliches Szenario für den Übergang vom Spätpaläozoikum zur Andinen Orogenese ist ein Suprasubduktionsmilieu, im initialen Stadium mit einer schrägen Subduktion mit NW-SE gerichteten Extensionstrukturen, welche später ein steileres Abtauchen der subduzierten Platte verursacht hat. Diese steilere Subduktion könnte die Magmengenese im subkontinentalen Mantel begünstigt haben. Die Subduktionszonengeometrie in Trias-Jura ermöglichte die Platznahme von Magmen mit extensionsbezogenen Signaturen bei gleichzeitig bedeutenden Beiträgen aus Mantelquellen. Das lässt darauf schließen, dass der Beginn der andinen Orogenese durch eine Rekonfiguration der Konvergenzbedingungen während einer kontinuierlichen Subduktion vom Paläozoikum bis heute verursacht wurde.

Resumen

El margen sudamericano es un margen activo por mas de 300Ma hasta hoy, registrando 2 estadios tectonomagmáticos: la Orogénesis del Paleozoico tardío y la Orogénesis Andina. El tema de este doctorado estudia la transición entre estos dos estadios tectonomagmáticos durante el Mesozoico temprano en la Cordillera de la Costa de Chile. En este trabajo se propone un modelo geodinámico con la ayuda de métodos petrológicos aplicados a las rocas magmáticas del Mesozoico temprano.

Edades presentadas en este trabajo agrupan la actividad magmática del Mesozoico temprano de la Cordillera de la Costa en tres pulsos: Magmatismo granítico a 225-220 Ma (Stock de Hualpén y Granito de Constitución), magmatismo bimodal a 210-197 Ma (Granito de la Estrella, Granito de Pichilemu y Plutón de Cobquecura), y el magmatismo máfico del Jurásico Medio a 175-150 Ma (Intrusivos de Cerros del Hualve y de Montecillos). Estos grupos magmáticos tienen características petrológicas y condiciones de cristalización distintivas, destacando la baja f_{O_2} y baja a_{H_2O} del magmatismo a 210-197 Ma.

Los intrusivos a 225-220 Ma y a 210-197 Ma están relacionados espacialmente a lineamientos de orientación NW-SE o N-S. Estas direcciones coinciden con las direcciones de estructuras mayores de edades Permo-Jurásicas que ocurren a lo largo de todo el margen continental chileno. El magmatismo del Mesozoico temprano presenta características geoquímicas de magmas relacionados a la subducción (anomalías negativas de Nb-Ta y anomalías positivas de Pb) y ocurren contemporáneamente con un prisma acrecionario. El magmatismo a los 210-197 Ma, muestra características geoquímicas y mineralógicas típicas de ambientes extensionales, particularmente el Granito de la Estrella (granito de arfvedsonita) y el Plutón de Cobquecura (con granitoides de fayalita).

El Plutón de Cobquecura presenta rocas graníticas (con fayalita) y gabroicas comagmáticas. Los granitoides con fayalita son una litología no muy corriente y hasta ahora no han sido relacionados a un margen continental. Su petrogénesis es controversialmente discutida. Los granitoides de fayalita han cristalizado desde magmas pobres en agua y con condiciones mas bajas que el buffer de fayalita-magnetita-cuarzo. La distribución de elementos mayores y trazas muestran que los granitoides de fayalita son un producto de cristalización fraccional desde los magmas máficos de esta suite que operó en un sistema abierto. Los gabros derivaron de una fuente máfica similar al manto subcontinental del subarco regional. Los granitoides de fayalita presentan composiciones isotópicas de Sr-Nd diferentes de las del manto y de las fuentes corticales conocidas (basamento Paleozoico regional).

Los gabros y granitoides de fayalita contienen xenolitos restíticos ricos en hierro (espinela-cordierita-cuarzo-plagioclasa), derivados de una corteza más profunda (corteza media a inferior) que la expuesta en la superficie. Características geoquímicas y composición de isótopos de Pb similares entre xenolitos restíticos y los granitos de fayalita apuntan a que la asimilación fue un proceso importante en la petrogénesis de estos últimos. Un proceso petrogenético no documentado en la literatura. Las fuentes magmáticas a los 210-197 Ma presentan una mayor influencia de contribuciones mantélicas, las cuales son notablemente más importantes que las del previo magmatismo de los 225-220 Ma y que las del magmatismo del Paleozoico tardío. Las condiciones de cristalización mostradas por el Granito de La Estrella y por el Plutón de Cobquecura son mas frecuentemente observadas en las rocas anorogénicas del Proterozoico. Sin embargo, características geoquímicas y geológicas avalan que un régimen de subducción ocurrió simultáneamente con el emplazamiento de las suites investigadas.

Las fuentes del magmatismo a los 225-220 Ma y a 175-150 son similares a aquellas del Batolito Nord-Patagónico, el cual es un ejemplo de magmatismo cordillerano relacionado con la subducción. Un escenario posible durante la transición entre el Paleozoico tardío y el comienzo del ciclo Andino para este esporádico magmatismo es un ambiente de suprasubducción. Este ambiente estaría precedido por una subducción oblicua que generaría extensión vinculada a estructuras NW-SE favoreciendo la fusión del manto subcontinental debido al empujamiento de la placa subductante. La geometría de subducción del Triásico-Jurásico permitió el emplazamiento de los magmas con una "signatura" extensional y con crecientes contribuciones de magmas mantélicos. Lo anterior sugiere que el comienzo de la Orogénesis Andina estuvo vinculada a reconfiguraciones de las condiciones de convergencia durante una continua subducción desde el Paleozoico.

Acknowledgements

This investigation was only made possible through the contribution, encouragement and the support of numerous people and institutions. First and foremost, I wish to express my sincere gratitude to my advisor, Prof. Dr. Gerhard Franz, for his guidance and invaluable criticism throughout this thesis. I'd like to thank him for all the support he has provided me in this scientific endeavor, and will always be grateful for giving me the opportunity to study in Berlin, also for the help in applying for scholarships and for providing me with all the necessary resources, which permitted me to develop my work.

I am especially grateful to Johannes Glodny and Dr. Rolf L. Romer from the GeoForschungsZentrum-Potsdam (GFZ-Potsdam) for instructing me on radiogenic isotopes. Also for their guidance, interesting discussions and for the access they granted me to use their laboratories.

I thank Oscar Figueroa (Universidad de Concepción), Francisco Hervé (Universidad de Chile), Reynaldo Charrier (Universidad de Chile) and Sven Nielsen (Kiel-Universität) for their invaluable input and useful ideas at the beginning of this thesis. I'd also like to thank Klaus Bandel (Hamburg Universität) for giving me access to infrastructure in the first stage of my "Doktorarbeit".

I would like to express my appreciation to the academic and technical staff at the Department of Geosciences of the Technical University Berlin, especially, Kirsten Drüppel (TUB), Friedrich Lucassen (GFZ-Potsdam), in acknowledgment of their valuable input, for stimulating discussions, and their constant and selfless assistance. I would like to express my gratitude to my colleague and friend Philipp Gleißner for his patience, and his unconditional help in the good as in the bad times. I thank my colleges Nicole Giliard, Andreas Hahn and Andreas Hösch for their friendship and their support. I thank François Galbert (TUB) for his assistance with the electronic microprobe; Maren Lewerenz (TUB) and Petra Marsiske (TUB) who helped with the XRF analysis. Christa Zecha (TUB) and Constanze von Engelhardt (TUB) for the thin section preparation.

I'd like to express my appreciation to Annette Meixner (GFZ-Potsdam) and Katrin Schultz (GFZ-Potsdam) for their friendly help in the isotopic laboratory, to Peter Dulski and Rudi Naumann at the GFZ Potsdam for providing geochemical data, and the use of their analytical instruments. Also to Hellmut Echtler, Robert Trumbull (GFZ-Potsdam) for their constructive criticism regarding the first manuscript. Sönke Brandt is also acknowledged for his useful help with PT condition calculation.

To the students of the Universidad de Concepción/Universidad de Chile (some of which are colleagues now) for their pleasant and enthusiastic company during different fieldtrips: Victor Hugo Venegas, Juan Figueroa, Hector Suazo, Ana Valdes, Alejandra Canales, Patricio Montecinos, Gabriela Tascón and Eduardo Inostroza.

From the Universidad de Concepción, many thanks to: Lucy Henriquez, Luis Arturo Quinzio and Gerardo. From the Universidad de Chile I thank Christian Creixell, for his help and discussions. Also Marcos Moreno (GFZ- Potsdam) and Daniel Melnick (Potsdam Universität) for giving me access to literature and data of the current Chilean subduction zones.

From other Institutions, I thank Klaus Wemmer (Universität Göttingen) for the K-Ar determinations, Dirk Frei (GEUS - Denmark) and Axel Gerdes (Universität Frankfurt) for his help and cooperation with the LA-ICPMS and Mark Hutchison for giving me accommodation in Copenhagen.

This investigation was financed by SFB- 267 "Deformation Processes in the Andes" of the Deutsche Forschungsgemeinschaft (DFG), a scholarship of the Deutscher Akademischer Austausch

Dienst (DAAD), and a scholarship from the „Berliner Programms zur Förderung der Chancengleichheit für Frauen in Forschung und Lehre“.

Last but not least, I'd like to express my gratitude to my friends Basia Cruz, Amerika Manzanares who stood by me at all times..... also to Ursula and Hartmut Nielsen for their love and uninterested support. Finally to my parents Mariela and Nelson that always accompanied me in my heart.

1. Introduction

Active continental margins have been an object of attention since the development of the plate tectonic theory. They involve many processes that modify the structure and composition of the continental lithosphere and are sites of economically important metal deposits as well as sites of large georisks such as volcanic eruptions and earthquakes. The Andean continental margin has been periodically active at least since the Early Paleozoic. Two significant orogenic phases occurred in the Southern Andes: the Pre-Andean Orogeny occurred between 300 and 250 Ma (Devonian-Permian) and is represented by a magmatic arc and an accretionary wedge, and the Andean Orogeny started about 200 Ma ago and is active until the present day. The exact starting time of the Andean Orogeny is unknown and probably occurred discontinuously along the Chilean continental margin. The tectonic setting of southwest Gondwana during the period 250 to 200 Ma is still a subject of discussion. Extensional basins with bimodal magmatism north of 34°S have been interpreted as an evidence for an extensional regime (Charrier 1979; Morata et al. 2000). However, south of 39°S a contemporaneous accretionary wedge was active from Carboniferous to Late Triassic (Martin et al. 1999; Glodny et al. 2005).

The absence of detailed geological, geochemical and isotopic studies in Triassic and Jurassic rocks between 34° and 37°S, and the different tectonic interpretations of the Triassic-Early Jurassic period, north (Mpodozis and Kay 1992; Parada et al. 1999; Morata et al. 2000) and south of the segment (Rapela and Pankhurst 1992; Duhart et al. 2001; Hervé and Fanning 2001; Willner et al. 2004) elucidate the need for new data, that help to answer the questions about the dominant tectonic regime during this period. The investigated segment in the Southern Andes between 34° and 37°S is therefore very important to understand the dominant tectonic setting during the Triassic to Early Jurassic.

The study of igneous rocks has long been used to unravel the tectonic processes involved in their petrogenesis. Field relations, petrography, geochemistry and isotopic studies of igneous rocks give information about the crystallization conditions, magma chamber processes, the nature of magma sources, and relation with geological features. The synthesis of these data is a powerful tool to obtain a reliable tectonic interpretation. Therefore, this study is focused on igneous rocks emplaced during the Late Triassic – Early Jurassic in order to gain a better understanding of the magmatic processes at the beginning of the Andean Orogeny.

During fieldwork, untypical and for the Andean continental margin undocumented magmatic rocks, such as fayalite granitoids and ardvedsonite granites, were recognized which motivated a detailed study of their petrogenesis. Ardvedsonite granites unfortunately display strong weathering and the outcrop quality is bad. Fayalite granites are exposed at the coast and display well preserved outcrops and are spatially associated with gabbroic rocks. The existent petrogenetic

models for the generation of these granitoids are controversial. Therefore, the investigation of the Chilean fayalite and ardvedsonites granites offers a unique opportunity to solve the petrogenesis of these kinds of granitoids in an untypical tectonic context.

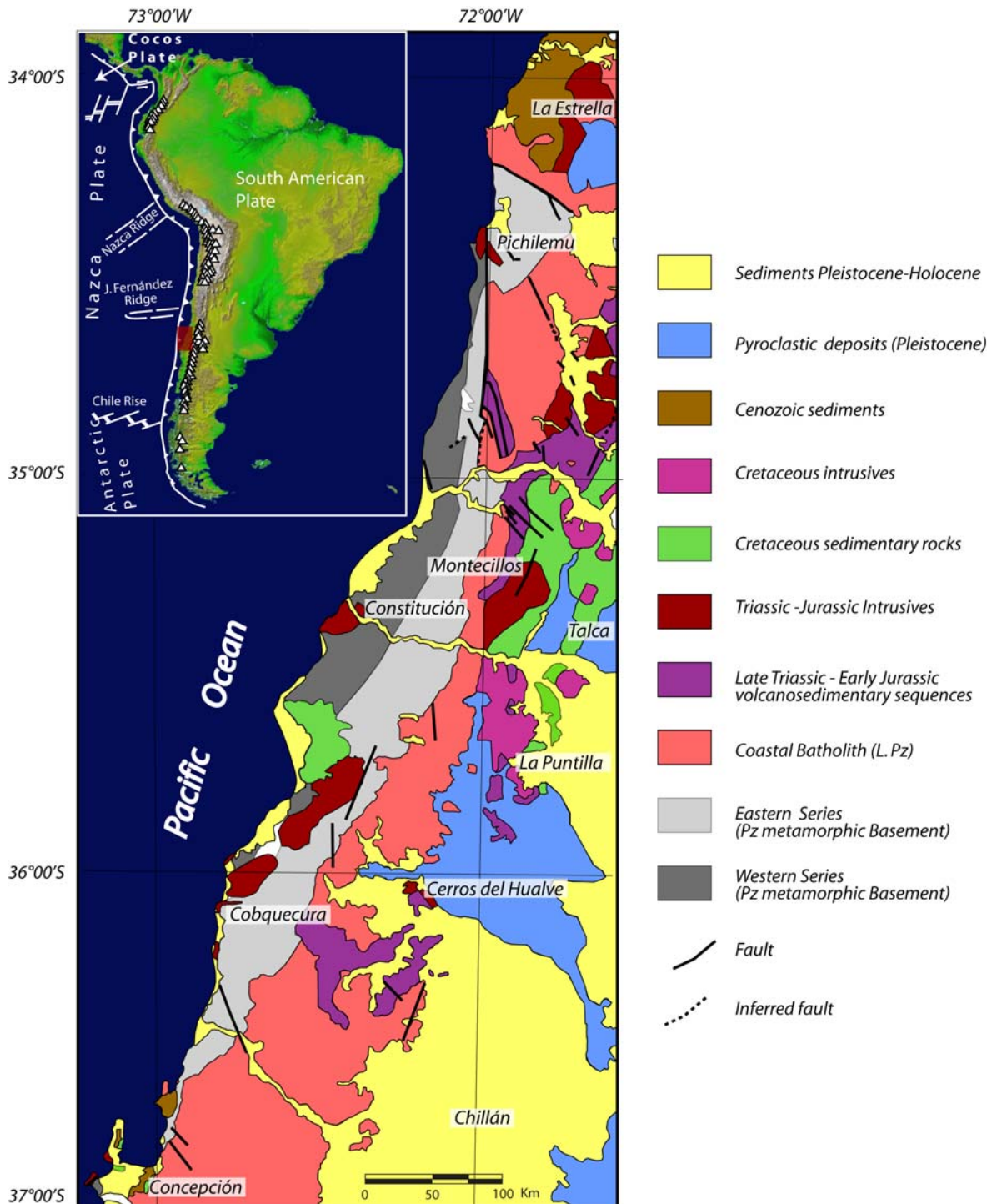


Figure 1.1 Geological map of the Cordillera de la Costa and part of the Central Valley of Central Chile (34°-37°S) (Modified and simplified after SERNAGEOMIN 2003). In the inset, the main geotectonic framework of the Andean continental margin is shown. White triangles represent Holocene volcanoes. The location of the study area is indicated by the red square.

In this study, I present new data of major and trace element compositions and Sr, Nd and Pb isotope compositions of selected Triassic and Jurassic igneous rocks, that, combined with U-Pb, Rb-Sr and K-Ar isotopical ages, contribute to the understanding of the magmatic evolution along the central Chilean Pacific margin during the initial stages of Mesozoic subduction. The Triassic-Jurassic magmatic evolution of this part of Gondwana is essential for the characterization and understanding of the initial stages of the Andean Orogeny. Furthermore, detailed petrography, mineral geochemistry, whole rock geochemistry and isotopic analyses were used to unravel the petrogenesis of the fayalite bearing granitoids.

This dissertation consists of five chapters, three of which were written as stand-alone manuscripts for publication in international scientific journals. Chapters 2 and 3 have been submitted or are in review in peer-reviewed journals, and Chapter 4 is in preparation to be submitted to a peer-reviewed journal. The methodology applied during this investigation is described in Chapters 2, 3, 4 and Appendix C.

Chapter 2: “Early Mesozoic plutonism of the Cordillera de la Costa (34-37°S), Chile: Constraints of the onset of Andean Orogeny” by Vásquez et al. was resubmitted in Marz, 2008 and currently is in review by the “*Journal of Geology*”. I am the first author of this manuscript, which was produced in cooperation with Gerhard Franz (TU Berlin), Johannes Glodny (GeoForschungsZentrum Potsdam), Rolf Romer (GeoForschungsZentrum Potsdam) and Dirk Frei (GEUS Copenhagen). This chapter offers a general overview of the tectonic setting during the Triassic-Jurassic and focuses on a characterization of the Late Triassic- Early Jurassic intrusives of the Cordillera de la Costa from a tectonicmagmatic point of view. The chapter presents new U-Pb, Rb-Sr and K-Ar geochronological ages, geological, geochemical and isotopic data from different Late Triassic- Jurassic intrusives. The magmatic evolution of the magmas is deduced and integrated in a tectonic model. The behavior of the magmatism in this zone is compared to other Late Triassic- Early Jurassic units exposed along the Chilean margin.

Chapter 3: “The Triassic Cobquecura Pluton (Central Chile): an example of a fayalite granite bearing A-Type intrusive massif at a continental margin” by Vásquez and Franz aimed for “*Tectonophysics*” was submitted in Marz 2006 and is currently *in press*. I am the first author of this manuscript, which was written in collaboration with Gerhard Franz (TU Berlin). Among all the Triassic intrusives exposed in the Cordillera de la Costa, the Cobquecura Pluton is the most exotic. It shows a wide lithological variability and is composed of granites with a special Fe-rich mineralogy. The mineral chemistry of the exposed rocks, the first reported K-Ar ages, and whole rock major and trace element geochemistry were presented in this manuscript. This paper mainly describes and evaluates the parameters that control the crystallization of this suite, especially the fayalite-granites.

Chapter 4: “Origin of fayalite granitoids: new insights from the Cobquecura pluton, Chile, and its metapelitic xenoliths” was submitted to “*Lithos*” in Juni, 2008. I am the first author of this manuscript, which was prepared in collaboration with Gerhard Franz (TU Berlin), Johannes Glodny (GeoForschungsZentrum Potsdam), Rolf Romer (GeoForschungsZentrum Potsdam) and Axel Gerdes (J.W. Goethe Universität Frankfurt). In this manuscript a discussion about the genesis of the fayalite granites is presented. This work mainly comprises geochemical and isotopic data. The different sources and their contribution to the generation of the fayalite bearing granitoids are characterized. Of special interest is the contribution of metapelitic xenoliths in the petrogenesis of these granites.

Chapter 6 summarizes the conclusions of the different chapters of this investigation and puts them in a broader context.

2. Early Mesozoic plutonism of the Cordillera de la Costa (34-37°S), Chile: Constraints on the onset of the Andean Orogeny

Abstract

New isotopic ages constrain the onset of the Andean Orogeny. They group the early Mesozoic magmatism in the Cordillera de la Costa, Chile (34°-37°S) into three pulses: Granitic magmatism at 225 - 220 Ma, bimodal magmatism at 210 - 197 Ma, and mafic magmatism at 170 - 150 Ma. Magmatic rocks have distinct field, petrographic, geochemical and isotopic characteristics, and crystallization conditions. Major sources are the subarc-subcontinental mantle and the Paleozoic Chilean continental crust, with a more important contribution of juvenile sources than the preceding Late Paleozoic magmatism. All three pulses of Early Mesozoic magmatism display geochemical signatures characteristic for subduction-related magmas, such as a Nb-Ta trough and a positive Pb anomaly. The 210 - 197 Ma magmatism also shows typical geochemical and mineralogical characteristics for an extensional setting, but a contemporaneous accretionary wedge indicates extension in a subduction-related setting. The two other magmatic pulses at 225 – 220 Ma and 170 – 150 Ma have mantle (like subarc-subcontinental mantle) and crustal sources (like the Paleozoic Chilean continental crust) similar to those of the North Patagonian Batholith (an example for subduction-related cordilleran magmatism).

A possible tectonic scenario for the transition between the Late Paleozoic and the Andean Orogeny is a suprasubduction setting with sporadic magmatism, preceded by an oblique subduction that would generate extension linked to NW-SE structures with subsequent steepening of the slab. The Early Mesozoic subduction geometry allows the emplacement of magmas with an extensional signature and enhanced contributions from the subcontinental mantle. This suggests that the onset of the Andean Orogeny was due to a reconfiguration of the convergence conditions during continuous subduction from the Paleozoic.

2.1 Introduction

The Andes are generally considered as the typical example of an orogen which was formed by subduction. Whereas the processes during subduction are fairly well understood, there is less information about the onset or renewed onset of subduction after a time of non-subduction. After the Late Proterozoic-Early Cambrian, the southwestern active continental margin of South America experienced two important periods of subduction-related magmatism, the Gondwana or Pre-

Andean orogeny (Carboniferous to Triassic) (e.g., Mpodozis and Ramos 1989; Bahlburg and Hervé 1997), and the Andean orogeny (Jurassic - Recent), with its ongoing subduction along the Andean Cordillera (e.g., Coira et al. 1982; Mpodozis and Ramos 1989).

Active continental margins are characterized by a distinct magmatic evolution, which is the result of parameters such as crustal thickness, heat flow and mass transport from the lower to the upper plate and in the mantle wedge. These are in turn the result of a special tectonic setting, and therefore the magmatic evolution is one of the key elements in order to understand the tectonic evolution.

The actual change in the tectonic setting and the related composition of the magmas between the two episodes of subduction, the Gondwana (Pre-Andean) and the Andean, is poorly constrained. It is the purpose of this paper to relate the geochemical parameters of igneous rocks from the transition period to a special tectonic setting. The intrusive rocks investigated here were intruded during the reorganization between the Gondwana and the Andean orogeny, and therefore should reflect in their chemistry the nature of these changes. Our new data on major and trace element compositions together with Sr, Nd and Pb isotope compositions of selected Triassic and Jurassic igneous rocks, combined with LA-ICP-MS single zircon U-Pb ages contribute to the understanding of the magmatic evolution along the central Chilean Pacific margin right before and during the initial stages of Andean subduction.

2.2 Tectonic evolution

At the transition from the Gondwana to the Andean subduction, the active margin experienced significant changes in the tectonic and magmatic regime in the Triassic to Jurassic. In the southern part of Central Chile, during the Carboniferous to Triassic, the subduction system is defined by a magmatic arc and an accretionary prism (Hervé et al. 1981; Parada 1990; Martin et al. 1999; Glodny et al. 2006). In this period, magmatism was characterized by predominance of crustal recycling processes with a coherent evolution along the 21-41°S section (Parada et al. 1999; Lucassen et al. 2004). In contrast, between 33° and 41°S the Andean subduction (Upper Jurassic? - Recent) is defined by a margin without major accretion, but with episodes of tectonic erosion, particularly in the northern part of the margin segment (e.g., Kay et al. 2005). The Andean subduction-related magmatism (Jurassic-Cenozoic) shows compositions with variable but generally lower crustal contributions and a more important juvenile component (Hildreth and Moorbath 1988; Parada et al. 1991; Lucassen et al. 2004). These different subduction styles – accretionary versus erosional - and geochemical magmatism signatures have justified the separation between the Gondwana Orogeny during the Carboniferous - Triassic? (e.g., Hervé et al. 1981; Ramos 1986;

Mpodozis and Ramos 1989) and the Andean Orogeny during the Upper Jurassic? - Recent (e.g., Coira et al. 1982; Mpodozis and Ramos 1989).

2.2.1 Gondwana orogeny and Late Paleozoic-Early Mesozoic convergence

Remains of the Late Paleozoic-Early Mesozoic Gondwana convergence occur at different locations and with different ages of formation along the Chilean continental margin (Fig. 2.1). A Late Paleozoic accretionary prism, which testifies to an accretionary subduction regime, is exposed in discontinuous outcrops in the western part of Central and Southern Chile near the present coastline, with younger ages towards the south (Hervé and Fanning 2001; Glodny et al. 2006). At Chañaral (~26°S, Fig. 2.1), this accretionary prism is represented by the Carboniferous Chañaral Melange (Bahlburg and Hervé 1997). Between 39°30' and 42°00'S, the accretionary prism (Western Series; Fig. 2.1) documents continuous subduction from the Carboniferous to the Late Triassic (Willner et al. 2004; Glodny et al. 2005). Between 44° and 47°S, the Chonos Metamorphic Complex (Fig. 2.1), comprised of Late Triassic sedimentary protoliths (Fang et al. 1998; Hervé and Fanning 2001) and metamorphosed in the Early Jurassic (Thomson et al. 2000) is also interpreted as an accretionary prism (Hervé et al. 2007a). South of 47°S, the accretion of the Madre de Dios exotic terrane (Fig. 2.1) documents convergence and subduction between the Middle Permian and the earliest Jurassic (Hervé et al. 2007a).

The magmatic activity in the Late Paleozoic between 34°S and 42°S, is typical for a magmatic arc, characterized mainly by crustal recycling, and continued into the Late Triassic, but with decreasing magma volumes (Martin et al. 1999; Lucassen et al. 2004; Willner et al. 2005). It indicates a continuous evolution in a largely unchanged setting at the convergent margin. In summary, the exposed Late Paleozoic (Pre-Andean) crust in the studied segment is volumetrically dominated by the magmatic rocks from an arc and metamorphic rocks from an accretionary wedge (Hervé 1988; Willner et al. 2005).

2.2.2 Change to extensional strike slip tectonics

During the Triassic-Jurassic, in Argentina there was important extensional tectonic activity, documented in large NW-SE to NNW-SSE oriented basins with fast subsidence and bimodal magmatism (Uliana et al. 1989; Ramos and Kay 1991; Franzese and Spalletti 2001). The occurrence of similar, but smaller, extensional basins in Chile (Fig. 2) suggests a similar extensional geotectonic setting for the western margin of South America (Charrier 1979). The NW-SE to NNW-SSE orientation of these Triassic and Early Jurassic basins was at least partly inherited from Late Paleozoic structures (Ramos 1994; Franzese and Spalletti 2001). This extensional regime has been related either to the first stage of break-up of Gondwana (Charrier 1979; Uliana et al. 1989) or to a possible interruption of subduction from the Late Permian to the Early Jurassic (e.g., Charrier 1979; Mpodozis and Kay 1992). Both inferred settings were associated with dextral strike-

slip tectonics parallel to the continental margin (Franzese and Spalletti 2001). Studies north of 33°S have related the dextral tectonics to a Triassic slab break-off, generating an asthenospheric window (Parada et al. 1999). The consequences of these changes were bimodal magmatism, uplift, thermal weakness, and gravitational collapse of the upper crust in an intracontinental extensional tectonic setting (Gana 1991; Parada et al. 1999; Morata et al. 2000; Franzese and Spalletti 2001).

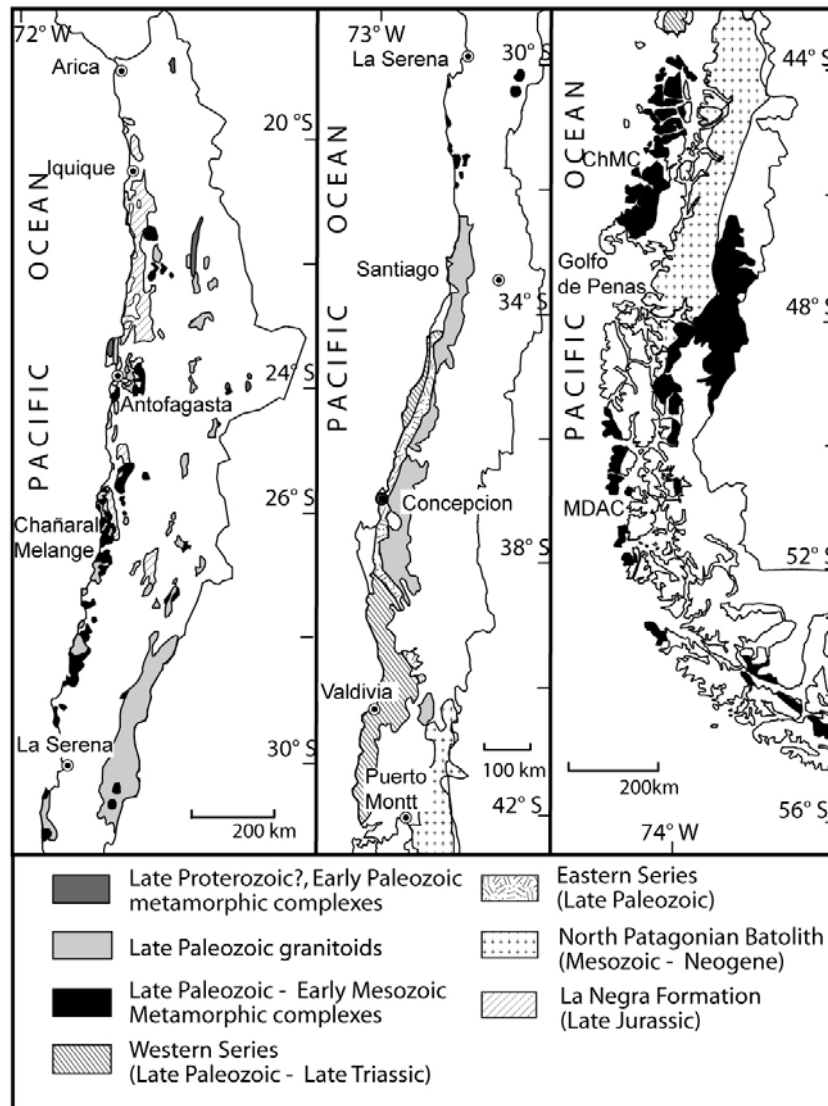


Figure 2.1 Geological sketch maps of Chile showing the distribution of outcrops of the metamorphic complexes, the Paleozoic plutonic belts (modified after Hervé et al. 2007a), the North Patagonian Batholith (Hervé et al. 2007b) and La Negra Formation (Lucassen et al. 2006). ChMC is the Chonos Metamorphic Complex and MDAC is the Madre de Dios Accretionary Complex.

2.2.3 Onset of the Andean Subduction

During the Jurassic, from North to South between 18°S and 37°S, the South American margin displayed a segmentation, with segment-specific tectonic evolutions (Mpodozis and Ramos, 1989). The Jurassic magmatic rocks, which mark the initiation of Andean subduction (e.g., Coira et

al. 1982; Mpodozis and Ramos 1989; Pichowiak 1994; Lucassen et al. 2006; Haschke et al. 2006), also display this segmentation. In the northernmost section between 18°S and 26°S the onset of the Andean subduction is well recorded in the La Negra volcanic Formation (e.g., Coira et al. 1982; Mpodozis and Ramos 1989; Pichowiak 1994; Lucassen et al. 2006; Oliveros et al. 2006). Its geochemical and isotopic characteristics define this magmatism as typical for an extensional arc-related environment (Bartsch 2004; Kramer et al. 2005). The succession consists of a thick, repeatedly altered volcanic sequence. Although this alteration has made it difficult to determine accurate absolute ages, the available geochronological age data as well as the biostratigraphical ages give a consistent picture that the major stages of magmatism occurred between 186 and 150 Ma (Rogers and Hawkesworth 1989; Kramer et al. 2005; Oliveros et al. 2006). The main geochemical signatures are calcalkaline-tholeiitic with minor alkaline components. The Pb isotopic composition and the high contents of Ba, Zr, and Th indicate an active continental margin setting for the La Negra Formation (Kramer et al. 2005).

Farther south, in the segment between 31° to 34° S the Middle Jurassic rocks are plutonic and their composition is mainly mafic. They reveal trace element patterns similar to subduction related basalts (Parada et al. 1999). These mafic rocks show typical characteristics of a subduction modified mantle such as the typical LILE enrichment and Nb depletion of a magmatic arc. In this segment, there is a progressive migration of the plutonic belts toward the east with time (e.g., Parada et al. 1999).

The plutonic rocks of the third, southernmost section between 34-37°S (Fig. 2.2) are the main focus of this paper and will be described in more detail in the next section.

2.3 Results - Characterization of the Early Mesozoic plutonic rocks (34°-37°S):

Geology, major, trace element and isotope geochemistry

Early Mesozoic plutonic rocks from the 34°-37°S section, which are important for the investigation of changes in the tectonic setting from the Gondwana to the Andean Orogeny crop out in the Cordillera de la Costa (Fig. 2.2). The area consists mainly of pre-Andean, Late Paleozoic magmatic and metamorphic rocks, associated with minor amounts of Upper Triassic sedimentary rocks and the Early Mesozoic igneous rocks (Hervé et al. 1988). Early Mesozoic intrusives of Late Triassic and Early Jurassic age are exposed at the western and eastern flanks of in the Cordillera de la Costa (Fig. 2.2) (Hervé et al. 1988; Vásquez and Franz, 2008). They were all emplaced at shallow crustal levels, display narrow contact aureoles, and are exposed in small and discontinuous areas of max. 290 km². These characteristics distinguish the Mesozoic intrusions from late Paleozoic granitoids in the Cordillera de la Costa, which cover large areas (Fig. 2.2) and display broad contact aureoles in the metasedimentary country rocks (Hervé 1977; our data).

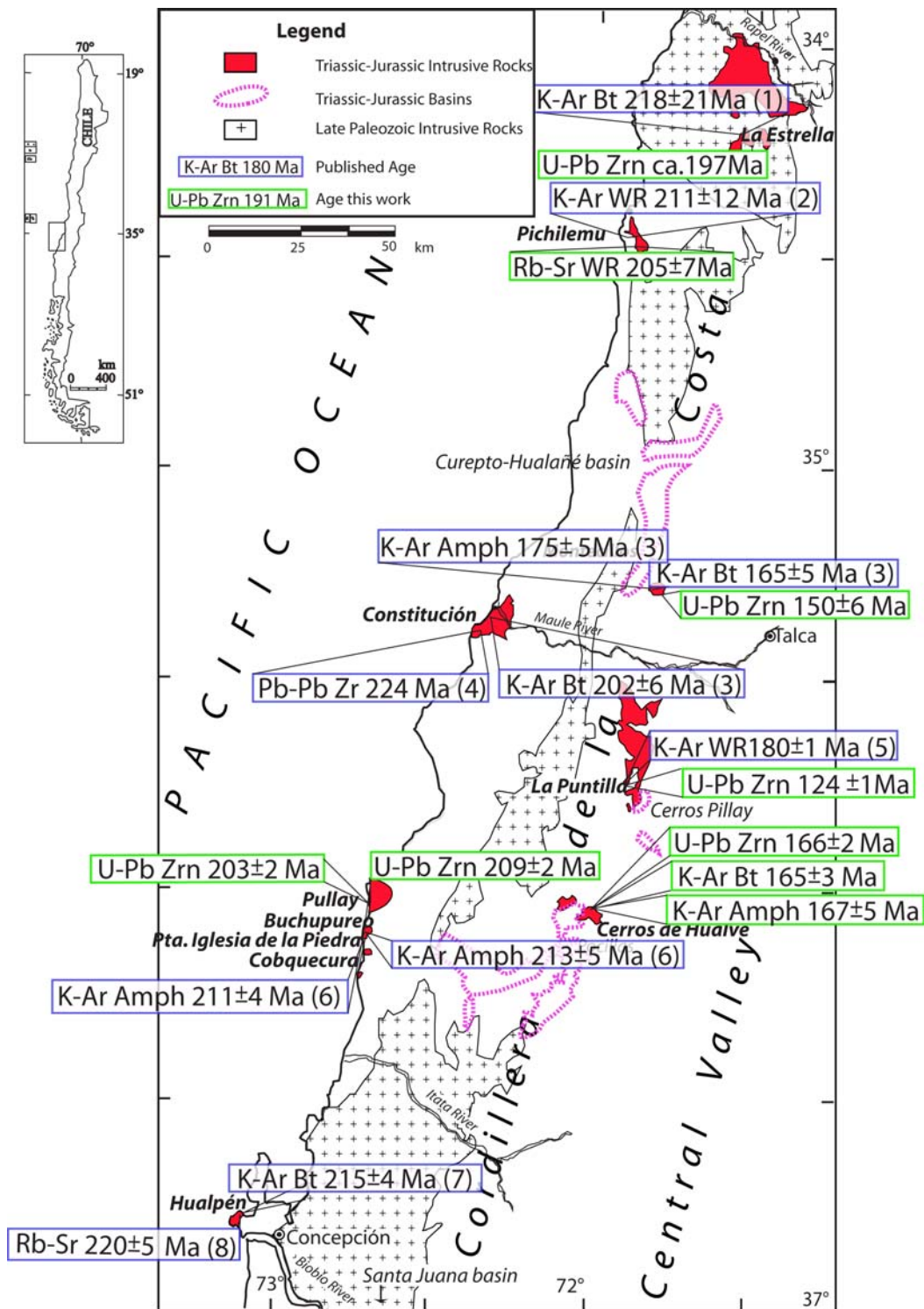


Figure 2.2 Distribution of Triassic and Jurassic intrusive rocks in the Cordillera de la Costa. The geologic units are outlined after Dávila et al. (1979), Escobar et al. (1977), Godoy (1970), Gajardo (1981), Gana and Hervé (1983), Hervé and Munizaga (1978), Vásquez et al. (2005), Vásquez and Franz (2008), and this work. The published ages are from: (1) Dávila et al. (1979) (2), Hervé et al. (1984) (3), Gana and Hervé (1983), (4) Willner et al. (2005) (5), Hervé and Munizaga (1978), (6) Vásquez et al. (2005), (7) Hervé et al. (1988), and (8) Lucassen et al. (2004). Abbreviations: Amph: Amphibole, Bt: Biotite, Wr: Whole rock, Zrn: Zircon. Triassic - Jurassic basin distribution after Escobar (1977). Outcrops of the Southern Coastal Batholith after SERNAGEOMIN (2003).

Early Mesozoic intrusions in the western part of the studied margin segment (Fig. 2.2) have been grouped as La Estrella Granite, Pichilemu Granite, Constitución Granite, Cobquecura Pluton and Hualpén Stock (Dávila et al. 1979; Hervé et al. 1988; Lucassen et al. 2004; Vásquez et al. 2005). Their compositions are mainly monzogranitic (Hervé et al. 1988), except for the Cobquecura Pluton, which also comprises gabbroic rocks (Vásquez et al. 2005). The intrusions are postkinematic with respect to the main foliation of their metamorphic host rocks. In the eastern part of the segment, intrusive rocks crop out around Cerros de Hualve and in Montecillos (Fig. 2.2); they are gabbroic to granitic in composition. A Cretaceous age was found (124 ± 5 Ma; see below) for the tonalitic-gabbroic intrusives at La Puntilla (Fig. 2.2), which were previously considered as Triassic (Hervé and Munizaga 1978). The main petrological characteristics of all these intrusions are summarized in Table 2.1. We analyzed 16 whole rock samples from the Constitución Granite, La Estrella Granite, Cerros del Hualve Pluton and Montecillos Intrusives for major elements, Nb, Sc, Ba, Ce, Co, Cr, Ga, Hf, Ni, V, Zn and Zr. A subset of 9 samples was analyzed for rare earth elements (REE), Rb, Sr, Sn, Ta, Tl, Pb, Th, U, Cs, Y, as well as for Sr-, Nd- and Pb-isotopes. Representative geochemical data are shown in Table 2.2. Sr, Nd and Pb isotopic compositions are compiled in Table 2.3. This database is enhanced by geochemical data of the Cobquecura Pluton from Vásquez and Franz (2008), and of the Hualpén Stock from Creixell et al. (2002) and Lucassen et al. (2004). Detailed analytical procedures are presented in appendix C.

All magmatic rocks are subalkaline (Fig. 2.3a) and show a tendency of increasing peraluminosity with increasing SiO_2 (Fig. 2.3c). Multielement variation diagrams of the trace elements normalized to primitive mantle (McDonough and Sun 1995) display a relatively similar pattern for all Early Mesozoic intrusives (Fig. 2.4). As evident from these diagrams, the rocks are enriched in incompatible elements (e.g., Rb, Th, U, with Ba as an exception). They show negative Sr-, P- and Ti- anomalies, positive Pb and K anomalies, and Nb-Ta troughs (Fig. 2.4a,b). All Early Mesozoic magmatic rocks show relatively flat REE patterns, with negative Eu anomalies in the more felsic rocks (Fig. 2.5) and positive Eu anomalies in the gabbroic rocks from the Cobquecura Pluton. The initial Pb – Sr - Nd isotopic composition for all the gabbroic rocks is shown in figures 2.6, 2.8 and Table 2.3.

The exact location of the samples used for geochemical and geochronological analysis is given in Table 2.2. In the following paragraphs, the intrusions will be described from north to south.

Table 2.1 Summary of characteristics of plutonic rocks of Late Triassic-Early Jurassic age of the Cordillera de la Costa of central Chile.

	Hualpén Stock ^(a)	Cobquecura Pluton	Constitución Granite	Pichilemu Granite	La Estrella Granite	Cerros del Hualve Stock	Montecillos Stock
Dominant lithology	granite	gabbro and granite	granite	granite	syenogranite	gabbro	monzonite
Minor lithology		tonalite, granodiorite, monzogabbros	tonalite, granodiorite			granite, granodiorite	monzodiorite
Outcrop area	13 km ²	75 km ²	65 km ²	16 km ²	280 km ²	30 km ²	10 km ²
SiO₂	~ 75 wt. %	48 - 76 wt. %	> 68 wt. %	> 76 wt. %	> 76 wt. %	54 - 63 wt. %	~ 60 wt. %
A/CNK^(b)	1.1 - 1.26	0.8 - 1.2	1 - 1.2	~1.1	0.94 - 0.95	1 - 1.2	0.98 - 0.99
⁸⁷Sr/⁸⁶Sr_T	~0.705	Gabbro: 0.704-0.707 Granite: ~ 0.707	~ 0.705	not constrained	~ 0.708	0.704 - 0.705	0.704 - 0.705
εNd_T	-2.3 - -1.9	Gabbro: 6.4 - -0.2 Granite: 0.5 - -1.9	-2.6 - -1.8	0.2	0 - 2.8	2.9 - 1.4	2.3 - 2.2
Country rocks	metapelites and quartzite of the Paleozoic metamorphic basement	metapelites and quartzite of the Paleozoic metamorphic basement	metapelites and metabasites of Paleozoic metamorphic basement	metapelites and metabasites of Paleozoic metamorphic basement	Paleozoic granitoids	Paleozoic granitoids	Paleozoic granitoids
Enclaves and xenoliths		rounded mafic enclaves and pelitic xenoliths	rounded and banded enclaves			rounded and centimetre-sized magma-tic enclaves and small pelitic xenoliths	
Contact with country rock	contact aureole of ~200 m width	several m wide contact aureole, increase of xenoliths towards the contact	contact aureole ~200 m wide	contact aureole ~100 m of wide	not exposed	not exposed	Several m wide contact aureole in the Triassic-Jurassic sedimentary sequences
Structural and textural features	miaroles filled with quartz, K-feldspar and tourmaline in otherwise medium to fine grained granitoid	hypidiomorphic medium- grained texture, locally coarse grained, locally miaroles filled with quartz, K-feldspar and tourmaline	centimetre-sized phenocrysts of orthoclase. Locally veins filled with tourmaline	Allotriomorphic coarse grained texture	Allotriomorphic coarse grained texture. Cavities with Fe-hydroxides.	hypidiomorphic medium-grained texture. Oscillatory and patchy zoning in plagioclase with resorbed cores	oscillatory and patchy zoning in plagioclase with rounded calcic cores

^(a) After Creixell et al. (2002) and Lucassen et al. (2004).

Table 2.2 Geochemical data of the Triassic-Jurassic intrusive of the Cordillera de la Costa, Chile (34°-37°S).

Sample N°		03-31	03-33	03-34	03-39	03-74	05-24	03-78	03-45	04-45	04-49	04-50	03-60	05-25
Locality		Constitución				Pichilemu	La Estrella		Cerro del Hualve				Montecillos	
Sample Coordinates		35°21'12.7"S/ 72°27'1.2"W	35°19'32.85"S/ 72°25'52.45"W	35°23'6.07"S/ 72°29'26.48"W	35°19'4.23"S/ 72°23'48.21"W	34°28'27"S/ 72°00'00"W	34°4'57.4"S/ 71°39'44.4"W	34°12'18.6"S/ 71°39'44.6"W	36°2'53.9"S/ 72°10'19.2"W	36°4'11.5"S/ 72°8'21.4"W	36°1'23.5"S/ 72°12'31.6"W	36°2'38.3"S/ 72°14'7.7"W	35°18'13.8"S/ 71°57'35.9"W	35°17'50.2"S/ 71°58'8"W
Rock		granite	granite	granodiorite (enclave)	granite	granite	granite	granite	gabbro	quartzdiorite	tonalite	gabbro	monzonite	monzodiorite
SiO ₂	%	71.9	70.5	68.7	70.7	76.5	77.0	76.0	55.9	61.7	62.7	54.8	60.6	59.9
Al ₂ O ₃	%	13.9	14.5	15.5	14.2	12.6	11.9	12.0	17.5	16.8	16.6	16.7	16.3	17.0
Fe ₂ O ₃	%	1.95	2.55	3.70	2.87	0.8	1.56	1.07	7.77	6.51	6.19	9.45	7.10	6.91
MnO	%	0.04	0.05	0.08	0.07	0.02	0.03	0.03	0.13	0.08	0.12	0.15	0.12	0.14
MgO	%	0.42	0.70	1.26	0.92	0.10	0.05	0.25	4.22	2.61	2.27	4.37	2.67	2.84
CaO	%	1.39	1.60	2.57	1.87	0.42	0.09	0.33	7.9	6.52	5.94	8.11	5.45	6.41
Na ₂ O	%	3.71	3.31	4.36	3.52	3.42	4.3	3.68	3.31	4.70	3.91	2.68	3.22	3.17
K ₂ O	%	4.07	4.34	1.90	3.78	4.58	4.17	4.54	1.09	0.47	0.21	1.43	3.09	2.70
TiO ₂	%	0.25	0.37	0.55	0.43	0.05	0.14	0.12	0.69	0.82	0.61	1.06	0.73	0.69
P ₂ O ₅	%	0.06	0.22	0.14	0.12	0.05	0.04	0.05	0.09	0.18	0.14	0.21	0.17	0.14
L.O.I	%	0.39	0.78	1.10	0.95	0.26	0.53	0.33	0.38	0.61	1.88	1.99	0.76	0.42
Total	%	98.2	99.1	100.0	99.6	98.8	99.8	98.6	98.9	101.1	100.7	101.2	100.4	100.5
Rb	ppm	250	n.d.	n.d.	217	299	147	195	41	n.d.	n.d.	47	141	108
Sr	ppm	88	n.d.	n.d.	107	10	16	33	319	n.d.	n.d.	288	328	315
Nb	ppm	10	13	15	12	24	28	15	2	6	6	6	5	8
Sn	ppm	8.8	n.d.	n.d.	11.2	8.3	10.0	4.4	1.0	n.d.	n.d.	1.0	1.8	2.0
Ta	ppm	1.3	n.d.	n.d.	1.4	2.3	2.5	1.4	0.2	n.d.	n.d.	0.4	0.3	0.3
Tl	ppm	1.2	n.d.	n.d.	1.3	1.4	0.7	0.9	0.2	n.d.	n.d.	0.2	0.5	0.4
Pb	ppm	31	n.d.	n.d.	27	27	14	23	9	n.d.	n.d.	5	13	30
Th	ppm	15	n.d.	n.d.	14	16	13	14	4	n.d.	n.d.	5	13	12.9
U	ppm	5.5	n.d.	n.d.	5.4	4.5	2.6	5.2	0.7	n.d.	n.d.	1.3	2.4	3.0
Cs	ppm	13	n.d.	n.d.	18	16	2	2	2	n.d.	n.d.	1	6	8
Y	ppm	22	n.d.	n.d.	24	47	89	45	19	n.d.	n.d.	26	26	23
La	ppm	26	n.d.	n.d.	28	16	51	45	10	n.d.	n.d.	20	21	18

Sample N°		03-31	03-33	03-34	03-39	03-74	05-24	03-78	03-45	04-45	04-49	04-50	03-60	05-25
Locality		Constitución				Pichilemu	La Estrella		Cerro del Hualve				Montecillos	
Sample Coordinates		35°21'12.7"S/ 72°27'1.2"W	35°19'32.85"S/ 72°25'52.45"W	35°23'6.07"S/ 72°29'26.48"W	35°19'4.23"S/ 72°23'48.21"W	34°28'27"S/ 72°00'00"W	34°4'57.4"S/ 71°39'44.4"W	34°12'18.6"S/ 71°39'44.6"W	36°2'53.9"S/ 72°10'19.2"W	36°4'11.5"S/ 72°8'21.4"W	36°1'23.5"S/ 72°12'31.6"W	36°2'38.3"S/ 72°14'7.7"W	35°18'13.8"S/ 71°57'35.9"W	35°17'50.2"S/ 71°58'8"W
Rock		granite	granite	granodiorite (enclave)	granite	granite	granite	granite	gabbro	quartzdiorite	tonalite	gabbro	monzonite	monzodiorite
Ce	ppm	51	n.d.	n.d.	57	32	59	90	23	n.d.	n.d.	44	50	42
Pr	ppm	6.1	n.d.	n.d.	7.1	4.6	13.2	11.0	3.1	n.d.	n.d.	5.6	6.7	5.3
Nd	ppm	22	n.d.	n.d.	26	17	51	43	13	n.d.	n.d.	24	27	22
Sm	ppm	4.7	n.d.	n.d.	5.5	5.4	10.8	9.4	3.2	n.d.	n.d.	5.4	5.9	4.9
Eu	ppm	0.6	n.d.	n.d.	0.9	0.2	1.6	1.0	1.0	n.d.	n.d.	1.3	1.1	1.0
Gd	ppm	4.3	n.d.	n.d.	5.1	6.6	10.5	9.0	3.4	n.d.	n.d.	5.3	5.3	4.5
Tb	ppm	0.8	n.d.	n.d.	0.9	1.4	2.1	1.6	0.6	n.d.	n.d.	0.9	0.9	0.8
Dy	ppm	4.3	n.d.	n.d.	4.9	8.8	13.2	9.4	3.7	n.d.	n.d.	4.7	5.0	4.2
Ho	ppm	0.8	n.d.	n.d.	0.9	1.9	2.8	1.8	0.8	n.d.	n.d.	0.9	1.0	0.9
Er	ppm	2.4	n.d.	n.d.	2.8	5.7	8.8	5.2	2.3	n.d.	n.d.	2.9	3.1	2.7
Tm	ppm	0.39	n.d.	n.d.	0.42	0.98	1.48	0.84	0.34	n.d.	n.d.	0.40	0.45	0.40
Yb	ppm	2.5	n.d.	n.d.	2.8	5.7	9.7	5.0	2.4	n.d.	n.d.	2.8	3.1	2.7
Lu	ppm	0.37	n.d.	n.d.	0.41	0.87	1.43	0.72	0.38	n.d.	n.d.	0.40	0.48	0.40
Sc	ppm	5	8	10	7	2	1	2	28	25	14	28	20	22
Ba	ppm	453	568	283	469	162	1170	753	301	177	196	390	571	498
Co	ppm	134	>140	>140	>140	155	<1	>140	95	54	39	36	102	43
Cr	ppm	<20	<30	34	<30	<20	<20	<30	28	<30	<30	39	<30	<30
Ga	ppm	19	18	20	19	24	28	23	13	21	21	22	21	15
Hf	ppm	<6	6	6	5	<6	15	5	>6	4	4	5	6	6
Ni	ppm	<20	15	15	10	<20	<20	<5	<20	7	5	11	12	<5
V	ppm	25	<30	50	31	21	<5	<30	209	180	127	255	170	171
Zn	ppm	33	73	76	69	51	90	52	64	<30	54	78	51	90
Zr	ppm	132	167	177	153	57	487	129	94	140	156	166	191	185

n.d. not determined

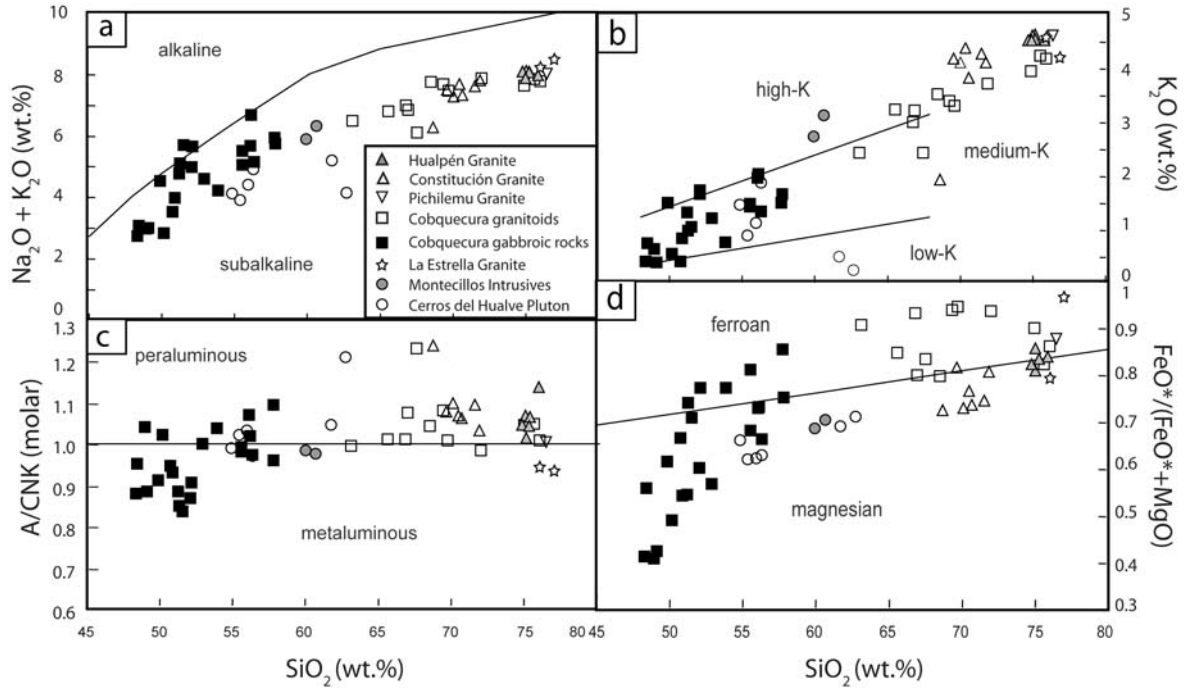


Figure 2.3 Classification diagrams of Triassic and Jurassic intrusive rocks in the Cordillera de la Costa: a) Total alkalis vs. SiO_2 ; b) K_2O vs. SiO_2 (classification after Le Maitre et al. 1989); c) $\text{A/CNK} = \text{Al}_2\text{O}_3/(\text{CaO} + \text{Na}_2\text{O} + \text{K}_2\text{O})$ [molar] vs. SiO_2 ; d) $\text{FeO}^*/(\text{FeO}^* + \text{MgO})$ vs. SiO_2 classification after Frost et al. (2001).

2.3.1 La Estrella Granite ($\sim 34^\circ 15'S$)

The La Estrella Granite crops out south of Rapel River near to the town of La Estrella ($\sim 34^\circ 15'S$, $71^\circ 45'W$) in the central part of the Cordillera de la Costa (Fig. 2.2). It is the largest Late Triassic intrusive body in the area and intrudes into Paleozoic granitoids. The main rock types are pink coarse-grained biotite-monzogranite and minor pink-colored arfvedsonite-granodiorite (Vásquez et al. 2006). Opaque minerals are ilmenite, often associated with pyrite.

The La Estrella Granite displays high SiO_2 contents, is moderately metaluminous (Fig. 2.3c), has high $\text{FeO}^*/(\text{FeO}^* + \text{MgO})$ ratios (0.80 - 0.96), and high K_2O -contents (4.2 - 4.5 wt.%) (Fig. 2.3b, d). It shows high Ba-contents (753 - 1169 ppm) and low Sr contents (16 - 33 ppm) (Fig. 2.7, Table 2.2). In mantle-normalized multielement diagrams, the La Estrella granites are richer in compatible elements and present a weaker Nb-Ta trough than other granites (Fig. 2.4). The La Estrella Granite has fairly flat REE patterns ($\text{La}_N/\text{Yb}_N = 3.6 - 6.1$), is rich in HREE, and has no pronounced negative Eu anomalies ($\text{Eu}^*/\text{Eu} = 0.33 - 0.45$) (Fig. 2.5b).

Among the Early Mesozoic granites studied here, the La Estrella Granite shows the highest ϵNd_i values between 0 and 2.8 with high $^{87}\text{Sr}/^{86}\text{Sr}_i$ ratios of ca. 0.708 (Fig. 2.6), which are, however, somewhat uncertain due to the imprecisely constrained crystallization age of this body (see below). It presents a broad range of initial $^{206}\text{Pb}/^{204}\text{Pb}$ and $^{208}\text{Pb}/^{204}\text{Pb}$ ratios between 18.1 - 18.5 and 38.1 - 38.4, respectively. Its $^{207}\text{Pb}/^{204}\text{Pb}$ isotopic composition is uniform with values of ca. 15.6 (Fig. 2.8b).

Table 2.3 Whole rock Nd, Sr and Pb isotope data of the Triassic-Jurassic intrusives rocks in the Cordillera de la Costa, Chile (34°-37°S)

Sample ^a	Age (Ma)	⁸⁷ Sr ^b	⁸⁷ Sr _(T) ^c	¹⁴³ Nd ^b	εNd _(T)	²⁰⁶ Pb ^d	²⁰⁷ Pb ^d	²⁰⁸ Pb ^d	²⁰⁶ Pb ^e	²⁰⁷ Pb ^e	²⁰⁸ Pb ^e	
		⁸⁶ Sr	⁸⁶ Sr	¹⁴⁴ Nd		²⁰⁴ Pb	²⁰⁴ Pb	²⁰⁴ Pb	²⁰⁴ Pb	²⁰⁴ Pb	²⁰⁴ Pb	
03-39	Constitución Granite ^f	224	0.725360±9	0.70540	0.512444±6	−1.8	18.748	15.660	38.763	18.22	15.64	38.33
03-31	Constitución Granite ^f	224	0.730167±9	0.70520	0.512407± 8	−2.6	18.727	15.650	38.735	18.27	15.63	38.33
03-78	La Estrella Granite ^f	197	0.749100±9	0.70800	0.512563± 4	0.0	18.577	15.641	38.546	18.07	15.62	38.12
05-24	La Estrella Granite ^f	197	0.781408±8	0.70800	0.512695±5	2.8	18.899	15.638	38.821	18.47	15.62	38.14
03-74	Pichilemu Granite ^f	205	0.940136±9	n.d.	0.512632±5	0.2	18.886	15.695	38.927	18.48	15.68	38.49
03-60	Montecillos Monzonite	155	0.706741±9	0.70409	0.512689±5	2.3	18.719	15.647	38.710	18.38	15.63	38.13
05-25	Montecillos Monzodiorite ^f	155	0.706323±8	0.70491	0.512686±4	2.2	18.597	15.613	38.525	18.42	15.60	38.28
03-45	C° Hualve Gabbro	166	0.704689±9	0.70384	0.512736±5	2.9	18.879	15.677	38.975	18.72	15.67	38.70
04-50	C° Hualve Gabbro ^f	166	0.706378±7	0.70547	0.512648±5	1.4	18.880	15.637	38.941	18.38	15.61	38.28

- a Samples were dissolved with 52% HF for four days at 160°C on the hot plate. Digested samples were dried and taken up in 6N HCl. Sr and Nd were separated and purified using ion-exchange chromatography as described in Romer et al. (2005). Pb was separated using the HBr-HCl ion-exchange procedure as described in Romer et al. (2005)
- b ⁸⁷Sr/⁸⁶Sr and ¹⁴³Nd/¹⁴⁴Nd normalized to ⁸⁷Sr/⁸⁶Sr = 0.1194 and ¹⁴³Nd/¹⁴⁴Nd = 0.7219 respectively. Isotopic data for Sr and Nd were obtained on a VG54 and Finnigan MAT262 multi-collector TIMS mass-spectrometer, respectively, using dynamic multicollection. Analytical uncertainties are given at 2σ_m level.
- c ⁸⁷Sr/⁸⁶Sr_(T) and ϵ Nd_(T) were calculated for the time of the intrusion using $\lambda^{87}\text{Rb} = 1.42\text{E-}11 \text{ y}^{-1}$ and $\lambda^{147}\text{Sm} = 6.54\text{E-}12 \text{ y}^{-1}$, (¹⁴⁷Sm/¹⁴⁴Nd)⁰ CHUR = 0.1967, (¹⁴³Nd/¹⁴⁴Nd)⁰ CHUR = 0.512638 and the concentration data given in Table 2.2.
- d Lead isotope data were obtained on a Finnigan MAT262 multi-collector TIMS mass-spectrometer using static multicollection. Lead isotope data were corrected for mass discrimination with 0.1% / A.M.U. Reproducibility at 2σ level is better than 0.1%.
- e Lead isotope data recalculated to the age of intrusions using the contents of Pb, Th and U (Tables 2.2 and 2.4) and the constants recommended by IUGS (Steiger and Jaeger. 1977).
- f ID-TIMS DATA

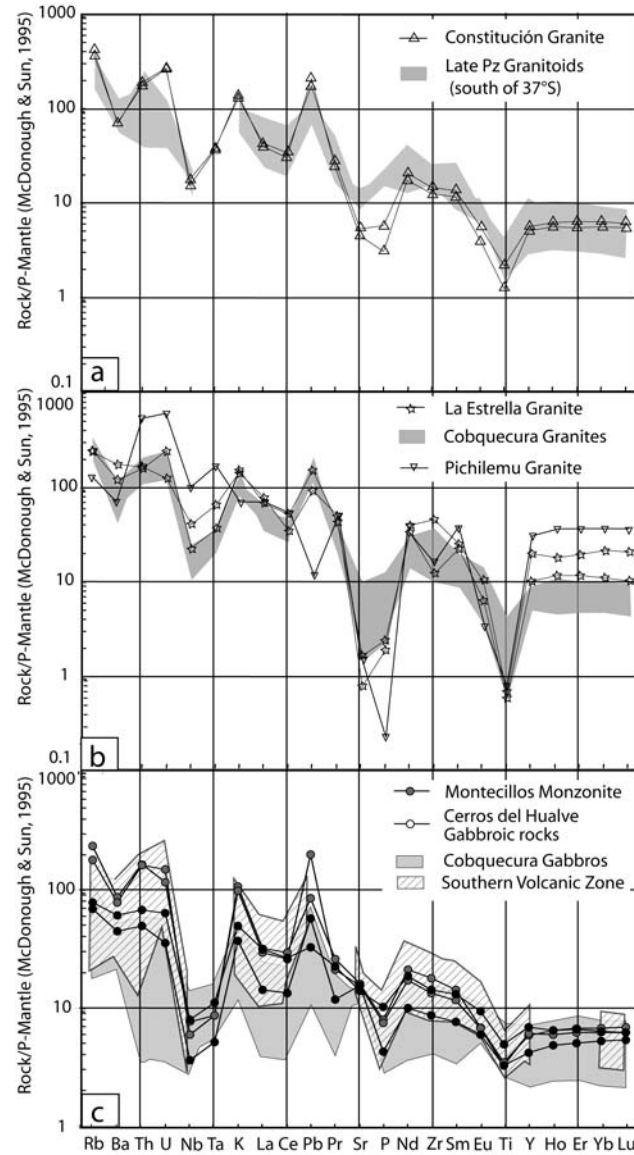


Figure 2.4 Selected trace element patterns of Triassic and Jurassic igneous rocks (33°S-37°S) normalized to primitive-mantle (McDonough and Sun 1995) a) Constitución Granite (225 -220 Ma). The field of Paleozoic granitoids was taken from Lucassen et al. (2004); b) La Estrella Granite (210 – 197 Ma). Shaded area represents the spectrum of the Cobquecura Granitoid (Vásquez et al., 2008a); c) Middle Jurassic Gabbroic Rocks from Cerros del Huave and Montecillos (170 – 150 Ma). Shaded area represents the spectrum of the Cobquecura Gabbroic rocks, and the hatched area represents the Southern Volcanic Zone (SVZ, taken from <http://georoc.mpch-mainz.gwdg.de/georoc/Entry.html>).

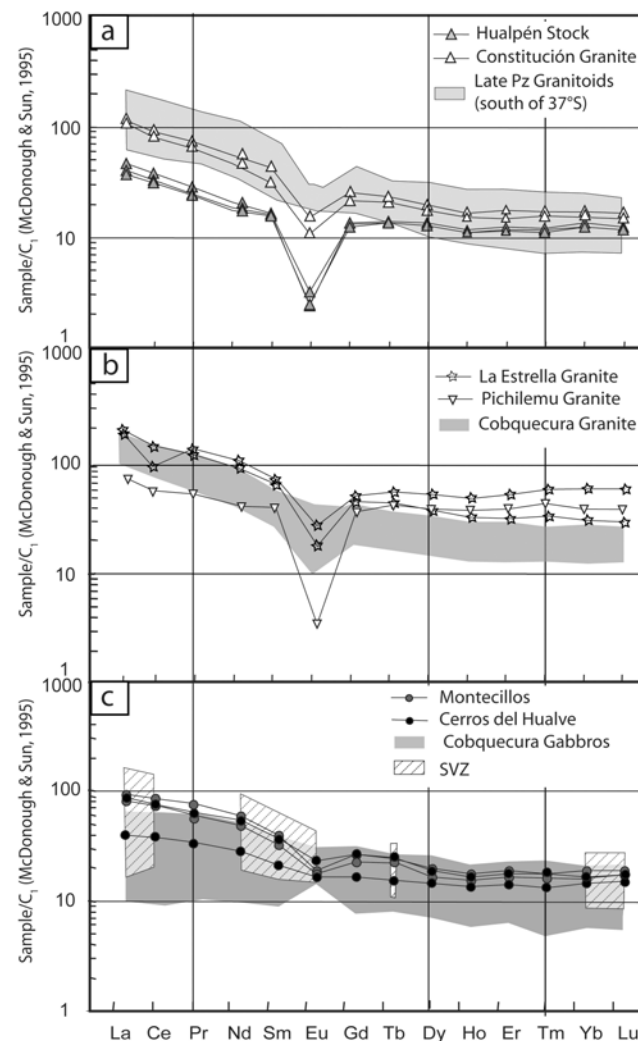


Figure 2.5 REE pattern of Triassic and Jurassic intrusive rocks in the Cordillera de la Costa normalized to Chondrite C_1 (McDonough and Sun, 1995) for a) Hualpén Stock (data from Lucassen et al. 2004), Constitución Granite and Pichilemu Granite (225 - 220 Ma). Shaded area represents the Paleozoic granitoids south of 37°S (data from Lucassen et al. 2004); b) La Estrella Granite (210 - 197 Ma). Shaded area represents the spectrum of the Cobquecura Granitoids (Vásquez et al., 2008a); c) Middle Jurassic Gabbroic rocks: Montecillos Intrusives and Cerros del Hualve Intrusives (170 - 150 Ma). Shaded area represents the spectrum of the Cobquecura Gabbroic rocks (~210 Ma). Hatched area represents the Southern Volcanic Zone (SVZ, data taken from <http://georoc.mpch-mainz.gwdg.de/georoc/Entry.html>).

2.3.2 Pichilemu Granite (34°30'S)

The granite is a small stock intruded into the metamorphic basement near the town of Pichilemu (Fig. 2.2, Table 2.1). Its composition is leucocratic (color index <10), and the mafic minerals are altered to chlorite. In the geological map of Richter et al. (2007), this stock is related to the N-S oriented Pichilemu- Vichuquen Fault.

It has high SiO_2 - (~76 wt.%) and K_2O -contents (~ 4.6 wt.%) and a $\text{FeO}^*/(\text{FeO}^*+\text{MgO})$ ratio of ca. 0.87 (Table 2.2, Fig. 2.3b, d). Its trace element signature is similar to that of the

Constitución Granite and the Hualpen Stock (Fig. 2.7), but with a flatter REE pattern than the other Late Triassic granitoids of this segment (Fig. 2.5). Its relatively high ϵNd_i value (~ 0.2) is similar to that of the Cobquecura granitoids. A reliable Sr_i cannot be calculated due to the very radiogenic Sr (0.9401, Table 2.3) and high $^{87}\text{Rb}/^{86}\text{Sr}$ (79.9) in our analyzed sample.

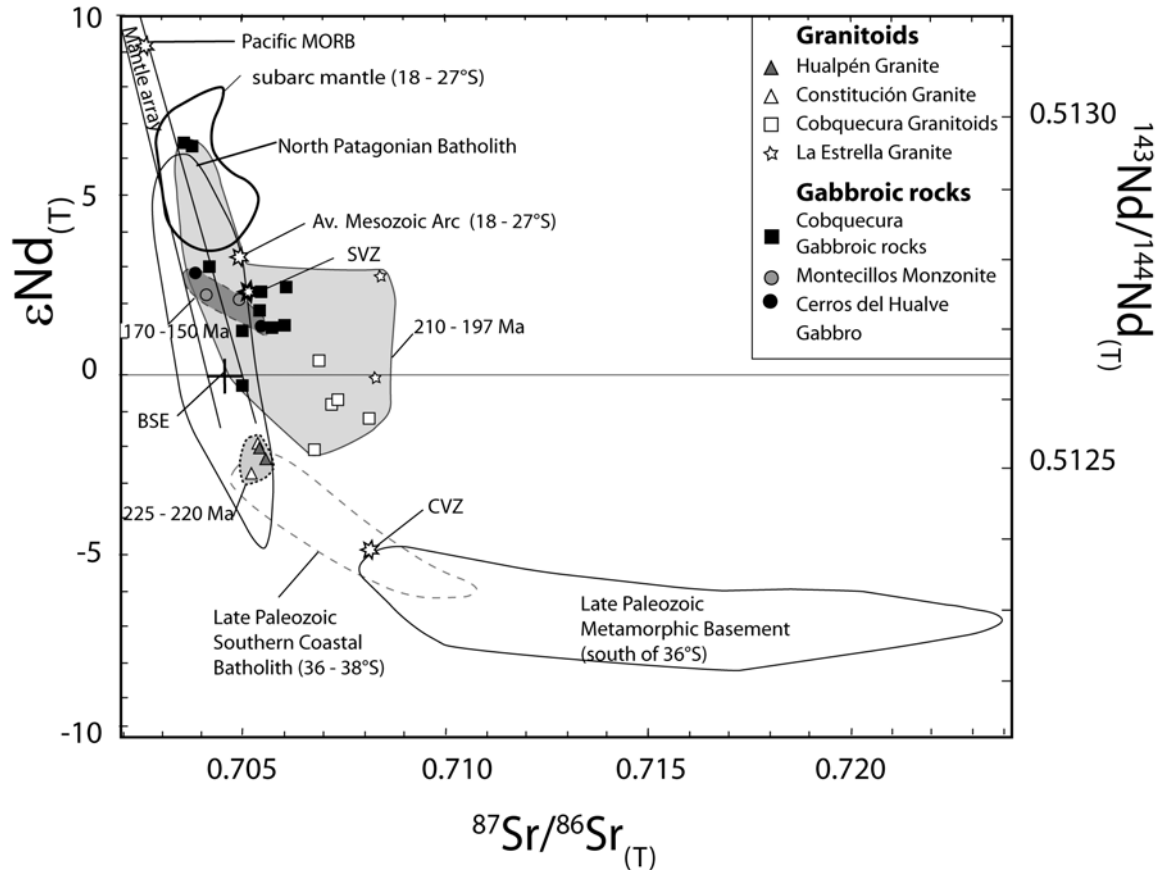


Figure 2.6 ϵNd vs. initial Sr isotopic compositions of the Triassic-Jurassic intrusives. For comparison the following $\text{Nd}_{(T)}$ and $\text{Sr}_{(T)}$ isotopic compositions are shown: Late Paleozoic Basement in the area (metamorphic rocks south of the 36°S) and the Late Paleozoic Southern Coastal Batholith (30-38°S) (Parada et al. 1999; Lucassen et al. 2004), the average Mesozoic arc between 18 and 27°S was calculated from the Jurassic magmatic rocks from northern Chile (Lucassen et al. 2006), Triassic volcanic rocks from northern Chile (18°-27°S; Lucassen et al. 2006), field of the North Patagonian Batholith (44°-47°S, Pankhurst et al. 1999), average of the Pacific MORB (Petrological database of the ocean floor <http://petdb.org>). The Nd isotope ratio is calculated for 210 Ma using a $^{147}\text{Sm}/^{144}\text{Nd}$ ratio of 0.214; the subarc-subcontinental mantle isotopic composition was calculated to 210 Ma (Lucassen et al. 2006). Bulk Silicate Earth values (BSE) are shown for the present day. Mantle array field is taken from Dickin, 1997. The average of the CVZ and SVZ (northern, central and southern volcanic zones) were calculated from the present-day data in <http://georoc.mpch-mainz.gwdg.de/georoc/Entry.html>.

2.3.3 Montecillos Intrusive Rocks ($\sim 35^\circ\text{S}$)

At Montecillos, along the road Talca-Curepto, a strongly altered pinkish gray amphibole- and biotite-monzonite to monzodiorite crops out. The stock intruded into Triassic-Jurassic sediments (Fig. 2.2, Table 2.1). The ubiquitous presence of orthopyroxene is a characteristic feature. The Montecillos body is not obviously related to any major tectonic structure. It presents a more mafic composition than the rocks at Pichilemu and La Estrella and is mildly peraluminous

(Table 2.1, Fig. 2.3). The Montecillos intrusive rocks present a high K_2O -content (2.7 - 3) and the $FeO^*/(FeO^*+MgO)$ ratios are low (~ 0.7) (Fig. 2.3). The negative Eu-anomalies ($Eu^*/Eu = 0.60 - 0.66$) in the fairly flat REE-patterns ($La_N/Yb_N = \sim 4.6$; Fig. 2.5c) are less pronounced than in the La Estrella granitoids. $^{87}Sr/^{86}Sr_i$ values are around 0.705, ϵNd_i values are positive between 2.2 and 2.3 (Fig. 2.6). Pb isotopic ratios are constrained to $^{206}Pb/^{204}Pb \sim 18.5$, $^{207}Pb/^{204}Pb \sim 15.6$ and $^{208}Pb/^{204}Pb \sim 38.3$ (Fig. 2.8).

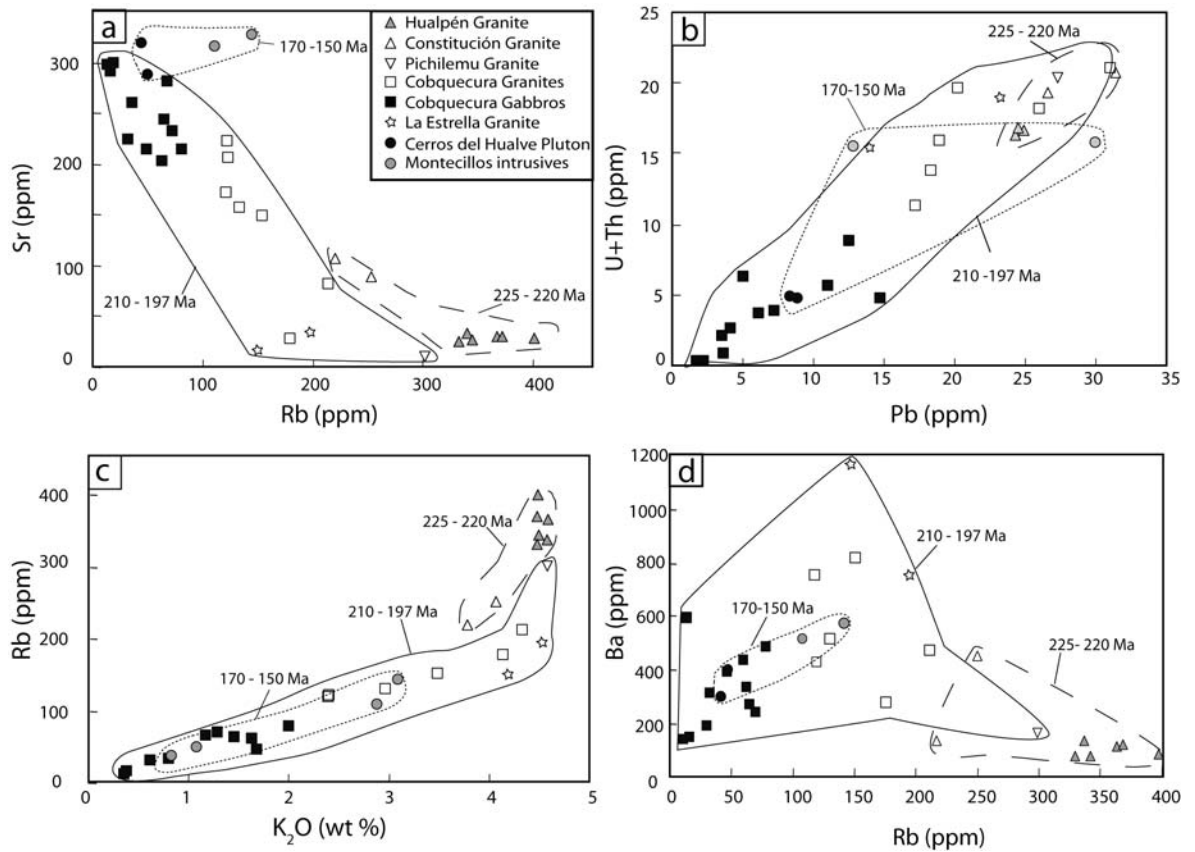


Figure 2.7 Trace element vs. trace element diagrams for the different magmatic age groups of Triassic and Jurassic intrusive rocks in the Cordillera de la Costa; a) Sr (ppm) vs. Rb (ppm); b) (U+Th) (ppm) vs. Pb (ppm); c) Rb (ppm) vs. K_2O (wt %); d) Ba (ppm) vs. Rb (ppm).

2.3.4 Constitución Granite ($\sim 35^\circ S$)

The Constitución Granite is located at the western flank of the Cordillera de la Costa, at the mouth of the Maule river (Fig. 2.2). This granite is a homogeneous, K-feldspar-porphyritic, biotite-monzogranite. It intrudes into metapelites and metabasites of the Late Paleozoic metamorphic basement.

The Constitución Granite is moderately peraluminous and shows high SiO_2 -, K_2O - (up to 4.6 wt. %, (Tables 2.1, 2.2, Fig. 2.3b), Rb-, U-, Th- and Pb- contents (Fig. 2.7), and high $FeO^*/(FeO^*+MgO)$ ratios (0.72 - 0.86; Fig. 2.3d). The samples have relatively flat REE-patterns ($La_N/Yb_N = 6.8 - 7.0$) with enrichment of LREE ($La_N/Sm_N = 3.2 - 3.4$) compared to the HREE

($\text{Lu}_N/\text{Gd}_N = \sim 0.7$) (Fig. 2.5a) and negative Eu-anomalies ($\text{Eu}^*/\text{Eu} = 0.4 - 0.5$). The $^{87}\text{Sr}/^{86}\text{Sr}_i$ values of ca. 0.705 and negative ϵNd values between -1.8 and -2.6 (Fig. 2.6) are identical to those of the Hualpén Granite. Its initial Pb isotope ratios are between the values from La Estrella Granite but lower than those of the Hualpén Granite (Fig. 2.8b; $^{206}\text{Pb}/^{204}\text{Pb} = \text{ca. } 18.2 - 18.3$; $^{207}\text{Pb}/^{204}\text{Pb} = \text{ca. } 15.6$ and Fig. 2.8a $^{208}\text{Pb}/^{204}\text{Pb} = \text{ca. } 38.3$).

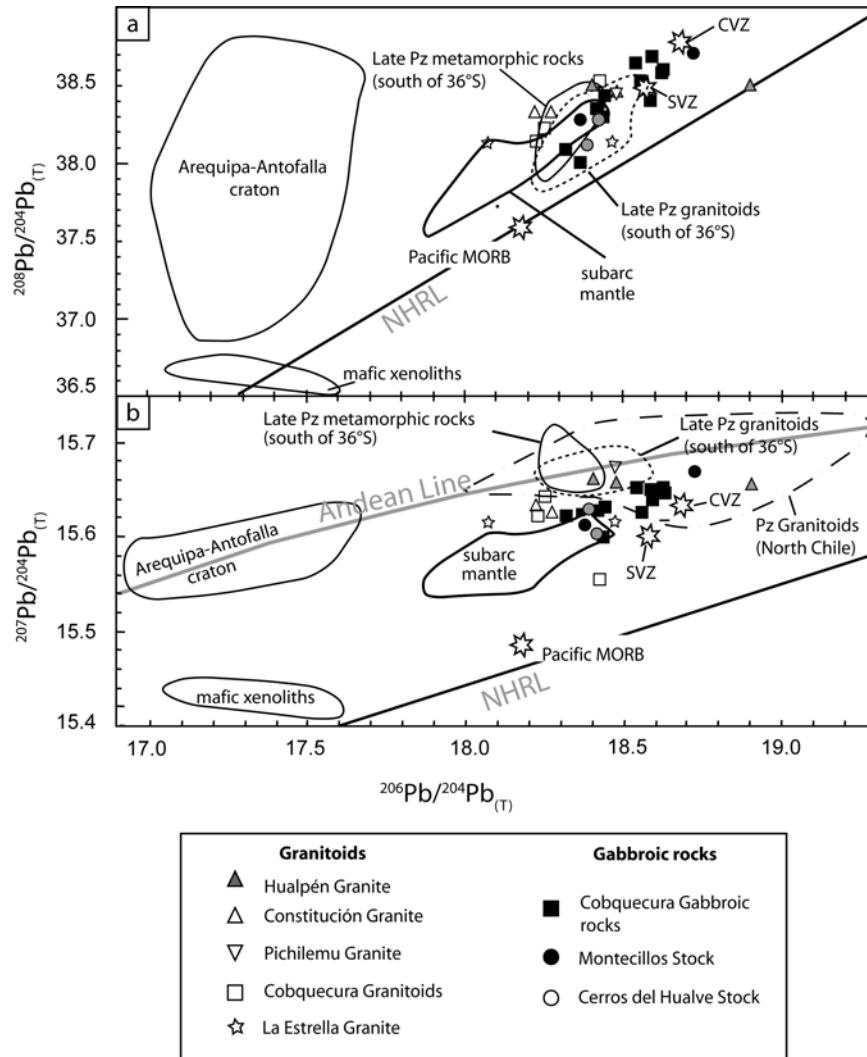


Figure 2.8 Initial Pb isotopic compositions of Triassic and Jurassic magmatic rocks of the Cordillera de la Costa (37 - 34°S). Field of Late Paleozoic metamorphic and igneous rock (south of 36°S) was taken from Lucassen et al (2004), Mesozoic lithospheric mantle at 210 Ma (18 - 27°S) from Lucassen et al. (2006), Pacific MORB at 210 Ma from Petrological database of the ocean floor (<http://petdb.org>), Arequipa-Antofalla craton at 210 Ma from Tosdal (1996). The field marked “mafic xenoliths” corresponds to xenoliths of the Basement of Precordillera, with values taken from Kay et al. (1996). Northern hemisphere reference line (NHRL; Hart, 1984). Data for Paleozoic granitoids from north Chile (21 - 27°S) and the Andean Pb line were taken from Lucassen et al. (2002). The average of the CVZ and SVZ (Central and Southern Volcanic Zones) were calculated from the data in <http://georoc.mpch-mainz.gwdg.de/georoc/Entry.html>.

2.3.5 Cobquecura Pluton (~36°S)

The Cobquecura Pluton crops out around the town of Cobquecura, north of the mouth of the Itata river on the western flank of the Cordillera de la Costa (Fig. 2.2), and intrudes into the metasedimentary metamorphic basement. It exhibits a wide lithologic and textural variety (described in detail by Vásquez and Franz, 2008) compared to the other intrusive bodies of this area. Its composition varies from fayalite-granite to olivine-gabbro. Its textures are typical for magma mingling (Vásquez and Franz, 2008), which together with geochemical and geochronological evidence (see below) suggests that the felsic and mafic magmas were coeval. Granites contain fayalitic olivine, Fe-rich clinopyroxene, amphibole, biotite, and ilmenite. Gabbroic rocks contain Mg-rich clino- and orthopyroxene, pyroxene, amphibole, and minor olivine and biotite. Opaque phases are ilmenite and accessory Cu-sulfides.

The rocks show a wide spectrum of compositions and A/CNK from metaluminous to peraluminous values which increase with increasing SiO₂-content (Fig. 2.3c; Vásquez and Franz, 2008). The granitoids are K-rich (2.4 - 4.19 wt.% K₂O; Fig. 2.3b) and have high FeO*/(FeO*+MgO) ratios (>0.8; Fig. 2.3d, Vásquez and Franz, 2008). The granitoid rocks have a gentle slope in the REE-patterns (La_N/Yb_N = 3.88 - 8) and slightly negative Eu-anomalies (Eu*/Eu = 0.42 - 0.85) (Fig. 2.5). In the εNd - ⁸⁷Sr/⁸⁶Sr_i diagram (Fig. 2.6) they comprise a field with both higher εNd and ⁸⁷Sr/⁸⁶Sr_i values (0.5 to -2.0; 0.706 to 0.708, respectively) than the Constitución and Hualpén granites. The ²⁰⁶Pb/²⁰⁴Pb (18.2 - 18.6), ²⁰⁷Pb/²⁰⁴Pb (~15.6; Fig. 2.8b) and ²⁰⁸Pb/²⁰⁴Pb ratios (38.1 - 38.5; Fig. 2.8a) are comparatively low, similar to those of La Estrella and Constitución granites.

REE patterns of the gabbroic rocks are gently sloped (La_N/Yb_N = 1.93 - 3.66) and have positive to absent Eu-anomalies. Their generally higher values in εNd (between 6.4 and -0.2) and lower values in ⁸⁷Sr/⁸⁶Sr_i (0.703 - 0.706; Fig. 2.6) partly overlap with the granitic rocks. Pb isotopic compositions of many gabbroic rocks are slightly more radiogenic (²⁰⁶Pb/²⁰⁴Pb = 18.3 -18.6, ²⁰⁷Pb/²⁰⁴Pb = 15.6 - 15.7; Fig. 2.8b, and ²⁰⁸Pb/²⁰⁴Pb = 38.0 - 38.7, Fig. 2.8a) than those of the associated granitoids.

2.3.6 Cerros del Hualve Pluton (~36°S)

Gabbro, quartz-diorites and tonalites occur on the eastern flank of the Cordillera de la Costa, north of Cerros del Hualve (Fig. 2.2, Table 2.1). Because of poor outcrop conditions, their relationship with the country rocks is unknown. The link between the pluton and major tectonic structures is not evident. The mafic rocks have amphibole and pyroxene as mafic minerals. The opaque minerals are magnetite with exsolution of ilmenite lamellae. Tonalite and quartz-diorite locally contain dioritic enclaves. Similarly as the intrusives at Montecillos, the Cerros del Hualve Pluton contains centimeter to millimeter sized pyroxene-rich enclaves but they are dominated by clinopyroxene and not by orthopyroxene as at Montecillos.

The predominantly mafic rocks have a K₂O-content similar to lithologies with similar SiO₂-content of the Cobquecura Pluton, but lower than those of the rocks from Montecillos (Fig. 2.3b). The FeO*/(FeO*+MgO) ratios range between 0.62-0.71. The negative Eu anomalies are less pronounced than those of the Montecillos samples (Fig. 2.5). Rocks from Cerros del Hualve Pluton and Montecillos are distinguished by small differences in the slopes of the REE-pattern with slightly steeper slopes for the LREE in the samples from Montecillos than for those from Cerros del Hualve (Fig. 2.5). U-, Th-, and Pb-contents in gabbroic rocks reach higher values in Montecillos Intrusives and Cerros del Hualve Pluton than in the gabbroic rocks from the Cobquecura Pluton (Fig. 2.7).

The Cerros del Hualve and Montecillos intrusives (both Middle Jurassic) display similar ⁸⁷Sr/⁸⁶Sr_i ratios, εNd_i values and Pb isotopic ratios as the Cobquecura gabbroic rocks (Figs. 2.6, 2.8), but slightly lower ²⁰⁸Pb/²⁰⁴Pb ratios (Figs. 2.6, 2.8).

2.3.7 Hualpen Stock (~37°S)

The Hualpén Stock is located at the mouth of the Biobío River, which follows a NW-SE oriented, most probably Paleozoic, lineament. It intrudes into metapelites of the Paleozoic metamorphic basement and is mainly a homogeneous two mica-monzogranite (described in detail by Creixell et al. 2002).

The previously reported isotopic data for the Hualpén Stock (⁸⁷Sr/⁸⁶Sr_i = ~0.705 and εNd = -1.9 to -2.3; Lucassen et al. 2004) are similar to those reported for the Constitución Granite (Figs. 2.6 and 2.8). Despite their geochemical and petrographical similarities, the Hualpén Stock displays higher ²⁰⁶Pb/²⁰⁴Pb ratios than the Constitución Granite (Fig. 2.8).

2.4 Age data: Methods, samples, and results

Several age determinations for the Hualpen, Constitución, Cerros del Hualve, Pichilemu, and La Estrella intrusive bodies, scattering between 165 and 230 Ma (Table 2.4), are available from the literature. For the intrusive bodies of unknown ages we present new age determinations. The new isotopic ages are based on laser ablation–inductively coupled plasma–sector field mass spectrometry (LA-ICP-MS) U-Pb analyses of zircon as well as on K-Ar-ages of amphibole and biotite (Table 2.4, Figs. 2.2 and 2.9 and appendices A and B). For the Pichilemu Granite, we present a Rb-Sr model age.

For U-Pb age determinations, zircons were separated using conventional magnetic separation and heavy liquid methods. Individual zircon grains were handpicked using an optical microscope. For analysis, the individual zircon grains were mounted in circular epoxy mounts and polished. Back-scattered electron (BSE) images of all grains were obtained with the aim to check

for internal structures. Finally, selected points were measured by LA-ICP-MS at GEUS, Copenhagen (for procedure details see the appendix C). Seven samples from the different plutons were selected (Table 2.4, appendix A). Three of these are from the Cobquecura Pluton (Buchupureo gabbro sample 03-27, the Pullay gabbro sample 04-22, and the La Iglesia de Piedra fayalite-granodiorite sample 03-08). The other four samples are from the Cerros del Hualve gabbro (sample 03-45), the La Estrella Granite (sample 03-79), the Montecillos monzonite (sample 03-60) and the La Puntilla tonalite (sample 03-58) (Table 2.4, Fig. 2.9, appendix A).

Data reduction and error treatment follow established standard procedures as usual for LA-ICP-MS dating (e.g., Frei et al. 2006). The size of the reported error is in part dependent on the number of analyzed spots, as the standard deviation is divided by the square root of the number of analyses. This procedure, which is also applied in SHRIMP dating, is based on the assumption that all the analyzed data are normally distributed around the mean. This assumption is correct for samples that are truly concordant, but not for samples with Pb-loss.

Gabbro samples of the Cobquecura Pluton from Buchupureo and Pullay have pink translucent, subhedral zircon grains. No internal zoning or inherited cores are visible with BSE. Forty-three U-Pb analyses from Buchupureo zircons form a concordant population with a mean of 209 ± 2 Ma (2σ) (Fig. 2.9a). A combined age of thirty-seven analyses from Pullay is 203 ± 2 Ma (2σ) (Fig. 2.9b). The fayalite granodiorite from Punta Iglesia de la Piedra, also from the Cobquecura Pluton, contains euhedral to subhedral, occasionally elongated pink translucent zircon grains. They display oscillatory zoning at their rims and resorbed cores that sporadically show an oscillatory concentric zoning visible with BSE. U-Pb zircon ages are discordant (see discussion below; Fig. 2.9c), but cluster near ≈ 200 Ma.

For the Pichilemu Granite, our Rb-Sr whole rock isotopic data (Table 2.3) facilitate calculation of a Rb-Sr model age. An assumed initial $^{87}\text{Sr}/^{86}\text{Sr}$ ratio of 0.707 ± 0.007 (allowing for hypothetically extremely variable mantle and crustal contributions to magma formation) combines with our analytical data for a Pichilemu Granite sample (see Table 2.4) to a model age of 205 ± 7 Ma (2σ).

For La Estrella Granite (sample 03-79), we obtained LA-ICP-MS ages for two zircon grains only, due to low abundance and a very small zircon grain size. One of these zircons plots nearly concordant at ~ 200 Ma and the other one plots near 180 Ma (Fig. 2.9d), rendering this dataset inconclusive.

The gabbro from Cerros del Hualve contains euhedral zircon grains with translucent pink color without zoning visible with BSE. Analyses on 18 zircon grains from Cerros del Hualve (sample 03-45) form a concordant population with a concordia age of 166 ± 2 Ma (2σ) (Fig. 2.9e). For the same sample, K-Ar isotopic ages determined for hornblende are 166 ± 5 Ma (2σ) and 165 ± 3 Ma (2σ) for biotite (see appendix B).

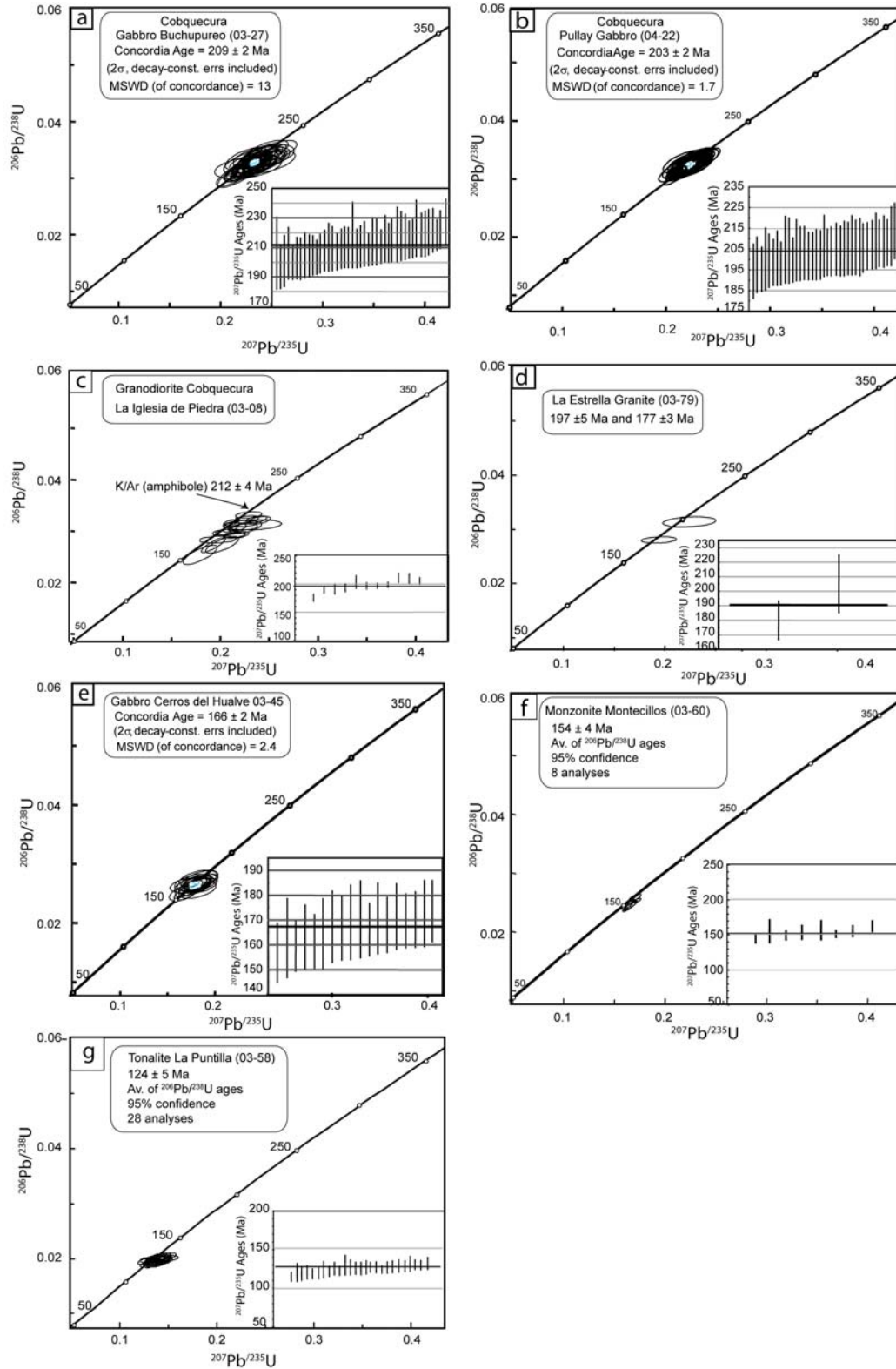


Figure 2.9 Results of LA-ICP-MS U-Pb age determinations on zircon from the Cordillera de la Costa (34°S - 37°S), Chile. Gabbroic rocks from Cobquecura (a, b) and Cerros del Hualve (e) yielded concordant ages. c) The oldest U-Pb ages from the fayalite-granodiorite coincide with the previously determined K-Ar age of amphibole for the same rocks (Vásquez et al. 2005). U-Pb ages from La Estrella Granite suggest an Early Jurassic age. U-Pb ages of zircon from Tonalite La Puntilla and Monzonite Montecillos (f, g) yield slightly discordant ages. Insets in all the figures show the ages derived from the Tukey's biweight mean of $^{207}\text{Pb}/^{235}\text{U}$ ages. Data point error ellipses and symbols are 2 σ .

The Montecillos monzonite (sample 03-60) has euhedral to subhedral zircon grains with strong zoning and some resorbed cores; their color is pink and the crystals are turbid. U-Pb zircon data are slightly discordant (Fig. 2.9f; see discussion below), with ages around 150 Ma (weighted mean of $8 \text{ }^{207}\text{Pb}/^{235}\text{U}$ ages is $152 \pm 5 \text{ Ma}$; weighted mean of $8 \text{ }^{206}\text{Pb}/^{238}\text{U}$ ages is $145 \pm 5 \text{ Ma}$; appendix A).

Table 2.4 Isotopic ages of intrusive rocks from the early Mesozoic rocks of the Cordillera de la Costa, 34-37°S, Chile.

Localities	Rock Types	Isotopic Age (literature)	Isotopic Age (this work)
Hualpén	two mica-monzogranite	$215 \pm 4 \text{ Ma}$, K-Ar, biotite ⁽²⁾ $220 \pm 5 - 222 \pm 2 \text{ Ma}$, Rb-Sr, mineral data ⁽¹⁾ $227 \pm 7 \text{ Ma}$, Rb-Sr, mineral data ⁽³⁾	_____
Constitución	biotite-monzogranite	$208 \pm 6 \text{ Ma}$; $202 \pm 6 \text{ Ma}$, K-Ar, biotite ⁽⁴⁾ $224 \pm 1 \text{ Ma}$, Pb-Pb, zircon ⁽⁵⁾	_____
Cobquecura	gabbro	$213 \pm 5 \text{ Ma}$, K-Ar, amphibole ⁽⁶⁾	$209 \pm 2 \text{ Ma}$ (Sample 03-27), U-Pb zircon (Buchupureo) $203 \pm 2 \text{ Ma}$ (Sample 04-22), U-Pb zircon (Pullay)
	fayalite-granodiorite	$212 \pm 4 \text{ Ma}$, K-Ar, amphibole ⁽⁶⁾	$212 \pm 4 \text{ Ma}$ (Sample 03-08), U-Pb zircon (Punta Iglesia de la Piedra)
La Estrella	biotite-monzogranite	$218 \pm 21 \text{ Ma}$, K-Ar biotite ⁽⁷⁾	$\sim 197 \text{ Ma}$ (Sample 03-79), U-Pb zircon
Pichilemu	hornfels at the contact with the monzogranite	$211 \pm 32 \text{ Ma}$, K-Ar crossite (metachert) ⁽⁸⁾	$205 \pm 7 \text{ Ma}$ (Sample 03-74); Rb-Sr whole rock
Cerro del Hualve	granite	$230 \pm 10 \text{ Ma}$, K-Ar biotite ⁽⁹⁾	_____
	gabbro	_____	$165 \pm 3 \text{ Ma}$ (Sample 03-45), K-Ar biotite $167 \pm 5 \text{ Ma}$ (Sample 03-45), K-Ar amphibole $166 \pm 2 \text{ Ma}$ (Sample 03-45), U-Pb zircon
Montecillos	monzonite/granodiorite	$165 \pm 5 \text{ Ma}$, K-Ar biotite ⁽⁴⁾ $175 \pm 5 \text{ Ma}$, K-Ar hornblende ⁽⁴⁾	$150 \pm 6 \text{ Ma}$ (Sample 03-60), U-Pb zircon
La Puntilla	tonalite	_____	$124 \pm 1 \text{ Ma}$ (Sample 03-58), U-Pb zircon (Cerro Pillay)

⁽¹⁾ Lucassen et al. (2004), ⁽²⁾ Hervé et al. (1988), ⁽³⁾ Glodny et al. (2006), ⁽⁴⁾ Gana and Hervé (1983), ⁽⁵⁾ Willner et al. (2005), ⁽⁶⁾ Vásquez et al. (2005), ⁽⁷⁾ Dávila et al. (1979), ⁽⁸⁾ Hervé et al. (1984), ⁽⁹⁾ Hervé and Munizaga (1978).

From La Puntilla, 28 euhedral to subhedral unzoned zircon grains from a tonalite (Cerros Pillay) were analyzed. The weighted mean of 26 $^{206}\text{Pb}/^{238}\text{U}$ ages is 124 ± 5 Ma (Fig. 2.9g, Table 2.4) suggesting an Early Cretaceous age for this granite. The La Puntilla body thus does not contribute any further to our understanding of the Triassic–Jurassic evolution, and its significance will be discussed elsewhere.

2.5 Discussion

2.5.1 Timing of magmatic pulses

The Early Mesozoic magmatism in the Cordillera de la Costa between 34°S and 37°S of the transition period from the Gondwana to the Andean orogeny is subdivided here into three magmatic pulses at 225 - 220 Ma, 210 – 197 Ma and 170 – 150 Ma (Table 2.4). The oldest rocks are from Hualpen and Constitución. The Rb-Sr ages from the Hualpen Stock cluster around 220 Ma, a K-Ar age of 215 ± 4 Ma is slightly younger and possibly related to cooling (Table 2.4). We accept an approximate age of 220 Ma as the most likely intrusion age. The zircon evaporation age of 224 ± 1 Ma (Willner et al. 2005) from the Constitución Granite indicates a contemporaneous magmatic pulse, and we interpret the younger K-Ar biotite ages of 208 ± 6 Ma and 202 ± 6 Ma (Gana and Hervé 1983) from this granite either as cooling-related or as being partially reset by supergene processes (cf. Jeong et al. 2006).

The second magmatic pulse is represented by the rocks from Cobquecura Pluton, La Estrella Granite and Pichilemu Granite. The amphibole K-Ar age (213 ± 5 Ma; 2σ) of the gabbroic rocks of the Cobquecura Pluton (Vásquez et al. 2005) is similar to the zircon U-Pb ages (209 ± 2 Ma; Fig. 2.9a and 203 ± 2 Ma, Fig. 2.9b) determined for the same rock. The fayalite-granodiorite sample of the Cobquecura Pluton displays scattered and discordant U-Pb zircon ages (Fig. 2.9c). These zircons show high U-contents (167 – 947 ppm) and Th/U ratios (0.6 - 1.4, appendix A). Discordance may thus be due to Pb loss, facilitated by radiation damage of the crystal structure (see Geisler et al. 2002). The amphibole K-Ar age of 212 ± 4 Ma (Vásquez et al. 2005) coincides with the highest $^{207}\text{Pb}/^{235}\text{U}$ ages determined for the fayalite-granodiorite (inset in Fig. 2.9c). Because the fayalite-granodiorites display mingling structures with the gabbroic rocks (Vásquez and Franz, 2008) and were therefore considered as comagmatic and contemporaneous with the gabbroic rocks, we adopt an age at around 210 Ma as the best estimate for the crystallization age of the entire upper crustal Cobquecura Pluton.

Age information for the La Estrella Granite is very limited. One of the two points of the U-Pb determination plots nearly concordant at 197 ± 5 Ma (Fig. 2.9d), the younger one at 177 ± 3 Ma. The older age is consistent with a published K-Ar biotite age of 218 ± 21 Ma (Dávila et al. 1979). Because also trace element characteristics (Fig. 2.7 a,c) and initial Sr-Nd isotope ratios (Fig. 2.6)

are similar to those from Cobquecura, we assume the La Estrella Granite to be formed during the 210 – 197 Ma pulse.

Also for the leucogranite from Pichilemu the age information is very limited. The best estimate for a crystallization age is the Rb-Sr whole rock model age of 205 ± 7 Ma (Table 2.4), given the observation that apparently no metamorphism or metasomatism has altered the sample. The new Rb-Sr whole rock age falls in the K-Ar crossite age range previously determined for the contact metamorphism (211 ± 32 Ma, Hervé et al. 1984; Table 2.4).

Rocks from Cerros del Hualve and Montecillos belong to the third magmatic pulse. The coincidence at Cerros del Hualve between the U-Pb age of 166 ± 2 Ma and K-Ar isotopic ages for hornblende (166 ± 5 Ma; 2σ) and biotite (165 ± 3 Ma; 2σ) (see appendix B) indicates intrusion and cooling below ≈ 300 °C in 4 Ma or less. For the Montecillos Monzonite, the slightly discordant zircon ages with a mean value of 154 ± 4 Ma (Fig. 2.9f) are younger than published K-Ar biotite and amphibole ages of 165 ± 5 and 175 ± 5 Ma, respectively (Gana and Hervé 1983). This discrepancy cannot be resolved with the current data and we use the zircon age of 154 ± 4 Ma as the best estimate for the crystallization age of the Montecillos Monzonite. Thus the youngest magmatic pulse is roughly constrained to 170 - 150 Ma (Middle Jurassic).

In summary, considering the zircons as comagmatic in all the lithologies in the segment between 34° and 37°S, three Mesozoic magmatic pulses have been identified. There are two Late Triassic pulses at the western flank of the Cordillera de la Costa. The Hualpen Stock and Constitución Granite represent the first pulse at 225 - 220 Ma. Next, the Cobquecura Pluton, Pichilemu Granite and possibly the La Estrella Granite represent a second Late Triassic pulse at 210 - 197 Ma. Younger plutonism at 170 – 150 Ma occurs at the eastern flank of the Cordillera de la Costa, represented by the Middle Jurassic Cerros del Hualve Pluton and Montecillos Intrusives. We will now refer to all this magmatism as ‘Early Mesozoic magmatism’, not considering the isolated Early Cretaceous mafic magmatism at Puntilla.

2.5.2 Changing contribution of the magmatic sources from ~225 to ~150 Ma

With the aim to evaluate the potential magmatic sources we compare the Sr-Nd-Pb isotopic data of the Early Mesozoic magmatism with the Sr-Nd-Pb isotopic data of regional possible crustal and mantle sources from the literature (Figs. 2.6, 2.8). The possible sources are an asthenospheric mantle, which might be represented by the isotope composition of Pacific MORB (calculated at 210 Ma), which is the existent and most probable approximation to the composition of the asthenosphere along the Chilean margin. The best estimate of the isotope composition for the subcontinental mantle source is that of the subarc-subcontinental mantle as characterized in northern Chile (Lucassen et al. 2006). The isotopic signatures of the Late Paleozoic metamorphic

and igneous basement at the outcrop level have been documented in detail (Lucassen et al. 2004) and are the best estimate for the isotopic composition of the regional crust.

The Nd-Sr isotope ratios of the gabbroic rocks cluster in a restricted field (Fig. 2.6). This field is near to the average composition of the young volcanic rocks from the Southern Volcanic Zone (SVZ) and also to the average value of the rocks from the Mesozoic arc in Northern Chile (at 18°S – 27°S). For the Mesozoic arc in Northern Chile, Lucassen et al. (2006) had outlined a field of Nd-Sr isotope ratios for the subarc mantle, and the isotope ratios of the two gabbro samples with the highest $\epsilon\text{Nd}_{\text{T}}$ plot into this field. Therefore we assume a similar mantle source for the Early Mesozoic magmatism in the transition period between the Gondwana and the Andean orogeny, as in the early stages of the magmatism in Northern Chile. The highest ϵNd -values of the Mesozoic-Cenozoic North Patagonian Batholith (a cordilleran batholith at 40° - 48°S; Pankhurst et al. 1999) also extend into field, indicating a similar ‘subarc mantle’ for the whole Chilean Andes.

The Early Mesozoic granitoids show Nd-Sr isotopic ratios between those of subarc mantle and the Late Paleozoic Basement ($\epsilon\text{Nd}_i = 2.8 - -2.6$; $^{87}\text{Sr}/^{86}\text{Sr}_i = 0.705 - 0.708$), suggesting that both are the more important sources for these magmas. However, it is remarkable that the Early Mesozoic granitoids display a more important contribution from mantle sources than the older Late Paleozoic granitoids (Fig. 2.6).

The Pb-isotopic ratios are generally considered as indicators for crustal contributions to magmas, because the radioactive parent isotopes are strongly concentrated in the crust compared to the mantle. Therefore, we compare the Pb isotopic ratios with other basement rocks from the region (Fig. 2.8) in order to evaluate the possible types of crustal contamination. Rocks considered similar to potential contaminants comprise late Paleozoic granitoids and metamorphic rocks south of 36°S (Cordillera de la Costa, Lucassen et al. 2004). These are the only available data from the area; unfortunately for the North Patagonian Batholith no Pb-isotope ratios are known. Other possible crustal contaminants hidden in the unexposed crust might be similar to Paleozoic granitoids of northern Chile (21-27°S, Lucassen et al. 2001), similar to basement gneisses of NW-Argentina, to the Middle Proterozoic Arequipa-Antofalla craton (21-27°S, N Chile-W Bolivia, Tosdal 1996), or to Precambrian xenoliths from the basement of the Precordillera terrane (31°S, Kay et al. 1996).

The Pb isotopic data from the Early Mesozoic intrusive rocks form a tight cluster (Fig. 2.8) indicating that more or less the same sources contributed to all this magmatism. There is no difference between the different magmatic pulses. Only one sample from Hualpén shows a slightly higher than average radiogenic $^{206}\text{Pb}/^{204}\text{Pb}$ ratio. The Pb isotopic data are less radiogenic in the $^{207}\text{Pb}/^{204}\text{Pb}$ ratios than the Andean Pb-Line (defined by Lucassen et al. 2002), but lie above the Northern Hemisphere Reference Line (NHRL; Hart 1984). The ‘Andean Pb-line’ fits the Pb isotopic composition of most pre-Carboniferous basement rocks in the Central Andes, including the Arequipa Massif (Tilton and Barreiro 1980; Damm et al. 1994; Wasteneys et al. 1995; Wörner et al. 2000, Lucassen et al. 2001), and various Paleozoic and older rocks from southern Bolivia,

northern Chile and NW-Argentina. Pre-Carboniferous rocks (i.e. Early Paleozoic and older) are not exposed in the area investigated here, and the only published isotopic data are from the Paleozoic Basement south of 36° (see Lucassen et al. 2004).

The different Pb isotopic ratios of the older Middle Proterozoic and Precambrian rocks from the northern Chilean margin (Arequipa-Antofalla craton and the xenoliths from the basement of the Precordillera terrane) rule out a contribution from such sources to the considerably more radiogenic Early Mesozoic magmatism (Fig. 2.8). The Late Paleozoic crust in the studied area is composed of granitoids and metamorphic rocks (Lucassen et al. 2004; Hervé 1977). This crust displays a $^{207}\text{Pb}/^{204}\text{Pb}$ and $^{206}\text{Pb}/^{204}\text{Pb}$ isotopic composition similar to, but more restricted than the Paleozoic crust at northern Chile (Lucassen et al. 2001). The Early Mesozoic intrusive rocks show a $^{207}\text{Pb}/^{204}\text{Pb}$ and $^{206}\text{Pb}/^{204}\text{Pb}$ isotopic trend from the field of the Paleozoic crust of northern Chile to the subarc subcontinental mantle.

The significance of the distinctive petrological and geochemical behavior (Figs. 2.3, 2.4, 2.5, 2.7; Table 2.1), the small differences in the Sr-Nd isotope ratios (Fig. 2.6) at the same Pb isotopic ratios (Fig. 2.8) for each magmatic pulse will be discussed in the next paragraph:

225-220 Ma magmatic pulse

The oldest group of intrusive rocks of this study, Hualpén Stock and Constitución Granite is very SiO₂-rich (< 68 wt.% SiO₂). The Fe-Mg phase is biotite; late magmatic white mica and tourmaline indicate crystallization in presence of water. These granites also display strong negative Eu- and Sr- anomalies, which together with a negative Ti-anomaly point to an important role of fractionation of low-pressure phases plagioclase and titanomagnetite. The relatively high peraluminosity (A/CKN = 1.1 - 1.3) and the strong enrichment in the incompatible elements K, Rb, U, Th, and Pb (Figs. 2.3, 2.4, 2.7 and Table 2.2) are characteristic either of important crustal contributions or of highly evolved granitic rocks as products of magmatic differentiation. The negative ϵNd_i (-1.8 to -2.6) confirms crustal contributions to the formation of these magmas, while the $^{87}\text{Sr}/^{86}\text{Sr}_i$ values (~ 0.705) are not distinctive. The Nd-Sr-Pb isotopic composition points to an important contribution of a crustal source for these granites, similar in composition to the known regional Paleozoic basement (Figs. 2.6, 2.7). In spite of the considerable crustal component in the highly differentiated granites, they are somewhat more influenced by mantle-derived components (Fig. 2.6) than the regional Late Paleozoic granitoids (Lucassen et al. 2004) (225 – 220 Ma granites with $\epsilon\text{Nd}_i = -1.8 - -2.6$; $^{87}\text{Sr}/^{86}\text{Sr}_i \sim 0.705$ vs. Late Paleozoic granitoids with $\epsilon\text{Nd}_i = -2.1 - -5.8$; $^{87}\text{Sr}/^{86}\text{Sr}_i = 0.71-0.72$)

210 - 197 Ma magmatic pulse

The second magmatic pulse at 210 – 197 Ma shows contemporaneous mafic and felsic magmas at the localities of Cobquecura, and felsic magmas at La Estrella and Pichilemu.

The felsic magmas are Fe-rich and contain anhydrous phases such as fayalite and hedenbergite or late arfvedsonite that suggest an H₂O-poor composition of the melt with low fO_2 crystallization conditions. The lower fO_2 in the granitoids at 210 – 197 Ma is also displayed by the not pronounced negative Eu-anomalies in comparison with the stronger negative Eu-anomalies in the first and third magmatic pulse (Fig. 2.5). Reducing conditions are a special feature for magmas from the second magmatic pulse in the area, documented here by the Cobquecura and La Estrella bodies, and previously reported for the Late Triassic (204 ± 11 - 197 ± 11 Ma) El León Unit at the Cordillera Frontal ($\sim 30^\circ S$) (Parada et al. 1991). The 210 - 197 Ma granitoids have considerably higher ϵNd_i values (2.8- -1.9) than the 225 - 220 Ma age group (-1.8 - -2.6; Constitución Granite and the Hualpén Stock) (Fig. 2.6). However, they plot to the right of the mantle array in Fig. 2.6, which may indicate interaction with crustal fluids. The $^{206}Pb/^{204}Pb_i$ isotope compositional range of the La Estrella Granite is wider than that displayed by the Cobquecura granitoids, while $^{207}Pb/^{204}Pb_i$ and $^{208}Pb/^{204}Pb_i$ isotopic ratios are similar with a narrow range (Fig. 2.8). The second magmatic pulse presents more reducing and water-poor crystallization conditions and more primitive, mantle-affine isotopic signatures than the first magmatic pulse.

The more primitive gabbros in the Cobquecura Pluton are similar to the subarc-subcontinental mantle from northern Chile (Fig. 2.6). The gabbros and intermediate rocks of Cobquecura Pluton display late amphibole, which indicates the presence of only small amounts of water in the crystallizing melts (Vásquez and Franz, 2008). In the Cobquecura gabbros, ilmenite and scarce Cu-Fe sulfides indicate a low fO_2 in the melt, as in the associated felsic magmas. This reveals a source of mantle magma similar to the subarc mantle in northern Chile, with low fO_2 and very low water content. The Cobquecura gabbroic rocks are characterized by slightly positive or absent Eu- and Sr-anomalies and by absence of a Ti-anomaly, indicating no major fractionation of plagioclase and Ti-rich phases during the crystallization (Fig. 2.4c). The array displayed for the mafic rocks in the Nd-Sr isotope diagram of the Cobquecura Pluton (Fig. 2.6) indicate that there were contamination or assimilation processes accompanying the fractional crystallization.

170 -150 Ma magmatic pulse

The similarities in the Nd-Sr and Pb isotopic compositions (Table 2.3 and Figs. 2.6, 2.8) of the Montecillos and Cerros del Hualve intrusives to the gabbroic rocks from Cobquecura Pluton suggest a similar melt source. Nevertheless, the gabbroic rocks of Cerros del Hualve have magnetite with exsolution of ilmenite lamellae, which indicate more oxidizing conditions than in the Cobquecura gabbroic rocks. The narrow distribution and primitive signature of the Nd-Sr isotopic ratios for the 170 - 150 Ma plutonic rocks suggests that the crustal contributions were not important (Fig. 2.6). The 170 - 150 Ma intrusive rocks have a trace element distribution similar to rocks from the Southern Volcanic Zone (SVZ, Andean Cordillera, 34-41°S, Fig. 2.4), where the magmas equally present unimportant crustal contributions (Hildreth and Moorbath 1988).

In summary, the three different magmatic pulses have distinctive geological, petrographical and geochemical characteristics. They evolved from dominantly SiO₂- rich felsic rocks at 225 - 220 Ma through bimodal magmatism at 210 - 197 Ma to predominantly mafic rocks in the 170 - 150 Ma intrusives, with characteristic trace element and isotopic compositions. The mantle source in our studied area is very similar in Sr, Nd and ²⁰⁶Pb/²⁰⁴Pb isotopic initial ratios to the Jurassic subarc mantle described for northern Chile (Lucassen et al. 2006). In the segment investigated here we find just slightly higher ²⁰⁷Pb/²⁰⁴Pb and ²⁰⁶Pb/²⁰⁴Pb ratios than those characteristic for subarc-subcontinental mantle from northern Chile, whereas signatures are different in all isotopic ratios from Pacific MORB (calculated to 210 Ma; Figs. 2.6, 2.8). In general, the Triassic granitoids display an important mantle contribution in comparison with the Late Paleozoic granitoids (Fig. 2.6). This mantle contribution increases in time from the 225 - 220 Ma magmatism to the 210 - 197 Ma magmatic pulse and is an even more important source of the 170 - 150 Ma plutonism, the trace element patterns of which are very similar to those in the SVZ subduction related magmas (Figs. 2.4 and 2.6). The compositional and isotopic magma evolution in this segment is in accordance with the magmatic source contributions proposed south of 37°S at the Cordillera de la Costa and the Main Cordillera (Lucassen et al. 2004). It also agrees with that proposed for the 31-34°S segment at the Cordillera de la Costa (Parada et al. 1999), where a decrease in the crustal component in the magmas from Late Paleozoic to the Cretaceous was observed. In comparison, the Sr-Nd signatures of the Mesozoic-Cenozoic North Patagonian Batholith (a cordilleran batholith at 40°-47°S, Pankhurst et al. 1999) are similar to those of the magmatic rocks at 225 - 220 Ma and 170 - 150 Ma. Nevertheless, the 210 - 197 Ma group displays notably higher radiogenic Sr for the same Nd isotopic composition (Fig. 2.6).

2.5.3 Possible tectonic setting

The geochemical and isotopic characteristics of the intrusive rocks allow us to evaluate a possible tectonic setting during the transition between the Gondwana and Andean orogenies. We first discuss the different geochemical features of these magmas that are characteristic for certain tectonomagmatic settings and then we evaluate these features considering the geological features and existent tectonic models for early Mesozoic times.

Anorogenic magma features

In general, the total REE content increases with time from values of 52 - 142 ppm in the older granites (Constitución and Hualpén) to values of 102 - 236 ppm for the younger (210 - 197 Ma) granitoids (Cobquecura and La Estrella; Fig. 2.5). High REE contents (except Eu) are considered to be typical for anorogenic magmas (e.g., Whalen et al. 1987). In addition, the Nb and Y contents of the Constitución granites are typical for arc-granites and in the Ce + Zr + Nb + Y vs.

$Ga \times 10,000/Al$ diagram (Fig. 2.10) they fall in the field of S + I-type granites, while the La Estrella Granite, Pichilemu Granite and the Cobquecura Granitoids (210 – 197 Ma) plot in the intraplate- and anorogenic granite fields of Whalen's and Pearce's discrimination diagrams (Fig. 2.10). Likewise, arfvedsonite and fayalite granitoids (like in the La Estrella and Cobquecura bodies) worldwide are commonly generated in an intraplate or postorogenic setting (Poitrasson et al. 1995; Mücke 2003). Therefore, there is a transition between granitic rocks with arc-affinities at 225 - 220 Ma to younger granitic rocks with anorogenic affinities with intraplate signatures at 210 - 197 Ma (Fig. 2.10). From these characteristics and from the establishment of contemporaneous extensional basins (Charrier 1979), it can be concluded that the Late Triassic-Early Jurassic rocks were generated in a continental extensional setting. However, the areal extent and nature of this extension is not yet clear. Further north between 30-33°S the Late Triassic - Early Jurassic (240 - 180 Ma) granitoids from the Cordillera de la Costa and the Cordillera Frontal show the same transitional chemistry between magmatic arc and intraplate affinities (e.g., Mpodozis and Kay 1990; Parada et al. 1991).

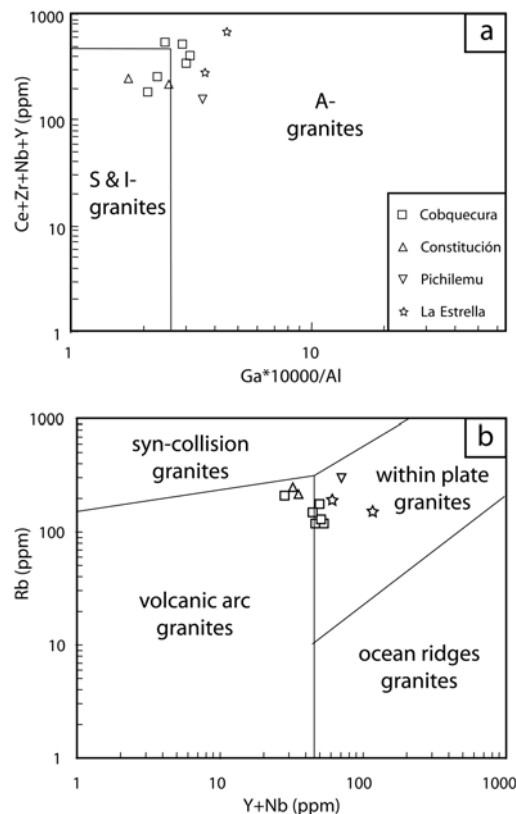


Figure 2.10 a) $Ce + Zr + Nb + Y$ vs. $Ga \times 10,000/Al$ discrimination diagrams of Whalen et al. (1987). The analyses are transitional between the S- and I- type granite and A-type granite. b) Rb vs. $Y+Nb$ diagrams of Pearce et al. (1984). The analyses also plot transitional between the volcanic arc granites and the within-plate granites.

Extension in a suprasubduction setting

The positive Pb-anomaly (normalized to primitive mantle) combined with negative Nb-Ta anomalies displayed by most of the magmatic rocks of our segment (Fig. 2.4) is characteristic of

arc magmas. These characteristics are more pronounced in the youngest magmatic pulse. The metamorphic ages of the accretionary prism south of our study area vary between 305 and 197 Ma (south of 38°S; Willner et al. 2004; Glodny et al. 2005, 2006) constraining a minimum duration of the Gondwana subduction. This fact, together with the trace element signatures of the contemporaneous Triassic-Jurassic magmatic rocks, shows that, most likely, the here studied magmatism is in some way subduction-related. This means that there is only a very narrow time window between the end of Gondwana and the onset of Andean subduction, if such a time window exists at all. There are various explanations in the literature for the development of this extensional setting along the Triassic-Jurassic Chilean margin:

1) Charrier (1979) and Uliana et al. (1989) proposed the beginning of rifting directly related to the first stages of the Gondwana break-up.

2) For Central Chile Parada et al. (1999) proposed rollback of the subducting slab resulting in detachment of the slab, based on geochemical and isotopic evidence.

3) Franzese and Spalletti (2001) proposed an extensional setting in a regime of slow or absent subduction. Dextral strike-slip movements parallel to the continental margin induced a break off of the slab and the generation of an asthenospheric window. Highly oblique plate configuration in the Jurassic has also been proposed for northern (e.g., Scheuber et al. 1994; Grocott and Taylor 2002) and southern Chile (Martin et al. 1999).

Given the fact that the Mesozoic magmatism in the Cordillera de la Costa of Central Chile occurred in the context of an overall active margin setting with only a short-term potential halt of subduction between the Gondwana and Andean stages, we consider that the properties of the local active margin system are much more important for the local magmatism than the possible far-field effects of the incipient Gondwana breakup. A link of the different magmatic pulses in the Cordillera de la Costa (Central Chile) to the Gondwana breakup appears unlikely, even more so in the absence of an obvious eastward-increasing intensity of extension-related phenomena.

The isotopic characteristics that the mafic magmatism in our segment shares with the recently described Jurassic subarc mantle of Chile (Lucassen et al. 2006), which differs compositionally from the Pacific mantle at 210 Ma, makes a slab detachment and a contribution of Pacific-MORB source type unlikely.

An extensional setting in a suprasubduction zone is possible under a strong slab-steepening regime, which can generate a strong thinning close to the trench with the consequent generation of subcontinental mantle-derived magmas by decompression. Oblique subduction has been documented for the Late Triassic-Early Jurassic in northern Chile (22-27°S, Scheuber and González 1999; Grocott and Taylor 2002) and for the Carboniferous-Jurassic in south Chile (38° - 41°S, Martin et al. 1999). This oblique subduction has generated a strike slip tectonic regime with NW and NE striking structures (Grocott and Taylor, 2002, Martin et al., 1999). The sporadic nature

of this Triassic-Jurassic magmatism and its occurrence linked to NW-SE structures suggests that the Early Mesozoic mantle magmas used these weak zones in the crust to rise.

2.6. Summary and conclusions

Geochronological data allow grouping the Triassic-Jurassic magmatism of the Chilean Coastal Cordillera (34°-37°S) into three magmatic pulses. The field, petrographical, geochemical and isotopic characteristics demonstrate that these three magmatic episodes had a separate evolution and are distinguished by differences in fO_2 , a_{H_2O} and composition. They show a transition from granitic magmatism with comparatively dominant crustal contributions at 225-220 Ma, through a bimodal magmatism at 210 – 197 Ma to dominantly mafic, mantle-derived melts at 170 – 150 Ma.

The sources of the magmas at 225 - 220 Ma and at 170 – 150 Ma are similar to those of the North Patagonian Batholith, an example of a subduction-related cordilleran batholith in southern Chile. The magmatic rocks also display many geochemical characteristics for subduction-related magmas, like the Nb-Ta trough and the positive Pb anomaly. Particularly, geochemical signatures of the magmatism at 210 - 197 Ma, represented by the La Estrella Granite, Pichilemu Granite and Cobquecura Pluton, are indicative of an overall extensional setting. However, the small exposed volume of this magmatic pulse suggests that extensional deformation occurred at a small scale rather than as a massive regional event. A possible scenario for this sporadic magmatism is an oblique subduction setting with a steepening slab, that would generate extension linked to NW-SE structures in a suprasubduction setting.

Our data are consistent with a continuous subduction since the Carboniferous, or with only a very narrow time window between the end of Gondwana and the onset of Andean subduction. The special Triassic-Jurassic subduction geometry allowed the emplacement of magmas with extensional signature and enhanced contribution of mantle sources. The onset of the Andean orogeny is thus interpreted as a further reconfiguration of the geometrically variable plate convergence conditions, in an overall setting of a continuous active margin evolution.

3. The Triassic Cobquecura Pluton (Central Chile): an example of a fayalite granite bearing A-Type intrusive massif at a continental margin

Abstract

The Late Triassic Cobquecura Pluton is a small epizonal intrusive body that was emplaced into the Paleozoic Basement at the western side of the Cordillera de la Costa, near to the town of Cobquecura (35°57'-36°12'S, central Chile). The pluton displays a wide spectrum of compositions that include gabbro and fayalite-granite, and less abundant hybrid rocks. SiO₂-content ranges from 48 to 76 wt.% with a compositional gap between 57 and 63 wt.% SiO₂. SiO₂-poor rocks have Mg-Fe minerals olivine (Fa₃₃₋₃₄), diopside-augite (Mg# = 56-91; Mg# = (Mg/(Mg+Fe²⁺)×100) and pargasite (Mg# = 4-8), which with progressive differentiation become Fe-rich olivine (Fa₈₉₋₉₈), hedenbergite-ferroaugite (Mg# = 10-43) and ferroedenite (Mg# = 8-29). Similar K/Ar isotopic ages, mingling structures, and coherent arrays in Harker diagrams, as well as mineral compositions show that the SiO₂-poor and SiO₂-rich rocks are comagmatic.

The Fe-rich mineralogy and Ga-content of the Cobquecura Pluton point to an anorogenic A-Type magmatism. The compositional similarities, as well as the bimodal character of the magmatism of Cobquecura and other Upper Triassic granitoids and lavas north of 30°S at the Chilean continental margin indicate a common origin of the magmatism, and coeval anorogenic processes along the southwestern margin of Gondwana in the Triassic.

Key Words: Fayalite, granite, A-Type, Triassic, magmatism, Chile

3.1 Introduction

Fayalite-bearing granites are relatively uncommon granitoids, which have been related mainly to alkaline and evolved magmatism (e.g., Njonfang and Moreau 2000; Frost et al. 2002). They are characterized by high FeO/(FeO+MgO) ratios, the occurrence of other Fe-rich mafic minerals such as hedenbergite, and the late crystallization of hydrous mafic minerals annite or Fe-rich amphibole (Turner et al. 1992; Mücke 2003). The Fe-rich mafic mineralogy indicates special crystallization conditions from an H₂O-poor magma at low *f*O₂ (Stephenson and Hensel 1978; Frost et al. 1988).

Fayalite-bearing granites and their Fe-rich mafic mineralogy are closely associated to so-called A-type granites and rapakivi granites, and they are often found in Precambrian terrains (e.g.,

Loiselle and Wones 1979; Eby 1990; Frost et al. 1999; Sakoma et al. 2000). A-type granites may be formed at the end of an orogeny or in continental rift zones (e.g., Eby 1992; Pitcher 1997; Wu et al. 2002). At the southwestern margin of Triassic Gondwana, along the Chilean coast and High Andes, A-type granitoids have been identified as an important constituent of the Triassic magmatism (Parada 1988; Gana 1991; Parada et al. 1991).

In this work, we report Triassic fayalite-bearing granitoids around Cobquecura (Fig. 3.1), in the Cordillera de la Costa of Central Chile, where they occur closely related to gabbros and gabbro-norites. This occurrence is of particular interest, because there are no previous records of fayalite-granitoids in the Cordillera de la Costa, and it can provide insights to the tectonic evolution of the southwestern margin of Gondwana during the Late Triassic. The aim of this study is to interpret this occurrence and its crystallization conditions on the basis of petrography, whole rock and mineral chemistry.

3.2 Geological setting and petrography

The southwestern margin of South-America has been a continental margin of Gondwana and pre-Gondwana at least since the Late Proterozoic-Early Cambrian (e.g., Coira et al. 1982). Between the Late Paleozoic and Andean (Late Jurassic to Present) cycle significant geodynamic changes occurred along the margin. In the southern part of Central Chile, the subduction regime between Carboniferous and Early Triassic was constituted by a magmatic arc and an accretionary prism (Hervé et al. 1981; Parada 1990; Martin et al. 1999) and characterized the Pre-Andean or Gondwana-Orogeny (e.g., Hervé et al. 1981; Ramos et al. 1986; Mpodozis and Ramos 1989). The Andean Cycle (Late Jurassic-Recent) between 33° and 41°S is defined by a non-accretionary margin with a magmatic arc that stayed nearly stationary in the present axis of the Cordillera Principal (Mpodozis and Ramos 1989). It was active since the Pennsylvanian and its geological evolution in the segment between 36° and 42°S are summarized in Glodny et al. (2006), the Recent picture of the geophysical signatures and the active tectonics is given in Krawczyk et al. (2006). The Late Paleozoic accretionary prism is exposed in discontinuous outcrops along the Chilean coast, with younger ages towards the south (Duhart et al. 2001; Hervé and Fanning 2001). At the latitude of Chañaral, (~26°S), the accretionary prism is represented by the late Carboniferous “Chañaral-Melange” (Bahlburg and Hervé 1997). Between 39°30' and 42°00'S, the prism documents a continuous subduction from Late Carboniferous to Late Triassic (Carnian) (Duhart et al. 2001; Willner et al. 2004, Glodny et al. 2005). More to the south, rocks of the Chonos Metamorphic Complex (between 44° and 47°S) have Late Triassic protolith ages (Late Norian) (Fang et al. 1998; Hervé and Fanning 2001), showing early Jurassic metamorphism (Thomson et al. 2000). On the other hand, several authors have associated the magmatic activity during the Triassic

with enhanced crustal melting (e.g., Choiyoi Group; Kay et al. 1989) in an extensional geotectonic setting (Parada 1990; Mpodozis and Kay 1992; Morata et al. 2000).

The time between Triassic and Early Jurassic was marked by the activity of large extensional basins with fast subsidence (Charrier 1979; Franzese and Spalletti 2001). These basins are oriented NW-SE to NNW-SSE, inherited from the main structures of the Late Paleozoic (Franzese and Spalletti 2001). The extension has been related to the first stage of break-up of Gondwana (Charrier 1979; Uliana et al. 1989), associated with hypothetical dextral strike-slip movements (Rapela and Pankhurst 1992), or as a consequence of a combined action of the cessation of the subduction from the Late Permian to the Early Jurassic with dextral strike-slip tectonics parallel to the continental margin (Franzese and Spalletti 2001). Studies north of 33°S have related this dextral tectonics with the slab break-off generating an asthenospheric window. The consequences of these changes were bimodal magmatism, uplift, thermal weakness and gravitational collapse of the upper crust (Gana 1991; Parada et al. 1999; Morata et al. 2000; Franzese and Spalletti 2001) generated in an intracontinental extensional tectonic setting (Parada et al. 1991; Morata et al. 2000). These studies exposed an ambiguity about the areal extension and the duration of the Gondwana Orogeny and the tectonic interpretation of the Triassic evolution in this part of Gondwana.

Late Triassic magmatic rocks south of 33°S, in the western flank of the Cordillera de la Costa, are exposed in small and discontinuous outcrops around Pichilemu, Constitución, and Hualpén (Fig. 3.1a; Hervé et al. 1988). The magmatic bodies intruded the metamorphic basement and are predominantly of monzogranitic composition with associated mafic dikes. The Cobquecura Pluton is located between the Constitución Granite and Hualpén Stock (Fig. 3.1b) and was not studied in detail up to now. It is exposed over approximately 75 km² and displays a wide lithologic and textural variety compared to the Constitución Granite and Hualpén Stock, which are relatively homogeneous. A K-Ar age of 211.6 ± 4.5 Ma was obtained for a fayalite-granodiorite from La Iglesia de la Piedra and 212.6 ± 4.9 Ma for a gabbro from Buchupureo (Fig. 3.1a), using amphiboles (ferroedenite and Mg-hornblende, respectively; Vásquez et al. 2005). Ongoing U/Pb isotopic work on zircon shows identical ages (Frei et al. 2006). The similar ages for granodiorite and gabbro of the Cobquecura Pluton and the close spatial occurrence confirm a comagmatic evolution.

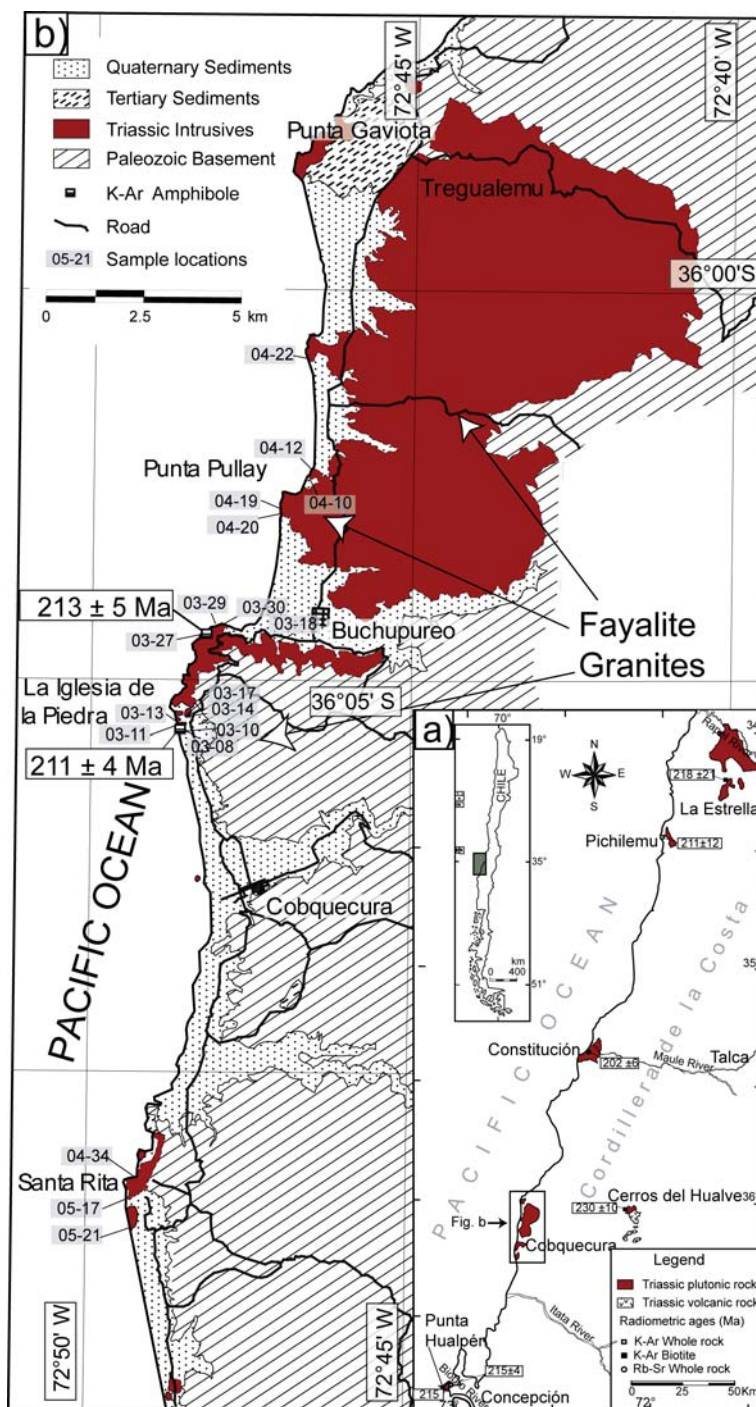


Figure 3.1 a) Distribution of late Triassic early Jurassic magmatism in the Cordillera de la Costa between 34° and 37°S; after Godoy (1970), Hervé and Munizaga (1978), Dávila et al. (1979), Gajardo (1981), and Gana and Hervé (1983). Additional radiometric ages were taken from Hervé et al. (1988) and Lucassen et al. (2004). b) Geological sketch map of the Cobquecura Pluton (see inset in a) and sample location; isotopic ages are taken from Vásquez et al. (2005). The arrows show the localities with fayalite-granite.

3.2.1 The Cobquecura Pluton

The different lithologies and their petrographic characteristics are summarized in Table 3.1. A more detailed description of the petrographical features is given in the Appendix, Table 3.1 and

shown in Figure 3.2. The Cobquecura Pluton crops out discontinuously along the coast between Tregualemu and Santa Rita (35°57' to 36°12'S; Fig. 3.1b). It intruded into low-grade regional metamorphic metapelites and metapsammities with coarsening of quartz, growth of chlorite and white mica. The intrusions generated an aureole, tens of meters wide, in the metapelites with neoblasts of cordierite, biotite, corundum and hercynite. Partially, Paleogene-Neogene and Quaternary sediments cover the Cobquecura Pluton.

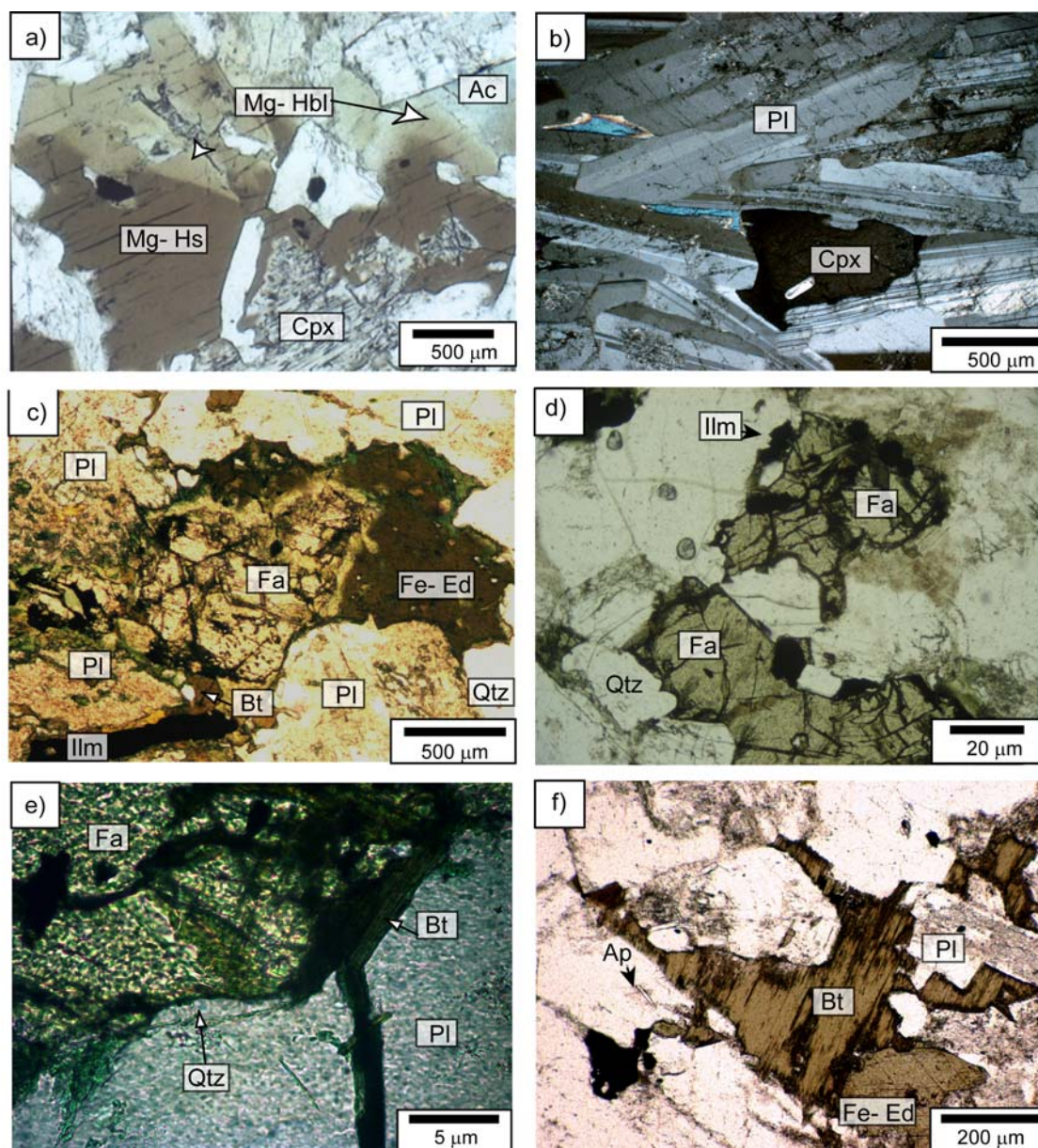


Figure 3.2 Microphotographs of textures and minerals from the Cobquecura Pluton. a) Replacement of clinopyroxene (Cpx) by magnesio-hastingsite (Mg-Hs), magnesio-hornblende (Mg-Hbl) and actinolite (Ac) in gabbro (sample 03-27), plane-polarized light. b) Trachytoidal texture in gabbro (sample 05-17; crossed polars) c) Replacement of fayalite by ferroedenite, in granodiorite (sample 04-08), plane-polarized light. d) Fayalite (Fa) in contact with quartz (Qtz), and ilmenite (Ilm) associated in fayalite granodiorite (sample 03-08), plane-polarized light. e) Rim of quartz and biotite between fayalite and plagioclase, in granite (sample 04-20), crossed polars. f) Interstitial biotite (Bt) between plagioclase (Pl) and ferroedenite (Fe-Ed) in fayalite granite, long-prismatic to needle shaped apatite (Ap) (sample 04-20), plain polarized light.

Most granitoid outcrops are limited to the coastal area, but further north, the outcrops continue inland into the Cordillera de la Costa (Fig. 3.1b). The major rock types are gabbro and granite, and less frequently granodiorite, tonalite and hybrid rocks. The hybrid rocks often contain mafic and metamorphic enclaves and are cross-cut by both synplutonic and postplutonic dikes (Fig. 3.3a) with acidic, granophyric and basic composition. Similar post-plutonic dikes intruded into the Paleozoic Basement, north of the area.

In the outcrops between Punta Gaviota and Buchupureo (Fig. 3.1b), only gabbros and granites were found. The gabbros vary in their composition between quartz-hornblende-bearing gabbro and pyroxene- and hornblende-bearing gabbro characterized by a trachytoidal texture. Gabbros are cross-cut by decimetric tonalitic dikes. Granites correspond to syenogranite and monzogranite; some of them contain olivine, biotite, amphibole and pyroxene as mafic minerals. They are relatively dark rocks and have a color index (CI) between 5 (olivine-absent varieties) and 28 (with olivine). They contain small microdioritic enclaves with a typical pink K-feldspar-rich halo. Towards the east, all rocks are strongly weathered and could not be used for geochemical and petrological work. The contacts between the olivine-bearing granites and the gabbros are not exposed here.

Between Buchupureo and La Iglesia de la Piedra, the intrusive contact of granitoids and gabbros with the metamorphic basement is exposed. South of Buchupureo the gabbros are coarse to very coarse-grained and associated gabbroic pegmatites contain large crystals of amphibole, pyroxene, plagioclase and quartz, intergrown in a graphic texture. Near La Iglesia de la Piedra, quartz-gabbro, monzogabbro, monzonite and granodiorite are exposed. In this area, diverse structures such as synplutonic composite dikes (Fig. 3.3a), net-vein complexes (Fig. 3.3b), mafic pillow-shaped enclaves (Fig. 3.3a), magmatic breccias, mafic and leucocratic synplutonic dikes with diffuse borders (Fig. 3.3c) and postplutonic diabase dikes (Fig. 3.3a) were found. The magmatic breccia is composed of metamorphic xenoliths and ellipsoidal mafic enclaves of decimeter to meter size. Here, a quartz-monzogabbro crops out, which has amphibole-coronas around quartz-feldspar cores (Fig. 3.3d). The composite synplutonic dikes are composed of oriented ellipsoidal enclaves in a leucocratic matrix with a thickness near 1 m (Fig. 3.3a). The leucocratic synplutonic dikes have a thickness between approximately 1 m and a few millimeters with irregular borders. They intruded approximately parallel to the main foliation of the metamorphic basement. The contact of the gabbroic rocks to the olivine-bearing granitoids, where they both intruded the metamorphic basement, is not exposed. There is a magmatic breccia in-between, which crops out over a distance of 50 to 100 m. Xenoliths of the basement were found in the breccia as well as in the granite.

In the south, near Santa Rita (Fig. 3.1b), gabbro and minor granophyre and granodiorite, the latter with microtonalitic enclaves, crop out. The gabbro contains miaroles

with diameters of about 2 cm composed of quartz, feldspar and biotite. The magmatic rocks are covered by sedimentary rocks, which show similarities to the continental Paleogene-Neogene sedimentary rocks of Arauco (Alfaro 1962), and are cross-cut by tonalitic dikes. They contain dark mafic globules also with gabbro-noritic composition.

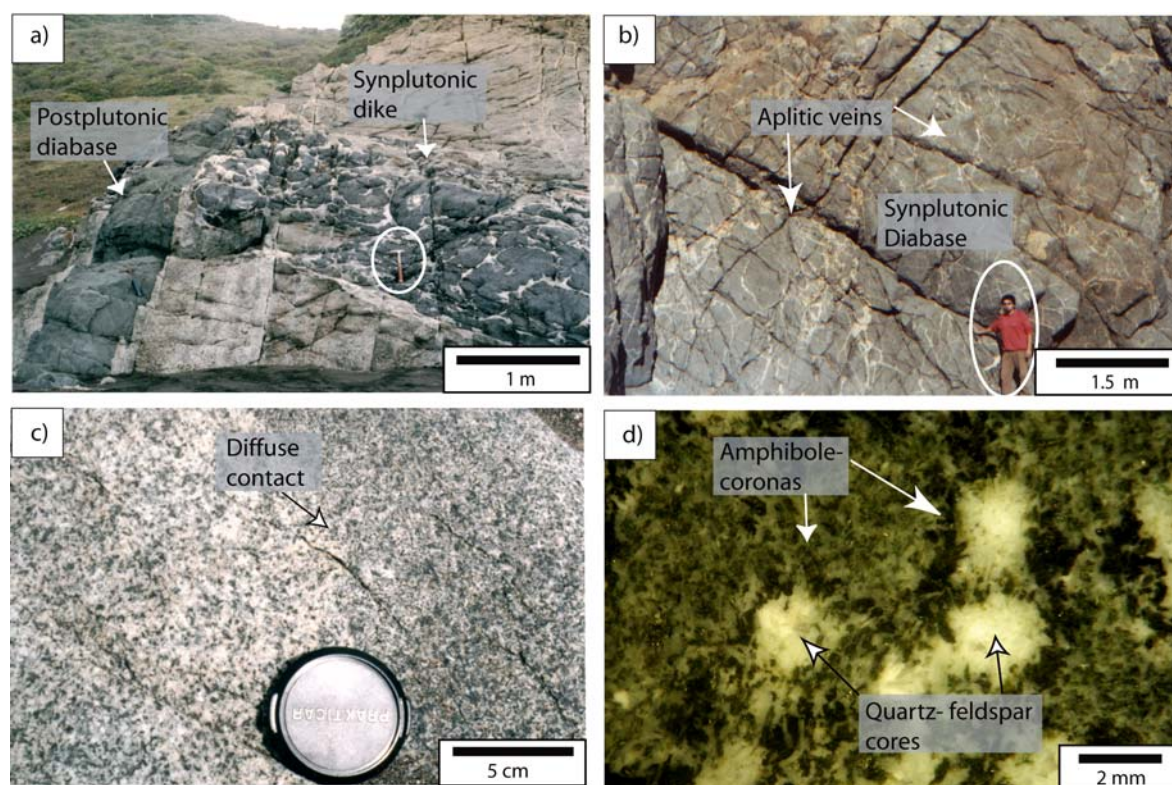


Figure 3.3 Petrographic structures in the Cobquecura Pluton (La Iglesia de la Piedra area). a) Synplutonic composite and postplutonic diabase dikes with sharp contact to the country rocks. The composite dike consists of mafic pillows with aplitic matrix; note hammer for scale. b) Net vein complexes formed by diabase with millimeter to centimeter wide aplitic veins; note person for scale. c) Synplutonic leucocratic granite dike with similar composition as the country rock, characterized by a diffuse contact. d) Quartz-feldspar intergrowth with a corona of amphibole crystals in quartz monzogabbro.

Table 3.1: Petrographic characteristics of the plutonic rocks and dikes of the Cobquecura Pluton.

	Plutonic rocks			Dikes		
	Gabbro-gabbronorite	Hybrids rocks	Granite-granodiorite	Composite dikes		Postplutonic Dikes
				Enclaves	Leucocratic Dikes	
Sample N°	03-11, 03-27, 03-29, 03-30, 04-22, 04-34, 04-35, 05-17, 05-21	03-18, 03-13	03-08, 04-10, 04-12, 04-19, 04-20	03-17, 04-15, 04-05	03-10, 03-14	03-15, 03-16, 04-16, 04-21, 04-23, 04-24, 04-27
SiO₂	48-57 wt. %	55 and 67 wt. %	63-76wt. %	49-53 wt. %	68 and 76 wt. %	51-57wt. %
A/CNK	0.87-1.00	0.99 and 1.24	0.99-1.01	0.87-0.91	1.01-1.05	0.84-1.02
Lithology	Gabbronorite, olivine-gabbronorite, pyroxene-hornblende-gabbro. Granitic and gabbroic pegmatite (in miaroles or veins). Mafic globules.	Biotite-tonalite, amphibole-tonalite, quartz- monzogabbro	Granite, olivine-granite, olivine-granodiorite	Diabase (pyroxene-hornblende-gabbro, hornblende-gabbro), minor granodiorite	Granite and tonalite. Diffuse borders to the country rock	Diabase, minor grano-phyes, and micrograno-diorite. Sharp borders to the country rock
Texture and fabric	Phaneritic medium- to coarse-grained (rare). Hypidiomorphic granular to heterogranular. Locally layering and poikilitic, ophitic to subophitic, trachytoidal textures (olivine-gabbronorites). Plagioclase with rounded calcic cores, and rare patchy and oscillatory zoning	Phaneritic medium-grained. Hypidiomorphic heterogranular. Oscillatory zonation in plagioclase. Coarse-grained varieties sometimes in veins or miaroles.	Phaneritic medium-grained. Hypidiomorphic granular to allotromorphic heterogranular. Minor poikilitic, myrmekitic, locally graphic. Rim of quartz and/or biotite around olivine	Phaneritic fine-grained. Hypidiomorphic heterogranular, intergranular. Minor ophitic, subophitic poikilitic.	Saccharoidal concertal. Local oscillatory zoning in plagioclase	Phaneritic fine- to medium-grained, porphyritic in fine-grained groundmass. Glomeroporphyritic. Minor intersertal and intergranular, graphic, myrmekites. Plagioclase with local oscillatory zoning
Color index	33-66	22-28	5-30	35-40	8-27	13-35
Felsic Minerals	Plagioclase	Plagioclase, quartz, alkali-feldspar	Plagioclase, quartz, alkali-feldspar	Plagioclase	Plagioclase, quartz, alkali-feldspar	Plagioclase, rare quartz and alkali-feldspar
Mafic Minerals	Olivine, diopside, augite, locally enstatite, amphibole, biotite	Biotite, amphibole, pyroxene relicts (rare)	Fayalite, ferroedenite, biotite, local hedenbergite, ferroaugite (local)	Amphibole, biotite, pyroxene	Biotite, amphibole	Clinopyroxene, olivine, orthopyroxene, amphibole, biotite

	Plutonic rocks			Dikes		
	Gabbro-gabbronorite	Hybrids rocks	Granite-granodiorite	Composite dikes		Postplutonic Dikes
				Enclaves	Leucocratic Dikes	
Sample N°	03-11, 03-27, 03-29, 03-30, 04-22, 04-34, 04-35, 05-17, 05-21	03-18, 03-13	03-08, 04-10, 04-12, 04-19, 04-20	03-17, 04-15, 04-05	03-10, 03-14	03-15, 03-16, 04-16, 04-21, 04-23, 04-24, 04-27
Accessory Minerals	Zircon, apatite, pyrite and tourmaline (in olivine-gabbronorite).	Zircon, apatite, sphene, allanite.	Allanite, zircon, apatite, sphene (local)	Zircon, apatite, sphene	Tourmaline, zircon, sphene.	Apatite, zircon
Opaque Minerals	Ilmenite, pyrite, Cu-Ni-Fe-sulphides (in mafic globules)	Ilmenite	Pyrite, ilmenite, rare titanomagnetite	-----	-----	Pyrite
Alteration	Sericite in plagioclase (moderate). Biotite in amphibole (weak). Uralitization of pyroxene (rare). Chlorite-sphene in biotite. Talc, chlorite/smectite and Fe-oxide in olivine.	Sericite-chlorite-zoisite-epidote in the core of plagioclase. Chlorite-epidote in biotite. Clay minerals in orthoclase (weak).	Sericite-clay minerals in plagioclase (moderate to strong). Chlorite/smectite-iddingsite in olivine (moderate) and pyrite (associated).	Sericite-clay minerals in plagioclase (weak to strong).	Clay minerals-sericite-zoisite in orthoclase (moderate). Sericite in the cores of plagioclase. Chlorite-epidote-prehnite-actinolite in biotite. Biotite-actinolite in amphibole (weak).	Clay minerals (moderate to strong), epidote, zoisite, pumpellyite and calcite (weak) in plagioclase. Serpentine in olivine (strong). Uralitization of pyroxene (moderate)

3.3 Analytical techniques

Major element whole rock composition including the minor and trace elements Cr, Cu, Ga, Ni, V, Zn and Zr were analyzed by XRF- techniques in 35 selected samples on fused disks at TU-Berlin using the software Oxiquant and X-40 Philips. The $\text{FeO}^*/(\text{FeO}^*+\text{MgO})$ ratios considered FeO as total iron (Table 3.2).

Mineral analyses were carried out at ZELMI (TU-Berlin) with a CAMEBAX Microbeam electron microprobe at operating conditions of 15 kV acceleration voltage, 17 nA sample current, 10 s measuring time on peak, 5 s on background twice, using minerals and synthetic materials as standards. Accuracy is estimated as approximately 1 % relative for major and 10 % relative for minor elements. Structural formulae were calculated on the basis of 4 oxygens for olivine, 6 oxygens for pyroxene, 22 oxygens for biotite and 8 oxygens for feldspar. Fe^{3+} for amphibole was calculated using the methods of Schumacher (1997), and the nomenclature proposed by Leake et al. (1997) was applied. X_{Mg} was calculated as molar ratio $\text{Mg}/(\text{Mg}+\text{Fe}^{2+})$. Fe^{3+} for pyroxene was estimated based on the method proposed by Droop (1987). Representative compositions of olivine, pyroxene, amphibole and biotite are shown in Tables 3.4 to 3.7.

3.4 Whole-rock geochemistry

The rocks of the Cobquecura Pluton have a wide spectrum of compositions ranging from 48 wt.% to 76 wt.% SiO_2 with a small compositional gap between 57 and 63 wt.% (Fig. 3.4, Table 3.2). This gap separates “mafic rocks” (gabbros, gabbronorites, synplutonic enclaves, and diabases = postplutonic dikes) from “granitic rocks” (granitic and granodioritic intrusives and granitic dikes). They have A/CNK ratios ($\text{Al}_2\text{O}_3/(\text{CaO}+\text{Na}_2\text{O}+\text{K}_2\text{O})$ molar) between 0.84 and 1.24 that increase with higher SiO_2 -content (Fig. 3.4a). Most analyses, including those of the fayalite granites fall in the subalkaline-series field (Fig. 3.4b); only the diabase dikes are more alkaline than the rest of the rocks.

Some major elements show a well defined trend for the whole suite in the Harker variation diagrams (Fig. 3.5). MgO , Al_2O_3 and CaO decrease, Na_2O increases with increasing SiO_2 in the gabbroic rocks, K_2O increases with increasing SiO_2 over the whole suite.

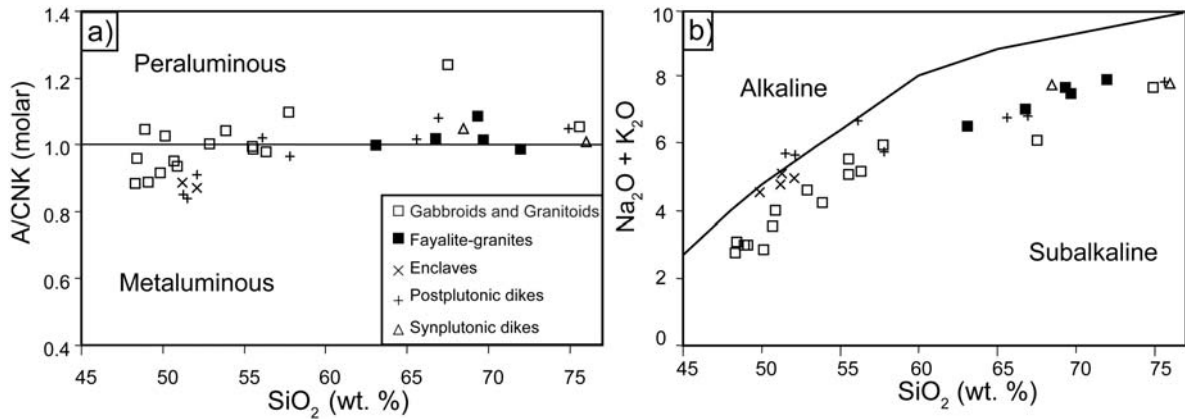


Figure 3.4 a) Variation of the A/CNK-index ($\text{Al}_2\text{O}_3/\text{CaO}+\text{Na}_2\text{O}+\text{K}_2\text{O}$ molar) with SiO_2 -content for the intrusive rocks of the Cobquecura Pluton. b) Variation of the alkali-content with SiO_2 -content; (symbols as in Fig. a); postplutonic dikes are slightly more alkaline than the plutonic rocks. Alkaline and subalkaline fields after Irvine and Baragar (1971).

The mafic rocks (48-57 wt.% SiO_2) show an increasing ratio of $\text{FeO}^*/(\text{FeO}^*+\text{MgO})$ from 0.41 to 0.85 with increasing SiO_2 (Fig. 3.5). Gabbro and gabbro fall mainly in the medium-K field (after Irvine and Baragar, 1971); they have a MgO-content between 2.26 and 9.92 wt.%, corresponding to an $\text{FeO}^*/(\text{FeO}^*+\text{MgO})$ ratio of 0.67 to 0.41 (Table 3.2), an A/CNK of 0.87-1.00 and TiO_2 -content of 0.54-3 wt.%. They have high contents of Co (39-87 ppm), Ni (up to 160 ppm) and Cr (up to 460 ppm, but is <100 ppm above 55 wt.% SiO_2), which is characteristic for relatively primitive rocks (Fig. 3.6; Table 3.2). TiO_2 , Al_2O_3 , CaO, MnO, FeO^* and V show variable scatter within the group of the mafic rocks with SiO_2 contents below 53% wt. In the mafic rocks with SiO_2 contents above 53% wt. the mafic rocks display a coherent trend for TiO_2 , Al_2O_3 , CaO, MnO, FeO^* and V. Gabbro and gabbro intrusives have scattered P_2O_5 -contents, but they also increase with increasing SiO_2 wt.%.

The mafic postplutonic dikes (51.2-57.8 wt.% SiO_2) have lower contents of MgO (3-4.5 wt.%) and Al_2O_3 (14.0-15.4 wt.%), higher contents of TiO_2 (1.8-2.5 wt.%) and FeO^* (8.4-12.2 wt.%), similar A/CNK ratios (0.84-1.02) than the mafic rocks, and fall in both the high and medium-K fields (after Irvine and Baragar, 1971; Figs. 3.4, 3.5). In general terms, the mafic postplutonic dikes behave similarly as the other mafic rocks.

The felsic rocks (63-76 wt.% SiO_2) show a coherent trend, are slightly more peraluminous (A/CNK = 0.99-1.24) than the mafic rocks and fall within the high-K field (Figs. 3.4, 3.5). The fayalite-bearing granites have $\text{FeO}^*/(\text{FeO}^*+\text{MgO})$ ratios significantly higher than those of the mafic rocks (0.8-0.94; Fig. 3.5). The olivine-granite and -granodiorite display high contents of Zn (88-119 ppm) and Ga (20-26 ppm). Zr-contents (226-406 ppm) increase with increasing SiO_2 up to 70 wt.% SiO_2 , where Zr reaches a maximum value of 406 ppm. At SiO_2 -contents above 70 wt.% Zr decreases with increasing SiO_2 (Fig. 3.6, Table 3.2).

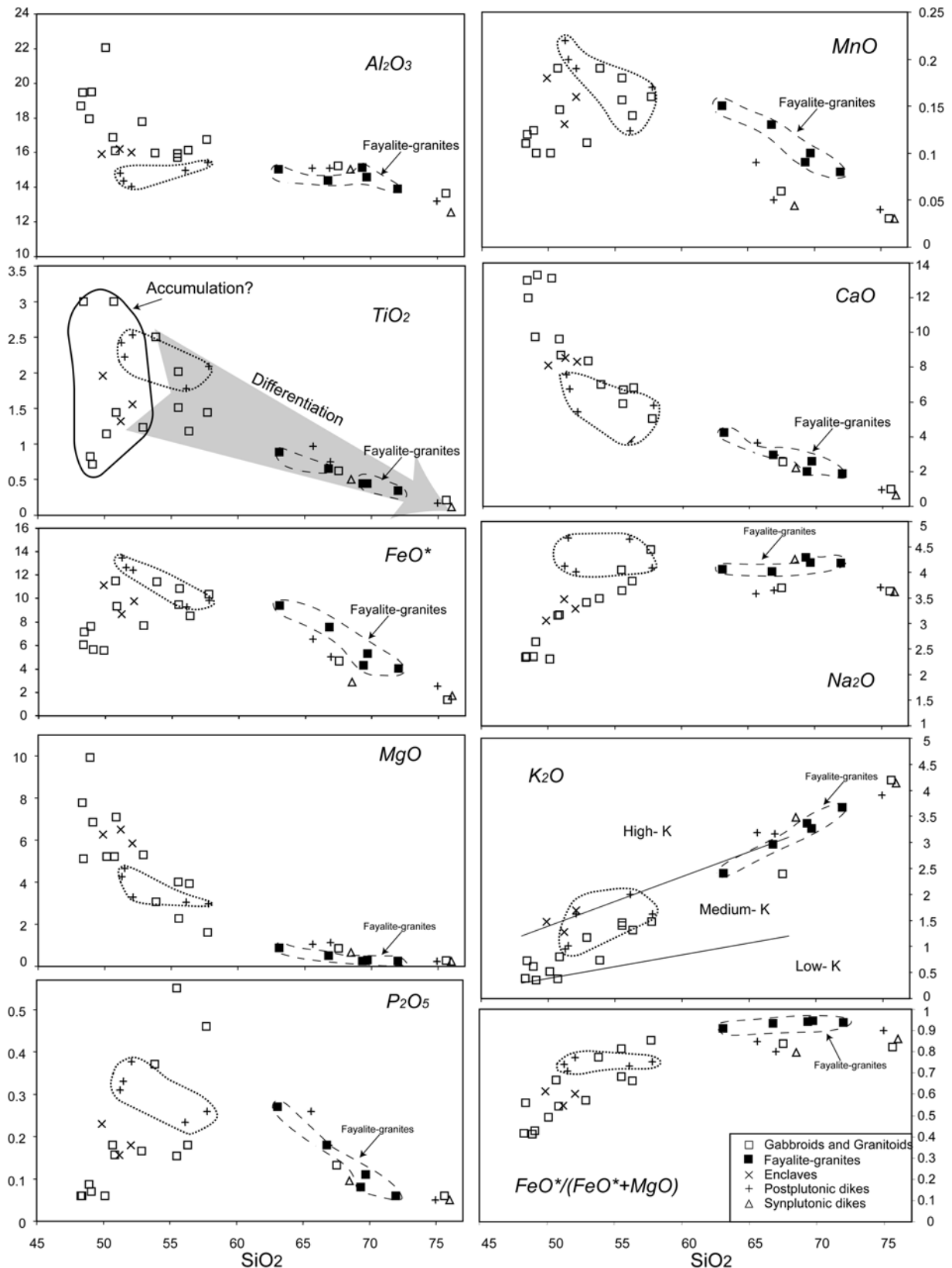


Figure 3.5 Variation diagrams of major elements content vs. SiO₂ wt.% (Harker diagrams). High-, medium- and low-K fields after Irvine and Baragar (1971). Data fields for fayalite-granitoids (dashed line) and postplutonic basic dikes (dotted line), are outlined. In the TiO₂ vs. SiO₂ diagram the field for mafic rocks with SiO₂ < 56 wt. % with a large scatter of the analyses that could indicate accumulation processes, a similar scatter is seen of the Al₂O₃, MnO and V correlations (see Fig. 3.6). The probable common differentiation trend for the mafic and the felsic suites is shown by the arrow.

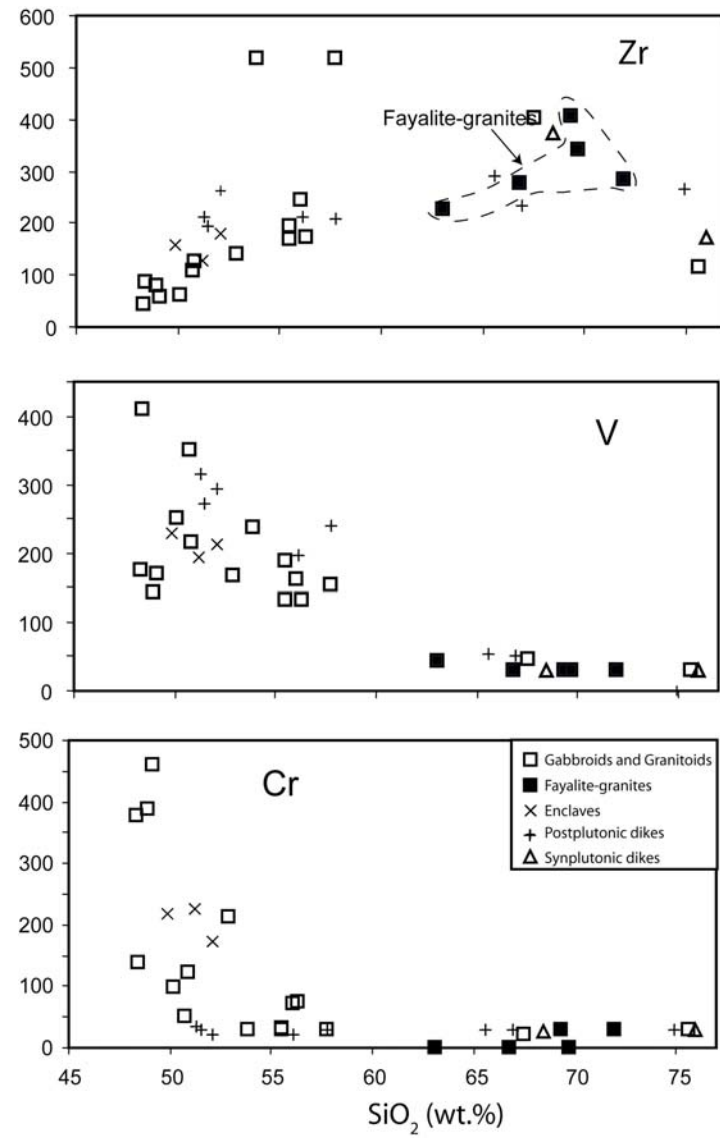


Figure 3.6 Variation diagrams of trace element content Zr, V and Cr (ppm) vs. SiO_2 (wt.%). The local high Zr- content could be due local accumulation of zircon.

Table 3.2: Whole-rock geochemical analyses of the Cobquecura Pluton

Sample	04-22	03-30	05-17	05-19	03-11	03-27	03-17	03-13	03-18	04-10	04-19	04-20	03-10	03-14	03-15	03-16
Lithology	Gabbronorite				Gabbro		Enclaves	Hybrid rocks	Fayalite-Granites				leucocratic synplutonic dikes	diabase postplutonic		
wt. %																
SiO ₂	50.7	48.9	49.1	48.3	52.9	50.1	51.2	55.5	67.5	63.1	66.8	72.0	76.0	68.5	52.1	56.1
Al ₂ O ₃	16.9	18.0	19.5	18.7	17.8	16.1	16.2	15.7	15.2	15.1	14.4	13.9	12.5	15.0	14.0	15.0
FeO*	10.46	6.86	5.06	5.45	6.96	8.43	7.78	8.55	4.20	8.46	6.79	3.68	1.57	2.63	11.19	8.39
MnO	0.19	0.12	0.1	0.11	0.11	0.15	0.13	0.16	0.06	0.15	0.13	0.08	0.03	0.04	0.19	0.12
MgO	5.22	9.92	6.83	7.76	5.28	7.09	6.50	4.01	0.83	0.87	0.50	0.25	0.25	0.67	3.30	3.06
CaO	9.61	9.72	13.28	12.99	8.35	8.70	8.54	5.91	2.56	4.24	2.94	1.87	0.64	2.20	5.44	3.75
Na ₂ O	3.15	2.34	2.63	2.33	3.41	3.16	3.47	4.05	3.69	4.06	4.02	4.18	3.62	4.26	4.01	4.66
K ₂ O	0.37	0.61	0.35	0.38	1.17	0.80	1.28	1.45	2.39	2.40	2.96	3.67	4.14	3.48	1.63	2.00
TiO ₂	3.00	0.82	0.71	0.54	1.23	1.44	1.32	1.51	0.62	0.88	0.65	0.34	0.12	0.50	2.53	1.78
P ₂ O ₅	0.18	0.09	0.07	0.06	0.16	0.16	0.16	0.15	0.13	0.27	0.18	0.06	0.05	0.10	0.38	0.23
L.O.I	0.06	1.47	1.38	2.30	1.33	1.35	1.65	1.05	1.05	0.41	0.61	0.39	0.33	0.82	2.51	2.01
SUM	101.3	99.8	99.7	99.7	99.4	99.7	99.1	99.2	99.0	100.9	100.9	100.9	100.2	98.7	98.7	98.2
FeO*/(FeO*+MgO)	0.67	0.41	0.43	0.41	0.57	0.54	0.54	0.68	0.84	0.91	0.93	0.93	0.86	0.80	0.77	0.73
ppm																
V	351	144	169	175	168	216	195	189	45	42	30	30	30	30	295	196
Cr	50	387	460	378	214	123	225	32	21	b.d.	b.d.	30	30	26	20	20
Co	58	73	47	39	64	72	66	87	106	46	49	59	140	151	43	55
Ni	19	160	63	51	39	45	45	b.d.	20	5	5	5	11	20	b.d.	20
Cu	30	40	63	38	20	33	20	20	20	30	30	30	30	b.d.	20	20
Zn	90	43	42	40	56	44	62	73	47	119	98	88	50	20	114	90
Ga	21	9	20	15	19	18	17	21	20	24	24	23	22	23	21	23
Sc	30	15	28	30	20	23	24	23	15	21	24	10	8	15	25	25
Zr	109	80	57	44	139	125	130	168	401	226	278	283	173	376	263	213

b.d. = Below detection limit

3.5 Mineral Chemistry

The principal features of the mineral chemistry of the different rocks are summarized in Table 3.8.

3.5.1 Olivine

Olivine with high fayalite contents of ≈ 33 and >90 mol% occurs in gabbro and granite respectively (Fig. 3.7b, Table 3.3). In gabbro, olivine is homogeneous with Fa₃₃ (Fig. 3.7). Olivine in mafic globules has a similar composition, but shows a slightly higher Ca-content (Table 3.3).

In the granite, olivine has slightly higher fayalite content than in the gabbro; it also displays slight zoning with the rim richer in MnO than the core (Table 3.3, 3.8). The MnO-contents in olivine are higher than in other mafic minerals (Fig. 3.9a), but similarly the MnO content increases with differentiation, i.e., from gabbro to granite (Figs. 3.8a, 3.9a).

Table 3.3: Representative olivine analyses from intrusive rocks of the Cobquecura Pluton.

Sample	03-08	03-08	04-10	04-19	04-19	04-20	05-21	05-21	05-17	05-17
Lithology	Granodiorite		Granite				Gabbro			
SiO ₂	30.10	30.30	30.96	30.62	30.31	31.22	37.20	37.33	38.09	38.10
TiO ₂	0.05	0.04	0.03	0.09	0.04	0.02	b.d.	0.05	b.d.	0.03
Al ₂ O ₃	b.d.	0.02	0.03	b.d.	0.02	0.01	b.d.	0.01	b.d.	0.00
FeO	66.48	66.43	64.00	64.24	64.70	65.29	29.24	29.73	28.72	28.87
MnO	1.58	1.59	1.51	1.47	1.51	2.02	0.47	0.48	0.51	0.49
MgO	1.29	1.22	3.31	3.45	2.60	1.49	32.35	32.28	32.97	32.59
CaO	0.15	0.15	0.07	0.11	0.11	0.08	0.19	0.09	0.06	0.06
Na ₂ O	0.06	0.03	b.d.	b.d.	b.d.	b.d.	b.d.	0.05	b.d.	0.03
K ₂ O	0.03	0.01	b.d.	b.d.	b.d.	b.d.	b.d.	b.d.	b.d.	b.d.
Total	99.74	99.79	99.90	99.97	99.32	100.12	99.45	100.05	100.35	100.18
Formula per 4 oxygens										
Si	1.01	1.01	1.02	1.01	1.01	1.03	1.01	1.01	1.02	1.02
Ti	0.00	0.00	0.00	0.00	0.00	---	---	0.00	---	0.00
Fe ²⁺	1.86	1.86	1.76	1.77	1.80	1.80	0.66	0.67	0.64	0.65
Mg	0.06	0.06	0.16	0.17	0.13	0.07	1.37	1.30	1.31	1.30
Mn	0.04	0.04	0.04	0.04	0.04	0.06	0.01	0.01	0.01	0.01
Ca	0.00	0.00	0.00	0.00	0.00	0.00	0.00	0.00	0.00	0.00
Total	2.99	2.99	2.98	2.99	2.99	2.97	2.99	2.99	2.98	2.98
mol %										
Fo	3	3	8	8	6	4	66	66	67	66
Tp	2	2	2	2	2	3	---	---	---	---
Fa	94	95	90	89	91	93	34	34	33	33

b.d. = below detection limit

3.5.2 Pyroxene

Clinopyroxene in gabbro and gabbro-norite is transitional between diopside and augite (Fig. 3.7a). Non-quadrilateral components are generally low, and there is almost no calculated Fe^{3+} . The Al_2O_3 - and TiO_2 -content of pyroxene is very low compared to amphibole (Table 3.4, Figs. 3.9b, c). However, in both minerals there is a similar trend, with two clusters of mineral analyses and decreasing contents in the more evolved rocks (Figs. 3.9b, c).

In gabbro-norite, clinopyroxene has a composition of $\text{Wo}_{42-46}\text{Fs}_{7-15}\text{En}_{42-50}$; the content of Cr_2O_3 is higher in the core than in the rim, and displays high X_{Mg} values (= $\text{Mg}/(\text{Mg}+\text{Fe})$ in atoms per formula unit) with notably high Al_2O_3 -contents in mafic globules. In gabbros, clinopyroxene composition is $\text{Wo}_{38-48}\text{Fs}_{10-17}\text{En}_{30-44}$ (Fig. 3.7) with lower X_{Mg} than in the gabbro-norites. Clinopyroxene is zoned with the core richer in TiO_2 , poorer in Al_2O_3 and Na_2O than the margin (Table 3.4, 3.8). An exception is clinopyroxene in gabbro-norites that displays a higher Al_2O_3 -content in the core than in the rim. Pyroxene from quartz-gabbro is occasionally Ca-poor due to the presence of microscopic exsolution of orthopyroxene (Fig. 3.7). $\text{Al}^{\text{VI}}/\text{Al}^{\text{IV}}$ ratios in clinopyroxene from the mafic rocks vary between 0.05 and 2.49, with a tendency to concentrate the highest values at the more mafic rocks and in the core.

In olivine-granodiorite and -granite the clinopyroxene is hedenbergite or Fe-rich augite (Fig. 3.7). In olivine-granodiorite, it is Fe-rich, with a lower X_{Mg} and low TiO_2 -content (Table 3.4, 3.8). In olivine-granite it is slightly richer in the enstatite component, with higher X_{Mg} and TiO_2 -content than in the granodiorites (Table 3.4). In granites the clinopyroxene displays a weak zoning with higher X_{Mg} in the cores than in the rims. Al^{VI} is mostly very low.

Orthopyroxene occurs as isolated grains in gabbro-norite and as exsolution lamellae in clinopyroxene in gabbros (Table 3.4). Crystals from gabbro-norite have a composition of $\text{Wo}_{2-3}\text{Fs}_{22-25}\text{En}_{53-74}$ and high X_{Mg} (0.69-0.75). Orthopyroxene presents a weak core-rim zoning in Al_2O_3 (0.5-0.86 wt.%), Cr_2O_3 (up to 0.05 wt.% in the rim) and TiO_2 (0.65-0.37 wt.%).

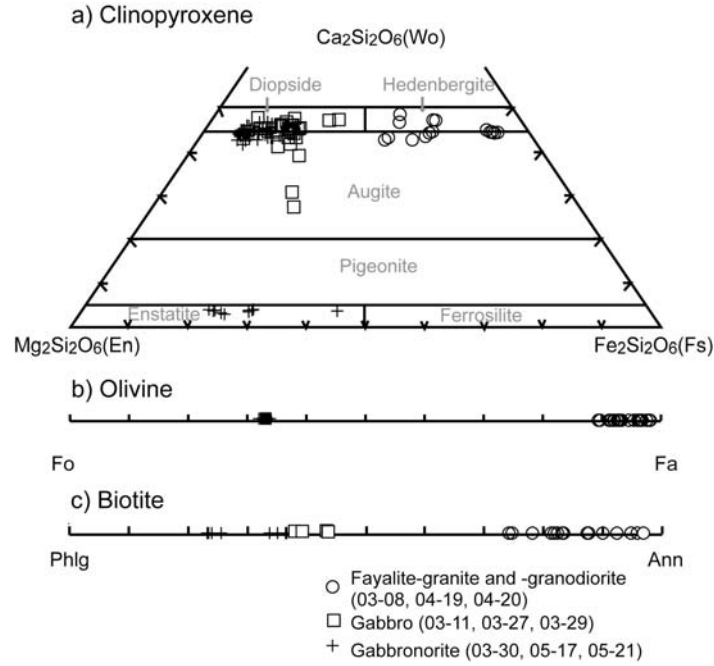


Figure 3.7 Quadrilateral components of (a) pyroxene; number of analyses $n = 141$, (b) olivine ($n = 38$) and (c) biotite ($n = 26$) from gabbros and fayalite-granodiorite of the Cobquecura Pluton. Classification of pyroxenes according to Morimoto (1989).

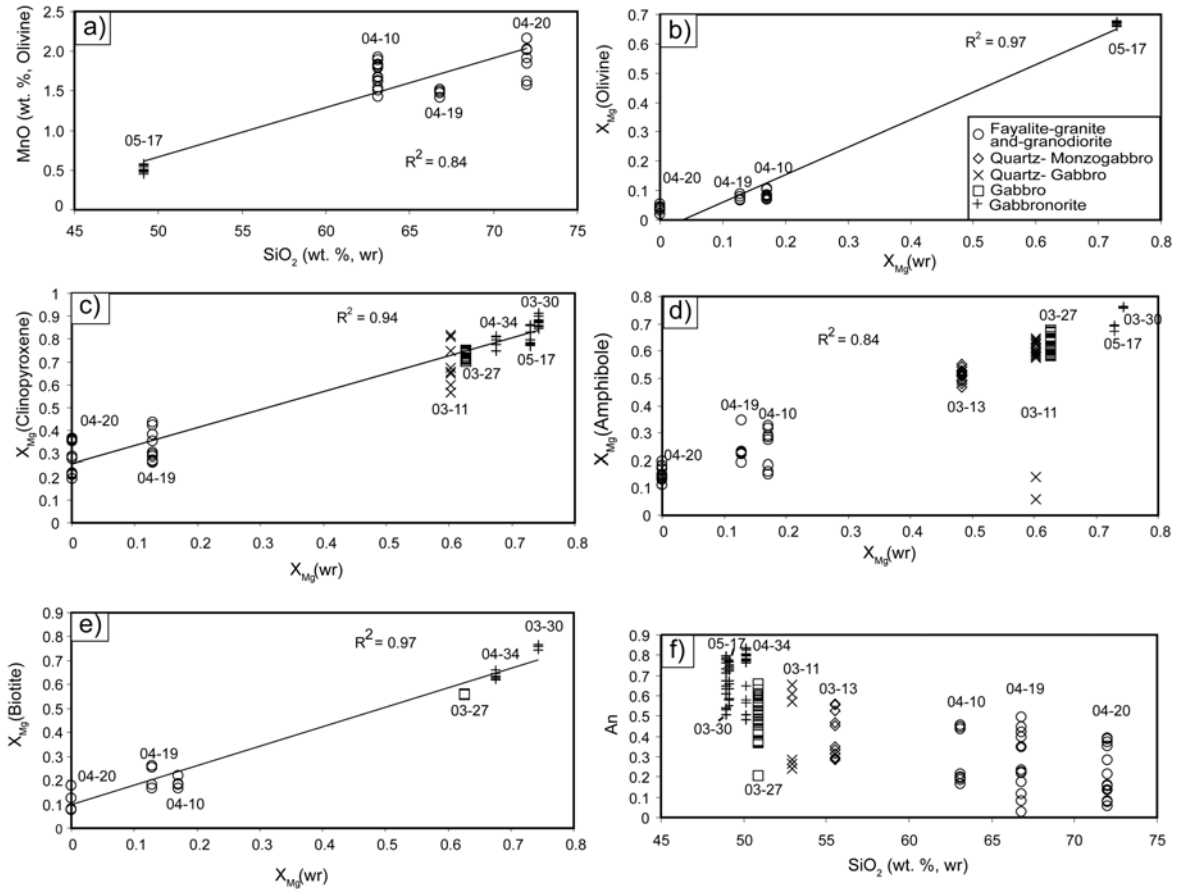


Figure 3.8 Diagrams of element content in mineral vs. element content in the whole rock (wr). a) MnO (in olivine) vs. SiO_2 (wr). b) X_{Mg} (in olivine) vs. X_{Mg} (wr). c) X_{Mg} (in pyroxene) vs. X_{Mg} (wr). d) X_{Mg} (in amphibole) vs. X_{Mg} (wr). e) X_{Mg} (in biotite) vs. X_{Mg} (wr). f) An-content (in plagioclase) vs. SiO_2 (wr). The numbers are sample numbers, for localities see Table 3.1. Lines are regression lines with correlation coefficient R^2 .

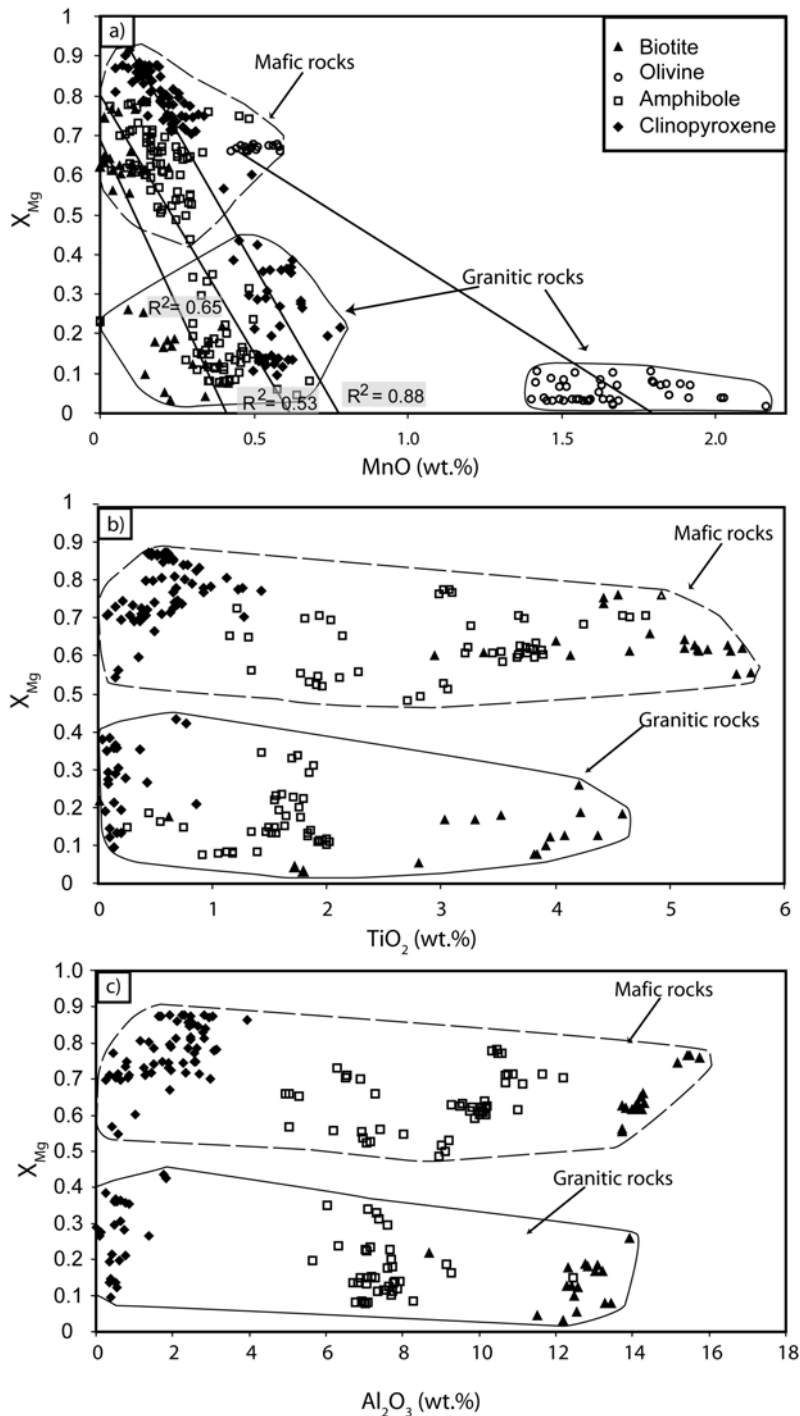


Figure 3.9 MnO (a), TiO_2 (b) and Al_2O_3 (c) vs. X_{Mg} in olivine, clinopyroxene, amphibole and biotite. Note the two clusters of mineral analyses with high and low X_{Mg} that occur in each mineral species and each cluster. There is a group of high Ti-Al-, low Mn and low Ti-Al-, high Mn analyses. Lines in (a) connect analyses points of the same minerals (biotite-biotite in mafic and granitic rocks etc.) with the correlation coefficient). Olivine is enriched in MnO, followed by clinopyroxene, amphibole and biotite (a), biotite is enriched in TiO_2 - Al_2O_3 , followed by amphibole and clinopyroxene (b,c).

Table 3.4: Representative pyroxene analyses from granites, granodiorites, gabbros and gabbro-norites of the Cobquecura Pluton.

Sample	03-08	03-08	04-19	04-19	03-27	03-29	03-11	03-30	05-17	05-21
Lithology	Granodiorite		Granite		Gabbro		Quartz-gabbro	Gabbro-norite		
SiO ₂	49.29	49.18	51.45	51.21	52.56	52.28	54.10	54.43	51.66	53.47
TiO ₂	0.20	0.14	0.09	0.15	0.67	0.30	0.49	0.58	1.43	0.55
Al ₂ O ₃	0.53	0.37	0.10	b.d.	2.59	1.50	1.92	0.86	3.08	2.81
Cr ₂ O ₃	n.a.	n.a.	n.a.	n.a.	n.a.	n.a.	n.a.	0.04	0.05	0.49
FeO	26.33	27.65	22.48	22.66	8.21	9.41	11.87	14.98	7.78	4.24
MnO	0.62	0.57	0.66	0.54	0.23	0.23	0.29	0.31	0.21	0.07
MgO	2.31	1.63	4.58	5.23	13.68	14.12	13.74	27.25	15.29	16.77
CaO	20.00	19.96	21.12	19.80	21.38	21.43	17.28	1.57	20.13	21.30
Na ₂ O	0.23	0.24	0.25	0.26	0.48	0.35	0.44	0.02	0.44	0.29
K ₂ O	0.02	b.d.	b.d.	b.d.	0.03	b.d.	0.12	b.d.	b.d.	b.d.
Total	99.52	99.75	100.74	99.86	99.85	99.60	100.25	100.07	100.06	100.01
Formula per 6 oxygens										
Si	2.01	2.01	2.03	2.03	1.95	1.96	2.00	1.96	1.99	1.94
Al	---	---	---	---	0.05	0.04	---	0.04	0.09	0.06
Al	0.02	0.02	0.01	---	0.06	0.03	0.08	---	0.04	0.06
Fe ³⁺	---	---	---	---	---	0.034	---	0.013	---	---
Cr	n.a.	n.a.	n.a.	n.a.	n.a.	n.a.	n.a.	0.001	0.002	0.014
Ti	0.01	0.00	0.00	0.00	0.02	0.01	0.01	0.02	0.04	0.02
Fe ²⁺	0.90	0.95	0.75	0.76	0.26	0.26	0.37	0.439	0.24	0.13
Mn	0.02	0.02	0.02	0.02	0.01	0.01	0.01	0.01	0.01	0.00
Mg	0.14	0.10	0.27	0.31	0.76	0.79	0.76	1.46	0.84	0.91
Ca	0.87	0.87	0.89	0.84	0.85	0.86	0.69	0.06	0.80	0.83
Na	0.02	0.02	0.02	0.02	0.04	0.02	0.03	0.00	0.03	0.02
K	0.00	---	---	---	0.00	---	0.01	0.00	---	---
Total	3.98	3.99	3.98	3.98	3.99	4.01	3.96	4.00	4.00	3.98
Wo	45	45	46	44	45	44	38	3	42	44
En	7	5	14	16	40	40	42	74	45	49
Fs	48	50	40	40	15	15	20	23	13	7
Mg/(Mg+Fe ²⁺) x100	14	10	27	29	75	75	67	77	78	88

b.d. = Below detection limit; n.a. = Not analysed

3.5.3 Amphibole

Amphibole is present in most rocks except in the postplutonic diabase dikes, the granophyres and the leucocratic dikes. The majority of the rocks have amphibole contents near 15 vol.%, in some enclaves up to 40 vol.%. They are calcic amphiboles with low Na-content and present a wide spectrum of compositions, but are predominantly magnesium-hornblende (Fig. 3.10, Table 3.5).

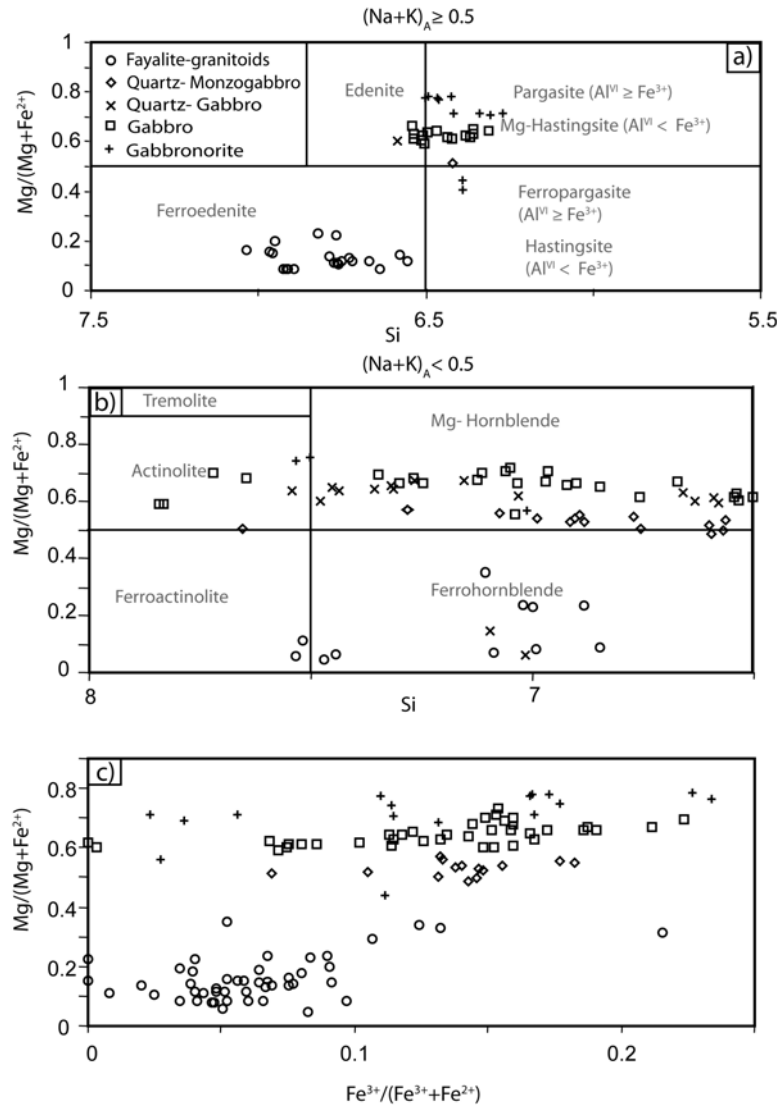


Figure 3.10 Composition of calcic amphiboles from the Cobquecura Pluton; a) and b) Fe-rich amphiboles develop from Fe-edenite to Fe-hornblende – Fe-actinolite; Mg-rich amphiboles from pargasite, Mg-hastingsite to Mg-hornblende – actinolite; compositional gap between Fe-rich and Mg-rich amphiboles corresponds to compositional gap in whole rock SiO_2 -content between 57 and 63 wt.%. Classification after Leake et al. (1997) $n = 116$. c) $Mg/(Mg+Fe^{2+})$ vs. $Fe^{3+}/(Fe^{3+}+Fe^{2+})$ diagram, ferric amphibole displays lower $Fe^{3+}/(Fe^{3+}+Fe^{2+})$ ratios (calculated from electron microprobe analyses) than the magnesian amphibole.

The scarce amphibole in gabbro-norite is mainly pargasite (Table 3.3). Kaersutite occurs only in mafic globules with low calculated $Fe^{3+}/(Fe^{3+}+Fe^{2+})$ ratios, moderate Ti-content, and a pargasitic rim (Table 3.5, 3.9).

Amphibole in gabbro and monzogabbro has concentric zoning (Fig. 3.2c). In the quartz-gabbro and -monzogabbro, the amphibole is magnesiohornblende. The darker zones in thin section are Si-poor than the lighter zones (Fig. 3.10). In amphiboles of the pyroxene- and hornblende-gabbros, the dark zones are mainly magnesiohastingsite with low Si-content, $(Na+K)_A$ near 0.5, and the lighter zones are magnesiohornblende with lower Ti-content.

Amphibole in the olivine-granite and -granodiorite is rich in Fe^{2+} compared to gabbro and gabbro-norite, mainly ferroedenite with minor ferrohornblende and ferroactinolite (Fig. 3.10). It has low $\text{Fe}^{3+}/(\text{Fe}^{3+}+\text{Fe}^{2+})_{\text{calc.}}$ ratios up to 0.22 (Fig. 3.10c). Ti content is variable, but this variation is not related to the zoning.

Table 3.5: Representative amphibole analyses from granites, monzogabbros, gabbros and gabbro-norites of the Cobquecura Pluton.

Sample	03-08	04-10	04-19	04-20	03-13	03-13	03-29	03-30	05-17	05-21
Lithology	Granodiorite	Granite				Quartz-monzogabbro	Gabbro	Gabbro-norite		
SiO_2	42.02	43.91	42.07	42.39	44.01	45.09	43.16	44.03	43.40	43.49
TiO_2	1.88	1.85	1.54	1.49	2.70	2.26	3.75	3.02	3.73	4.78
Al_2O_3	7.54	7.60	7.06	7.29	8.94	8.13	10.06	10.45	12.21	10.87
FeO	31.07	26.51	26.45	30.18	20.27	19.59	14.43	9.74	11.15	10.50
MnO	0.38	0.33	0.41	0.50	0.25	0.20	0.03	0.15	0.17	0.17
MgO	2.12	5.56	4.33	2.68	9.21	9.73	11.79	15.28	13.23	13.80
CaO	10.31	9.91	12.79	9.57	10.53	10.68	11.01	11.20	10.97	11.03
Na_2O	1.79	2.16	1.70	1.92	1.88	1.63	2.11	2.28	2.40	2.65
K_2O	1.09	0.76	0.72	0.96	0.65	0.71	0.90	0.68	0.75	0.54
Total	98.20	98.60	97.07	96.98	98.44	98.02	97.25	96.83	98.01	97.84
Formula per 23 oxygens										
Si	6.72	6.77	6.77	6.80	6.59	6.75	6.43	6.42	6.31	6.34
Al^{IV}	1.28	1.23	1.23	1.20	1.41	1.25	1.57	1.58	1.69	1.66
Al^{VI}	0.14	0.15	0.19	0.18	0.17	0.20	0.22	0.40	0.20	0.20
Ti	0.22	0.21	0.25	0.18	0.30	0.42	0.33	0.41	0.52	0.52
Fe^{3+}	0.25	0.36	---	0.37	0.36	0.32	0.14	0.27	0.16	0.07
Fe^{2+}	3.91	3.06	3.62	3.68	2.18	2.13	1.66	0.92	1.20	1.21
Mg	0.51	1.23	1.04	0.64	2.06	2.17	2.62	3.32	2.87	3.00
Mn	0.05	0.04	0.06	0.07	0.03	0.02	0.00	0.02	0.02	0.02
Ca	1.77	1.64	2.20	1.64	1.69	1.71	1.76	1.75	1.71	1.72
Na	0.94	0.65	0.53	0.60	0.54	0.47	0.61	0.64	0.68	0.75
K	0.22	0.15	0.15	0.20	0.12	0.14	0.17	0.13	0.14	0.10
Total	14.15	15.15	15.15	15.20	15.13	15.14	15.17	15.13	15.14	15.10
$\text{Mg}/(\text{Mg}+\text{Fe}^{2+}) \times 100$	12	30	22	15	49	50	61	78	70	71

3.5.4 Biotite

In gabbro and gabbro-norite, biotite has an X_{Mg} between 0.55 and 0.77 (Fig. 3.7), TiO_2 -contents between 4.42 and 5.71 wt.%, Al_2O_3 -content between 13.72 and 15.74, and low MnO-content (<0.10 wt.%), with higher X_{Mg} and Al_2O_3 values in gabbro-norite (Table 3.6). In olivine-granodiorite and -granite it has lower X_{Mg} , TiO_2 -contents, and Al_2O_3 -contents than in gabbros, but with higher values in the olivine granite than in the olivine-granodiorite (Fig. 3.7). The MnO-content is higher in biotite from the fayalite-granite than in biotite from the gabbros, resembling the behavior of the MnO-content in olivine (Fig. 3.9a). Biotite from the rim to olivine has a low content of TiO_2 (Table 3.6), which confirms the textural indication for a subsolidus origin.

Table 3.6: Representative biotite analyses from granites, granodiorites, gabbros and gabbroonorites of the Cobquecura Pluton. (*) Rim of biotite in olivine.

Sample	03-08	03-08	04-10	04-19	04-20	04-20 (*)	03-27	03-27	03-30	03-30	04-34	04-34
Lithology	Granodiorite		Granite				Gabbro		Gabbroonorite			
SiO ₂	34.14	33.69	34.79	34.21	34.57	35.73	36.75	36.88	38.13	38.30	38.21	38.33
TiO ₂	3.92	2.81	3.30	3.52	3.82	0.61	5.58	5.71	4.54	4.42	5.13	4.82
Al ₂ O ₃	12.47	12.54	13.04	12.84	13.45	12.31	13.74	13.72	15.45	15.74	14.22	14.27
FeO	33.18	35.01	32.45	31.43	34.19	34.04	17.73	17.33	9.93	10.16	14.47	14.18
MnO	0.15	0.21	0.23	0.18	0.41	0.35	0.10	0.04	0.04	0.06	0.01	0.10
MgO	2.05	1.10	3.68	3.92	1.62	4.11	12.41	12.44	18.26	17.91	14.96	15.54
CaO	0.10	0.10	0.02	0.15	0.06	0.03	0.02	0.02	0.02	0.02	0.04	0.04
Na ₂ O	0.22	0.19	0.10	0.09	0.03	0.03	0.25	0.24	0.98	1.10	0.24	0.22
K ₂ O	7.65	7.93	7.86	7.65	8.09	7.62	8.47	8.64	7.92	7.70	8.45	8.40
total	93.87	93.58	95.48	93.98	96.23	94.83	95.04	95.02	95.26	95.42	95.72	95.91
Formula per 22 oxygens												
Si	5.68	5.69	5.65	5.62	5.62	5.87	5.57	5.58	5.52	5.53	5.63	5.60
Ti	0.49	0.36	0.40	0.44	0.48	0.08	0.64	0.65	0.49	0.48	0.57	0.53
Al ^{IV}	2.32	2.31	2.35	2.38	2.38	2.13	2.43	2.42	2.48	2.47	2.37	2.40
Al ^{VI}	0.12	0.19	0.14	0.11	0.20	0.25	0.02	0.02	0.15	0.21	0.09	0.06
Fe ²⁺	4.61	4.95	4.40	4.32	4.65	4.68	2.25	2.19	1.20	1.23	1.78	1.73
Mn	0.02	0.03	0.03	0.02	0.06	0.05	0.01	0.00	0.00	0.01	0.00	0.01
Mg	0.51	0.28	0.89	0.96	0.39	1.00	2.80	2.80	3.94	3.86	3.28	3.38
Ca	0.02	0.02	0.00	0.03	0.01	0.00	0.00	0.00	0.00	0.00	0.01	0.01
Na	0.07	0.06	0.03	0.03	0.01	0.01	0.07	0.07	0.28	0.31	0.07	0.06
K	1.62	1.71	1.63	1.60	1.68	1.60	1.64	1.67	1.46	1.42	1.59	1.57
total	15.46	15.59	15.53	15.51	15.47	15.67	15.43	15.42	15.53	15.51	15.39	15.35
Mg/(Mg+Fe ²⁺) x100	10	5	17	18	18	8	56	56	77	76	65	66

3.5.5 Feldspar

Gabbros have plagioclase with normal zoning (An₆₀-An₃₇). Feldspar in quartz-gabbro and monzogabbro is more sodic than in gabbros, also with a more sodic (An₆₀-An₂₈) border. Quartz-monzogabbro also has alkali-feldspar with a composition of Or₇₉Ab₂₀An₁.

Plagioclase in gabbroonorite displays different zoning patterns; (1) normal zoning (An₇₇-An₆₆), (2) reverse zoning with cores (An₅₈-An₈₀), and (3) zoning with Ca-rich intermediate zones (An₇₄) with comparatively Ca-poor (An₆₁) cores and rims.

Fayalite-bearing granitoids contain plagioclase and alkali-feldspar. The alkali-feldspar has a composition of Or₆₈₋₇₃Ab₃₀₋₃₂An₀₋₁, which occasionally becomes K-richer (Fig. 3.8f). The plagioclase has normal zoning (An₅₀-An₀₈) with Na-rich patches (An₁₆) in the core.

3.5.6 Ilmenite-titanomagnetite

Ilmenite occurs as small grains associated commonly to mafic silicates, and only locally occurs as lamellae in titanomagnetite. In the fayalite-bearing assemblages, ilmenite is the most abundant Fe-Ti-oxide and its composition approaches that of the end-member. MnO-contents between 0.57 and 2.02 wt.% (Table 3.7) are not correlated with MgO content. Rare titanomagnetite with ilmenite lamellae occurs in the more differentiated fayalite granite.

In the gabbros, ilmenite is often the only Fe-Ti oxide, but locally titanomagnetite occurs as small inclusions in amphibole. Ilmenite in gabbros and gabbro-norites has an MnO-content between 0.91 and 1.09 wt.%, in monzogabbro and quartz-gabbro between 1.81 and 1.62 wt.%, and in gabbro-norites between 0.82 and 2.35 wt.% (Table 3.7), with the lowest values in the mafic globules.

Table 3.7: Representative ilmenite analyses from granites, granodiorites, gabbros and gabbro-norites of the Cobquecura Pluton.

Sample	03-08	04-19	04-20	03-13	03-27	03-27	03-29	03-30	03-30
Lithology	Granodiorite	Granite		Monzogabbro	Gabbro			Gabbro-norite	
TiO ₂	53.39	53.70	51.92	55.09	52.65	51.46	51.66	53.10	52.80
FeO	44.72	45.54	45.53	44.73	46.85	46.81	46.59	43.96	44.04
MnO	2.02	1.44	1.57	1.81	1.09	1.01	0.91	1.37	2.35
MgO	---	0.07	0.02	---	0.13	0.14	0.36	1.53	0.06
total	100.13	100.75	99.06	101.63	100.71	99.43	99.52	99.97	99.26
Formula per 3 oxygens									
Ti	1.01	1.01	1.00	1.02	0.99	0.99	1.00	1.00	0.93
Fe ²⁺	0.94	0.95	0.97	0.92	0.98	1.00	0.99	0.92	0.05
Mn	0.04	0.03	0.03	0.04	0.02	0.02	0.02	0.03	0.00
Mg	0.00	0.00	0.00	---	0.00	0.00	0.01	0.06	0.98
total	1.99	1.99	2.00	1.98	2.00	2.01	2.02	2.01	1.96

Table 3.8: Resume of the mineral chemistry characteristic of the plutonic rocks of the Cobquecura Pluton.

Rock Mineral	Fayalite granite	Hybride rocks	Gabbro	Gabbronorite
Olivine	subhedral Fa ₈₉₋₉₈ CaO (0.7-0.37 wt.%) MnO (1.4-2.16 wt.%) with the rim richer in MnO than the core.	absent	absent	elongated (4×1mm) Fa _{~33} CaO (0.06-0.19 wt.%) MnO (0.42-0.58 wt. %) Mafic globules: CaO (0.09-0.25)
Clinopyroxene	scarce tabular/anhedra (less than 5 vol. %) hedenbergite- Fe-rich- augite Wo ₄₁₋₄₈ Fs ₃₃₋₅₀ En ₅₋₂₅ X _{Mg} (0.09-0.43) TiO ₂ (0.04-0.77 wt.%) Al ₂ O ₃ (<1.86 wt.%) Na ₂ O (0.11-0.46 wt.%) Al ^{VI} very low	absent	large and subhedral diopside-augite Wo ₃₈₋₄₈ Fs ₁₀₋₁₇ En ₃₀₋₄₄ X _{Mg} (0.7-0.77) TiO ₂ (0.73-0.15 wt.%) Al ₂ O ₃ (1.63-3.08 wt.%) Na ₂ O (0.26-0.43 wt.%) Al ^{VI} /Al ^{IV} (0.09-2.49)	anhedral/subhedral diopside-augite Wo ₄₂₋₄₆ Fs ₇₋₁₅ En ₄₂₋₅₀ X _{Mg} (0.70-0.9) TiO ₂ (1.43-0.41) Al ₂ O ₃ (4.6-1.37 wt.%) Na ₂ O (0.21-0.44 wt.%) Al ^{VI} /Al ^{IV} (0.06-2.15)
Amphibole	anhedral ferroedenite to ferrohornblende-ferroactinolite X _{Mg} (0.04-0.35) Fe ³⁺ /(Fe ³⁺ +Fe ²⁺) <0.22 TiO ₂ (0.25-2 wt.%)	subhedral/anhedral Mg-Hornblende core poorer in Si X _{Mg} (0.48-0.56) Fe ³⁺ /(Fe ³⁺ +Fe ²⁺) (0.11-0.18) TiO ₂ (1.3-3 wt.%)	anhedral and interstitial between plagioclase. Mg-hastingsite-edenite to Mg-hornblende X _{Mg} (0.59-0.73) Fe ³⁺ /(Fe ³⁺ +Fe ²⁺) <0.22 TiO ₂ (1.01-3.9 wt.%)	scarce, euhedral or interstitial. Mg-hastingsite, minor kaersutite and actinolite X _{Mg} (0.56-0.78) Fe ³⁺ /(Fe ³⁺ +Fe ²⁺) <0.23 TiO ₂ (0.02-4.78 wt.%)
Biotite	interstitial X _{Mg} (0.03-0.26) TiO ₂ (1.7-7.4 wt.%) Al ₂ O ₃ (9-14wt.%) MnO (0.09-0.41 wt.%)	absent	scarce, large and anhedral X _{Mg} (0.55-0.62) TiO ₂ (4.6-5.7 wt.%) Al ₂ O ₃ (13.7-14.17 wt.%) MnO (0.04-0.22 wt.%)	scarce and interstitial X _{Mg} (0.62-0.77) TiO ₂ (4.4-5.6 wt.%) Al ₂ O ₃ (13.71-15.74 wt.%) MnO (0.01-0.13 wt.%)

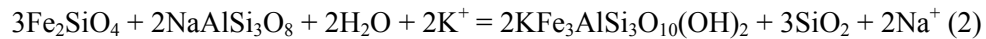
3.6. Discussion

3.6.1 Crystallization and emplacement conditions

In gabbros and gabbro-norites plagioclase crystallized first, followed by olivine and pyroxene, which sometimes contains inclusions of plagioclase; amphibole and biotite crystallized in a late stage as indicated by the interstitial habit and the inclusions. Amphibole in the gabbroic rocks shows an evolution from pargasite, Mg-hastingsite to Mg-hornblende – actinolite (Figs. 3.2c, 3.10a and b). In the fayalite-granites, the crystallization sequence is zircon ~ apatite, plagioclase, then hedenbergite and fayalite. However, fayalite and hedenbergite were not found in contact, although they show similar texture. The high Fe/(Fe+Mg) ratio of fayalite (Fig. 3.7) indicates that it crystallized when the magma was already strongly enriched in Fe. Allanite, amphibole, biotite, quartz and alkali-feldspar are late crystallization products. Amphibole in the felsic rocks evolves from Fe-edenite to Fe-hornblende – Fe-actinolite (Fig. 3.10). Fayalite relicts in amphibole (Fig. 3.2c) indicate a reaction:



in the late stage of the magma development. The reaction is simplified, neglecting the Mg-Fe substitution, Fe^{2+} - Fe^{3+} reaction and the Na-content, but shows that with increasing water content fayalite becomes unstable. The reaction rims of biotite and quartz between olivine and plagioclase (Fig. 3.3e) can be explained by a subsolidus reaction with a hydrous fluid phase and the albite component:



The anhydrous minerals (olivine and clinopyroxene) in the gabbros indicate an initially H_2O -poor magma. During fractionation it remained relatively poor in H_2O , as shown by the late crystallization of fayalite.

The calculated $\text{Fe}^{3+}/(\text{Fe}^{3+}+\text{Fe}^{2+})$ ratios in amphibole and the Ti-content of amphibole and biotite decrease with differentiation (Fig. 3.10c, Table 3.5) indicating a decreasing f_{O_2} and T with differentiation (Spear, 1981; Foley, 1990). The two arrays of mineral analyses at high and low X_{Mg} in TiO_2 and Al_2O_3 vs. X_{Mg} diagrams (Fig. 3.9b, c) for clinopyroxene and amphiboles, and in MnO vs. X_{Mg} for all the Fe-Mg minerals (Fig. 3.9a) correspond to mafic and evolved rocks which are separated by the compositional gap between 57 and 63 wt.% SiO_2 . In each mineral species and each cluster there is a group of high-Ti-Al, low-Mn, and low-Ti-Al, high Mn analyses, indicative for high- and low-temperature crystallization, respectively.

The coexistence of ilmenite with fayalite and quartz and the absence of magnetite in the fayalite granitoids (Table 3.1) constrain the f_{O_2} to conditions below the QFM buffer (Harrison et al. 1990; Anderson et al. 2003). In the mafic rocks the wide variation in the Al^{VI}/Al^{IV} in clinopyroxene reflects polybaric crystallization (Simonetti et al. 1996) from higher pressure at the early stages of crystallization in the more mafic magmas to lower pressures. This polybaric crystallization is also evident in the composition of amphibole, which displays a large range of Al content (Fig. 3.9b). In the fayalite-granites the negligible $Al^{IV} = Al_{Tot}$ in clinopyroxene supports a shallow-level crystallization (Simonetti et al. 1996).

There are several characteristics recognizable in the field, such as the predominance of a medium grain-size, the presence of miaroles and the occurrence of a magmatic breccia at La Iglesia de la Piedra and north of Santa Rita, that are indicators for an epizonal emplacement of the Cobquecura Pluton. The low-grade assemblage of the regional metamorphic basement rocks (chlorite, white mica and quartz, without minerals such as biotite and garnet) confirms that these rocks were at shallow depth and low temperature at the time of intrusion. The narrow contact aureole (<100 m) is another argument for a shallow emplacement, especially when it is compared with the much wider aureole (>20 km) from the Paleozoic granitoids in Cordillera de Nahuelbuta (Cordillera de la Costa, south of 37°S), which were emplaced at pressures of ~3 kbar and generated a contact metamorphism up to granulite facies conditions (Hervé 1977; own data). A shallow emplacement with small contact aureole requires quick cooling of the pluton. This is confirmed by the fine-grained granophyres. Skeletal habits of zircon and acicular apatite crystals in the hybrid rocks and related quartz-gabbros also indicate crystallization during mingling and quick cooling (Wyllie et al. 1962, Didier 1977, Baxter and Feely 2002). Zircon fission track data of the segment between 34° and 35°30'S show that the present day erosion level was at temperature of 200-250°C in the Late Triassic (Willner et al. 2005).

Intermediate rocks with magma-mixing features have the paragenesis and the compositional range, which allow the application of the Al-in hornblende geobarometer (Anderson and Smith 1995) and the edenite-richterite thermometer (Holland and Blundy 1994). A maximal pressure of 3.8 kbar at 736°C was estimated for the contact zone that shows many features for the roof of the magma chamber. The inconsistency between the calculated pressure for the contact (corresponding to a depth of ≈ 10 km) and the field indication for a subvolcanic intrusion is essentially due to the low f_{O_2} , which can exaggerate the calculated pressure by a factor of two to three (Anderson and Smith 1995).

3.6.2 Magmatic Evolution

The X_{Mg} of clinopyroxene, amphibole and biotite displays an excellent correlation ($R^2 = 0.97-0.84$) with the X_{Mg} of the corresponding whole rock, with higher X_{Mg} ratios in the

gabbro-norites and gabbros than in the granites (Figs. 3.8, 3.10c). MnO of the mafic minerals (olivine, clinopyroxene, amphibole, biotite) shows a similar behavior; it increases with differentiation and shows for all the minerals a compositional gap between mafic mineral in the mafic and felsic rocks, respectively (Fig. 3.9a). Despite the compositional gap, CaO, K₂O and MgO display coherent arrays in Harker and variation diagrams for all lithologies (Figs. 3.5, 3.8). These geochemical and mineralogical characteristics together with the narrow spatial relationships and the similar ages of the mafic and felsic suites indicate that the rocks in the Cobquecura Pluton are comagmatic.

The scatter in the contents of Al₂O₃, TiO₂, Fe₂O₃, MnO, CaO, and V (Figs. 3.5, 3.6) for mafic rocks, with SiO₂-contents < 53 wt. %, probably indicates variable modal proportions of plagioclase, Fe-Mg minerals and ilmenite in an early stage of the differentiation, typical of cumulate rocks. Mafic rocks with SiO₂-contents between 53-57 wt.% display a trend for these elements, which is coherent with the felsic rocks. Postplutonic dikes are similar as the mafic rocks with 53-57 wt.% SiO₂ compatible with a common origin.

On the SiO₂ –rich side of the gap > 63 wt. %, the arrays in the Harker Diagrams (except for MnO) and in the Zr vs. SiO₂ diagram are coherent. The slopes of these arrays are in agreement with the arrays from the mafic rocks with 53-57 wt.% SiO₂. Therefore we propose a scenario of cogenetic felsic and mafic magmas in the Cobquecura Pluton with accumulation in the early stages of crystallization (< 53% wt. SiO₂), followed by fractional crystallization as the dominant processes. Contamination is not obvious from the major element chemistry, but trace element and isotope analyses (own unpublished data) show that it was an important process for some of the mafic rocks.

The compositional gap that divides the mafic and felsic suites of the Cobquecura Pluton covers ~ 6 wt.% SiO₂. Bimodal magmatism with such a compositional gap between mafic and felsic suites could have been produced as consequence of the intrusion of hot mafic and mantle-derived magma into a crust that produces a compositionally distinct silicic magma (e.g., Myers and Marsch 1981; Christiansen 1984). Another explication is that this compositional gap was formed during the fractional crystallization with no or little input of crustal material (e.g., Mac Donald, 1987; Bacon and Druitt 1988; Brophy 1991). The coherent trend on both sides of this compositional gap favors the second alternative; a detailed study of the magma sources with trace element studies and isotope data is in progress.

3.6.3 Tectonic environment of the Cobquecura Pluton

The Cobquecura Pluton exhibits geological, petrographical, mineral chemical and whole rock geochemical characteristics typical of A-type anorogenic granites. The absence of foliation in the granites and a late crystallization of the hydrated mafic minerals amphibole and biotite (Collins

et al. 1982) are typical for such an environment. Fayalite and hedenbergite reflect crystallization with a low fO_2 and H_2O -activity. Major element compositions of the granites and granodiorites are characterized by high $FeO^*/(FeO^*+MgO)$ ratios and high K_2O contents. Trace elements show high values of Ga with a Ga/Al ratio of $10,000Ga/Al = 2-3.15$, which are typical for A-type granitoids (Whalen et al. 1987). The high Zr-contents for the majority of the granites (Fig. 3.11, Zr- Ga/Al discrimination diagram of Whalen et al., 1987) are also in favor for A-type granites, with some granites transitional between I- and A-type. The high Ti + Cr- contents vs. the low Ca + Na- contents of clinopyroxene in gabbros and gabbronorites (Fig. 3.12) is also typical for an anorogenic setting, but with a tholeiitic-calcalkaline affinity (Leterrier et al. 1982).

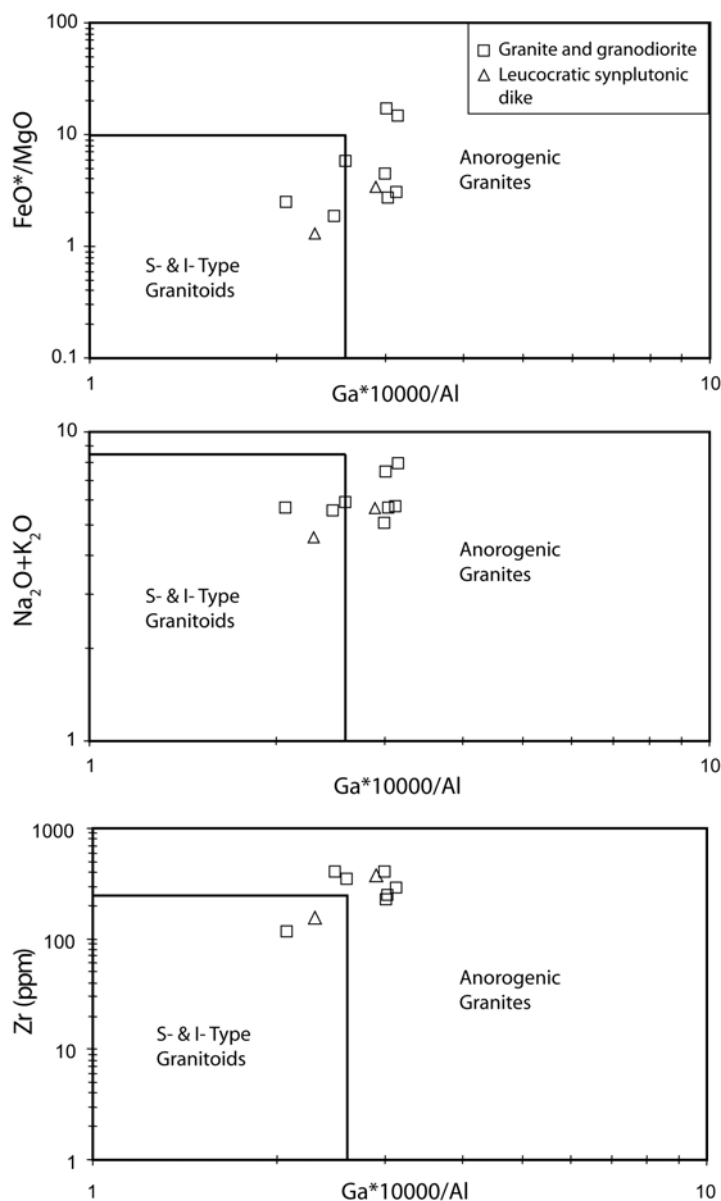


Figure 3.11 FeO^*/MgO , Na_2O+K_2O , Zr vs. $10,000Ga/Al$ discrimination diagrams of Whalen et al. (1987) for granitic rocks and leucocratic dikes. The analyses are transitional between anorogenic granites and S- and I-type granite.

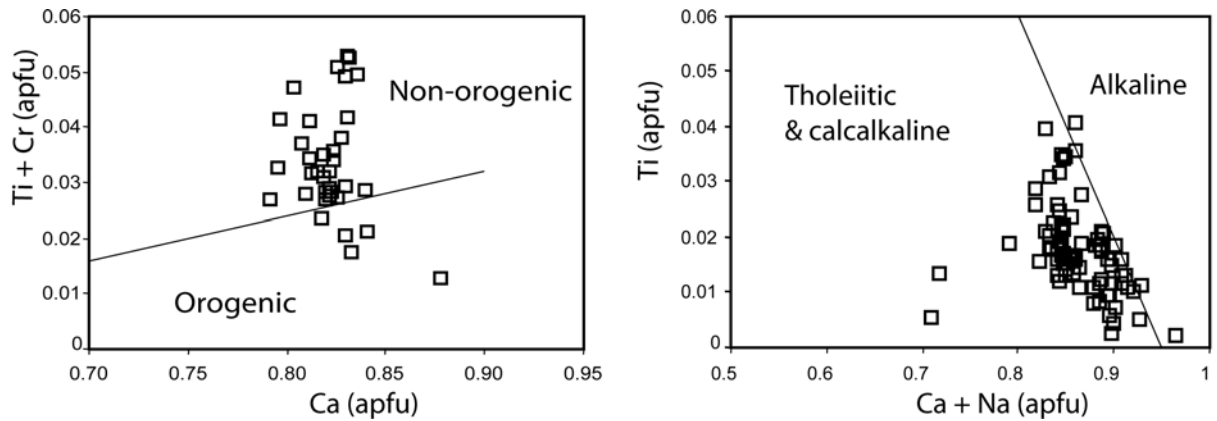


Figure 3.12 Non-quadrilateral components Ti, Cr and Na for clinopyroxene from gabbroic rocks in the Cobquecura Pluton. Discrimination lines after Leterrier et al. (1982). a) Ti + Cr vs. Ca in atoms per formula unit. b) Ti vs. Ca + Na. Clinopyroxene composition is not typical for alkaline rocks, but consistent with a non-orogenic setting of the magmatism.

3.6.4 Comparison with other Late Triassic-Early Jurassic bodies in the Cordillera de la Costa

In the Cordillera de la Costa, between 30° and 33°S, there is also a Late Triassic-Early Jurassic bimodal plutonic association of gabbro – monzodiorite and leucogranite (Gana 1991). These rocks have Rb-Sr ages of 220 to 200 Ma, with similar K-Ar ages, both interpreted as indicative of rapid cooling (Parada et al. 1991). These Late Triassic to Early Jurassic granitoids were classified as A-type to transitional and they are associated with I-type granitoids (Gana 1991; Parada et al. 1991; Mpodozis and Kay 1992). Early work on rocks in this segment proposed that the bimodality was generated in an extensional environment that promoted the generation and emplacement of gabbroic magmas through partial melting of the upper mantle, and of felsic magmas derived through melting of the crust (Gana 1991; Parada et al. 1991). A common character among the Triassic granitoids is their shallow emplacement level (Hervé et al. 1988), evidenced by the narrow contact aureoles of the different bodies, the low-pressure metamorphic mineralogy in the country rocks and the presence of miaroles. Another common characteristic is the predominance of orthoclase as alkali-feldspar in the Triassic granitoids, which distinguishes them from the microcline-bearing Paleozoic granitoids.

The Triassic intrusive granites on the western side of the Cordillera de la Costa (Fig. 3.1a), except the La Estrella Granite, crop out along the coast, and intruded the metamorphic basement. Except for the Hualpén Stock (Lucassen et al. 2004) there are no detailed geochemical and isotopic studies on the Triassic intrusives within the segment 34°-37°S. However, the available data of the bodies of La Estrella, Pichilemu, Constitución and Hualpén show compositionally homogeneous rocks at the outcrop level (Dávila et al. 1979; Hervé et al. 1988; Lucassen et al. 2004; our data). In comparison, the Cobquecura Pluton shows a large compositional and textural diversity, from

gabbro-norite to syenogranite. The Cobquecura Pluton differs also from the Triassic intrusives located north of 33°S by the presence of fayalite, which is absent in the granitoids of the northern area. Only in the Cordillera Frontal, at El León (~30°00'S/72°30'W), exists one granite body with Fe-rich mafic minerals (ferrohornblende and ferrohedenbergite; Parada et al. 1991; see details in Parada 1988).

A-type granites can be formed in both postorogenic and extensional settings (Eby 1992). It is difficult to differentiate between these settings, because there are no distinctive petrological, mineralogical or geochemical attributes (Whalen et al. 1987; Eby 1992). The end of major orogenic processes is marked by uplift and erosion, transcurrent to extensional tectonic regimes induced partly by gravitational collapse of the thickened crust, partly by delamination of the lithosphere, and emplacement of voluminous igneous formations (Bonin 2004). The timing of the end of the Paleozoic orogenesis is unclear, and occurs diachronically along the western margin of Gondwana. However, the Choiyoi Formation, a voluminous felsic Late Permian-Triassic magmatism (24°-40°S), may mark its end (Llambías and Sato 1995). The similar ages and petrological features of the Cobquecura Pluton and other Triassic bodies could point to a common origin, and thus the Cobquecura Pluton is a manifestation of a magmatic event at the Gondwana margin during the Late Triassic together with other small and sporadic intrusions along the coast and at the Cordillera Frontal (29°30'-31°S).

Chapter 4: Origin of fayalite granitoid: new insights from the Cobquecura pluton, Chile, and its metapelitic xenoliths

Abstract

Fayalite granitoids of the Cobquecura Pluton, Central Chile occur in an active continental margin setting, which is unusual for such rocks. They are closely associated with gabbros. Both lithologies contain hercynite-rich metapelitic xenoliths. The primitive magmas of the Cobquecura Pluton are derived from a mafic source, similar to the regional subarc subcontinental mantle. Sr-Nd-Pb isotope data demonstrate that crustal contributions were important in the petrogenesis of the fayalite granitoids. The crustal contribution, however, does not consist of rocks similar to the regionally exposed Paleozoic basement rocks, but rather resembles restitic metapelitic lower crustal rocks, which occur as Fe-rich xenoliths in the granitoids. A relatively high content of REE and HFSE elements in the fayalite granitoids is linked to selective assimilation of deeper crust, as evident from the abundant presence of REE- and HFSE-rich accessory minerals in the leucosome of the deep crustal xenoliths which are entrained in the fayalite granitoids. These Fe-rich rocks from the deep continental crust could have acted as a chemical buffer keeping the oxygen fugacity low, which is crucial for the generation of fayalite bearing granitoids.

Keywords: Fayalite granitoid, Sr-Nd-Pb isotopes, restitic metapelitic xenoliths, selective assimilation, Chile, petrogenesis.

4.1 Introduction

Granitoids are the most abundant rocks in the Earth's upper continental crust and their formation is linked to a wide spectrum of different tectonic and geodynamic processes. Granitoids may either form by differentiation of mafic, mantle-derived melts, or by partial melting of crustal rocks. In many crustal continental settings, granitoid petrogenesis involves both fractional crystallization of mantle-derived melts, and wallrock assimilation within the crust. Fayalite-bearing granitoids are fairly uncommon and are mainly related to alkaline magmatism, usually of intraplate setting, or anorogenic magmatism (e.g., Njonfang and Moreau 2000; Frost et al. 2002, and references therein).

Most fayalite granitoids occur in Precambrian terrains (e.g., Pikes Peak Batholith, Central Colorado, USA, Smith et al. 2001; Sherman Batholith, Wyoming, USA, Frost et al. 1999; Padthaway Ridge, South Australia, Turner et al. 1992). Only few fayalite granitoids are known from Phanerozoic terrains, e.g., the anorogenic province of Corsica (France) (Poitrasson et al.

1995) and the Tibchi anorogenic ring complex of Nigeria (Mücke 2003). Fayalite granitoids are characterized by comparatively high overall Fe contents, high $\text{FeO}/(\text{FeO}+\text{MgO})$ ratios, the occurrence of Fe-rich anhydrous mafic minerals such as fayalite and hedenbergite, and the late crystallization of hydrous mafic minerals like annite or Fe-rich amphibole (Turner et al. 1992; Mücke 2003). These characteristics indicate distinct crystallization conditions from an H_2O -poor magma at low f_{O_2} (Stephenson and Hensel 1978; Frost et al. 1988).

The petrogenesis of fayalite granitoids has been a longstanding subject of discussion. Some authors proposed that these granites were generated by fractionation from mafic magmas (e.g., Loiselle and Wones 1979; Frost et al. 2002). Other authors favored fayalite granitoid formation by partial melting of dehydrated lower crustal sources like granulites (Collins et al. 1982; Clemens et al. 1986) or tonalites (Creaser et al. 1991).

At the southwestern margin of Triassic Gondwana, along the South-Central Chilean coast, A-type granitoids (cf. Whalen et al. 1987) have been identified as an important constituent of the regional Triassic magmatism (Gana 1991; Parada et al. 1991; Vásquez and Franz 2008). Fayalite granites were discovered in the Triassic Cobquecura Pluton (Coastal Cordillera, $\sim 36^\circ\text{S}$; Vásquez and Franz 2008). Here we discuss the petrogenesis of the fayalite granitoids in the light of their petrographical, geochemical and Sr-Nd-Pb isotopic characteristics, with particular attention to the metapelitic xenoliths entrained in the magmas.

4.2 Geological setting and petrography

The southwestern margin of South America has been a continental margin of Gondwana and pre-Gondwana at least since the Late Proterozoic-Early Cambrian (e.g., Coira et al. 1982). In the southern part of Central Chile, the subduction regime between the Late Carboniferous and the Early Triassic generated a magmatic arc and an accretionary prism (Hervé et al. 1981; Parada 1990; Martin et al. 1999). The metamorphic basement in south-central Chile is subdivided in two metamorphic complexes: the Western and the Eastern Series (Aguirre et al. 1972 and Fig. 4.1a). The Eastern Series consists of metagreywacke and metapelite, and is almost devoid of metabasites. It shows metamorphic gradients from very low-grade rocks to amphibolite-granulite gneisses, related to the proximity of Late Paleozoic calcalkaline granitoids (Hervé et al. 1988; Beck et al. 1991; Martin et al. 1999). The Western Series comprises low-grade metapsammite with metabasite intercalations and serpentinite, in transitional greenschist to blueschist facies. The Western Series is interpreted as a paleoaccretionary complex built by basal accretion, and the Eastern Series shows all characteristics of frontally accreted sediments (Glodny et al. 2005; Richter et al. 2007). According to this interpretation, the Western Series most probably represents the composition of the lower crust of the forearc in this region.

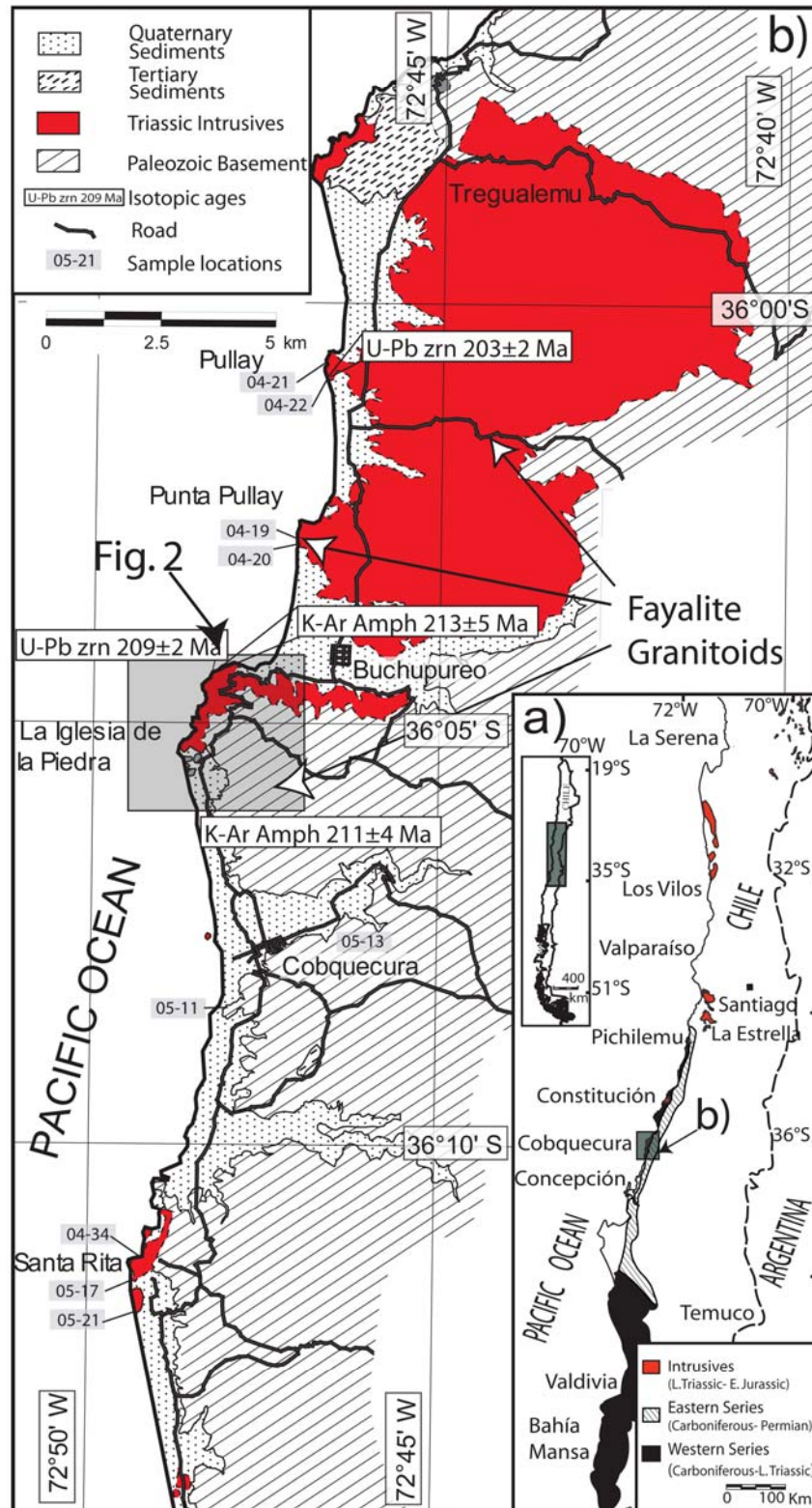


Figure 4.1 a) Distribution of late Triassic-early Jurassic magmatism in the Cordillera de la Costa between 29° and 37°S; compiled after Godoy (1970), Hervé and Munizaga (1978), Dávila et al. (1979), Gajardo (1981), Gana and Hervé (1983), Mpodozis and Kay (1992), Parada et al. (1999) and Willner et al. (2004). Western and Eastern Series distribution after Hervé et al. 2007. b) Geological sketch map of the Cobquecura Pluton (after Vásquez and Franz 2008) and sample location. Isotopic ages are taken from Vásquez et al. (2005) and Vásquez et al. (2008b). The arrows show the localities with fayalite granite.

Triassic granitoids with minor gabbros occur as scattered epizonal intrusive bodies in today's Coastal Cordillera of Central- South Chile, between 29° and ~37°S (Fig. 4.1a). They intrude into the Paleozoic metamorphic and granitoid rocks. Their composition is mainly granitic, with isolated occurrences of gabbros and intermediate rocks. Several authors have associated the Triassic magmatic activity with enhanced crustal melting (e.g., Choiyoi Group; Kay et al., 1989) in an extensional geotectonic setting (Parada 1990; Mpodozis and Kay 1992; Morata et al. 2000). Permo-Triassic magmatic rocks occur at variable distances to the deep-sea trench, so magmatism of the same age could have different geotectonic settings. Vásquez et al. (2008b) propose, based on the study of the magmatism of the Chilean Cordillera de la Costa (34-37°S), that the Triassic magmatism in today's forearc region could have been generated in a suprasubduction setting with slab rollback, which favors the melting of the subcontinental mantle. The coincidence of the Triassic plutonic bodies with NW-SE trending lineaments suggests that, previous to the steepening of the slab, there was oblique subduction generating extension-related NW-SE structures, which in turn facilitated the ascent of magmas (Vásquez et al. 2008b).

4.2.1 The Cobquecura Pluton (~36°S, ~72°45'W)

The Cobquecura Pluton is an epizonal, complex intrusive body, cropping out at the western side of the Cordillera de la Costa (Fig. 4.1). Vásquez and Franz (2008) have previously described it and we only give a short summary here. The Cobquecura Pluton displays a wide lithologic and textural variety compared to other Triassic intrusives of this crustal segment of the SW continental margin of Gondwana. The major rock types are gabbro and granite, and less frequently hybrid rocks. A peculiarity is that some granitoids are fayalite-bearing. The gabbros range from hornblende-bearing gabbros to olivine gabbro-norites. They are composed of plagioclase, clinopyroxene, amphibole and minor olivine, biotite and orthopyroxene. Fayalite granitoids are medium-grained and are composed of fayalite, Fe-rich clinopyroxene, Fe-rich edenite, quartz, plagioclase, annite, potassic feldspar and ilmenite. In both granitoids and gabbros, amphibole and biotite are late magmatic minerals. Medium-grained fayalite-free granitoids are composed of quartz, potassic feldspar, plagioclase and minor biotite. The suite of hybrid rocks consists of tonalite with magma mixing features (resorbed cores of plagioclase) and mingled rocks (composite dikes, mafic pillow-shaped enclaves and net-vein complexes) that contain mafic-igneous and metamorphic enclaves. Hybrid rocks generally are crosscut by both synplutonic and postplutonic dikes with acidic and basic compositions.

Magmatic breccia occurs at the La Iglesia de la Piedra locality (Fig. 4.2) and is composed of matrix-embedded igneous and metapelitic xenoliths (Fig. 4.3 a, b). The matrix has a variable composition from amphibole-bearing tonalite to amphibole and biotite-bearing granodiorite.

Magma mingling-related mafic enclaves, present as composite dikes and mafic pillow-shaped enclaves, display intergranular texture and contain plagioclase, clinopyroxene and

amphibole. These enclaves result from injection of mafic magma into felsic melts (Vásquez and Franz, 2008).

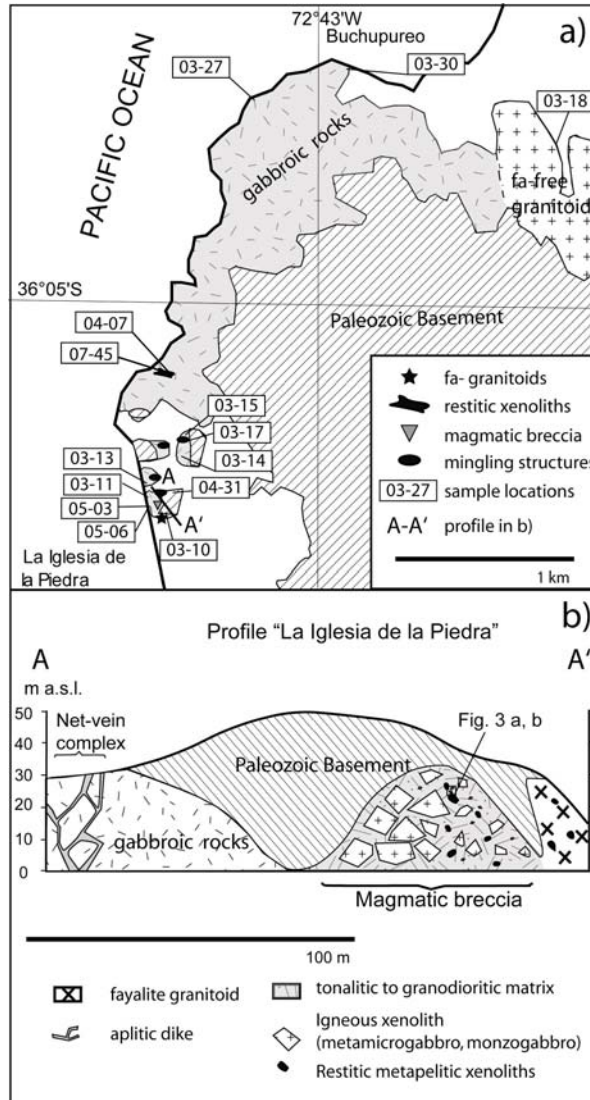


Figure 4.2 a) Detailed map of the Punta Iglesia de la Piedra area. b) "La Iglesia de la Piedra Profile" that shows the contact relationship between the gabbros, magmatic breccia and fayalite granitoids.

A K-Ar age of 212 ± 5 Ma (2σ) on ferroedenitic amphibole was obtained for a fayalite granodiorite from La Iglesia de la Piedra (Fig. 4.1b), and a K-Ar Mg-hornblende age of 213 ± 5 Ma (2σ) for a gabbro from Buchupureo (Fig. 4.1b) (Vásquez et al. 2005). LA-ICP-MS zircon U-Pb data gave similar Late Triassic ages for these intrusives, namely an age of 209 ± 2 Ma (2σ) for a gabbro from Buchupureo, while Pullay gabbro zircons yielded 203 ± 2 Ma (2σ) (Vásquez et al. 2008b). Isotopic ages thus cluster around 210 Ma. They suggest a comagmatic evolution for all Cobquecura igneous rocks (Vásquez and Franz 2008). This inference is backed up by the close spatial relationship between different lithologies, the evidence for magma mingling, and major

element correlations for fayalite granitoids and gabbro of the Cobquecura Pluton. The small analytical errors for the U-Pb zircon age data may indicate separate magmatic events, whereas the field evidence strictly shows that the magmas of the Cobquecura Pluton were contemporary. We therefore hypothesize that some of the nominally ‘youngest’ U-Pb zircon ages were affected by minor Pb loss, which is not resolvable by LA-ICP-MS dating, and that Cobquecura magmatism occurred at around 210 Ma (Vásquez et al. 2008b).

4.2.2 Country rocks

The low-grade metamorphic basement in the Cobquecura area is represented by rocks of the Eastern Series (Fig. 4.1a), which around the Cobquecura Pluton, is mainly composed of phyllite, with subordinate quartz-rich metapsammite. The foliation in the phyllite is defined by white mica. Other constituents are granoblastic quartz, albite and scarce tourmaline. Quartz-rich metapsammite with alternating quartz- and phyllosilicate-rich layers of white mica, chlorite and minor biotite crops out at the Iglesia de la Piedra, and is located directly above the roof of the Cobquecura Pluton. The metamorphic rocks of the area belong to the Paleozoic to Mesozoic accretionary wedge, which is exposed in many outcrops along the coast of Central and Southern Chile. The available isotopic age data to this unit indicate that metamorphism occurred mainly in the Late Paleozoic (Permo-Carboniferous; Willner et al. 2005; Glodny et al. 2006, and references therein).

4.2.3 Characteristics of the xenoliths in the Cobquecura Pluton

The Cobquecura Pluton displays different types of xenoliths related to diverse structures (Table 4.1, Figs. 4.3, 4.4). There are igneous, metapelitic and meta-igneous fragments present mainly in the magmatic breccia and in gabbro, and less abundant in fayalite granitoid.

There are different types of metapelitic xenoliths included in gabbros. The first is very similar to the metamorphic basement at the outcrop level, and is described here as upper crustal xenoliths (UCX). They are brown to gray and display a strong foliation, and folds with segregated quartz (Fig. 4.3c, d). They contain white mica, chlorite, quartz and opaque minerals and, at the contact with the intrusive rocks pinitized cordierite.

Another type of metapelitic xenoliths included in gabbro is also present in the fayalite granitoids, but with smaller dimensions in the latter (<1 – 30 cm). The shape of these xenoliths is stretched, indicating plastic deformation and there is a quartz-feldspar-rich aureole in the surrounding gabbro, indicating mass transport from the xenolith into the gabbro (Fig. 4.3e, f). Their mineralogy and their leucosome content indicate that they are restitic xenoliths, which, while entrained into the gabbro, preserved their original foliation and some relict leucosome. There are two types of restitic xenoliths, one with high leucosome content (high-leucosome restitic xenoliths, HLRX) and other with low leucosome content (low-leucosome restitic xenoliths, LLRX) (see

Table 4.1). Both show similar melanosomes with granolepidoblastic textures, abundant hercynite (ca. 30 vol.%), cordierite, corundum, plagioclase, scarce sillimanite and opaque minerals together with late biotite; the opaque minerals are mainly ilmenite with minor magnetite and Fe-sulphides (Fig. 4.4a, b, c). This mineralogy is typical for high temperature-low pressure metamorphism in metapelites. The HLRX occasionally display a layered structure with coarse-grained granitic leucosomes. The LLRX display a leucosome with high concentrations of zircon, with minor apatite, monazite and xenotime.

The high concentration of zircon in the leucosome of LLRX (Fig. 4.4d) allowed us to date zircon in situ by U-Pb methods using LA-ICPMS (see Appendix C for methodology). Some zircon grains display inherited rounded cores, mantled by apparently magmatic overgrowths. Using data from zircon cores and mantle, a discordia line is defined with an upper intercept at $651 \pm 88/-91$ Ma and a lower intercept at $202 \pm 16/-19$ Ma (Fig. 4.5; data in Table 4.2). We interpret the cluster of concordant age data at about 200 to 210 Ma (Fig. 4.5, inset) as the crystallization age of the magmatic, latest zircon generation, whereas the upper intercept age only suggests presence of a Neoproterozoic inherited zircon component.

The magmatic breccia contains fragments of metapelite, quartzite, monzogabbroic xenoliths (MX) and metamicrogabbroic xenoliths (MMX), all mostly with cusped forms, (Table 4.1, Fig. 4.3a, b), in a tonalitic to granodioritic matrix. MMX show ophitic to subophitic texture with plagioclase and clinopyroxene, together with recrystallized amphibole, orthopyroxene and biotite (Table 4.1). Metapelitic xenoliths with lepidogranoblastic texture (Fig. 4.3a, b) are similar to HLRX (Table 4.1).

Table 4.1: Petrographic characteristics of the different xenoliths included in the Cobquecura Pluton, Cordillera de la Costa, Chile (~36°S, 72°45'W)

Type of xenolith	Texture	Metamorphic grade	Mineral assemblage	Leucosome	Occurrence	Chemical features
Upper crustal xenoliths (UCX)	with strong foliation	low-grade metamorphism up to greenschist facies	white mica, quartz, albite, with pinitized cordierite near xenolith rims	absent	in gabbro	similar to the regional upper crust
High-leucosome restitic xenolith (HLRX)	with foliation, presence of leucosome and melanosome	high-temperature metamorphism (granulite facies)	melanosome: hercynite, cordierite, corundum leucosome: quartz, K-feldspar, plagioclase, biotite	abundant (~30 vol. %)	in magmatic breccia	extremely rich in FeO and Al ₂ O ₃
Low-leucosome restitic xenolith (LLRX)	with foliation, presence of leucosome and melanosome	high-temperature metamorphism (granulite facies)	melanosome: hercynite, cordierite leucosome: quartz, plagioclase, biotite, zircon, monazite	scarce (~5 vol. %)	in gabbro, fayalite granitoid	extremely rich in FeO and Al ₂ O ₃ , rich in REE and HFSE
Monzogabbro xenolith (MX)	without foliation	magmatic without recrystallization texture	clinopyroxene, plagioclase, K-feldspar, amphibole	absent	in magmatic breccia	similar to the gabbroic rocks
Metamicrogabbros (MMX)	without foliation	magmatic with local recrystallization texture	clinopyroxene, plagioclase, opaque minerals, late amphibole, biotite	absent	in magmatic breccia	similar to the gabbroic rocks

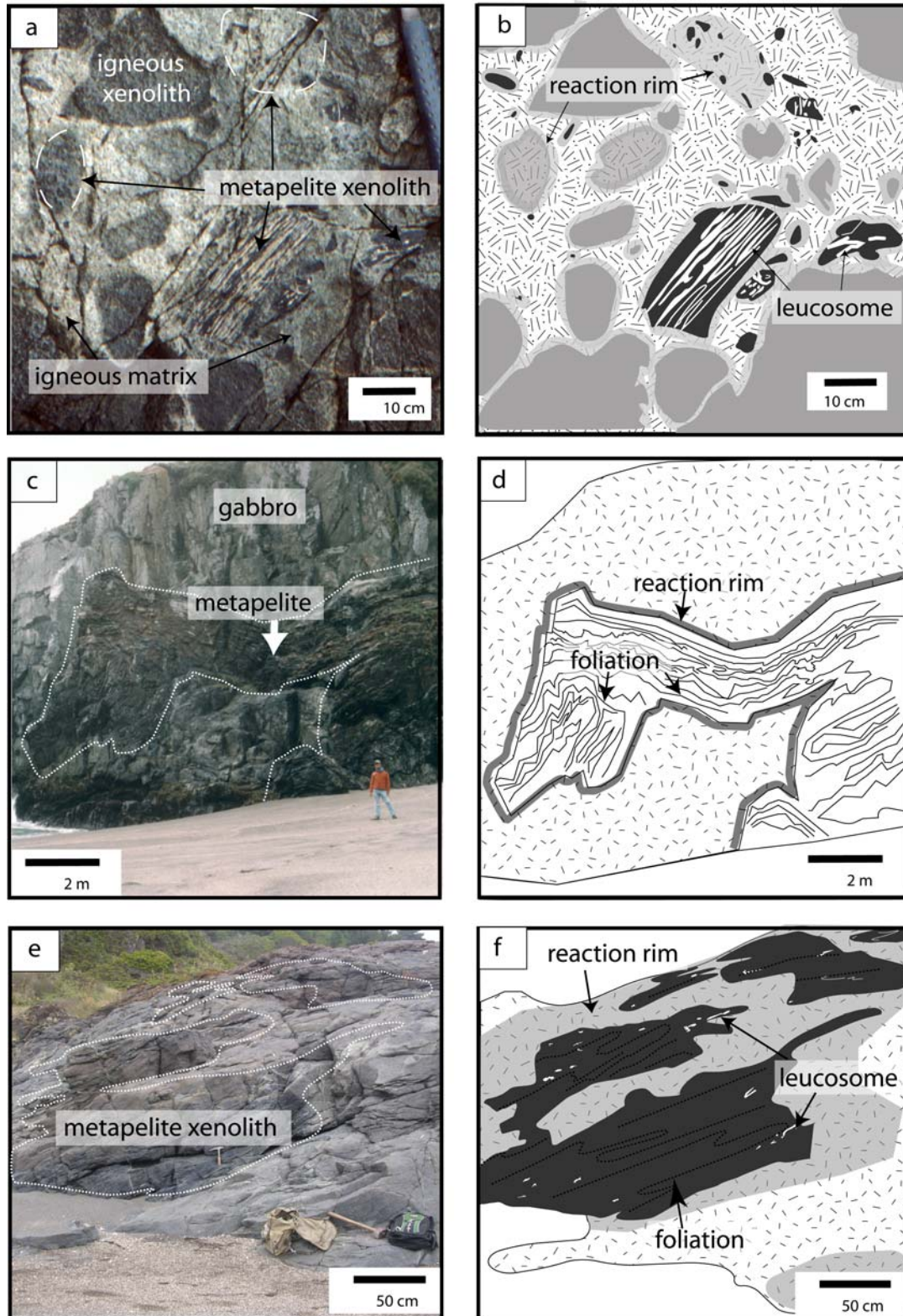


Figure 4.3 Different types of enclaves and xenoliths. a) and b) image and drawing of different xenoliths in the magmatic breccia. Metapelitic xenoliths (similar to HLRX) display abundant leucosome and a quartz-feldspar rich reaction rim. Igneous enclaves show indications for interaction with surrounding melts. c) and d) image and drawing of a large metapelitic xenolith included in gabbro, showing a strong foliation of the xenolith with folding and a thin quartz-feldspar rich – reaction rim (indicating partial assimilation). e) and f) image and drawing of a low leucosome restitic xenolith in gabbro (LLRX), displaying an quartz-feldspar rich – reaction rim (assimilation), and relict leucosome in the xenolith. Dashed line indicates the direction of the foliation.

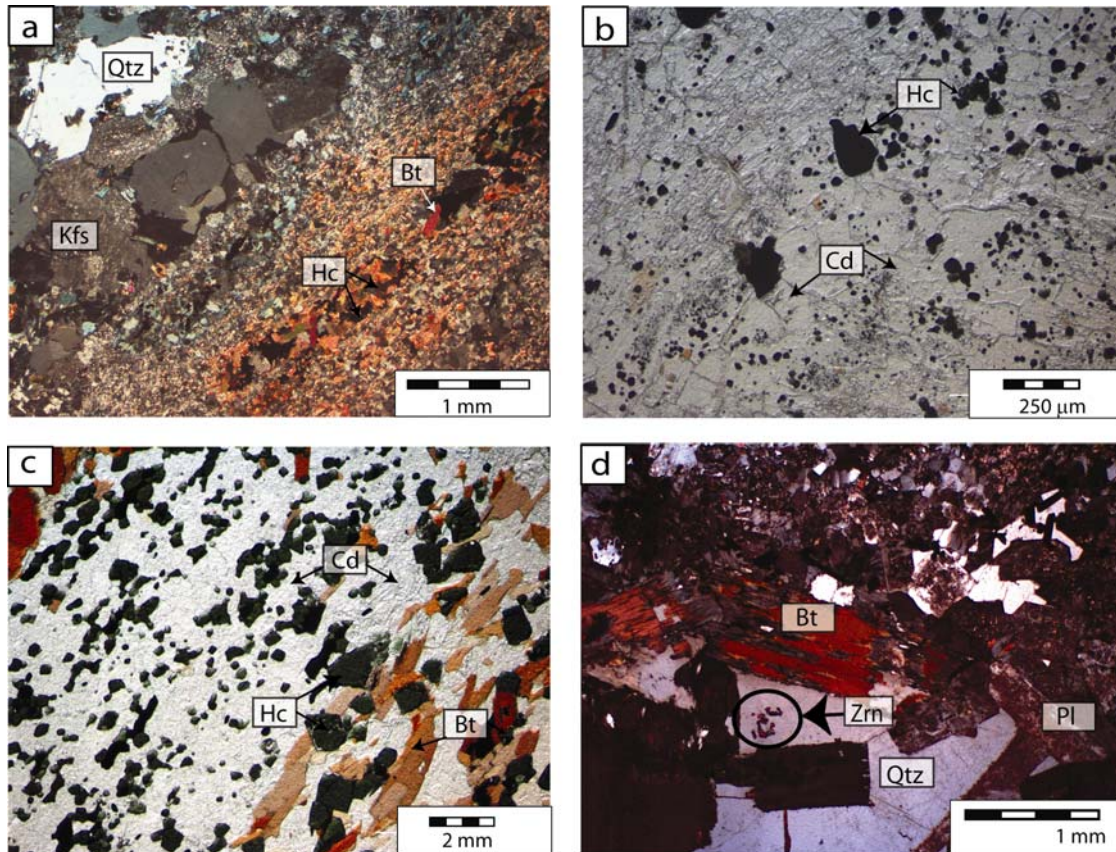


Figure 4.4 Textures and minerals of Cobquecura Pluton xenoliths. a) Xenoliths in a granodioritic to tonalitic matrix (high leucosome restitic xenolith, HLRX) with a granitic leucosome of quartz, altered potassic feldspar, and biotite, side by side with restitic melanosomes with strong foliation with late biotite, hercynite and corundum (sample 04-31). b) Strongly foliated xenolith in gabbro (low leucosome restitic xenolith, LLRX, cordierite-rich restite with hercynite, sample 04-07). c) Foliated xenolith in gabbro (LLRX) composed of hercynite-rich restite with cordierite and late biotite (sample 07-44). d) Leucosome from the LLRX, with coarse-grained quartz, plagioclase, biotite and zircon (sample 07-45). Abbreviation: Bt = biotite, Cd = cordierite, Hc = hercynite, Kfs = potassic feldspar, Qtz = quartz, Zrn = zircon.

Table 4.2: U, Th and Pb isotope analyses for zircon from a low leucosome restitic xenolith (LLRX; sample 07-45), included in gabbros of the Cobquecura Pluton Cordillera de la Costa, Chile (~36°S, 72°45'W)

Analysis No.	²⁰⁷ Pb ^a (cps)	U ^b (ppm)	Pb ^b (ppm)	Th ^b U	Age (Ma)													
					²⁰⁶ Pb ²⁰⁴ Pb	²⁰⁶ Pb ^c ²³⁸ U	±2σ	²⁰⁷ Pb ^c ²³⁵ U	±2σ	rho ^e	²⁰⁷ Pb ^c ²⁰⁶ Pb	±2σ	²⁰⁶ Pb ²³⁸ U	±2σ	²⁰⁷ Pb ²³⁵ U	±2σ	²⁰⁷ Pb ²⁰⁶ Pb	±2σ
					(%)	(%)	(%)	%	%									
48	3932	502	21	1.79	9851	0.0357	1.1	0.254	2.8	0.40	0.0515	2.6	226	3	230	6	261	60
49*	2103	274	199	128	6210	0.0380	1.3	0.285	3.6	0.36	0.0544	3.3	241	3	255	8	386	74
2b	1390	153	5.4	0.54	798	0.0334	1.3	0.234	4.7	0.28	0.0509	4.5	212	3	214	9	235	104
2c	2038	159	11	0.32	3476	0.0691	1.5	0.563	3.7	0.40	0.0591	3.4	431	6	453	14	570	74
10	3193	169	8.8	0.38	5060	0.0504	1.7	0.399	3.8	0.45	0.0574	3.4	317	5	341	11	507	75
51	1813	159	8.8	0.57	5714	0.0542	1.2	0.417	4.0	0.31	0.0558	3.8	340	4	354	12	444	85
52	2112	190	11	0.51	3078	0.0557	1.0	0.428	4.8	0.21	0.0557	4.7	350	3	362	15	439	105
53	1471	183	6.7	0.85	2822	0.0336	1.6	0.235	4.9	0.32	0.0506	4.7	213	3	214	10	222	108
54	607	79	2.6	0.50	1616	0.0328	3.4	0.235	6.9	0.50	0.0519	5.9	208	7	214	13	283	136
4	690	81	2.9	0.54	1235	0.0350	1.6	0.244	8.3	0.20	0.0505	8.1	222	4	222	17	218	188
55	1465	161	6.4	0.51	2836	0.0384	1.6	0.273	5.6	0.29	0.0515	5.4	243	4	245	12	265	124
6	572	98	3.2	0.79	866	0.0319	2.5	0.221	6.8	0.37	0.0502	6.3	203	5	203	13	206	147
56	1036	120	5.0	0.77	799	0.0406	2.6	0.294	5.5	0.48	0.0526	4.8	256	7	262	13	311	109
29	1600	210	7.7	0.52	1181	0.0342	2.4	0.236	7.7	0.32	0.0501	7.3	217	5	215	15	200	169
31b	2278	184	6.7	0.42	2093	0.0348	2.0	0.248	5.0	0.39	0.0517	4.6	220	4	225	10	271	106
31	1424	97	3.6	0.42	1845	0.0347	2.4	0.252	7.1	0.34	0.0526	6.7	220	5	228	15	313	151
32	1434	167	5.4	0.31	1880	0.0325	2.4	0.222	6.5	0.38	0.0497	6.0	206	5	204	12	180	141
33	1527	187	6.4	0.45	1017	0.0326	2.4	0.220	5.7	0.42	0.0489	5.2	207	5	202	11	144	122
35	2929	526	43	1.93	1674	0.0869	3.4	0.756	6.0	0.56	0.0631	4.9	537	18	572	26	711	105
34	1949	346	11	0.38	1785	0.0318	2.4	0.229	6.6	0.37	0.0522	6.2	202	5	209	13	294	141
28	1482	179	6.2	0.49	542	0.0336	2.4	0.231	6.7	0.36	0.0500	6.2	213	5	211	13	196	144
27	1555	257	8.6	0.44	480	0.0326	1.6	0.232	3.7	0.43	0.0516	3.4	207	3	212	7	266	77
26	2004	152	5.7	0.44	2384	0.0365	2.1	0.258	5.3	0.39	0.0514	4.9	231	5	233	11	258	112
38	2511	201	7.2	0.44	1121	0.0346	2.3	0.233	4.8	0.47	0.0487	4.2	219	5	212	9	134	99
37	1713	254	9.1	0.61	1869	0.0334	2.1	0.229	8.0	0.26	0.0497	7.7	212	4	209	15	181	180
40	1422	147	5.2	0.43	1510	0.0337	2.2	0.230	8.7	0.25	0.0495	8.4	214	5	210	17	170	196
39	1611	110	4.5	0.43	900	0.0351	2.6	0.251	9.9	0.26	0.0520	9.5	222	6	228	20	285	218
23	1413	160	5.4	0.45	1426	0.0325	2.3	0.215	7.1	0.32	0.0480	6.8	206	5	198	13	97	160

Analysis No.	Age (Ma)																	
	²⁰⁷ Pb ^a	U ^b	Pb ^b	Th ^b	²⁰⁶ Pb	²⁰⁶ Pb ^c	±2σ	²⁰⁷ Pb ^c	±2σ	rho ^e	²⁰⁷ Pb ^c	±2σ	²⁰⁶ Pb	±2σ	²⁰⁷ Pb	±2σ	²⁰⁷ Pb	±2σ
	(cps)	(ppm)	(ppm)	U	²⁰⁴ Pb	²³⁸ U	(%)	²³⁵ U	(%)		²⁰⁶ Pb	%	²³⁸ U		²³⁵ U		²⁰⁶ Pb	
45	1585	210	7.6	0.51	967	0.0342	2.4	0.235	8.0	0.30	0.0499	7.6	217	5	215	15	189	177
19	1419	146	5.4	0.54	1629	0.0348	2.0	0.264	7.4	0.27	0.0551	7.1	220	4	238	16	418	159
18	1713	231	8.2	0.48	1258	0.0340	2.0	0.255	6.4	0.32	0.0545	6.0	215	4	231	13	391	135
20	1074	192	7.3	0.46	1384	0.0318	2.4	0.209	9.4	0.25	0.0478	9.1	202	5	193	17	88	215
21	1563	185	6.4	0.53	2271	0.0326	2.0	0.235	5.9	0.34	0.0523	5.5	207	4	214	11	297	126
15	1423	152	5.7	0.43	1439	0.0361	2.3	0.259	5.9	0.39	0.0520	5.4	228	5	234	12	288	123
14	1546	221	7.7	0.56	1280	0.0325	2.3	0.223	5.7	0.40	0.0497	5.2	206	5	204	11	182	122
13	1391	232	10	0.44	164	0.0318	2.3	0.208	9.4	0.24	0.0474	9.1	202	5	192	17	67	217
17	1609	223	7.6	0.48	1306	0.0324	2.3	0.226	6.0	0.38	0.0506	5.6	206	5	207	11	223	129
16	1687	192	6.8	0.54	1984	0.0320	2.4	0.229	5.5	0.44	0.0519	4.9	203	5	209	10	280	113
11	1947	297	12	0.66	616	0.0356	2.6	0.255	6.8	0.38	0.0520	6.3	226	6	231	14	286	145
10	1672	218	7.6	0.41	1712	0.0336	2.2	0.245	6.2	0.36	0.0529	5.8	213	5	223	12	325	131
12	1608	214	7.6	0.45	1315	0.0335	2.2	0.228	7.4	0.29	0.0493	7.1	212	5	209	14	164	165
8	1600	217	7.9	0.47	1724	0.0345	1.9	0.241	6.0	0.32	0.0506	5.7	219	4	219	12	222	131
9	1485	182	6.2	0.49	1923	0.0325	2.2	0.223	7.3	0.30	0.0496	7.0	206	5	204	14	178	163
4	1637	163	6.3	0.55	1669	0.0359	2.3	0.253	8.0	0.29	0.0510	7.6	227	5	229	16	242	176
5	34099	303	122	4.15	16937	0.0325	1.8	0.227	2.0	0.88	0.0508	1.0	206	4	208	4	231	23
7	2081	284	9.5	0.31	1599	0.0316	2.4	0.231	7.9	0.30	0.0529	7.5	201	5	211	15	323	171
3	2474	596	24	0.55	1454	0.0377	1.7	0.266	4.5	0.38	0.0512	4.1	239	4	240	10	249	95
1	1450	144	5.6	0.62	1912	0.0354	1.8	0.237	11.1	0.17	0.0485	11.0	224	4	216	22	122	258
2	1464	167	6.0	0.38	1239	0.0349	2.0	0.227	12.0	0.17	0.0472	11.8	221	4	208	23	61	281
44	1580	180	6.2	0.47	1324	0.0320	2.4	0.228	6.4	0.37	0.0516	6.0	203	5	208	12	270	137
43	1772	300	11	0.58	2204	0.0345	1.6	0.228	7.2	0.22	0.0478	7.0	219	3	208	14	88	166

^a Within run background-corrected mean ²⁰⁷Pb signal in counts per second.

^b U and Pb content and Th/U ratio were calculated relative to GJ-1 reference (LA-ICP-MS values. Gerdes. unpublished).

^c corrected for background and within-run Pb/U fractionation and subsequently normalised GJ-1 reference (ID-TIMS value/measured ratio)

^d mass bias corrected by normalising to GJ-1 (ID-TIMS/measured ratio; c. 0.5% per amu).

^e error correlation defined as $\text{err}^{206}\text{Pb}/^{238}\text{U} / \text{err}^{207}\text{Pb}/^{235}\text{U}$.

*Analysis in monazite

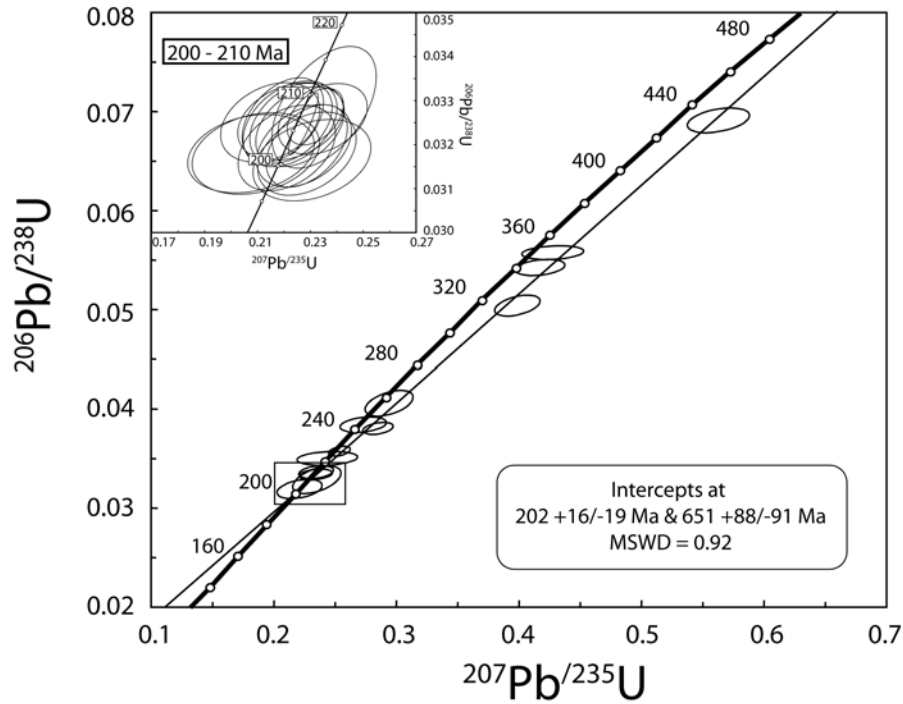


Figure 4.5 Results of in situ LA-ICP-MS U-Pb age determinations on zircon from leucosome of a low-leucosome restitic xenolith (LLRX, sample 07-45). Age data for the youngest zircon generation cluster at around 210 to 200 Ma (see inset), which is the magmatic age of the Cobquecura pluton.

4.3. Geochemical characteristics

4.3.1 Intrusive rocks

The Cobquecura Pluton comprises a subalkaline suite with SiO_2 - content between 48 and 76 wt.% and a small compositional gap between 57 % and 63 % wt.% SiO_2 (Vásquez and Franz 2008). The most differentiated rocks are leucocratic dikes and granitoids without fayalite. Compositional continuity exists between metaluminous mafic rocks and slightly peraluminous, more differentiated rocks richer in K_2O and with a higher $\text{FeO}^*/(\text{FeO}^*+\text{MgO})$ (total iron as FeO ; Vásquez and Franz 2008).

The rocks of the Cobquecura Pluton have gently sloped REE patterns, with a steeper slope in the LREE ($\text{La}_\text{N}/\text{Sm}_\text{N} = 1.12 - 3.39$) than in the HREE ($\text{Lu}_\text{N}/\text{Gd}_\text{N} = 0.59 - 0.76$; Fig. 4.6). The HREE patterns are almost parallel, whereas LREE patterns gradually increase their slopes with increasing SiO_2 -content, which is typical for fractional crystallization processes (Fig. 4.6a).

REE patterns of the mafic rocks are more gently sloped ($\text{La}_\text{N}/\text{Yb}_\text{N} = 1.93 - 3.66$) than those of the felsic rocks ($\text{La}_\text{N}/\text{Yb}_\text{N} = 3.88 - 8$). Gabbro displays a positive Eu anomaly ($\text{Eu}/\text{Eu}^* = 1.4 - 1.6$). Gabbros have no or only a weak negative Eu anomaly ($\text{Eu}/\text{Eu}^* = 0.9 - 1$; Fig. 4.6a).

The total REE-contents of the fayalite granitoids are higher than those of the fayalite-free granitoids, despite their lower SiO₂-content compared to the fayalite-free granitoids (Fig.4.6a, b). All felsic rocks consistently have negative Eu anomalies ($Eu/Eu^* = 0.85 - 0.29$), which are markedly less pronounced in the fayalite granitoids despite of their higher overall REE-contents (Fig. 4.6a, b).

In primitive-mantle normalized multielement diagrams, all rocks of the Cobquecura Pluton show positive Pb and negative P anomalies and display only a weak Nb-Ta trough (Fig. 4.7). The felsic rocks are richer in incompatible elements (e.g., Rb, Th, and U) than the mafic rocks and display strong negative Sr- and Ti-anomalies. Complementary Eu-, Sr- and Ba-anomalies point to feldspar fractionation, whereas negative Ti-anomalies could indicate ilmenite fractionation (Fig. 4.7a, b). The mafic rocks have weak positive Ba-, Sr- and Ti-anomalies that may indicate accumulation processes of feldspar and ilmenite in the mafic rocks. Among the felsic rocks, the fayalite granitoids show the smallest Eu-, Sr- and Ti-anomalies and among the intrusive rocks they are the richest in compatible elements (e.g., HREE) and HFSE (Zr, Nb and Y).

Most of the variation diagrams of trace elements show a well-defined trend for the whole suite (Fig. 4.8). U, Th, and Pb display a positive correlation with SiO₂ content. Nb increases with increasing SiO₂ content up to 57 wt.% (compositional gap) and decreases from 63 wt.% SiO₂ content. Zr vs. Nb and Y vs. Nb show positively correlated trends with Y-, Zr-, and Nb-poor gabbroic rocks and Y-, Zr-, and Nb-rich felsic rocks (Fig. 4.8).

4.3.2 Metamorphic basement and xenoliths

The metamorphic basement in the Cobquecura area consists of metapelite and quartz-metapsammite with SiO₂ contents between 57.7 and 78.1 wt.%, Al₂O₃ of 10.8-17 wt.%, Fe₂O₃ of 3.2–8.0 wt.%, TiO₂ of 0.6-0.9 wt.% and K₂O of 2.2-3.5 wt.% (Table 4.3). The REE concentrations range between 163 and 203 ppm with uniform REE patterns. They display $La_N/Yb_N = 7.9-8.5$, combined with negative Eu anomalies ($Eu/Eu^* = 0.6-0.7$). The trace element patterns normalized to the average continental crust composition are also rather uniform for most samples and show negative anomalies of Ba, Nb, Ta, Sr, and Ti (Fig. 4.7c). The trace element signatures of the basement around Cobquecura (36°S), of the regional metamorphic basement south of 37°S (Figs. 4.6c, 4.7c), and of North American Shale Composite (NASC, Gromet et al., 1984, not shown) are generally similar.

Restitic xenoliths in gabbro and fayalite granitoid (HLRX and LLRX) contain 46 to 56 wt.% SiO₂, with notably higher content of Al₂O₃ (20 to 26 wt.%), Fe₂O₃ (7.6 to 11.1 wt.%), TiO₂ (0.9 to 1.5 wt.%) and K₂O (1.2 to 6.3 wt.%) than the metamorphic basement around Cobquecura (Table 4.3). These metapelite-restitic xenoliths also are richer in compatible elements (e.g., HREE), in HFSE (Y, Zr, and Nb), and in Th and Pb (15–22 and 12-26 ppm, respectively) than the regionally exposed basement. Restitic xenoliths have high REE contents (218-378 ppm), with

steeper slopes in the REE patterns ($La_N/Yb_N = 7.4\text{--}11.4$) than the exposed metamorphic basement, and a small negative Eu anomaly ($Eu/Eu^* = 0.71\text{--}0.72$). Their U-, Pb-, Nb- compatible element and HFSE contents are similar to those of fayalite granitoid (Figs. 4.7, 4.8). The LLRX have less SiO_2 , K_2O , and Rb, and are enriched in Al_2O_3 , Fe_2O_3 , TiO_2 , REE, and HFSE compared to the HLRX.

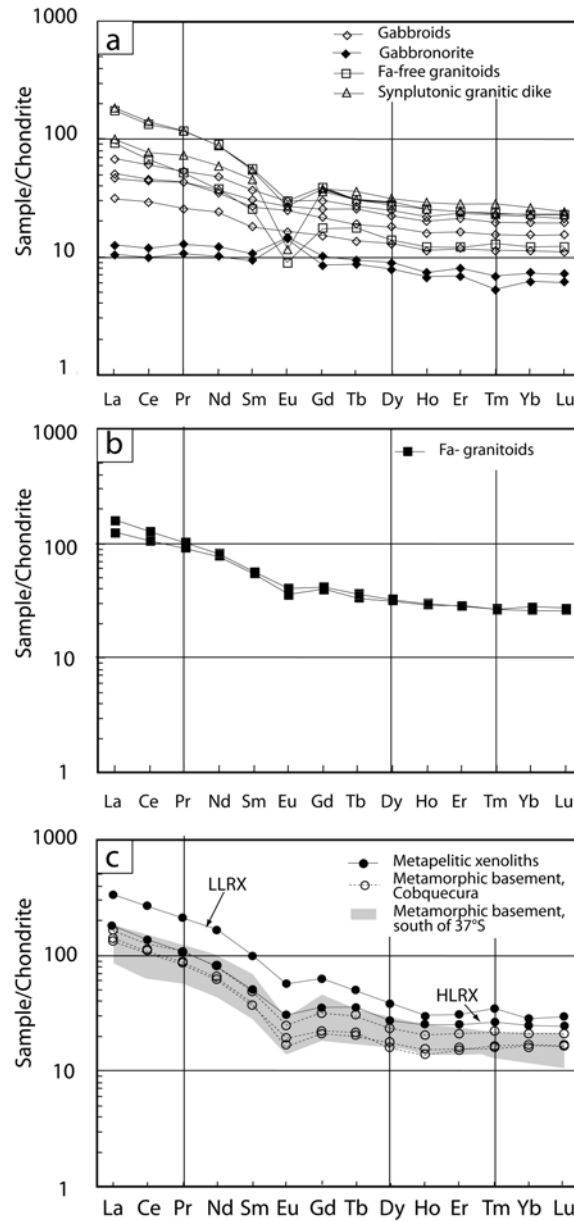


Figure 4.6 Chondrite-normalized rare earth element spectra (cf. McDonough and Sun 1995), Cobquecura Pluton and environs: a) gabbros (48 - 55% wt. SiO_2) and fayalite-free granitoids (67 - 76% wt. SiO_2), b) fayalite granitoids (63 - 72% wt. SiO_2) and c) metamorphic basement in the Cobquecura area and metapelitic xenoliths. The gray area represents the compositions of the Paleozoic metamorphic basement of the Cordillera de la Costa south of the 37°S (adapted from Lucassen et al. 2004).

Table 4.3: Major and trace elements: composition of granitoids, xenoliths and country rocks from the Cobquecura Pluton, Cordillera de la Costa, Chile (~36°S, 72°45'W)

Sample	Mafic rocks				Fayalite granitoids		Fa-free Granites		Granitic dike	Mafic dike	metapelitic xenoliths		Metamorphic Basement		igneous xenoliths	
No	03-11*	03-30*	05-19*	Mafic enclave 03-17*	04-10*	04-19*	03-18*	04-28*	03-10*	03-15*	04-31 HLRX	04-07 LLRX	05-11	05-13	05-06	05-03
SiO ₂	52.9	48.9	48.3	51.2	63.1	66.8	67.5	75.6	76.0	52.1	56.1	46.0	73.3	57.7	49.5	56.7
Al ₂ O ₃	17.8	18.0	18.7	16.2	15.1	14.4	15.2	13.6	12.5	14.0	20.0	26.6	13.1	17.0	16.8	15.7
Fe ₂ O ₃ *	7.74	7.62	6.06	8.65	9.40	7.55	4.67	1.39	1.74	12.4	7.68	11.1	3.91	8.54	10.4	7.95
MnO	0.11	0.12	0.11	0.13	0.15	0.13	0.06	0.03	0.03	0.19	0.08	0.11	0.03	0.06	0.19	0.13
MgO	5.28	9.92	7.76	6.50	0.87	0.50	0.83	0.27	0.25	3.30	2.29	3.69	1.05	2.15	8.55	3.92
CaO	8.35	9.72	13.0	8.54	4.24	2.94	2.56	0.99	0.64	5.44	1.35	2.95	0.19	4.20	9.57	7.18
Na ₂ O	3.41	2.34	2.33	3.47	4.06	4.02	3.69	3.63	3.62	4.01	3.6	3.31	0.81	1.26	2.11	3.35
K ₂ O	1.17	0.61	0.38	1.28	2.40	2.96	2.39	4.19	4.14	1.63	6.34	1.17	2.95	3.53	1.15	1.90
TiO ₂	1.23	0.82	0.54	1.32	0.88	0.65	0.62	0.21	0.12	2.53	0.90	1.58	0.67	0.95	1.30	1.31
P ₂ O ₅	0.16	0.09	0.06	0.16	0.27	0.18	0.13	0.06	0.05	0.38	0.14	0.25	0.10	0.18	0.16	0.22
LOI	1.33	1.47	2.30	1.65	0.41	0.61	1.05	0.55	0.33	2.51	1.85	2.90	3.70	4.05	0.83	1.63
Y	22	16	9	24	37	37	33	21	39	43	43	54	26	35	29	31
Rb	64	29	16	69	120	130	118	211	176	60	205	43	142	159	65	106
Sr	281	225	300	232	205	157	171	82	28	203	168	323	74	97	192	216
Co	33	43	41	32	6	3	7	2	0	24	16	25	2	7	39	21
Ga	20	16	16	18	24	24	23	17	21	24	28	40	20	26	18	20
Nb	7	4	2	6	17	14	13	7	10	13	16	25	12	15	4	7
Pb	7	4	2	6	17	18	20	26	31	15	26	12	14	11	7	14
Th	3	2	0	3	9	11	16	13	17	4	14	22	12	12	1	5
U	0.9	0	0	0.7	2	3	3	5	4	1	4	3	3	3	0	2
Sc	25	21	36	29	28	25	11	4	4	29	22	34	16	18	30	27
Zr	139	80	44	130	226	278	401	107	173	263	171	271	150	162	103	158
La	12	8	2	12	29	37	42	23	24	22	45	76	33	40	7	15
Ce	28	18	6.1	29	64	77	83	46	48	53	89	159	72	84	19	33
Pr	4	2	1	4	8	9	11	5	7	7	10	18	8	10	3	4
Nd	16	11	5	17	35	36	41	18	27	32	38	70	30	37	14	18
Sm	4	3	1	4	8	8	8	4	7	8	7	13	6	7	4	4

Eu	1.4	0.9	0.8	1.4	2.3	2.0	1.7	0.6	0.7	2.4	1.9	3.6	1.7	1.6	1.2	1.5
Gd	4.3	3.0	1.7	4.7	8.2	7.9	7.8	3.4	7.1	8.3	6.7	11.0	4.3	6.3	4.4	4.8
Tb	0.7	0.5	0.3	0.8	1.3	1.2	1.1	0.6	1.3	1.4	1.3	1.9	0.8	1.1	0.9	0.9
Dy	4.5	3.2	1.9	4.9	8.0	7.7	6.8	3.8	7.8	8.6	7.5	10.0	4.6	6.4	5.3	5.5
Ho	0.9	0.6	0.4	1.0	1.6	1.6	1.4	0.7	1.6	1.8	1.4	1.9	0.9	1.2	1.0	1.1
Er	2.6	1.9	1.1	3.0	4.5	4.5	3.9	2.1	4.6	5.0	4.2	5.4	2.8	3.6	2.9	3.1
Tm	0.38	0.28	0.13	0.43	0.67	0.65	0.58	0.33	0.71	0.75	0.66	0.80	0.43	0.53	0.43	0.46
Yb	2.5	1.8	1.0	2.8	4.2	4.4	3.7	2.1	4.2	4.7	4.3	5.2	2.9	3.5	2.8	2.9
Lu	0.38	0.27	0.15	0.43	0.64	0.66	0.57	0.31	0.59	0.72	0.63	0.77	0.45	0.52	0.40	0.44

(*) Major elements are from Vásquez and Franz (2008).

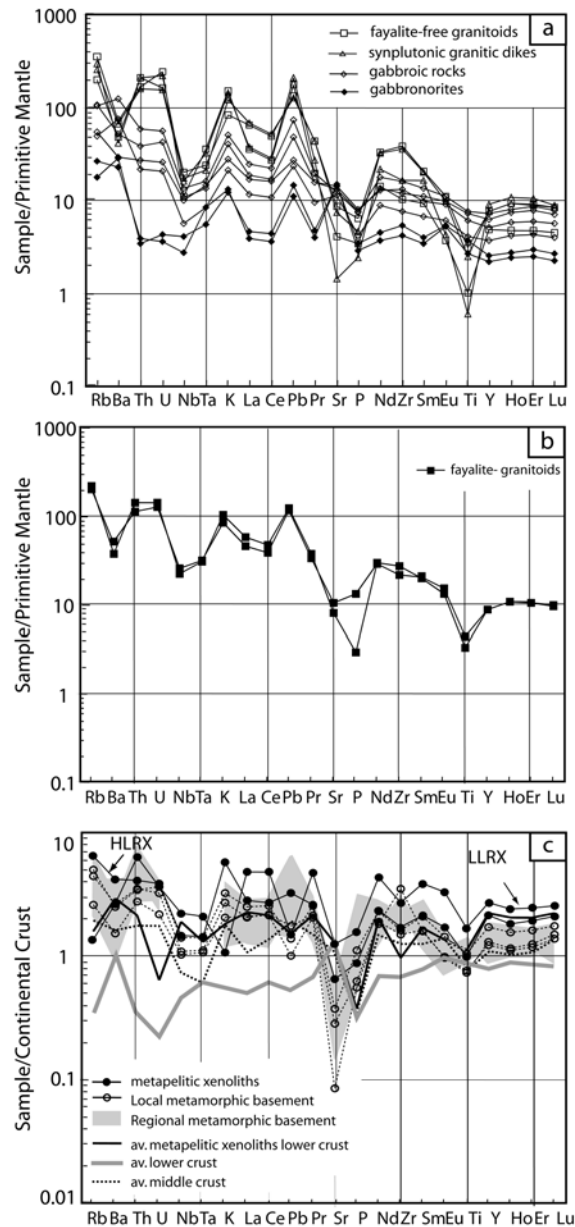


Figure 4.7 Primitive mantle-normalized (McDonough and Sun 1995) trace element diagrams for a) Gabbros (48 - 55% wt. SiO_2) and fayalite-free granites (67 - 76%wt. SiO_2) b) Fayalite granites and c) Continental crust-normalized (Taylor and McLennan 1995) multielement diagrams for rocks from the metamorphic basement at the Cobquecura area and metapelitic xenoliths. The gray area represents the compositions of the Paleozoic metamorphic basement at the Cordillera de la Costa south of the 37°S (adapted from Lucassen et al. 2004).

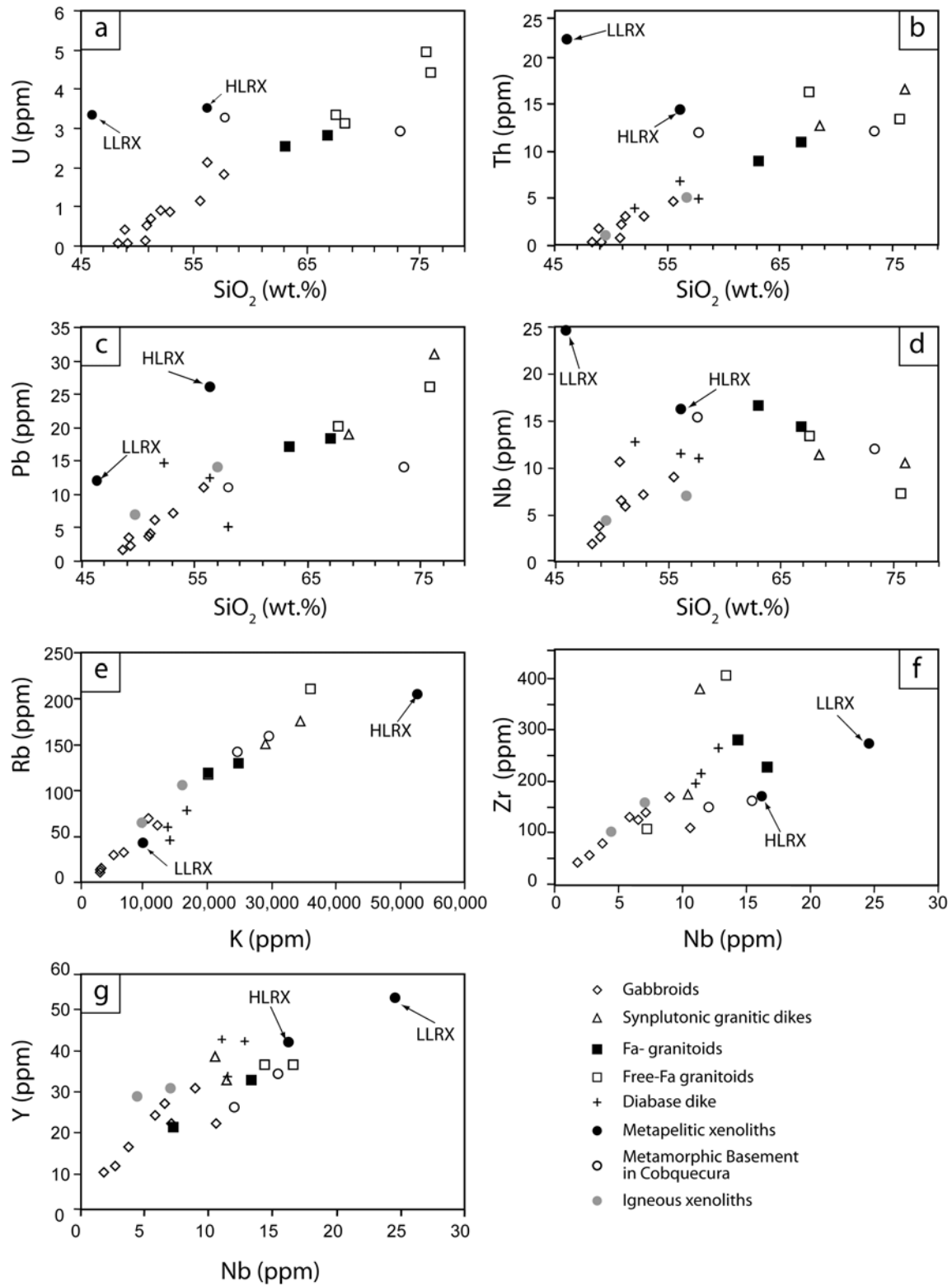


Figure 4.8 Correlations of trace element concentrations with SiO₂, and trace element intercorrelations in the Cobquecura intrusive suite.

4.4 Pb, Nd and Sr isotopic composition

We analyzed 22 whole rock samples from the Cobquecura Pluton, its different enclaves and xenoliths, and the surrounding metamorphic basement for Nd-Sr-Pb isotopic composition (see Appendix C for methodology).

Results are presented in Table 4.4 and in Figures 4.9 and 4.10.

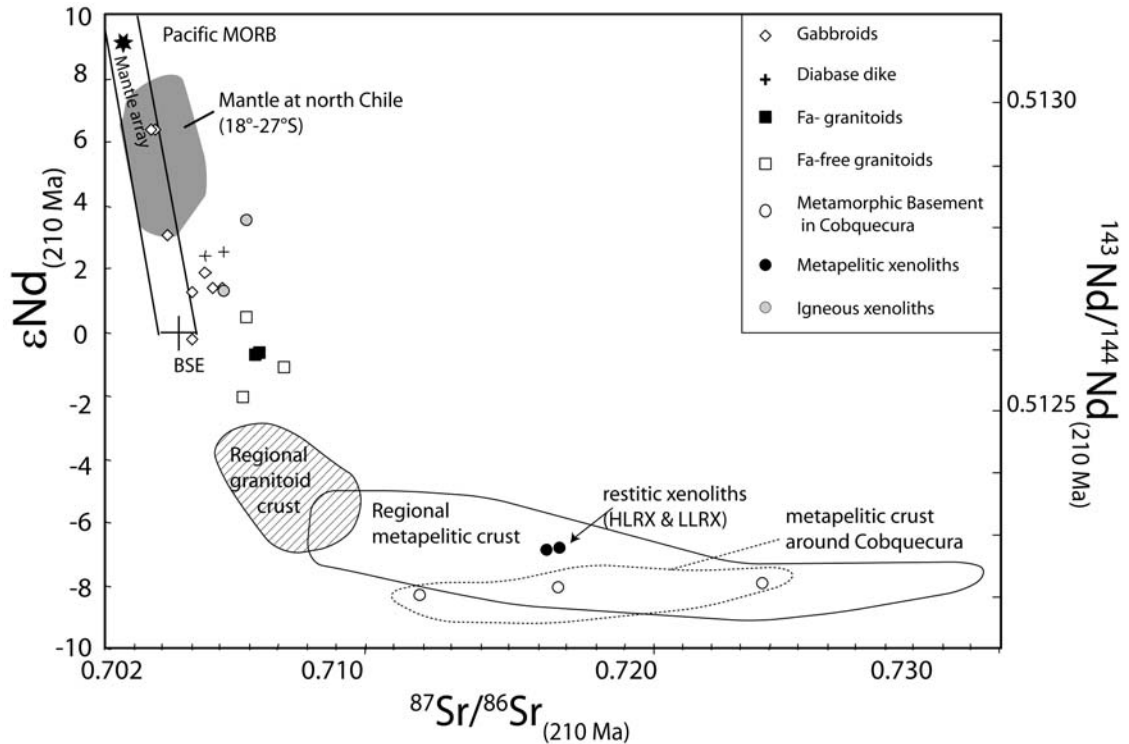


Figure 4.9 Initial Nd and Sr isotopic compositions (at 210 Ma), Cobquecura Pluton and related rocks. Fields are shown for a) the regional metapelitic crust and the regional granitoid crust (Southern Coastal Batholith 30-38°S and metamorphic basement of the Chilean Coastal Cordillera (36° - 41°S; Parada et al. 1999, Lucassen et al. 2004), b) the subarc subcontinental mantle of northern Chile (18° - 27°S; Lucassen et al. 2006), c) average of the Pacific MORB (Petrological database of the ocean floor <http://petdb.org>); the Nd isotope composition is corrected for in-situ decay to 210 Ma using a $^{147}\text{Sm}/^{144}\text{Nd}$ ratio of 0.214; d). Sr isotope composition of Bulk Silicate Earth (BSE) is calculated at 210 Ma assuming a Rb/Sr ratio of 0.03 (McDonough and Sun 1995) and a present day $^{87}\text{Sr}/^{86}\text{Sr}$ of 0.7045 (Salters and Stracke 2004). Mantle array field was taken from Dickin 1997.

Table 4.4: Whole-rock Sr, Nd and Pb isotope data of granitoids, xenoliths and of country rocks from the Cobquecura Pluton, Cordillera de la Costa, Chile (~36°S)

Sample ^a N°	Lithologic unit	Rock type	Age Ma	Rb ppm	Sr ppm	⁸⁷ Sr ^b ⁸⁶ Sr	⁸⁷ Sr _(T) ^c ⁸⁶ Sr	Nd ppm	Sm ppm	¹⁴³ Nd ^b ¹⁴⁴ Nd	εNd _{c(T)}	Pb ppm	U ppm	Th ppm	²⁰⁶ Pb ^d ²⁰⁴ Pb	²⁰⁷ Pb ^d ²⁰⁴ Pb	²⁰⁸ Pb ^d ²⁰⁴ Pb	²⁰⁶ Pb ^e ²⁰⁴ Pb	²⁰⁷ Pb ^e ²⁰⁴ Pb	²⁰⁸ Pb ^e ²⁰⁴ Pb
05-19	Cobquecura Pluton	Gabbronorite	203±2	16	300	0.704156±7	0.70373	5	1.4	0.512948±8	6.4	2	0.1	0.3	18.728	15.652	38.737	18.63	15.65	38.60
05-17	Cobquecura Pluton	Gabbronorite	203±2	11	297	0.703854±7	0.70355	6	1.6	0.512937±6	6.4	2	0.1	0.3	18.512	15.634	38.441	18.42	15.63	38.35
04-22	Cobquecura Pluton	Gabbronorite	203±2	13	291	0.705344±9	0.70498	13	3.7	0.512671±6	1.3	4	0.1	0.7	18.525	15.636	38.577	18.44	15.63	38.44
04-19	Cobquecura Pluton	Fa-Granitoid	209±2	130	157	0.714081±9	0.70719	36	8.0	0.512518±5	-0.7	18	2.8	11.0	18.603	15.661	38.659	18.22	15.64	38.20
04-10	Cobquecura Pluton	Fa-Granitoid	209±2	120	205	0.712219±9	0.70735	35	8.2	0.512532±5	-0.6	17	2.5	8.9	18.564	15.640	38.512	18.20	15.62	38.12
03-30	Cobquecura Pluton	Gabbro	209±2	29	224	0.705258±9	0.70418	11	2.7	0.512729±5	3.1	4	0.4	1.7	18.609	15.659	38.619	18.32	15.64	38.24
03-27	Cobquecura Pluton	Gabbro	209±2	33	260	0.706037±7	0.70498	17	4.5	0.512576±7	-0.2	4	0.5	2.1	18.849	15.669	39.046	18.54	15.65	38.64
03-18	Cobquecura Pluton	Fa-free Granitoid	209±2	118	171	0.713876±7	0.70813	41	8.4	0.512484±5	-1.1	20	3.3	16.4	18.721	15.643	38.718	18.32	15.62	38.09
03-17	Cobquecura enclave	Microgabbro	209±2	69	232	0.707895±7	0.70542	17	4.3	0.512678±4	1.9	6	0.7	3.0	18.865	15.664	38.786	18.59	15.65	38.40
03-15	Cobquecura dike	Microgabbro	209±2	60	202	0.707932±9	0.70546	32	7.9	0.512698±6	2.4	15	0.9	3.9	18.585	15.608	38.500	18.44	15.60	38.29
03-14	Cobquecura dike	Granite	209±2	151	149	0.715335±9	0.70689	40	8.1	0.512483±4	0.5	19	3.1	12.7	18.959	15.647	39.046	18.56	15.63	38.52
03-13	Cobquecura Pluton	Monzogabbro	209±2	62	244	0.708149±9	0.70603	22	5.5	0.512649±4	1.4	11	1.1	4.6	18.875	15.666	38.907	18.62	15.65	38.58
03-11	Cobquecura Pluton	Gabbro	209±2	64	281	0.707607±9	0.70571	16	4.0	0.512645±5	1.4	7	0.9	3.1	18.657	15.642	38.779	18.35	15.63	38.01
05-11	Cobquecura, country rock	Metapelite	298	71	132	0.733701±9	0.71089	30	5.7	0.512122±4	-7.2	14	3.9	12.2	18.924	15.662	39.072	18.19	15.62	38.11
05-13	Cobquecura, country rock	Metapelites	298	80	105	0.736040±7	0.71997	38	7.3	0.512114±5	-6.9	11	3.3	12.0	19.022	15.654	39.089	17.97	15.60	37.88
04-31	Cobquecura, xenoliths	Metapelites	298	85	91	0.726557±9	0.71333	38	7.4	0.512182±5	-6.0	26	3.5	14.5	18.723	15.632	38.688	18.25	15.61	38.08
04-07	Cobquecura, xenoliths	Metapelitic Restite	298	22	15	0.718326±9	0.71749	77	13	0.512183±5	-5.9	12	3.3	22.0	18.906	15.654	39.055	17.93	15.60	37.02
04-28	Cobquecura Pluton	Fa-free Granite	209±2	73	200	0.730518±7	0.70675	18	3.8	0.512447±4	-1.9	26	5.0	13.4	18.892	15.679	38.932	18.43	15.66	38.53
05-06	Cobquecura xenoliths	Microgabbro	210	141	19	0.708049±8	0.70686	14	4.0	0.512729±5	3.5	7	0.3	1.0	18.539	15.635	38.498	18.44	15.63	38.39
04-21	Cobquecura dike	Microgabbro	210	207	36	0.707559±8	0.70608	26	6.0	0.512689±4	2.5	5	1.8	4.4	19.483	15.684	39.380	18.59	15.64	38.68
05-03	Cobquecura, xenoliths	Microgabbro	209±2	211	86	0.709643±9	0.70611	18	4.5	0.512645±5	1.3	14	1.6	5.0	18.720	15.645	38.678	18.44	15.63	38.40

- a Samples were dissolved with 52% HF for four days at 160°C on the hot plate. Digested samples were dried and taken up in 6N HCl. Sr and Nd were separated and purified using ion-exchange chromatography as described in Romer et al. (2005). Pb was separated using the HBr-HCl ion-exchange procedure as described in Romer et al. (2005)
- b $^{87}\text{Sr}/^{86}\text{Sr}$ and $^{143}\text{Nd}/^{144}\text{Nd}$ normalized to $^{87}\text{Sr}/^{86}\text{Sr} = 0.1194$ and $^{143}\text{Nd}/^{144}\text{Nd} = 0.7219$ respectively. Isotopic data for Sr and Nd were obtained on a VG54 and Finnigan MAT262 multi-collector TIMS mass-spectrometer using dynamic multicollection respectively. Analytical uncertainties are given at 2σ level.
- c $^{87}\text{Sr}/^{86}\text{Sr}_{(\text{T})}$ and $\varepsilon\text{Nd}_{(\text{T})}$ were calculated for the time of the intrusion using $\lambda^{87}\text{Rb} = 1.42\text{E-}11 \text{ y}^{-1}$ and $\lambda^{147}\text{Sm} = 6.54\text{E-}12 \text{ y}^{-1}$, $(^{147}\text{Sm}/^{144}\text{Nd})_{0\text{CHUR}} = 0.1967$, $(^{143}\text{Nd}/^{144}\text{Nd})_{0\text{CHUR}} = 0.512638$ and the concentration data given in Table 4.2.
- d Lead isotope data were obtained on a Finnigan MAT262 multi-collector TIMS mass-spectrometer using static multicollection. Lead isotope data were corrected for mass discrimination with 0.1% / A.M.U. Reproducibility at 2σ level is better than 0.1%.
- e Lead isotope data recalculated to the age of intrusions using the contents of Pb, Th and U (Vásquez et al. 2005, Vásquez et al. 2008b.) and the constants recommended by IUGS (Steiger and Jäger 1977).

4.4.1 Intrusive rocks

$^{87}\text{Sr}/^{86}\text{Sr}_i$ (at 210 Ma) ratios of Cobquecura Pluton igneous rocks range from 0.703 to 0.708 with dominantly positive εNd_i between 6.4 and -1.9 (Fig. 4.9). $^{87}\text{Sr}/^{86}\text{Sr}_i$ ratios of gabbros (0.703 - 0.706) are well correlated with the SiO_2 -content (Fig. 4.11); their εNd_i values range from 6.4 to -0.2 (Fig. 4.9). Fayalite granitoids have $^{87}\text{Sr}/^{86}\text{Sr}_i$ near 0.707 and εNd_i from -0.6 to -0.7 , similar to the more differentiated gabbroic rocks (Fig. 4.9), whereas the fayalite-free granitoids have slightly more negative εNd_i values (0.5 to -1.9), but display similar $^{87}\text{Sr}/^{86}\text{Sr}_i$ ratios (0.707-0.708). $^{87}\text{Sr}/^{86}\text{Sr}_i$ and εNd_i ratios in fayalite granitoids and fayalite-free granitoids display no correlation with SiO_2 (Fig. 4.11).

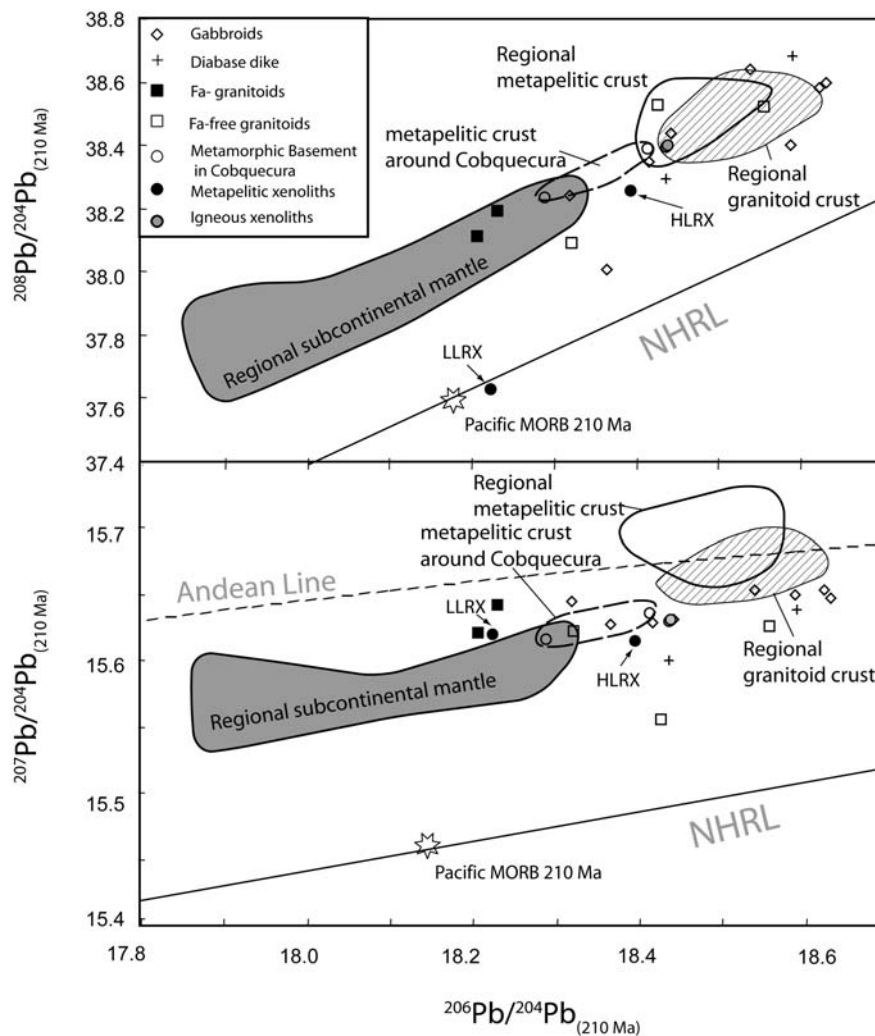


Figure 4.10 Initial Pb isotopic composition of the Cobquecura Pluton. Average of the continental crust (Coastal Cordillera of Chile 36° - 41°S) calculated at 210 Ma using data of Lucassen et al 2004. Average of the Mesozoic magmatic arc of northern Chile (18 - 27°S) calculated at 210 Ma (data of Lucassen et al. 2006). Pacific MORB at 210 Ma (Petrological database of the ocean floor <http://petdb.org>). Northern hemisphere reference line (NHRL; Hart 1984).

Pb initial ratios range from 18.27 - 18.66 ($^{206}\text{Pb}/^{204}\text{Pb}_i$), 15.6 - 15.66 ($^{207}\text{Pb}/^{204}\text{Pb}_i$), and 38.15 - 38.68 ($^{208}\text{Pb}/^{204}\text{Pb}_i$), respectively. They plot below the Andean Pb-line as defined by

Lucassen et al. (2002) that shows the evolution of the average Andean crust (Fig. 4.10). $^{206}\text{Pb}/^{204}\text{Pb}_i$ ratios show a trend from 18.31 - 18.62 in gabbros through 18.42 - 18.55 in fayalite-free granitoids to 18.22 - 18.25 in fayalite granitoids. Gabbros and fayalite granites display similar $^{207}\text{Pb}/^{204}\text{Pb}_i$ of 15.60 - 15.65, and $^{208}\text{Pb}/^{204}\text{Pb}_i$ of 38.01 - 38.68. Fayalite-free granitoids show similar but restricted $^{208}\text{Pb}/^{204}\text{Pb}_i = 38.09 - 38.22$, and a wider range of $^{207}\text{Pb}/^{204}\text{Pb}_i = 15.62 - 15.66$ isotopic ratios than the gabbros and fayalite granitoids. Pb isotopes of the entire suite are not correlated with the SiO_2 -content (not shown).

4.4.2 Metamorphic basement and xenoliths

The metamorphic basement in the Cobquecura area displays $^{87}\text{Sr}/^{86}\text{Sr}_{(210\text{Ma})}$ ratios from 0.712 to 0.724 with strongly negative $\epsilon\text{Nd}_{(210\text{Ma})}$ values (-7.9 to -8.3) (Fig. 4.9). It shows a broad range of $^{206}\text{Pb}/^{204}\text{Pb}_{(210\text{Ma})}$ ratios (18.29 to 18.41), $^{207}\text{Pb}/^{204}\text{Pb}_{(210\text{Ma})}$ (15.61 to 15.64), and $^{208}\text{Pb}/^{204}\text{Pb}_{(210\text{Ma})}$ (37.23 to 38.39) (Fig. 4.10).

The restitic xenoliths (HLRX and LLRX) show $^{87}\text{Sr}/^{86}\text{Sr}_{(210\text{Ma})}$ ratios and $\epsilon\text{Nd}_{(210\text{Ma})}$ values similar to the surrounding regional metamorphic basement (0.713 to 0.717 and ~ -6 , respectively). However, the $^{206}\text{Pb}/^{204}\text{Pb}_{(210\text{Ma})}$, $^{207}\text{Pb}/^{204}\text{Pb}_{(210\text{Ma})}$ and $^{208}\text{Pb}/^{204}\text{Pb}_{(210\text{Ma})}$ ratios of the restitic xenoliths tend to be lower than those of the regional metamorphic basement, with ranges between 18.22-18.39 (6/4), 15.61-15.62 (7/4) and 37.63–38.26 (8/4), respectively, with more radiogenic lead in the HLRX than in the LLRX (Fig. 4.10).

The igneous xenoliths enclosed by the magmatic breccia present Sr-Nd-Pb compositions that fall in the range of those of the gabbroic rocks ($^{87}\text{Sr}/^{86}\text{Sr}_i \sim 0.706$, $\epsilon\text{Nd}_i = 1.3-3.5$, $^{206}\text{Pb}/^{204}\text{Pb}_{(210\text{Ma})} \sim 18.44$, $^{207}\text{Pb}/^{204}\text{Pb}_{(210\text{Ma})} \sim 15.63$, and $^{208}\text{Pb}/^{204}\text{Pb}_{(210\text{Ma})} = 38.39-38.40$).

4.5 Discussion

4.5.1 Nature of the continental crust

Late Paleozoic granitoids and metapelites form the upper crust at the present outcrop level of the Central Chilean continental margin. The formation of the upper crust in this segment is mainly related to recycling of Proterozoic continental basement in a continental margin setting, with a resulting composition close to the average of the old continental crust of SW Gondwana (as described by Lucassen et al. 2004). This upper crust is isotopically and lithologically relatively homogeneous along the Chilean continental margin (Lucassen et al. 2004). The granitoid crust displays higher ϵNd_i and $^{206}\text{Pb}/^{204}\text{Pb}_i$, lower $^{87}\text{Sr}/^{86}\text{Sr}_i$ and similar $^{207}\text{Pb}/^{204}\text{Pb}_i$ and $^{208}\text{Pb}/^{204}\text{Pb}_i$ compared to values of the metapelitic crust. It has similar petrological, geochemical, Sr-Nd and $^{206}\text{Pb}/^{204}\text{Pb}_i$ characteristics and displays slightly lower $^{207}\text{Pb}/^{204}\text{Pb}_i$ and similar $^{208}\text{Pb}/^{204}\text{Pb}_i$ ratios than the rest of the metamorphic basement along the Chilean margin south of 37°S (Fig. 4.10). The

metamorphic metapelitic crust displays a homogeneous and narrow composition in Pb isotopes ($^{206}\text{Pb}/^{204}\text{Pb}_{(210\text{Ma})}$ 18.14 - 18.6, $^{207}\text{Pb}/^{204}\text{Pb}_{(210\text{Ma})}$ 15.64 - 15.70 and $^{208}\text{Pb}/^{204}\text{Pb}_{(210\text{Ma})}$ 38.1 - 38.6), $\epsilon\text{Nd}_{(210\text{Ma})}$ (-5 to -9) and displays a wide range of $^{87}\text{Sr}/^{86}\text{Sr}_{(210\text{Ma})}$ ratios (Figs. 4.9, 4.10).

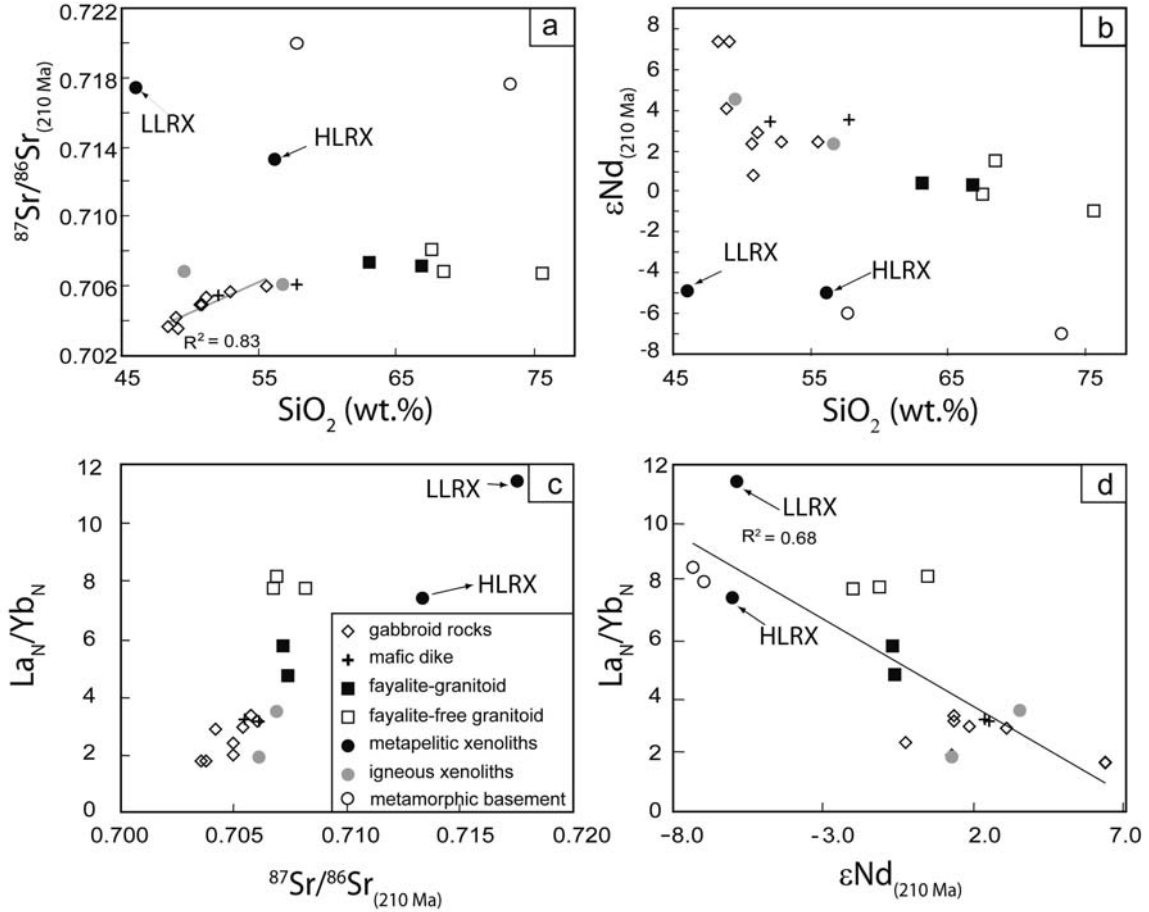


Figure 4.11 Sr-Nd initial isotopic ratios vs. SiO_2 -content and $\text{La}_\text{N}/\text{Yb}_\text{N}$ ratios: a) Initial $^{87}\text{Sr}/^{86}\text{Sr}$ vs. SiO_2 -content. The correlation line shows the good correlation present in the gabbroids ($r = 0.8$), b) $\epsilon\text{Nd}_{(210\text{Ma})}$ vs. SiO_2 -content, with no obvious correlation in gabbroic rocks. c) $^{87}\text{Sr}/^{86}\text{Sr}_{(210\text{Ma})}$ vs. $\text{La}_\text{N}/\text{Yb}_\text{N}$ ratios (chondrite-normalized), d) $\epsilon\text{Nd}_{(210\text{Ma})}$ vs. $\text{La}_\text{N}/\text{Yb}_\text{N}$ ratios.

The restitic xenoliths (HLRX and LLRX) of the Cobquecura Pluton have distinctive petrographical, geochemical and isotopic characteristics with respect to the metamorphic basement neighboring the Cobquecura Pluton as well as to the xenoliths that come from this basement. The restitic xenoliths (HLRX and LLRX) are rich in hercynite and cordierite, a typical paragenesis for metapelites at upper amphibolite to granulite facies. The association cordierite – hercynite – quartz, without garnet, is stable at high temperatures at a pressure of 2 to 8 kbar (Bucher and Frey, 2002; Spear 1993). Some of these restitic xenoliths preserve layers of granitic leucosomes, reflecting a stage of anatexis melting. The compositional layering with both hercynite and cordierite, which follow the main foliation, is indicative for an origin of these minerals by regional rather than contact metamorphism by the intrusives. The low leucosome contents in LLRX, compared to those included in fayalite granitoid suggests that the former had experienced a stage of melt extraction

(with a melt composition like the leucosome of the HLRX). The increasing REE and HFSE contents, and decreasing Rb, K₂O and Pb, with decreasing leucosome-content from the HLRX to the LLRX, is probably related to the early feldspar melting during leucosome formation, and subsequent extraction of felsic melt. Furthermore, the high contents of Th, HFSE and REE in the LLRX with scarce leucosome are related to the presence of zircon, apatite, monazite and xenotime in the leucosome.

The restitic xenoliths (HLRX and LLRX) have, compared to the average value for metapelitic xenoliths of granulite or amphibolite facies conditions (Rudnick and Fountain 1995), similar compatible element and Rb contents, but are enriched in Th. The xenoliths display similar Sr-Nd initial isotopic ratios to those from the local and regional Cobquecura crust (Figs. 4.9, 4.10). Their ²⁰⁷Pb/²⁰⁴Pb ratios are slightly lower than typical for the regional upper continental crust (Figs. 4.9, 4.10), but are similar to those from the local Cobquecura crust. However, the xenoliths display high La_N/Yb_N ratios (Figs. 4.6, 4.11), are richer in FeO, Al₂O₃, TiO₂, Th, REE, and HFSE concentration and display lower ²⁰⁸Pb/²⁰⁴Pb and ²⁰⁶Pb/²⁰⁴Pb ratios than the surrounding metapelitic basement. These geochemical differences, together with the higher metamorphic grade and the restitic nature of the xenoliths, suggest that they were not derived from the surrounding metamorphic basement, but from a “deeper level” with a different history, probably from the middle crust. The enrichment combined with low initial (at 210 Ma) ²⁰⁸Pb/²⁰⁴Pb ratios (Fig. 4.10) indicates that the restitic xenoliths do not represent ancient deep crust but that today's geochemical signatures were acquired in the Phanerozoic.

4.5.2 Mantle-derived melts and crustal influence

The most primitive rocks in the Cobquecura Pluton are gabbro-norites. They display the highest εNd_i, the lowest ⁸⁷Sr/⁸⁶Sr_i ratios and show the most depleted incompatible element signatures of the entire suite. Their Nd-Sr isotope signature is similar to that of other primitive magmatic rocks along the Chilean Mesozoic arc, which are considered to reflect the composition of the subarc subcontinental mantle including additions from the subduction zone (Lucassen et al. 2006). The subarc subcontinental mantle shows lower εNd_i and higher ⁸⁷Sr/⁸⁶Sr_i values than the asthenospheric Pacific oceanic mantle, the source of MORB (source: <http://www.petdb.org>) at 210 Ma (Fig. 4.9). The increase of ⁸⁷Sr/⁸⁶Sr_i ratios of 0.703-0.706 with εNd_i decreasing from 6.4 to -0.2 indicates contamination of the mantle-derived melts by significant amounts of continental crust. Accordingly, the gabbroic rocks display higher ²⁰⁷Pb/²⁰⁶Pb and ²⁰⁸Pb/²⁰⁴Pb ratios than the subarc subcontinental mantle and Pacific MORB at 210 Ma. The absence of negative Eu- and Sr-anomalies and the low ratios of La_N/Yb_N (1.7-3.3) in the mafic rocks suggest that neither plagioclase nor garnet were residual phases in their source (Vásquez et al. 2008b). The LILE enrichment, the positive Pb anomaly and the negative Nb-Ta trough present in both gabbros and

granitoids (Fig. 4.7) are typical of magmatic rocks generated in continental magmatic arcs (e.g., Hawkesworth et al. 1993).

4.5.3 Petrogenesis of the Cobquecura Pluton

Previous models have explained the fayalite granitoids as granitic residual melts from the fractional crystallization of mafic magmas (i.e., Pitcher 1997; Frost and Frost 1997; Turner et al. 1992). Another hypothesis is that fayalite granitoids originate from partial melting of a dehydrated source, like granulites of the lower continental crust (e.g., Collins et al. 1982). Possible regional sources for the formation of the fayalite granitoids of the Cobquecura Pluton are the subarc-subcontinental mantle, Late Paleozoic upper continental crust (granitic and metamorphic) or a deeper level crust represented by the restitic xenoliths described above. It is noteworthy that the restitic xenoliths (HLRX and LLRX) were not found in fayalite-free granitoids. Based on the field, petrographic and geochemical characteristics, possible processes contributing to fayalite granitoids petrogenesis are fractional crystallization and assimilation of the continental crust. These processes and the role of the possible sources in the generation of the fayalite granitoids magmas are evaluated in the next sections.

Evidence of fractional crystallization

Major and trace element arrays demonstrate that fractional crystallization and accumulation processes were important in the petrogenesis of the Cobquecura magmas. CaO, K₂O and MgO display coherent arrays in Harker diagrams and the X_{Mg} of mafic minerals displays an excellent correlation with the X_{Mg} of the corresponding whole rock (Vásquez and Franz 2008). Fractional crystallization processes are also indicated by the correlations of trace element contents such as Y and Nb (Fig. 4.8g) and the complementary Ba- Eu- and Sr-anomalies displayed by the gabbros and granites in the primitive mantle normalized multielement diagrams and the REE patterns, respectively (Figs. 4.6, 4.7). An exclusive origin of the fayalite granitoids by fractional crystallization from the primitive mafic magmas can be ruled out by their different Sr-Nd isotope signatures (Fig. 4.9). However, it is remarkable that fayalite granitoid and the more contaminated gabbros display similar ϵNd_i (Fig. 4.9), suggesting an origin of this granitoid from the more contaminated gabbros. For pure fractional crystallization processes, parallel patterns with increasing contents of REE and more pronounced negative Eu-anomalies with increasing differentiation could be expected. However, although the REE-patterns are fairly parallel (Fig. 4.6), fayalite-bearing granitoids (63 - 71 wt.% SiO₂) have higher REE contents and smaller negative Eu-anomalies than the fayalite-free granitoids (67 - 76 wt.% SiO₂) (Fig. 4.6). Therefore, the REE patterns disagree with an origin for the fayalite granitoids from closed-system fractional crystallization from a mafic magma. Instead, the fayalite granitoids must have originated from

open-system fractional crystallization from a gabbroic, mantle-derived magma with associated assimilation processes.

Assimilation processes

The Cobquecura Pluton displays abundant field evidence for assimilation of metapelitic crust, such as foreign metapelitic xenoliths with quartz-feldspar rich assimilation aureoles (Fig. 4.3). The average isotopic composition of the upper crust at the outcrop level is ϵNd_i of -5.9 , $^{87}\text{Sr}/^{86}\text{Sr}_i$ of 0.71 and $^{207}\text{Pb}/^{204}\text{Pb}_i$ of 15.68 (values taken from Lucassen et al. 2004). The restitic xenoliths, representing a deeper crust, are even more radiogenic in $^{87}\text{Sr}/^{86}\text{Sr}_i$ compared to Cobquecura signatures of $^{87}\text{Sr}/^{86}\text{Sr}_i < 0.707$ and $\epsilon\text{Nd}_i > -2$ (Fig. 4.9, Table 4.4). These isotope signatures indicate that the above crustal lithologies are not the only and apparently not even the dominant sources for Cobquecura granitoids. The primitive mafic rocks of the Cobquecura Pluton have compositions of ϵNd_i of 6.4 , $^{87}\text{Sr}/^{86}\text{Sr}_i$ of 0.703 , close to the regional sub-arc mantle, but show considerably higher $^{207}\text{Pb}/^{204}\text{Pb}_i$ ratios. This points to a mantle source contaminated with minor amounts of crust characterized by more radiogenic lead, similar to that of the regional granitoid crust (Fig. 4.10). Therefore, the Pb, Nd, and Sr isotope compositions of the Cobquecura Pluton rule out a magma source exclusively from the upper crust, deeper crust or the mantle.

The good correlation between the $^{87}\text{Sr}/^{86}\text{Sr}_i$ ratios and the SiO_2 for the gabbroic rocks (Fig. 4.11) also suggests that the fractional crystallization processes were accompanied by assimilation of ambient crust. The strong positive correlation of the $^{87}\text{Sr}/^{86}\text{Sr}_i$ ratios with SiO_2 -contents and La_N/Yb_N suggests an increasing assimilation of a deeper crust (similar to the LLRX leucosome) during the differentiation (Fig. 4.11). The Pb isotopic composition is a very sensitive tracer for crustal assimilation because of the relatively high Pb content of crustal compared to mantle sources. At the Chilean continental margin, the regional continental crust and subarc subcontinental mantle also show distinct Pb isotopic compositions. The latter displays similar $^{206}\text{Pb}/^{204}\text{Pb}_i$ but higher $^{207}\text{Pb}/^{204}\text{Pb}_i$ and $^{208}\text{Pb}/^{204}\text{Pb}_i$ ratios compared to the continental crust (Fig. 4.10). The crustal restitic xenoliths included in the intrusives of Cobquecura take up an intermediate position between the upper continental crust and the subarc subcontinental mantle with respect to the $^{207}\text{Pb}/^{204}\text{Pb}_i$ ratios.

The fayalite bearing granitoids and the fayalite-free granitoids display many differences such as the content of Al- and Fe-rich restitic xenoliths, the higher REE and HFSE content (Figs. 4.6, 4.7, 4.8) and the H_2O poor- Fe-rich mineralogy and consequently a lower $f\text{O}_2$ and H_2O activity in the former. This shows that assimilation of a Fe-rich medium or deep continental crust compositionally similar to the Al- and Fe-rich restitic xenoliths and different from the exposed upper crust could be an important process in the petrogenesis of the fayalite granitoids. The relatively elevated $a_{\text{H}_2\text{O}}$, $f\text{O}_2$ and $^{206}\text{Pb}/^{204}\text{Pb}_i$ of the fayalite-free granitoids with respect to those of

fayalite granitoids suggest an assimilation of a more hydrated crust, similar to the upper crust at the outcrop level, during the fractional crystallization. Furthermore, the fayalite granitoids crystallized at oxygen fugacities below the fayalite-magnetite-quartz (FMQ) buffer (Vásquez and Franz 2008), which suggests a major influence of reduced sources. Both the primitive mafic rocks (with their presence of sulphide phases) and restitic xenoliths (HLRX and LLRX, with their occasional presence of sulphide and Fe²⁺-rich minerals, like hercynite and cordierite) display indications for low oxygen fugacities, which is consistent with the low oxygen fugacities recorded by the fayalite granitoids (this work, and Vásquez and Franz 2008).

Selective assimilation processes

Anatectic processes are indicated by the presence of the pair restite-leucosome in the restitic xenoliths, and may facilitate selective assimilation processes (c.f. Hogan and Sinha 1991, Zeng et al. 2005). Selective assimilation of restitic crust is suggested by field evidence (Fig. 4.3), and is also indicated by the chemical and isotopic behavior of the Cobquecura rocks. The differences in the leucosome composition present in the restitic xenoliths included in the Cobquecura Pluton suggest two types of leucosome: a feldspar-rich, accessory minerals-poor leucosome of the HLRX, and a feldspar-poor, accessory mineral-rich leucosome of the LLRX.

The leucosome of the HLRX is generated in an anatectic process and represents an initial and feldspar-quartz rich melt (minimum melt), with a remaining zircon – monazite - rich residuum. Fayalite-free granitoids could have been generated through the assimilation of a melt similar to the leucosome of the HLRX. The paragenesis of potassic feldspar, plagioclase and quartz suggest a low melt temperature similar to the eutectic melt in granitic system, i.e. ca. 650°C. After this first-stage melt extraction processes and with an increasing degree of melting, the ‘later’ melt will increase the zircon and monazite content and decrease the feldspar content as it is observed in the leucosome of the LLRX. The modal differences in feldspar, zircon, apatite, monazite and xenotime between the leucosomes of the HLRX and LLRX lead to differences in the Rb, K₂O, Pb, Th, HFSE, and REE contents and initial Pb, Sr and Nd isotopic ratios in the restitic xenoliths included in gabbros and fayalite granitoids.

The initial Pb isotopic composition of anatectic melts are a mixture of Pb derived from major minerals with characteristic low ²³⁸U/²⁰⁴Pb and ²³²Th/²⁰⁴Pb ratios (i.e. feldspar) with Pb contributed from dissolved accessory minerals with characteristically high ²³⁸U/²⁰⁴Pb and ²³²Th/²⁰⁴Pb ratios (i.e. zircon, monazite) (Hogan and Sinha 1991). In the Cobquecura Pluton, LLRX with low leucosome content and higher accessory mineral contents display lower initial Pb isotopic composition than the HLRX with high leucosome content and lower accessory mineral contents. This observation calls for a two-step evolution that can be explained in two different ways:

- A first generation of leucosome of the HLRX is composed of plagioclase, potassic feldspar and quartz. The early new feldspars that compose the leucosome of the HLRX would be enriched in radiogenic Pb, partially released by both dissolution of accessory minerals like zircon, monazite, or xenotime, and by Pb loss from such phases. After melt extraction from HLRX-type xenoliths, continued or renewed melting leads to the development of LLRX xenoliths. Their leucosome consists of quartz, biotite, less feldspar and abundant newly crystallized accessory minerals like zircon and monazite. Element sources for the new accessory minerals may have been Zr- and REE-bearing phases of the protolith, (like older zircon and monazite), which also supplied the unradiogenic Pb now dominating the whole rock (see Fig. 4.10). The ages of ~210 Ma obtained from zircon of the leucosome of the LLRX (Fig. 4.5) are similar to the ages obtained for the Cobquecura Pluton intrusive rocks, (Vásquez et al. 2005, 2008b), which indicates (re)crystallization of zircon contemporaneous with the magmatic event, as expected in such a scenario.

- Another possibility to explain the high radiogenic lead content in the LLRX is the action of fluids, generated for instance by metamorphic dehydration reactions, and enriched in radiogenic Pb from recrystallization of metamict protolith phases like zircon or monazite. Plagioclase-bearing rocks could then receive variable additions of more radiogenic Pb from these fluids.

The Cobquecura magmatic suite displays mafic rocks with relatively radiogenic $^{206}\text{Pb}/^{204}\text{Pb}_i$ and $^{208}\text{Pb}/^{204}\text{Pb}_i$ ratios, and felsic rocks with less radiogenic $^{206}\text{Pb}/^{204}\text{Pb}_i$ and $^{208}\text{Pb}/^{204}\text{Pb}_i$ ratios, whereas $^{207}\text{Pb}/^{204}\text{Pb}_i$ ratios are fairly constant. Fayalite granitoids display $^{206}\text{Pb}/^{204}\text{Pb}_i$ and $^{207}\text{Pb}/^{204}\text{Pb}_i$ ratios that are identical to those of the restitic xenoliths, but with higher $^{208}\text{Pb}/^{204}\text{Pb}_i$ ratios (Fig. 4.10). The relatively high contents of REE and HFSE elements in the fayalite granitoids (Fig. 4.6, 4.7) could be due to the high content of accessory minerals rich in these elements in the assimilated leucosome of the LLRX. These close similarities between the trace element characteristics (Table 4.3), $^{207}\text{Pb}/^{204}\text{Pb}_i$ ratios and $^{206}\text{Pb}/^{204}\text{Pb}_i$ ratios of the restitic xenoliths and fayalite granitoids (Fig. 4.10) point to a contribution of the leucosome of the LLRX to the magmas of the fayalite granitoids.

In summary, we conclude that the fayalite granitoids formed by means of an open-system fractional crystallization from a gabbroic, mantle-derived magma with geochemical and isotopic evidences of various grades of assimilation of continental crust during the differentiation. The sampled fayalite granitoids display relatively constant $^{87}\text{Sr}/^{86}\text{Sr}_i$ isotopic ratios, and Pb isotope signatures broadly similar to those of the restitic xenoliths. This might indicate a role of a source similar to the restitic xenoliths in the fayalite-granitic magmas, because the geochemical signatures, as well as $^{206}\text{Pb}/^{204}\text{Pb}_i$ and $^{207}\text{Pb}/^{204}\text{Pb}_i$ isotopic ratios match between the fayalite bearing granitoids

and these xenoliths. The relatively high content of REE and HFSE elements in the fayalite granitoids is most probably linked to selective assimilation of deep crust (similar to the LLRX), the leucosome of which may have been the source of those elements.

4.5.4 Comparison with other fayalite-granitoids worldwide

Fayalite granitoids from Cobquecura occur in an unusual extensional subduction related geodynamic setting (Vásquez et al. 2008b). This tectonic setting differs from the typical intracratonic setting of Precambrian fayalite bearing granitoids and from the extensional setting of most Phanerozoic fayalite granitoids. Worldwide, the Precambrian fayalite-bearing granitoids are commonly closely associated to rapakivi granites, anorthosite – mangerite – charnockite - granite suites (AMCG), and the Phanerozoic fayalite granitoids to anorogenic ring complexes (e.g., Frost et al. 2002; Poitrasson et al. 1995).

The petrogenesis of AMCG suites has been subject of discussion for a long time and its relation with fayalite granitoids is still problematic owing to the suggested different origins for the fayalite granitoids in the different localities where they occur. One of the best-studied fayalite-bearing suites is the Laramie Anorthosite Complex (LAC) in Wyoming (Frost and Frost 1997, Frost et al. 2002; Anderson et al. 2003). Anderson et al. (2003) conclude that the fayalite granitoids of the LAC were formed by the interaction of a hot, dry ferrodioritic magma derived by fractional crystallization or partial melting from a tholeiitic parent, with assimilated felsic crust. This ferrodioritic magma had high $\text{FeO}^*/(\text{FeO}^*+\text{MgO})$ ratios and high REE and Zr contents.

The fayalite granitoids of Cobquecura have characteristics (such as crystallization condition, mineralogical association, trace element and Sr-Nd isotopes initial ratios) that are very similar to those from the Sherman Batholith and Mule Creek fayalite granitoids (associated with the LAC, described by Frost et al. 2002). In the Cobquecura Pluton there is no evidence of a residual ferrodiorite, but restitic xenoliths also present high $\text{FeO}^*/(\text{FeO}^*+\text{MgO})$, are rich in REE and Zr, and display a signature of low oxygen fugacities. Our data show that a deep crust similar to the restitic xenoliths has contributed to the magmas of the fayalite granitoids. Probably the assimilation of this hypothetical metapelitic deep crust has enhanced the REE and HFSE contents and $\text{FeO}^*/(\text{FeO}^*+\text{MgO})$ ratios in the fayalite granitoids.

A common aspect of all different models for fayalite granitoids genesis is involvement of a lithology with low oxygen fugacity (mafic rocks, ferrodiorite, granulitic felsic lower crust). This lithology is required as a chemical buffer to keep the redox condition below or near to the FMQ buffer, which together with low $a_{\text{H}_2\text{O}}$ could favors the generation of fayalite-bearing granitoids.

4.6 Concluding remarks

The Cobquecura Pluton displays comagmatic and genetically related fayalite granitoids and gabbroic rocks. Both lithologies contain restitic metapelitic xenoliths. Our data show that the important processes involved in the generation of the fayalite granitoids were fractional crystallization combined with assimilation. Major element and trace element data show that an open-system fractional crystallization from a mafic magma with associated selective assimilation were the key processes in the generation of the granitoids of Cobquecura. The Sr-Nd-Pb isotope signature of the most primitive mafic magma is similar to that of the regional subarc-subcontinental mantle. Isotopic data show that the assimilated crustal component has striking similarities with the restitic metapelitic xenoliths from the deep crust, found in gabbros and fayalite granitoids. Different degree of assimilation could explain why there are fayalite-free and fayalite-bearing-granitoids. fayalite-free granitoids could have assimilated a granitic leucosome similar to the HLRX, whereas the fayalite granitoids have assimilated melts similar to the accessories mineral-rich leucosome from the LLRX.

Fayalite granitoids from Cobquecura occur in a subduction-related extensional geodynamic setting (Vásquez et al. 2008b), which is atypical and differs from the usual intracratonic and extensional setting where most of the fayalite granitoids worldwide occur. From comparison of existing models for fayalite granite genesis with our observations it appears that the important and common feature critical for fayalite granitoids generation is the presence of a lithology with low oxygen fugacity (certain mafic rocks, ferrodiorite, or, as in our case, a certain type of lower crust), which have a role as a chemical buffer and keep the oxygen fugacities near to the FMQ buffer. In the case of the Cobquecura Pluton this low oxygen fugacity component most likely had a composition similar to the restitic xenoliths present in the mafic rocks and the fayalite granitoids.

5. Conclusions

The results of the present study place new constraints on the evolution of the Andean continental margin during an enigmatic stage: the onset of the Andean Orogeny. The main motivation of this study was the contrasting existing tectonic models for this period north and south of the 34°-37°S segment of the Cordillera de la Costa. For this reason, the present study was focused on the intrusive rocks in the 34°-37°S segment of the Cordillera de la Costa, for which only little geological and petrological information is available. By the integration of new field observations, isotopic ages, petrography, mineral chemistry, geochemistry and isotopic data, this investigation provides a tectonic model for the petrogenetic setting in which the magmatism of the Triassic-Jurassic boundary was generated.

Three generations of magmatism (~224Ma, ~210Ma and Middle Jurassic) have been identified for the early Mesozoic, all of them cropping out as small epizonal intrusive bodies. The differences in their composition and magma sources help to a better understanding of the igneous evolution during this period. All of these magmatic generations show typical subduction-signature, which, together with the contemporaneous accretionary prism, confirms a continuous subduction from the Late Paleozoic until the onset of the Andean Orogeny. The magmatism at ~224 Ma is dominated by leucogranitic rocks. Their isotopic composition reveals that the most important magma sources were the continental crust at the current outcrops level and the regional subarc subcontinental mantle. This magmatism shows a higher contribution of crustal sources than the younger magmatic generations, but with notably more mantle contribution than the older Late Paleozoic magmatic suites.

Of special interest was the magmatism at ~210 Ma, because it displays mineralogical and geochemical characteristics uncommon for an active continental margin. At ~210 Ma the magmatism was bimodal with contemporaneously emplaced mafic and felsic melts. The felsic magmas are composed of lithologies rather uncommon in subduction-related setting, such as fayalite granitoids and arvedsonite granites. These rocks are commonly associated with extensional or anorogenic regimes. The ~210 Ma magmatism shows distinct crystallization conditions with notably lower f_{O_2} and a_{H_2O} , when compared to the previous and later igneous suites. Their sources are predominantly the regional subarc subcontinental mantle with a contribution of deeper restitic crust with geochemical characteristics different to those of the crust at the present outcrop level. In conclusion, the geochemical signatures of the magmatic suites at ~210 Ma are indicative for an overall extensional setting. However, the scarce and sporadic occurrence of this magmatism suggests that extensional structures were locally restricted, and represents no regional

extensional event. They also preserved typical geochemical subduction signatures, which suggest that the extension occurred in an overall active continental margin context.

The Middle Jurassic magmatism is predominantly mafic in composition. Its geochemical characteristics and the nature of its sources are very similar to those of volcanic rocks from the recent Southern Volcanic Zone (located at the same latitude) and similar to those of the North Patagonian Batholith, a typical subduction-related cordilleran batholith. These similarities suggest that during the Middle Jurassic, the subduction-related magmatism had sources similar to other subduction-related magmas of the Andean Orogeny, with a significantly higher contribution of mantle than during the previous Late Paleozoic tectonomagmatic stage. This enhanced mantle component of the Mesozoic magmas was previously recognized north of this segment along the Chilean margin (Parada et al. 1999; Lucassen et al. 2004).

The spatial relation of the intrusives at ~224 and ~210 Ma with NW-SE trending lineaments suggests that these intrusions used older structures as pathways. A possible tectonic scenario is a suprasubduction setting preceded by an oblique subduction that would generate extensional NW-SE trending structures, followed by steepening of the slab. The latter process would favor the melting of the subcontinental mantle. This Triassic-Jurassic subduction geometry allowed the emplacement of magmas with extensional signature with enhanced contribution of mantle sources suggesting that the onset of the Andean Orogeny was caused by reconfiguration of the convergent conditions during continuous subduction. Previous works show that NW-SE extensional structures trending structures frequently occur along the Chilean margin both north and south of the segment studied and have been dated as Permian to Jurassic (Martin et al. 1999; Grocott and Taylor 2002). The model presented here reconciles these different interpretations for the regions north and south of the studied area. Fayalite granite and ardevsonite granite are classical examples for the so-called anorogenic granites. However, the results of this work demonstrate that this nomenclature must be used very carefully and highlights the need for observation and integration of all available geological and petrological characteristics before this tectonic classification is considered.

As another important result of this thesis the petrogenesis of fayalite granitoids in this very untypical tectonic setting has been resolved. These fayalite granitoids were generated through open-system fractional crystallization from mantle-derived magmas similar to the regional subarc-subcontinental mantle with assimilation of restitic middle-lower crustal rocks. The geochemical characteristics and Pb isotopic signatures suggest that this process of assimilation of restitic metapelitic material has an important effect on the petrogenesis of the fayalite granitoids. These metapelitic rocks, preserved as rare xenoliths in granitoids and gabbros, show a restitic nature with

geochemical and Pb isotopic characteristics different from those of the metapelitic crust in the outcrop level. In the case of the Cobquecura Pluton, these metapelitic restitic xenoliths may be acted as a buffer for the f_{O_2} , keeping the oxygen fugacities near the FMQ buffer and allowing the crystallization of fayalite in the differentiated granitic magmas.

6. References

Aftalion, M., Bowes, D.R., Vřana, S., 1989. Early Carboniferous U-Pb zircon ages for garnetiferous perpotassic granulites, Blansky Les Massif, Czechoslovakia. *Neues Jahrbuch Mineralogie, Abhandlungen* 4, 145-152.

Aguirre, L., Hervé, F., Godoy, E., 1972. Distribution of metamorphics facies in Chile an outline. *Krystalinikum* 9, 7-19.

Alfaro, G., 1962. Geología del área de Cobquecura. *Geoandes* 2, 1-65.

Anderson, I.C., Frost, C.D., Frost, B.R., 2003. Petrogenesis of the Red Mountain pluton, Laramie anorthosite complex, Wyoming: implications for the origin of A- type granite. *Precambrian Research* 124, 243-267.

Anderson, J.L., Smith, D.R., 1995. The effects of temperature and f_{O_2} on the Al-in-hornblende barometer. *American Mineralogist* 80, 549-559.

Bacon C.R., Druitt, T.H., 1988. Compositional evolutions of the zoned calc-alkaline magma chamber of Mount Mazama, Crater Lake, Oregon. *Contributions to Mineralogy and Petrology* 98, 224-256.

Bahlburg, H., Hervé, F., 1997. Geodynamic evolution and tectonostratigraphic terranes of northwestern Argentina and northern Chile. *Geological Society of America Bulletin* 119, 869-884.

Bartsch, V., 2004. Magmengenese der obertriassischen bis unterkretazischen Vulkanite der mesozoischen Vulkanzone in der Küstenkordillere von Nord-Chile zwischen 24° und 27°S. Dissertation. Technical University Berlin. 348 pp.

Baxter, S., Feely, M., 2002. Magma Mixing and mingling textures in granitoids: examples from the Galway Granite, Connemara, Ireland. *Mineralogy and Petrology* 76, 63-74.

Beck, M.E., García, A., Burmester, R.F., Munizaga, F., Hervé, F., Drake, R.E., 1991. Paleomagnetism and geochronology of late Paleozoic granitic rocks from the Lake District of southern Chile: implications for accretionary tectonics. *Geology* 19, 332–335.

6. References

- Bonin, B., 2004. Do coeval mafic and felsic magmas in post-collisional to within-plate regimes necessarily imply two contrasting, mantle and crustal sources? A review. *Lithos* 76, 1-24.
- Brophy, J.G., 1991. Compositional gaps, critical crystallinity, and fractional crystallization in orogenic (calc-alkaline) magmatic systems. *Contributions to Mineralogy and Petrology* 91, 173-182.
- Bucher, K., Frey, M., 1992. Petrogenesis of metamorphic rocks. Springer Verlag, Berlin, Heidelberg, New York. 317 p.
- Charrier, R., 1979. El Triásico en Chile y regiones adyacentes de Argentina: Una reconstrucción paleogeográfica y paleoclimática. *Comunicaciones* 26, 1-37.
- Christiansen, R.L., 1984. Yellowstone magmatic evolution: its bearing on understanding large-volume explosive volcanism. In *Explosive Volcanism: inception, evolution, and hazards*. National academy Press, Washington, DC, pp 84-95.
- Coira, B., Davidson, J., Mpodozis, C., Ramos, V., 1982. Tectonic and magmatic evolution of the Andes of northern Argentina and Chile. *Earth-Sciences Reviews* 18, 303-332.
- Clemens, J.D., Holloway, J.R., White, A.J.R., 1986. Origin of an A-type granite: Experimental constraints. *American Mineralogist*, 71, 317-324.
- Collins, W.J., Beams, S.D., White, A.J.R., Chappel, B.W., 1982. Nature and origin of A-type granites with particular reference to southeastern Australia. *Contributions to Mineralogy and Petrology* 80, 189-200.
- Creaser, R., Price, R., Wormald, R., 1991. A-type granites revisited: Assessment of a residual-source model. *Geology* 19 (2), 163-166.
- Creixell, C., Lucassen, F., Franz, G., Vásquez, P., Figueroa, O., 2002. Petrology of Hualpén stock: evidences of Late Triassic crustal epizonal plutonism at the western margin of Gondwana (36°45'S – 73°10'W). 5th International Symposium on Andean Geodynamics, Toulouse, France, 167-170.
- Damm, K. W., Harmon, R. S., Kelley, S., 1994. Some isotope and geochemical constraints on the origin and evolution of the Central Andean basement (19°–24°S). In Reutter, K. J., Scheuber, E., Wigger, P. J., eds. *Tectonics of the Southern Central Andes*. Heidelberg, Springer, 263–275.

- Dávila, A., Hervé, F., Munizaga, F., 1979. Edades K/Ar en granitoides de la Cordillera de la Costa de la provincia de Colchagua, VI Región, Chile Central. 2º Congreso Geológico Chileno, F107-120.
- Dickin, A.P., 1997. Radiogenic Isotope Geology. Cambridge University Press, Cambridge. 490 p.
- Didier, J., 1977. Granite and their enclaves; the bearing of enclaves on the origin of granites, Elsevier, Amsterdam, 393 p.
- Droop, G.T.R., 1987. A general equation for estimating Fe^{3+} concentration in ferromagnesian silicates and oxides from microprobe analyses, using stoichiometric criteria. Mineralogical Magazine 51, 431-435.
- Duhart, P., McDonough, M., Muñoz, J., Martin, M., Villeneuve, M., 2001. El complejo metamórfico Bahía Mansa en la Cordillera de la Costa del centro-sur de Chile (39°30'–42°00'S): geocronología K–Ar, $^{40}\text{Ar}/^{39}\text{Ar}$ y U–Pb e implicancias en la evolución del margen sur-occidental de Gondwana. Revista Geológica de Chile 28, 179–208.
- Dulski, P., 2001. Reference Materials for Geochemical Studies: New Analytical Data by ICP-MS and Critical Discussion of Reference Values, Geostandard Newsletter 25, 87-125.
- Eby, G.N., 1990. The A- type granitoids: A review of their occurrence and chemical characteristics and speculations on their petrogenesis. Lithos 26, 115-134.
- Eby, G.N., 1992. Chemical subdivision of the A-type granitoids: Petrogenetic and tectonic implication. Geology 20, 641-644.
- Escobar, F, Guzmán, R., Vieira, C., 1977. Avance Geológico de las hojas Rancagua-Curicó-Talca-Linares-Chanco-Concepción-Chillan. Instituto de Investigaciones Geológicas (Unpublished). 55 p.
- Fang, Z., Boucot, A., Covacevich, V., Hervé, F., 1998. Late Triassic fossils in the Chonos Metamorphic Complex, southern Chile. Revista Geológica de Chile 25, 165-173.
- Foley, S. F., 1990. Experimental constraints on phlogopite chemistry in lamproites: 2. Effect of pressure- temperature variations. European Journal of Mineralogy 2, 327–341.

6. References

Franzese, J., Spalletti, L., 2001. Late Triassic-early Jurassic continental extension in southwestern Gondwana: tectonic segmentation and pre-break-up rifting. *Journal of South American Earth Sciences* 14, 257-270.

Frei, D., Hollis, J. A., Gerdes, A., Harlov, D., Karlsson, C., Vásquez, P., Franz, G., Johansson, L., Knudsen, C., 2006. Advanced *in-situ* trace element and geochronological microanalysis of geomaterials by laser ablation techniques. *Geological Survey Denmark and Greenland Bulletin* 10, 25-28.

Frost, C.D., Frost, B.R., 1997. Reduced rapakivi-type granites: The tholeiite connection. *Geology* 25, 647-650.

Frost, B.R., Barnes, C.G., Collins, W.J., Arculus, R.J., Ellis, D.J., Frost, C.D. 2001. A Geochemical classification for granitic rocks. *Journal of Petrology* 42, 2033-2048.

Frost, C.D., Frost, B.R., Bell, J.M., Chamberlain, K.R., 2002. The relation between A-type granites and residual magmas from anorthosite: evidence from northern Sherman batholith, Laramie Mountains, Wyoming, USA. *Precambrian Research* 119, 45-71.

Frost, C.D., Frost, B.R., Chamberlain, K.R., Edwards, B.R., 1999. Petrogenesis of the 1,43 Ga Sherman Batholith, SE Wyoming, USA: a reduced, Rapakivi-type anorogenic granite. *Journal of Petrology* 40, 1771-1802.

Frost, B.R., Lindsey, D.H., Andersen, D.J., 1988. Fe-Ti oxide-silicate equilibria: Assemblages with fayalitic olivine. *American Mineralogist* 73, 727-740.

Gajardo, A., 1981. Hoja Concepción-Chillán, Mapas geológicos preliminares de Chile, escala 1:250.000. Instituto de Investigaciones Geológicas, 56 p.

Gana, P., 1991. Magmatismo bimodal del Triásico superior-Jurásico inferior en la Cordillera de la Costa, provincias de Elqui y Limarí. *Revista Geológica de Chile* 18, 55-68.

Gana, P., Hervé, F., 1983. Geología del Basamento cristalino de la Cordillera de la Costa entre los ríos Mataquito y Maule, VII Región. *Revista Geológica de Chile* 19, 37-56.

- Geisler, T., Pidgeon, R.T., Bronswijk, W.van, Kurtz, R., 2002. Transport of uranium, thorium, lead in metamict zircon under low-temperature hydrothermal conditions. *Chemical Geology* 191, 141-154.
- Gerdes, A., Zeh, A., 2006. Combined U-Pb and Hf isotope LA-(MC)-ICP-MS analyses of detrital zircons: Comparison with SHRIMP and new constraints for the provenance and age of an Armorican metasediment in Central Germany. *Earth and Planetary Sciences Letters* 249, 47-61.
- Glodny, J., Lohrmann, H., Echtler, H., Gräfe, K., Seifert, W., Collao, S., Figueroa, O., 2005. Internal dynamic of a paleoaccretionary wedge: insights from combined isotope tectonochronology and sandbox modeling of the South-Central Chilean forearc. *Earth and Planetary Science Letters* 231, 23-39.
- Glodny, J., Echtler, H., Figueroa, O., Franz, G., Gräfe, K., Kemnitz, H., Kramer, W., Krawczyk, C., Lormann, J., Lucassen, F., Melnick, D., Rosenau, M., Seifert, W., 2006. Long-term geological evolution and mass-flow balance of the South-Central Andes. In O. Oncken, G. Chong, G. Franz, P. Giese, H.-J. Götze, V. A. Ramos, M. R. Strecker, P. Wigger ,eds. *Frontiers in Earth Sciences: The Andes*, Springer, pp 401-428.
- Godoy, E., 1970. Estudio petrológico del granito de Constitución y su aureola metamórfica. Tesis para optar al título de geólogo (Unpublished Ms Thesis). Universidad de Chile, Santiago. 144 p.
- Grocott, J., Taylor, G.K., 2002. Magmatic arc fault system, deformation partitioning and emplacement of granitic complexes in the Coastal Cordillera, north Chilean Andes. (25°30'S to 27°00'S). *Journal of the Geological Society London* 159, 425-442.
- Gromet, L.P., Dymek, R.F., Haskin, L.A., Koroter, R. L., 1984. The North American shale composite, its compilation, major and trace elements characteristics. *Geochimica et Cosmochimica Acta*, 48, 2469-2482.
- Harrison, T.N., Parson, I., Brown, P.E., 1990. Mineralogical evolution of the fayalite-bearing rapakivi granites from Prins Christians Sund pluton, South Greenland. *Mineralogical Magazine* 54, 57-66.
- Hart, S.R., 1984. A large-scale isotopic anomaly in the southern hemisphere mantle. *Nature* 309, 753-757.

6. References

- Haschke, M., Günther, A., Melnick, D., Echtler, H., Reutter, K.-J., Scheuber, E., Oncken, O. 2006. Central and southern Andean tectonic evolution inferred from arc magmatism. In Oncken, O., Chong, G., Franz, G., Giese, P., Götze, H.-J., Ramos, V.A., Strecker, M.R., Wigger, P., eds. *Frontiers in Earth Sciences: The Andes* 16, 337-353.
- Hawkesworth, C.J., Gallagher, K., Hergt, J.M., McDermott, F., 1993. Mantle and slab contributions in arc magmas. *Annual Reviews Earth Planetary Sciences*, 21, 175-204.
- Hervé, F., 1977. Petrology of crystalline basement of the Nahuelbuta Mountains, south central Chile. In Ishikawa, T., Aguirre, L., eds. *Comparative Studies on the Geology on the Circumpacific Orogenic Belts in Japan-Chile*. Japan Society for the Promotion of Science, 1-51.
- Hervé, F., 1988. Late Palaeozoic Subduction and accretions in Southern Chile. *Episodes* 11, 183-188.
- Hervé, F., Kawashita, K., Munizaga, F., Bassei, M., 1984. Rb-Sr isotopic ages from late Palaeozoic metamorphic rocks of central Chile. *Journal of the Geological Society London* 141, 877-884.
- Hervé, F., Fanning, C.M., 2001. Late Triassic detrital zircon in metaturbidites of Chonos Metamorphic Complex, southern Chile. *Revista Geológica de Chile* 28, 91-104.
- Hervé, F., Munizaga, F., 1978. Evidencias geocronológicas de un magmatismo intrusivo Triásico Superior-Jurásico en la Cordillera de la Costa de Chile entre los 35°30'S y 36°30'S. 7° Congreso Geológico Argentino 2, 43-52, Neuquén.
- Hervé, F., Davidson, J., Godoy, E., Mpodozis, C., Covacevic, V., 1981. The Late Palaeozoic in Chile: stratigraphy, structure and possible tectonic framework. *Anais da Academia Brasileira de Ciencias* 53, 361-363.
- Hervé, F., Munizaga, F., Parada, M.A., Brook, M., Pankhurst, R., Snelling, N., Drake, R., 1988. Granitoids of the Coast Range of central Chile: Geochronology and geologic setting. *Journal of South American Earth Sciences* 1, 185-194.
- Hervé, F., Faundez, V., Calderón, M., Massonne, H.-J., Willner, A.P., 2007a. Metamorphic and plutonic basement complexes. In Moreno, T., Gibbons, W. eds. *The Geology of Chile*. London, The Geological Society, 5-19.

Hervé, F., Pankhurst, R.J., Fanning, C.M., Calderón, M., Yaxley, G.M., 2007b. The South Patagonian batholith: 150 my of granite magmatism on a plate margin. *Lithos* 97, 373-394.

Hildreth, W., Moorbath, S., 1988. Crustal contributions to arc magmatism in the Andes of Central Chile. *Contributions to Mineralogy and Petrology* 98, 455-489.

Hogan, J.P., Sinha, A.K., 1991. The effect of accessory minerals on the redistribution of lead isotopes during crustal anatexis: A Model. *Geochimica and Cosmochimica Acta* 55, 335-348.

Holland, T., Blundy, J., 1994. Non-ideal interactions in calcic amphiboles and their bearing on amphibole-plagioclase thermometry. *Contributions to Mineralogy and Petrology* 116, 433-447.

Horstwood, M., Foster, G.L., Parrish R.R., Noble, S.R., 2003. Common-Pb corrected in situ U–Pb accessory mineral geochronology by LA-MC-ICP-MS. *Journal of Analytical Atomic Spectrometry* 18, 837–846.

Irvine, T.N., Baragar, W.R.A., 1971. A guide to the chemical classification of the common volcanic rocks. *Canadian Journal of Earth Sciences* 8, 523-548.

Jackson, S., Pearson, N.J., Griffin, W.L., Belousova, E.A., 2004. The application of laser ablation – inductively coupled plasma – mass spectrometry to in situ U-Pb zircon geochronology. *Chemical Geology* 211, 47-69.

Jeong, G.Y., Cheong, C-S., Kim, J. 2006. Rb–Sr and K–Ar systems of biotite in surface environments regulated by weathering processes with implications for isotopic dating and hydrological cycles of Sr isotopes. *Geochimica and Cosmochimica Acta* 70, 4734-4749.

Kay, S.M., Ramos, V.A., Mpodozis, C., Sruoga, P., 1989. Late Paleozoic to Jurassic silicic magmatism at the Gondwana margin: Analogy to the middle Proterozoic in North America? *Geology* 17, 324-328.

Kay, S.M., Orrel, S., Abbruzzi, J.M., 1996. Zircon and whole rock Nd-Pb isotopic evidence for a Grenville age and Laurentian origin for the basement of the Precordillera in Argentina. *Journal of Geology* 104, 637-638.

6. References

- Kay, S.M., Godoy, E., Kurtz, A., 2005. Episodic arc migration, crustal thickening, subduction erosion, and magmatism in the south-central Andes. *Geological Society of America Bulletin* 117, 67–88, doi: 10.1130/B25431.1.
- Kramer, W., Siebel, W., Romer, R., Haase, G., Zimmer, M., Ehrlichmann, R., 2005. Geochemical and isotopical characteristics and evolution of the Jurassic volcanic arc between Arica (18°30'S) and Tocopilla (22°S), North Chilean Coastal Cordillera. *Chemie der Erde* 65, 47-78.
- Krawczyk, C. M., Mechie, J., Lüth, S., Tasárova, Z., Wigger, P., Stiller, M., Brasse, H., Echtler, H. P., Araneda, M., Bataille, K., 2006. Geophysical signatures and active tectonics at the South-Central Chilean margin. In O. Oncken, G. Chong, G. Franz, P. Giese, H.-J. Götze, V. A. Ramos, M. R. Strecker, P. Wigger, eds. *Frontiers in Earth Sciences: The Andes*, Springer, pp 171-192.
- Leake, B.E., Wolley, A.R., Arps, C.E.S., Birch, W.D., Gilbert, M.C., Grice, J.D., Hawthorne, F.C., Kato, A., Kisch, H.J., Krivovichev, V.G., Linthout, K., Laird, J., Mandarino, J., Maresch, W.V., Nickel, E.H., Rock, N.M.S., Shumacher, J.C., Smith, D.C., Stephenson, N.C.N., Ungaretti, L., Whitaker, E.J.W., Youzhi, G., 1997. Nomenclature of amphiboles. Report of the Subcommittee on Amphiboles of the International Mineralogical Association Commission on New Minerals and Mineral Names. *European Journal of Mineralogy* 9, 623-651.
- Le Maitre, R.W., Bateman, P., Dudek, A., Keller, J., Lameyre, J., Le Bas, M.J., Sabine, P.A., Schmid, R., Sorensen, H., Streckeisen, A., Woolley, A.R., Zanettin, B., 1989. *A Classification of Igneous Rocks and Glossary of terms: Recommendations of the International Union of Geological Sciences Subcommittee on the Systematics of Igneous Rocks*. Blackwell Scientific Publications, Oxford, U.K.
- Leterrier, J., Maury, R.C., Thonon, P., Girard, D., Marchal, M., 1982. Clinopyroxene composition as a method of identification of the magmatic affinities of paleo-volcanic series. *Earth and Planetary Sciences Letters* 59, 139-154.
- Llambías, E.J., Sato, A.M., 1995. El Batolito de Colangüil: transición entre orogénesis y anórogenesis. *Revista de la Asociación Geológica* 50(1-4), 111-131.
- Loiselle, M.C., Wones, D.R., 1979. Characteristics and origin of anorogenic granites. *Geological Society of America Abstracts with Programs* 11, 468.

6. References

- Lucassen, F., Becchio, R., Harmon, R., Franz, G., Trumbull, R., Wilke, H-G., Romer, R.L., Dulski, P., 2001. Composition and density model of the continental crust at an active continental margin—the Central Andes between 21° and 27°S. *Tectonophysics* 341, 195–223.
- Lucassen F., Harmon R., Franz G., Romer R.L., Becchio R., Siebel W., 2002. Lead evolution of the Pre-Mesozoic crust in the Central Andes (18-27°S): progressive homogenisation of Pb. *Chemical Geology* 186, 183-197.
- Lucassen, F., Trumbull, R., Franz, G., Creixell, C., Vásquez, P., Romer, R. L., Figueroa, O., 2004. Distinguishing crustal recycling and juvenile additions at active continental margins: the Paleozoic to Recent compositional evolution of the Chilean Pacific margin (36 – 41°S). *Journal of South American Earth Sciences* 17, 103-119.
- Lucassen, F., Kramer, W., Bartsch, V., Wilke, H-G., Franz, G., Romer, R.L., Dulski, P. 2006. Nd, Pb, Sr isotope composition of juvenile magmatism in the Mesozoic large magmatic province of northern Chile (18-27°S): indication for a uniform subarc mantle. *Contributions to Mineralogy and Petrology* 152, 571-589.
- Ludwig K.R., 2003. *Isoplot 3: A geochronological toolkit for Microsoft Excel*. Berkely Geochronology Centre Special Publication, 4.
- Mac Donald, R., 1987. Quaternary peralkaline silicic rocks and caldera volcanoes of Kenya. In *Alkaline Igneous rocks*, Fitton, J.G., Upton, B.G.J. Geological Society London, Special Publication 30, 313-333.
- Martin, M., Kato, T., Rodriguez, C., Godoy, E., Duhart, P, McDonough, M., Campos, A., 1999. Evolution of the late Paleozoic accretionary complex and overlying forearc-magmatic arc, south central Chile (38°-41°S): Constraints for the tectonic setting along the southwestern margin of Gondwana. *Tectonics* 18, 582-605.
- McDonough, W.F., Sun, S., 1995. The composition of the Earth. *Chemical Geology* 120, 223-253.
- Morata, D., Aguirre, L., Oyarzún, M., Vergara, M., 2000. Crustal contribution in the genesis of the bimodal Triassic volcanism from the Coastal Range, central Chile. *Revista Geológica de Chile* 27, 83-98.
- Morimoto, N., 1989. Nomenclature of pyroxenes. *Canadian Mineralogist* 27, 143-156.

6. References

- Mpodozis, C., Kay, S.M., 1990. Provincias magmáticas ácidas y evolución tectónica de Gondwana: Andes chilenos (28°-31°S). *Revista Geológica Chilena* 17, 153-180.
- Mpodozis, C., Kay, S.M., 1992. Late Paleozoic to Triassic evolution of the Gondwana margin: Evidence from Chilean Frontal Cordilleran batholiths (28°S to 31°S). *Geological Society of America Bulletin* 104, 999-1014.
- Mpodozis, C., Ramos, V., 1989. The Andes of Chile and Argentina. In Ercksen, G.E., Cañas Pinochet, M.T., Reinemund, J. A., eds. *Geology of the Andes and its relation to hydrocarbon and mineral resources* 11, 59-90.
- Mücke, A., 2003. Fayalite, pyroxene, amphibole, annite and their decay products in mafic clots within the Younger Granites of Nigeria: Petrography, mineral chemistry and genetic implications. *Journal of African Earth Sciences* 36, 55-71.
- Myers, J.D., Marsch, B.D., 1981. Geology and petrogenesis of the edgacumber volcanic field, SE Alaska: Interaction of basalt and sialic crust. *Contributions to Mineralogy and Petrology* 77, 272-287.
- Njonfang, E., Moreau, C., 2000. The mafic mineralogy of the Pandé massif, Tikar plain, Cameroon: implications for a peralkaline affinity and emplacement from highly evolved alkaline magma. *Mineralogical Magazine* 64, 525-537.
- Oliveros, V., Féraud, G., Aguirre, L., Fornari, M., Morata, D., 2006. The Early Andean Magmatic Province (EAMP): $^{40}\text{Ar}/^{39}\text{Ar}$ dating on Mesozoic volcanic and plutonic rocks from the Coastal Cordillera, northern Chile. *Journal of Volcanology and Geothermal Research* 157, 311-330.
- Pankhurst, R.J., Weaver, S.D., Hervé, F., Larrondo, P., 1999. Mesozoic-Cenozoic evolution of the North Patagonian Batholith in Aysén, southern Chile. *Journal of the Geological Society, London* 156, 673-695.
- Parada, M.A., 1988. Pre-Andean peraluminous and metaluminous leucogranitoid suites in the High Andes of central Chile. *Journal of South American Earth Sciences* 1, 211-221.

6. References

- Parada, M.A., 1990. Granitoid plutonism in central Chile and its geodynamic implications: a review. In Kay, S.M., Rapela, C.W., eds. *Plutonism from Antarctica to Alaska*: Boulder, Colorado, Geological Society of America Special Paper 241, 51-66.
- Parada, M.A., Levi, B., Nyström, J., 1991. Geochemistry of the Triassic to Jurassic plutonism of central Chile (30 to 33°S): Petrogenetic implications and a tectonic discussion. In Harmon, R.S., Rapela, C.W., eds. *Andean magmatism and its tectonic setting*: Boulder, Colorado. Geological Society of America Special Paper 265, 99-112.
- Parada, M.A., Nyström, J., Levi, B., 1999. Multiple sources for the Coastal Batholith of central Chile (31-34°S): geochemical and Sr-Nd isotopic evidence and tectonic implications. *Lithos* 46, 505-521.
- Pearce, J.A., Harris, N.B.W., Tindle, A.G., 1984. Trace element discrimination diagrams for the tectonic interpretation of granitic rocks. *Journal of Petrology* 25, 956-983.
- Pichowiak, S. 1994. Early Jurassic to Early Cretaceous magmatism in the coastal Cordillera and the central depression of North Chile. In Reutter, K.J., Scheuber, E., Wigger, P., eds. *Tectonics of the southern central Andes*. Berlin Heidelberg New York, Springer, p. 203–217.
- Pitcher, W.S., 1997. *The nature and origin of granite*. Blackie Academic and Professional, 386p.
- Poitrasson, F., Duthou, J-L., Pin, C., 1995. The relationship between petrology and Nd isotopes as evidence for contrasting anorogenic granitic genesis: Example of Corsican province (SE France). *Journal of Petrology* 36, 1251-1274.
- Ramos, V., Jordan, T., Allmendinger, R., Mpodozis, C., Kay, S., Cortés, J., Palma, M., 1986. Paleozoic terrains of Central Argentine-Chilean Andes. *Tectonics* 5, 855-880.
- Ramos, V.A., Kay, S.M., 1991. Triassic rifting and associated basalts in the Cuyo basin, central Argentina. In Harmon, R.S., Rapela, C.W., eds. *Andean magmatism and its tectonic setting*: Boulder, Colorado, Geological Society of America Special Paper 265, 79-91.
- Ramos, V. 1994. Terranes of southern Gondwanaland and their control in the Andean structure (30°-33°S latitude). In Reutter, K-J, Scheuber, E., Wigger, P., eds. *Tectonics of the South Central Andes*. Springer Verlag, Berlin, Heidelberg, New York: 249-261.

6. References

- Rapela, C., Pankhurst, R., 1992. The granites of northern Patagonia and the Gastre Fault System in relation to the break-up of Gondwana. In Storey, B., Alabaster, T., Pankhurst, R., eds. *Magmatism and the Causes of Continental Break-up*. Geological Society Special Publication 68, 209-220.
- Richter, P.P., Ring, U., Willner, A.P., Leiss, B., 2007. Structural contacts in subduction complexes and their tectonic significance: the Late Paleozoic coastal accretionary wedge of central Chile. *Journal of the Geological Society, London* 164, 203-214.
- Rogers, G., Hawkesworth, C. J., 1989. A geochemical traverse across the North Chilean Andes: evidence for crust generation from the mantle wedge. *Earth and Planetary Sciences Letters* 91, 271–285.
- Romer, R.L., Heinrich, W., Schröder-Smeibidl, B., Meixner, A., Fischer, C.O., Schulz, C., 2005. Elemental dispersion and stable isotope fractionation during reactive fluid-flow and fluid immiscibility in the Bufa del Diente aureole, NE-Mexico: evidence from radiographies and Li, B, Sr, Nd, and Pb isotope systematics. *Contributions to Mineralogy and Petrology* 149, 400-429.
- Rudnick, P., Fountain, D.M., 1995. Nature and composition of the continental crust: a lower crustal perspective. *Reviews of Geophysics* 33, 267-309.
- Sakoma, E.M., Martin, R.F., Williams-Jones, A.E., 2000. The late stages of evolution of the Kwandonkaya A-type granite complex, Nigeria, as deduced from mafic minerals. *Journal of African Earth Sciences* 30, 320-350.
- Salters, V., Stracke, A., 2004. Composition of the depleted mantle. *Geochemistry, Geophysics, Geosystems* 5 (5).
- Scheuber, E., Bogdanic, T., Jensen, A., Reutter, K.-J., 1994. Tectonic Development of the North Chilean Andes in Relation to Plate Convergence and Magmatism Since the Jurassic. In Reutter, K.-J., Scheuber, E., Wigger, P., eds. *Tectonics of the Southern Central Andes*, 121-139, Springer Verlag, Berlin
- Scheuber, E., González, G., 1999. Tectonic of the Jurassic-Early Cretaceous magmatic arc of the north Chilean Coastal Cordillera (22°-26°S): a story of crustal deformation along a convergent plate boundary. *Tectonics* 18, 895-910.

6. References

Schumacher, J.C., 1997. The estimation of iron in electron microprobe analysis of amphiboles. *European Journal of Mineralogy* 9, 643-651.

SERNAGEOMIN, 2003. Mapa Geológico de Chile: versión digital, Servicio Nacional de Geología y Minería, Publicación Geológica Digital, No. 4 (CD-ROM, versión 1.0, 2003), Santiago, Chile.

Simonetti, A., Shore, M., Bell, K., 1996. Diopside phenocrysts from nephelinite lavas, Napak volcano, eastern Uganda: evidence for magma mixing. *Canadian Mineralogist* 34, 411-421.

Smith, D.R., Noblet, J., Wobus, R.A., Unruh, D., Douglas, J., Beane, R., Davis, C., Goldman, S., Kay, G., Gustavson, B., Saltoun, B., Stewart, J., 1999. Petrology and geochemistry of late stage intrusions of the A-type, mid-Proterozoic Pikes Peak Batholith (Central Colorado, USA): implications for petrogenetic models. *Precambrian Research* 98, 271-305.

Spear, F.S., 1981. An experimental study of hornblende stability and compositional variability in amphibolite. *American Journal of Sciences* 281, 691-734.

Spear, F.S., 1993. Metamorphic phase equilibria and pressure-temperature-time path. Mineralogical Society of America. Monograph. Washington, D.C. 799 p.

Steiger, R. H., Jaeger, E., 1977. Subcommittee on geochronology - Convention on use of decay constants in geochronology and cosmochronology. *Earth and Planetary Sciences Letters* 36, 359-362.

Stephenson, N.C.N., Hensel, H.D., 1978. A Precambrian fayalite granite from the south coast of Western Australia. *Lithos* 11, 209-218.

Taylor, S.R., McLennan, S.M., 1995. The geochemical evolution of the continental crust. *Reviews of Geophysics* 33 (2), 241-265.

Thomson, S.N., Hervé, F., Fanning, C.M., 2000. Combining fission track and U-Pb SHRIMP zircon ages to establish stratigraphic and metamorphic ages in basement sedimentary rocks in southern Chile. 9° Congreso Geológico Chileno 2, 769-773. Puerto Varas.

Tilton, G. R., Barreiro, B. A. 1980. Origin of lead in Andean calc-alkaline lavas, southern Peru. *Science* 210, 1245-124

6. References

Tosdal, R., 1996. The Amazon-Laurentian connection as viewed from the Middle Proterozoic rocks in the central Andes, western Bolivia and northern Chile. *Tectonics*, 15, 827-842.

Turner, S.P., Foden, J.D., Morrison, R.S., 1992. Derivation of some A-type magmas by fractionation of basaltic magma: An example from Padthaway Ridge, South Australia. *Lithos* 28, 151-179.

Uliana, M., Biddle, K., Cerdán, J., 1989. Mesozoic extension and formation of Argentina sedimentary basins. *Extensional Tectonics and Stratigraphy of the North Atlantic margin*, American Association of Petroleum Geologist, Memoir 46, 599-613.

Vásquez, P., Franz, G., Wemmer, K., 2005. Fe-rich silicates in the Cobquecura pluton: An indicator of A-type granitoids in the Triassic magmatism of south-central Chile. 6th International Symposium on Andean Geodynamics, 773-775. Barcelona.

Vásquez, P., Franz, G., Frei, D., 2006. Petrology of the Late Triassic arfvedsonite-granitoid at La Estrella (Central Chile). XI Congreso Geológico Chileno. 573-576. Antofagasta.

Vásquez, P., Franz, G., 2008. The Cobquecura Pluton (Triassic, Central Chile), an example of a fayalite granite bearing A-Type granitoid massif at a continental margin. *Tectonophysics*, in press

Vásquez, P., Glodny, J., Franz, G., Frei, D., Romer, R.L., 2008. Early Mesozoic plutonism of the Cordillera de la Costa (34-37°S), Chile: Constraints on the onset of the Andean Orogeny. *Journal of Geology*, in review.

Vásquez, P., Franz, G., Glodny, J., Romer, R., 2008. Origin of fayalite granitoids: new insights from metapelitic xenoliths. *Lithos*, submitted.

Wasteneys, H. A., Clark, A. H., Farrar, E., Langridge, R. J., 1995. Grenvillian granulite-facies metamorphism in the Arequipa Massif, Peru: a Laurentia-Gondwana link. *Earth and Planetary Sciences Letters* 132, 63-73.

Whalen, J.B., Currie, K.L., Chappell, B.W., 1987. A-type granites: geochemical characteristics, discrimination and petrogenesis. *Contributions to Mineralogy and Petrology* 95, 407-419.

6. References

Willner, A.P., Glodny, J., Gerya, T.V., Godoy, E., Massonne, H.J., 2004. A counterclockwise PTt path of high pressure- low temperature rocks from the Cordillera de la Costa accretionary complex of South Central Chile: Constraints for the earliest stage of subduction mass flow. *Lithos* 75, 283-310.

Willner, A.P., Thomson, S.N., Kröner, A., Wartho, J.-A., Wijbrans, J.R., Hervé, F., 2005. Time markers for the evolution and exhumation history of a Late Paleozoic paired metamorphic belt in north-central Chile (34°-35°30'S). *Journal of Petrology* 46, 1835-1858.

Wörner, G., Lezaun, J., Beck, A., Heber, V., Lucassen, F., Zinngrebe, E., Röbling, R., Wilke, H.G. 2000. Geochronology, metamorphic petrology and geochemistry of basement rocks from Belén (N. Chile) and C. Uyarani (W. Bolivian Altiplano): implications for the evolution of Andean basement. *Journal of South American Earth Sciences* 13, 717-737.

Wu, F., Sun, D., Li, H., Jahn, B., Wilde, S., 2002. A-type granites in northeastern China: age and geochemical constraints on their petrogenesis. *Chemical Geology* 187, 143-173.

Wyllie, P.J., Cox, K.G., Biggar, G.M., 1962. The habit of apatite in synthetic system and igneous rocks. *Journal of Petrology* 3, 238-243.

Yañez, G., Gana, P., Fernández, R., 1998. Origen y significado geológico de la Anomalía Melipilla, Chile central. *Revista Geológica Chilena* 25, 175-198.

Zeng, L., Asimov, P.D., Saleeby, J.B., 2005. Coupling of anatectic reactions and dissolution of accessory phases and the Sr and Nd isotope systematics of anatectic melts from a metasedimentary source. *Geochimica and Cosmochimica Acta* 69, 3671-3682.

Zuleger, E., Erzinger, J., 1988. Determination of the REE and Y in silicate materials with ICP-AES. *Fresenius Zeitschrift für Analytische Chemie* 332, 140-143.

Appendix A: U-Pb data for Early Mesozoic rocks of the Cordillera
de la Costa (34-37°S)

Appendix A: U-Pb data for Early Mesozoic rocks of the Cordillera de la Costa (34-37°S)

Sample Analysis						Atomic Ratios							Ages					Conc [%] ^g
	²⁰⁷ Pb ^a [cps]	U ^b [ppm]	Pb ^b [ppm]	²⁰⁶ Pb/ ²⁰⁴ Pb	Th/U	²⁰⁷ Pb/ ²³⁵ U ^c [%] ^e	²⁰⁶ Pb/ ²³⁸ U ^c [%] ^e	rho ^d	²⁰⁷ Pb/ ²⁰⁶ Pb ^f [%] ^e	²⁰⁷ Pb/ ²³⁵ U 2σ [Ma]	²⁰⁶ Pb/ ²³⁸ U 2σ [Ma]	²⁰⁶ Pb/ ²³⁸ U 2σ [Ma]	²⁰⁶ Pb/ ²³⁸ U 2σ [Ma]					
03-08	48 4725	235	8	25100	0.6	0.229	4.8	0.0324	1.5	0.31	0.0514	4.6	210	10	205	3	98	
03-08	49 4445	192	7	38900	1.2	0.222	6.0	0.0307	1.6	0.26	0.0525	5.8	203	12	195	3	96	
03-08	52 21650	947	37	13600	0.1	0.198	7.8	0.0276	2.0	0.26	0.0519	7.5	183	14	175	4	96	
03-08	62 4359	200	6	16600	0.9	0.205	5.1	0.0290	1.7	0.33	0.0514	4.9	190	10	184	3	97	
03-08	63 3481	167	6	16900	1.0	0.227	4.4	0.0315	1.8	0.41	0.0523	4.0	208	9	200	4	96	
03-08	64 7908	366	13	61900	1.3	0.212	3.4	0.0304	1.2	0.35	0.0505	3.2	195	7	193	2	99	
03-08	65 7150	268	10	33500	1.4	0.211	2.9	0.0308	1.4	0.50	0.0496	2.5	194	6	196	3	101	
03-08	70 13782	693	24	74000	1.3	0.210	2.7	0.0296	1.6	0.60	0.0515	2.2	194	5	188	3	97	
03-08	71 5248	261	8	13100	1.0	0.205	4.1	0.0290	1.4	0.35	0.0513	3.8	190	8	184	3	97	
03-08	76 10734	498	17	14600	1.3	0.218	3.4	0.0299	1.8	0.54	0.0528	2.9	200	7	190	4	95	
03-27	04 4898	140	5	20300	1.4	0.232	6.6	0.0320	4.8	0.72	0.0526	4.6	212	14	203	10	96	
03-27	05 3025	84	3	14200	1.3	0.230	6.3	0.0322	4.8	0.75	0.0518	4.2	210	13	204	10	97	
03-27	06 4395	126	4	68300	0.9	0.218	5.7	0.0318	4.8	0.84	0.0497	3.0	200	11	202	10	101	
03-27	07 4230	126	4	11100	0.9	0.228	6.6	0.0322	4.8	0.72	0.0513	4.6	208	14	204	10	98	
03-27	08 1819	51	2	48800	1.1	0.224	7.1	0.0317	4.8	0.68	0.0513	5.2	205	15	201	10	98	
03-27	09 2207	59	2	12400	1.1	0.233	7.2	0.0324	4.9	0.68	0.0522	5.2	213	15	206	10	97	
03-27	10 3294	96	3	19500	1.5	0.223	6.6	0.0324	4.9	0.74	0.0500	4.5	205	14	205	10	100	
03-27	11 2625	71	3	33700	1.4	0.240	6.9	0.0329	4.8	0.70	0.0529	4.9	219	15	209	10	95	
03-27	12 3658	107	4	16100	1.6	0.226	6.0	0.0326	5.0	0.83	0.0504	3.3	207	12	207	10	100	
03-27	13 3031	84	3	41900	1.0	0.226	6.4	0.0323	4.9	0.76	0.0507	4.1	207	13	205	10	99	
03-27	17 2547	70	3	11600	1.4	0.225	8.5	0.0330	5.2	0.60	0.0493	6.8	206	18	210	11	102	
03-27	18 2145	61	2	24100	1.0	0.219	8.7	0.0313	7.2	0.82	0.0507	4.9	201	17	199	14	99	
03-27	20 2143	61	2	21300	1.4	0.223	7.6	0.0337	4.8	0.63	0.0481	5.9	205	16	213	10	104	

Sample Analysis	²⁰⁷ Pb ^a		Pb ^b	²⁰⁶ Pb/ ²⁰⁴ Pb	Th/U	Atomic Ratios							Ages				Conc	
	[cps]	U ^b [ppm]				²⁰⁷ Pb/ ²³⁵ U ^c	2σ ^e	²⁰⁶ Pb/ ²³⁸ U ^c	2σ ^e	rho ^d	²⁰⁷ Pb/ ²⁰⁶ Pb ^f	2σ ^e	²⁰⁷ Pb/ ²³⁵ U	2σ ^e	²⁰⁶ Pb/ ²³⁸ U	2σ ^e		
			[ppm]										[Ma]	[Ma]	[Ma]	[Ma]	[%] ^g	
03-27	21	4759	133	5	40300	1.4	0.235	6.0	0.0334	4.8	0.79	0.0511	3.6	215	13	212	10	99
03-27	22	4974	138	5	92900	1.6	0.237	6.0	0.0331	4.8	0.80	0.0518	3.6	216	13	210	10	97
03-27	23	2053	55	2	51800	1.5	0.237	7.4	0.0330	4.9	0.66	0.0521	5.6	216	16	209	10	97
03-27	24	1675	46	2	15500	1.1	0.230	7.7	0.0325	4.9	0.63	0.0514	6.0	210	16	206	10	98
03-27	25	10358	298	10	16600	1.0	0.231	5.3	0.0331	4.7	0.90	0.0506	2.3	211	11	210	10	99
03-27	26	2389	63	2	23600	0.9	0.234	7.3	0.0328	4.8	0.66	0.0518	5.5	214	16	208	10	97
03-27	30	9092	265	10	86200	1.5	0.222	5.8	0.0317	5.2	0.90	0.0509	2.6	204	12	201	11	99
03-27	31	4271	119	4	25600	1.6	0.229	6.4	0.0326	4.8	0.76	0.0509	4.2	209	13	207	10	99
03-27	32	2183	62	2	10700	1.4	0.214	7.5	0.0310	5.8	0.77	0.0500	4.8	197	15	197	11	100
03-27	33	2107	56	2	15800	1.2	0.235	7.7	0.0333	5.1	0.66	0.0511	5.8	214	16	211	11	99
03-27	34	2098	53	2	46700	1.5	0.245	5.8	0.0340	5.0	0.85	0.0522	3.0	222	13	216	11	97
03-27	35	4223	118	4	51900	1.5	0.229	6.6	0.0331	4.8	0.73	0.0502	4.5	210	14	210	10	100
03-27	36	1698	43	2	19600	1.1	0.239	7.9	0.0339	4.8	0.61	0.0511	6.2	217	17	215	10	99
03-27	37	1479	38	1	79900	1.1	0.221	7.1	0.0315	5.0	0.71	0.0509	4.9	203	14	200	10	99
03-27	38	6933	197	8	77500	1.9	0.228	5.3	0.0331	4.8	0.91	0.0499	2.2	208	11	210	10	101
03-27	39	2184	57	2	33700	1.4	0.230	6.7	0.0323	4.9	0.74	0.0517	4.5	210	14	205	10	97
03-27	43	1479	38	1	13800	1.1	0.221	7.1	0.0315	5.0	0.71	0.0509	4.9	202	14	200	10	99
03-27	44	2435	64	2	37700	1.4	0.235	6.9	0.0341	5.0	0.72	0.0500	4.8	214	15	216	11	101
03-27	45	2673	69	3	40200	1.6	0.243	7.0	0.0332	5.1	0.73	0.0531	4.7	221	15	210	11	95
03-27	46	1535	38	1	18600	1.4	0.240	10.2	0.0340	5.2	0.51	0.0513	8.7	219	22	215	11	99
03-27	48	2074	53	2	19900	1.0	0.241	8.7	0.0335	5.2	0.60	0.0521	7.0	219	19	212	11	97
03-27	50	1942	44	2	12800	1.4	0.246	8.5	0.0330	4.9	0.58	0.0540	6.9	223	19	209	10	94
03-27	51	2541	68	3	19000	1.7	0.233	6.5	0.0338	5.2	0.80	0.0500	3.9	213	14	214	11	101
03-27	52	1181	29	1	10600	1.2	0.225	11.9	0.0322	5.2	0.44	0.0508	10.7	206	25	204	11	99
03-27	56	2392	68	3	72000	1.1	0.252	6.9	0.0350	4.4	0.64	0.0522	5.3	228	16	221	10	97
03-27	57	1926	58	2	53900	1.5	0.239	7.1	0.0342	4.1	0.58	0.0506	5.8	217	15	217	9	100

Sample Analysis	²⁰⁷ Pb ^a		U ^b	Pb ^b	²⁰⁶ Pb/ ²⁰⁴ Pb	Th/U	Atomic Ratios					Ages					Conc	
	[cps]	[ppm]					²⁰⁷ Pb/ ²³⁵ U ^c	2σ ^e	²⁰⁶ Pb/ ²³⁸ U ^c	2σ ^e	rho ^d	²⁰⁷ Pb/ ²⁰⁶ Pb ^f	2σ ^e	²⁰⁷ Pb/ ²³⁵ U ^{2σ}	[Ma]	²⁰⁶ Pb/ ²³⁸ U ^{2σ}		[Ma]
03-27	58	2544	77	3	91000	1.5	0.241	7.1	0.0337	4.1	0.58	0.0520	5.8	219	16	213	9	97
03-27	59	3179	99	4	22500	1.5	0.244	6.8	0.0351	4.1	0.61	0.0505	5.4	222	15	222	9	100
03-27	60	3088	96	4	18200	1.4	0.228	7.6	0.0330	4.2	0.55	0.0501	6.3	209	16	209	9	100
03-27	62	6795	219	9	16400	1.6	0.240	4.8	0.0339	4.0	0.84	0.0514	2.6	218	11	215	9	98
03-45	63	2023	83	3	91000	2.8	0.173	6.8	0.0255	4.5	0.67	0.0491	5.1	162	11	162	7	100
03-45	64	1567	64	2	22500	3.0	0.180	8.7	0.0263	4.1	0.48	0.0495	7.6	168	15	167	7	100
03-45	65	3046	118	4	18200	2.1	0.184	7.8	0.0266	4.1	0.52	0.0501	6.7	171	13	169	7	99
03-45	70	1842	77	3	16400	3.3	0.184	8.5	0.0269	4.7	0.56	0.0495	7.0	171	14	171	8	100
03-45	72	2213	91	3	20600	2.5	0.179	7.9	0.0258	4.5	0.57	0.0505	6.5	167	13	164	7	98
03-45	73	2447	103	3	29000	3.4	0.178	6.4	0.0263	4.1	0.64	0.0492	5.0	167	11	167	7	100
03-45	74	1760	73	2	5000	2.6	0.186	7.8	0.0264	4.9	0.63	0.0511	6.1	173	14	168	8	97
03-45	75	2352	98	3	6000	3.0	0.186	7.2	0.0260	4.0	0.56	0.0520	6.0	174	13	165	7	95
03-45	76	2072	87	3	10000	2.7	0.180	6.7	0.0261	4.2	0.62	0.0501	5.3	168	11	166	7	99
03-45	77	1475	62	2	53000	3.2	0.174	9.9	0.0261	4.1	0.41	0.0483	9.0	163	16	166	7	102
03-45	78	1367	55	2	19000	2.8	0.183	6.4	0.0264	4.1	0.64	0.0504	4.9	171	11	168	7	98
03-45	82	1606	63	2	101000	3.1	0.182	6.5	0.0260	4.1	0.63	0.0509	5.1	170	11	165	7	97
03-45	83	2084	88	3	6480	2.7	0.170	6.4	0.0248	4.5	0.70	0.0499	4.6	160	10	158	7	99
03-45	84	1540	63	2	142000	3.5	0.176	8.6	0.0265	4.3	0.50	0.0483	7.5	165	14	169	7	102
03-45	86	1244	48	2	20800	3.0	0.175	8.0	0.0260	4.2	0.53	0.0487	6.8	163	13	165	7	101
03-45	87	1067	38	1	130200	2.5	0.182	8.9	0.0252	4.5	0.51	0.0523	7.7	169	15	160	7	95
03-45	88	2514	109	3	6500	3.2	0.167	7.7	0.0248	4.7	0.61	0.0490	6.1	157	12	158	7	100
03-45	91	1659	69	2	17600	3.6	0.183	9.2	0.0272	4.3	0.46	0.0489	8.1	171	16	173	7	101
03-58	04	2823	99	2	4800	0.8	0.134	5.2	0.0198	2.4	0.47	0.0492	4.6	128	7	126	3	99
03-58	05	1340	61	1	64400	0.7	0.137	7.9	0.0194	3.1	0.40	0.0513	7.3	130	10	124	4	95
03-58	06	3085	158	4	9100	1.3	0.130	5.8	0.0190	2.8	0.49	0.0497	5.0	124	7	121	3	98
03-58	07	2091	101	2	8600	0.9	0.132	5.3	0.0188	2.6	0.49	0.0508	4.6	126	7	120	3	96

Sample Analysis	Atomic Ratios										Ages					Conc [%] ^g		
	²⁰⁷ Pb ^a [cps]	U ^b [ppm]	Pb ^b [ppm]	²⁰⁶ Pb/ ²⁰⁴ Pb	Th/U	²⁰⁷ Pb/ ²³⁵ U ^c	2σ ^e	²⁰⁶ Pb/ ²³⁸ U ^c	2σ ^e	rho ^d	²⁰⁷ Pb/ ²⁰⁶ Pb ^f	2σ ^e	²⁰⁷ Pb/ ²³⁵ U [Ma]	2σ ^e [Ma]	²⁰⁶ Pb/ ²³⁸ U [Ma]		2σ ^e [Ma]	
03-58	08	1885	88	2	3400	0.9	0.140	5.2	0.0202	2.6	0.50	0.0500	4.5	133	7	129	3	97
03-58	09	1760	85	2	4096	0.7	0.134	6.9	0.0190	2.4	0.34	0.0512	6.5	128	9	121	3	95
03-58	10	1440	67	1	79800	0.8	0.138	5.8	0.0196	2.7	0.46	0.0512	5.2	131	8	125	3	95
03-58	12	1487	72	2	7900	0.9	0.137	6.7	0.0196	2.7	0.40	0.0506	6.2	130	9	125	3	96
03-58	13	1514	71	2	50100	0.9	0.137	6.2	0.0196	3.1	0.51	0.0507	5.3	130	8	125	4	96
03-58	17	1373	65	1	3400	0.9	0.131	5.7	0.0191	2.3	0.41	0.0499	5.2	125	7	122	3	97
03-58	18	1876	95	2	58400	1.2	0.129	7.5	0.0187	2.8	0.37	0.0499	7.0	123	9	120	3	97
03-58	19	1638	81	2	14000	1.0	0.140	10.0	0.0198	2.6	0.26	0.0510	9.7	133	13	127	3	95
03-58	20	1434	67	1	10100	0.9	0.139	6.6	0.0197	2.3	0.36	0.0512	6.2	132	9	126	3	95
03-58	21	1224	58	1	65600	0.9	0.138	6.3	0.0195	2.9	0.46	0.0512	5.6	131	8	125	4	95
03-58	22	1357	65	1	17600	0.8	0.134	6.6	0.0197	2.6	0.40	0.0494	6.0	128	8	126	3	98
03-58	23	1912	94	2	4500	1.3	0.139	5.8	0.0202	2.5	0.43	0.0500	5.3	132	8	129	3	97
03-58	24	1855	91	2	2200	1.4	0.143	6.1	0.0202	2.7	0.44	0.0515	5.5	136	8	129	3	95
03-58	25	1408	68	1	8200	0.9	0.136	7.1	0.0194	2.4	0.33	0.0508	6.7	130	9	124	3	96
03-58	26	1826	88	2	5800	1.0	0.133	4.3	0.0193	2.4	0.55	0.0502	3.6	127	6	123	3	97
03-58	30	1272	64	1	40600	0.9	0.137	7.9	0.0198	2.8	0.35	0.0501	7.4	130	10	127	4	97
03-58	31	2055	110	3	14200	1.3	0.123	5.7	0.0193	2.4	0.43	0.0463	5.2	118	7	123	3	104
03-58	32	1553	76	2	74500	1.1	0.131	7.0	0.0191	2.6	0.37	0.0498	6.5	125	9	122	3	98
03-58	33	1817	94	2	16400	1.2	0.132	6.2	0.0192	2.7	0.43	0.0498	5.6	126	8	122	3	97
03-58	34	1413	72	1	29000	0.7	0.131	5.7	0.0189	2.6	0.46	0.0502	5.1	125	7	121	3	97
03-58	35	983	47	1	9800	0.9	0.136	8.8	0.0194	3.0	0.35	0.0509	8.3	129	11	124	4	96
03-58	36	1492	75	2	52900	0.8	0.133	9.7	0.0195	2.6	0.27	0.0494	9.3	127	12	125	3	98
03-60	12	7295	473	14	64400	1.3	0.153	3.2	0.0215	1.3	0.41	0.0514	2.9	144	5	137	2	95
03-60	20	10828	707	22	9000	0.2	0.162	2.4	0.0228	1.0	0.40	0.0513	2.2	152	4	146	1	96
03-60	24	6353	426	13	9000	3.2	0.158	3.3	0.0231	1.1	0.35	0.0498	3.1	149	5	147	2	99
03-60	43	8670	375	12	34100	0.1	0.167	4.4	0.0241	2.6	0.58	0.0501	3.6	157	7	154	4	98

Sample Analysis						Atomic Ratios							Ages					
	²⁰⁷ Pb ^a [cps]	U ^b [ppm]	Pb ^b [ppm]	²⁰⁶ Pb/ ²⁰⁴ Pb	Th/U	²⁰⁷ Pb/ ²³⁵ U ^c	2σ ^e [%]	²⁰⁶ Pb/ ²³⁸ U ^c	2σ ^e [%]	rho ^d	²⁰⁷ Pb/ ²⁰⁶ Pb ^f	2σ ^e [%]	²⁰⁷ Pb/ ²³⁵ U [Ma]	2σ ^e [Ma]	²⁰⁶ Pb/ ²³⁸ U [Ma]	2σ ^e [Ma]	Conc [%] ^g	
03-60	44	13101	514	13	4100	0.2	0.164	3.7	0.0234	3.2	0.85	0.0508	1.9	154	6	149	5	97
03-60	46	13169	564	18	79800	0.1	0.173	3.3	0.0244	2.3	0.71	0.0514	2.3	162	5	155	4	96
03-60	58	3878	293	9	8000	1.1	0.170	5.8	0.0248	4.4	0.77	0.0498	3.7	160	9	158	7	99
03-60	59	5771	443	11	50100	0.6	0.166	7.2	0.0234	6.6	0.92	0.0514	2.8	156	11	149	10	96
03-79	33	7236	129	5	21700	2.0	0.194	7.3	0.0278	1.7	0.23	0.0507	7.1	180	13	177	3	98
03-79	30	2233	97	3	8200	1.2	0.224	9.6	0.0311	2.5	0.26	0.0523	9.3	205	20	197	5	96
04-22	04	4548	223	8	10800	0.7	0.212	5.4	0.0305	4.9	0.89	0.0506	2.4	196	11	193	9	99
04-22	05	5333	266	10	21700	0.9	0.227	5.4	0.0319	4.8	0.89	0.0518	2.5	208	11	202	10	97
04-22	06	6086	312	11	3500	0.9	0.216	5.6	0.0315	4.7	0.85	0.0498	2.9	199	11	200	9	101
04-22	07	8857	466	17	14400	1.0	0.218	5.4	0.0312	4.7	0.88	0.0506	2.6	200	11	198	9	99
04-22	08	2445	120	4	6000	0.7	0.232	6.7	0.0328	5.0	0.74	0.0513	4.5	212	14	208	10	98
04-22	09	9451	477	19	14800	1.0	0.227	5.5	0.0321	4.7	0.86	0.0512	2.8	207	11	204	10	98
04-22	10	4301	213	8	13700	0.8	0.226	5.5	0.0321	4.8	0.87	0.0510	2.7	207	11	204	10	99
04-22	11	3173	159	6	19300	0.8	0.225	7.2	0.0319	4.9	0.68	0.0512	5.3	206	15	202	10	98
04-22	12	1396	66	2	6300	0.5	0.224	7.9	0.0325	4.7	0.60	0.0499	6.3	205	16	206	10	101
04-22	13	4538	231	8	33400	0.8	0.220	5.8	0.0314	4.9	0.84	0.0509	3.1	202	12	199	10	99
04-22	17	4409	216	8	40500	0.6	0.235	6.2	0.0331	4.7	0.76	0.0515	4.1	214	13	210	10	98
04-22	18	9584	512	20	13000	0.9	0.215	5.3	0.0316	4.7	0.89	0.0494	2.4	198	10	201	9	101
04-22	19	2571	132	4	13000	0.4	0.224	6.1	0.0326	4.8	0.80	0.0499	3.7	205	12	207	10	101
04-22	20	1805	89	3	7900	0.5	0.229	6.4	0.0326	4.7	0.74	0.0510	4.3	210	13	207	10	99
04-22	21	4400	228	9	188000	0.9	0.228	5.7	0.0330	4.8	0.84	0.0502	3.0	209	12	209	10	100
04-22	22	3703	197	7	5100	0.7	0.223	5.8	0.0325	5.0	0.87	0.0498	2.9	205	12	206	10	101
04-22	23	2653	139	5	4400	0.8	0.224	5.8	0.0326	4.9	0.84	0.0498	3.1	205	12	207	10	101
04-22	24	2106	111	4	109000	0.8	0.211	6.9	0.0312	5.2	0.76	0.0490	4.4	194	13	198	10	102
04-22	25	3952	206	8	27100	1.0	0.222	5.6	0.0319	4.8	0.86	0.0505	2.9	203	11	202	10	99
04-22	26	2890	154	5	4600	0.5	0.219	6.3	0.0313	4.8	0.76	0.0508	4.1	201	13	199	10	99

Sample Analysis	²⁰⁷ Pb ^a U ^b		Pb ^b [ppm]	²⁰⁶ Pb/ ²⁰⁴ Pb	Th/U	Atomic Ratios				rho ^d	²⁰⁷ Pb/ ²⁰⁶ Pb ^f		Ages		Conc [%] ^g			
	[cps]	[ppm]				²⁰⁷ Pb/ ²³⁵ U ^c	2σ ^e [%] ^e	²⁰⁶ Pb/ ²³⁸ U ^c	2σ ^e [%] ^e		2σ ^e [Ma]	²⁰⁶ Pb/ ²³⁸ U 2σ ^e [Ma]						
04-22	30	1269	66	2	15500	0.5	0.223	7.8	0.0318	4.9	0.63	0.0508	6.0	204	16	202	10	99
04-22	31	2346	123	4	21900	0.9	0.221	6.4	0.0318	4.9	0.77	0.0505	4.0	203	13	202	10	99
04-22	32	2154	115	4	27500	0.9	0.226	6.8	0.0325	4.9	0.72	0.0506	4.7	207	14	206	10	99
04-22	34	2252	120	4	25800	0.7	0.221	6.0	0.0320	4.8	0.80	0.0501	3.6	203	12	203	10	100
04-22	36	2547	138	5	5000	0.9	0.224	6.2	0.0322	4.8	0.77	0.0505	4.0	205	13	204	10	100
04-22	37	2517	139	5	10000	0.9	0.217	6.5	0.0315	5.3	0.82	0.0500	3.7	199	13	200	11	100
04-22	38	3743	204	7	36800	0.6	0.221	5.8	0.0321	4.8	0.83	0.0500	3.2	203	12	204	10	100
04-22	39	1827	98	3	28700	0.8	0.215	6.8	0.0318	5.1	0.76	0.0490	4.4	197	13	202	10	102
04-22	43	2517	139	5	28200	0.9	0.219	6.5	0.0318	5.3	0.82	0.0500	3.7	201	13	202	11	100
04-22	44	2192	114	4	8400	0.4	0.225	6.3	0.0322	4.8	0.76	0.0507	4.1	206	13	205	10	99
04-22	45	4840	262	10	10600	0.9	0.224	5.8	0.0317	4.8	0.82	0.0513	3.3	205	12	201	10	98
04-22	46	1444	75	3	8400	0.8	0.223	7.2	0.0321	4.8	0.66	0.0504	5.4	205	15	204	10	100
04-22	47	2452	135	5	22100	0.9	0.220	5.7	0.0320	4.8	0.84	0.0498	3.1	202	11	203	10	101
04-22	48	1100	58	2	3100	0.5	0.218	7.6	0.0326	4.9	0.65	0.0484	5.7	200	15	207	10	103
04-22	49	4480	239	9	6700	1.0	0.225	6.4	0.0318	4.8	0.75	0.0512	4.2	206	13	202	10	98
04-22	50	1184	61	2	22500	0.8	0.226	7.0	0.0330	4.9	0.70	0.0497	5.0	207	14	209	10	101
04-22	51	2345	119	5	48900	1.0	0.228	6.0	0.0331	4.8	0.80	0.0501	3.6	209	13	210	10	100

^a Within-run background-corrected mean ²⁰⁷Pb signal in counts per second [cps]

^b U and Pb concentrations and Th/U ratios are calculated relative to GJ-1 reference

^c Corrected for background and within-run Pb/U fractionation and normalised to reference GJ-1 (ID-TIMS values/measured value); ²⁰⁷Pb/²³⁵U calculated using (²⁰⁷Pb/²⁰⁶Pb)/(²³⁸U/²⁰⁶Pb * 1/137.88)

^d Rho is the error correlation defined as the quotient of the propagated errors of the ²⁰⁶Pb/²³⁸U and the ²⁰⁷/²³⁵U ratio

^e Quadratic addition of within-run errors (2 SD) and daily reproducibility of GJ-1 (2 SD)

^g Degree of concordance = (²⁰⁶Pb/²³⁸U age * 100/²⁰⁷Pb/²³⁵U age)

Appendix B: K/Ar ages of intrusive rocks from Cerros del Hualve

Appendix B: K/Ar ages of intrusive rocks from Cerros del Hualve

Sample	Rock	Mineral	Spike (No.)	K ₂ O (wt%)	⁴⁰ Ar * (nl/g STP)	⁴⁰ Ar * (%)	Age (Ma)	2σ-Error (Ma)
03-45	gabbro	hornblende	3379	0.64	3.60	73.71	166.5	2.9
03-45	gabbro	biotite	3341	8.76	48.82	96.36	165.0	2.8

Appendix C: Sample preparation and analytical techniques

Appendix C: Sample preparation and analytical techniques

A. In-situ U-Pb zircon geochronology by laser ablation – magnetic sector field - inductively coupled plasma mass spectrometry (LA-ICP-MS)

Sample preparation

For LA-ICP-MS age determinations, zircons were separated from the bulk samples using conventional heavy liquid and magnetic separation methods. The final separation step was made by handpicking of individual zircon grains from the heavy and non-magnetic fraction using an optical microscope. For analysis, the individual zircon grains are mounted on double-sided, transparent adhesive tape and subsequently embedded in 1-inch diameter circular epoxy mounts for polishing. In order to study their internal structure, backscatter electron (BSE) images of all analysed zircons were obtained using a Philips XL 40 scanning electron microscope at GEUS.

Analytical methods

The methodology applied at GEUS for *in-situ* U-Pb zircon analysis essentially follows that described by Gerdes and Zeh (2006) and Frei et al. (2006). All analyses were carried out using a ThermoFinnigan Element2 single-collector double focusing magnetic sector ICPMS coupled to a NewWave/Merchantek UP213 laser ablation system. The UP213 laser ablation system is equipped with a frequency quintupled ND-YAG laser emitting at a wavelength of 213 nm. The nominal pulse width of the laser is 5 ns with a pulse-to-pulse stability of 2 % (2 r.s.d.). The laser was operated at a repetition rate of 10 Hz and a nominal energy output of 45 %, corresponding to a laser energy of ~0.03 mJ and a laser fluency of 3 to 4 J cm⁻². All data were acquired with a single spot analysis on each individual zircon grain with a beam diameter of 30 µm. During the 35 s ablation the laser drilled approximately 30 µm deep. Samples and standards were held in a low-volume ablation cell specially developed for U-Pb-dating (Horstwood et al. 2003). Helium was used to flush the sample cell and was mixed downstream with the Ar sample gas of the mass-spectrometer. The washout time for this configuration is < 15 s. All sample mounts were rigorously cleaned before introduction into the sample cell to remove surface Pb contamination.

The total acquisition time for each isotopic analysis was 90 s with the first 30 s used to measure the gas blank, followed by 35 s ablation and 25 s sample cell flush out. The mass-spectrometer was tuned to give large, stable signals for the ²⁰⁶Pb and ²³⁸U peaks, low background count rates (typically around 150 counts per second for ²⁰⁷Pb) and low oxide production rates (²³⁸U¹⁶O/²³⁸U generally below 2.5 %). All measurements were performed in low-resolution mode using electrostatic scanning (E-scan) with the magnetic field resting at mass ²⁰²Hg. The following

masses were measured: ^{202}Hg , $^{204}(\text{Pb} + \text{Hg})$, ^{206}Pb , ^{207}Pb , ^{208}Pb , ^{232}Th , ^{235}U , and ^{238}U . All data were acquired on four samples per peak with a sampling and a settling time of 1 ms for each isotope. Mass ^{202}Hg was measured to monitor the ^{204}Hg interference on ^{204}Pb (using a $^{202}\text{Hg}/^{204}\text{Hg}$ -ratio of 4.36). Because of the large uncertainties in ^{204}Pb determinations due to the Hg contamination of the carrier gas (Jackson et al. 2004) a correction for common lead is only applied if the net intensities for mass ^{204}Pb , corrected for ^{204}Hg , are significantly above the limit of detection (i.e. $^{204}\text{Pb} > 3$ standard deviations of the background ^{204}Hg signal). For all analysis presented in this study the ^{204}Pb signal was below this level and hence no common lead correction was applied. The laser induced elemental fractionation and the instrumental mass bias on measured isotopic ratios were corrected by matrix-matched external standardization using the GJ-1 zircon standard (Jackson et al. 2004). Samples were analyzed in sequences: three standards are analyzed initially, followed by ten samples, again three standards, and so on.

The raw data were exported in ASCII format and processed offline using in-house developed data reduction spreadsheets that integrate corrections for laser-induced U-Pb fractionation and instrumental mass bias. All errors (2σ confidence level on ratios and ages) are propagated with the reproducibility of the standard over the session taken into account. The Plesovice zircon standard (Aftalion et al. 1989; provided by Jan Kosler, Charles University, Prague) was regularly analyzed as an unknown. Long-term precision based on 109 analyses of the Plesovice zircon by two different operators during a period of 6 months was (2 r.s.d.) 2 %, 2.3 % and 1.1 % for the $^{206}\text{Pb}/^{238}\text{U}$, $^{207}\text{Pb}/^{235}\text{U}$ and $^{207}\text{Pb}/^{206}\text{Pb}$ ratios, respectively (Frei et al. 2006). The calculation of concordia ages and weighted averages, as well as plotting of concordia diagrams was performed using Isoplot/Ex 3.0 (Ludwig 2003).

B. Whole rock, trace elements and isotope geochemistry methodes

Macroscopically fresh samples without alteration along joints and secondary mineral formations have been selected for analysis. All samples have been checked under the petrographic microscope for absence of secondary alterations. Whole rock analyses for major elements have been carried out by XRF at Technical University Berlin. For some samples, REE were determined by ICP-MS (cf. Dulski 2001) at GeoForschungsZentrum Potsdam. For other samples, REE analyses were carried out together with analyses of Y, La, and Sc by ICP-AES at GFZ Potsdam (cf. Zuleger and Erzinger 1988). All other trace elements were analyzed either by ICP-MS methods (GFZ Potsdam / ACTLABS, Ancaster, Ontario) or by ID-TIMS (Rb, Sr; GFZ Potsdam).

U–Th–Pb, Sm–Nd, and Rb–Sr isotopic and concentration analyses were performed on different splits from one solution of ~100 mg sample powder. Nd, Sr and Pb isotopic ratios have been determined at the GeoForschungsZentrum Potsdam (for analytical procedures for Sr and Pb, see Romer et al. 2005; for Nd, see Lucassen et al. 2004). Sr has been analyzed on a VG Sector 54 TIMS instrument in dynamic multicollector mode. During the period of analytical work the NBS

987 Sr standard yielded $^{87}\text{Sr}/^{86}\text{Sr} = 0.710268 \pm 10$ (2σ ; $n = 9$). Nd was analyzed on a Finnigan MAT262 TIMS in dynamic multicollector mode. The La Jolla Nd standard yielded $^{143}\text{Nd}/^{144}\text{Nd} = 0.511850 \pm 4$ (2σ , $n = 14$). Nd isotopic ratios have been normalized to $^{146}\text{Nd}/^{144}\text{Nd} = 0.7219$, Sr isotopic ratios to $^{86}\text{Sr}/^{88}\text{Sr} = 0.1194$. Pb isotopic ratios have been measured on a Finnigan MAT262 TIMS, at controlled temperatures between 1200–1250°C. Instrumental mass-fractionation has been corrected using 0.1% per a.m.u. The 2σ reproducibility of all Pb isotope ratios of the NBS SRM 981 standard ($^{206}\text{Pb}/^{204}\text{Pb} = 16.90 \pm 0.01$, $n = 52$) is better than 0.1% and a 2σ error of 0.1% is assumed for the measured samples. Procedural blanks were <30 pg for Pb, <50 pg Nd and <100 pg for Sr. No blank corrections have been applied to the measured ratios because blank contribution were insignificant in comparison with the amount of the respective elements in the sample.

Appendix D: Detailed petrography of the Cobquecura Pluton

Appendix D: Detailed petrography of the Cobquecura Pluton

1. Gabbros

The gabbros vary from hornblende-gabbro and orthopyroxene-gabbro to olivine-gabbro norite, with more mafic compositions towards the south. Hornblende-bearing and olivine-free gabbros occasionally contain quartz. Euhedral to subhedral plagioclase has normal zoning, patchy and oscillatory zonings, occasionally with rounded calcic cores, and contains multiple small amphibole, pyroxene and apatite inclusions. Anhedral amphibole is zoned with brown cores and green rims (Fig. 3.2a) and often has multiple and lamellar twinning. The amphibole locally contains inclusions of plagioclase, apatite, zircon, opaque minerals and small cores of clinopyroxene. Amphibole is interstitial between plagioclase crystals and associated with large anhedral biotite. Diopside-augite occurs in large euhedral crystals, which show sporadic orthopyroxene exsolutions. It is often surrounded by amphibole and contains inclusions of euhedral plagioclase (An₆₅), quartz and biotite. Scarce interstitial quartz is slightly fractured and includes plagioclase (with irregular borders), apatite, zircon, clinopyroxene, amphibole and opaque minerals. Anhedral to subhedral ilmenite and pyrite are often associated with mafic minerals like amphibole and biotite.

Orthopyroxene gabbro and olivine gabbro norite (the latter characterized by a trachytoidal texture; Fig. 3.2b), contains euhedral to subhedral plagioclase with inclusions of clinopyroxene, biotite, apatite and opaque minerals. Locally plagioclase is zoned with resorbed calcic cores. Anhedral to subhedral diopside-augite shows multiple or simple twinning with inclusions of zoned plagioclase and opaque minerals. It occurs in clusters together with orthopyroxene; locally it is mantled by amphibole and biotite (Fig. 3.2a), which also occur in its fractures. Subhedral and anhedral enstatite presents lamellae of clinopyroxene. Orthopyroxene and clinopyroxene in the olivine-gabbro norite occur in close association with olivine and contain scarce inclusions of plagioclase. Elongated olivine crystals (4 × 1 mm) are locally mantled by biotite. Rare amphibole is euhedral or interstitial and fractured. In olivine-gabbro norite biotite occurs interstitially. Subhedral and interstitial opaque minerals are often associated with mafic minerals. The mafic globules also have an olivine-gabbro norite composition, and similar characteristics as the olivine gabbro norite described above, but with a higher CI (~60) and larger olivine crystals.

2. Granite, Granodiorite and Quartz Monzonite

The more differentiated rocks consist of olivine-bearing monzogranite, syenogranite, granodiorite and quartz-monzonite with similar petrographic characteristics. Anhedral K-feldspar has simple twinning and perthites, it is occasionally interstitial and has inclusions of plagioclase with embayed or diffuse grain boundaries, quartz, zircon, apatite and mafic and opaque minerals.

Occasionally it is intergrown with quartz in a graphic texture. Euhedral plagioclase presents sharp-defined calcic cores with zoning at the border, also with oscillatory and patchy zoning and contains inclusions of amphibole, smaller plagioclase, euhedral apatite and opaque minerals. Anhedral quartz is embayed and includes plagioclase with diffuse borders, elongated opaque minerals, allanite, apatite and rarely amphibole. Subhedral fayalitic olivine has a greenish color probably due to alteration and occurs associated with biotite and opaque minerals by which it is sometimes included. It occurs also as a relict in amphibole (Fig. 3.2c). Olivine is interstitial between plagioclase crystals (Fig. 3.2d) and a rim of quartz and biotite is common between olivine and albite rich plagioclase (An_{20} ; Fig. 3.2e). Scarce tabular or anhedral clinopyroxene (less than 5 vol.%) has a pale green color and is included in plagioclase or K-feldspar or as cores in amphibole. Clinopyroxene is not observed in contact to olivine. Anhedral amphibole in clusters has simple, lamellar or multiple twinning and occasionally displays embayment. Inclusions in amphibole are plagioclase, opaque minerals, zircon and apatite. Interstitial biotite (Fig. 3.2f) includes plagioclase, olivine, amphibole, apatite and opaque minerals. Anhedral ilmenite and pyrite occur disseminated in the rock in association with mafic minerals.

Olivine-free granite and granodiorite are medium-grained phaneritic rocks often containing abundant metapelite xenoliths. Subhedral plagioclase with oscillatory zoning at the border includes elongated apatite and some altered mafic minerals. Interstitial quartz and anhedral K-feldspar includes embayed plagioclase and accessory phases. Euhedral to subhedral amphibole with simple twinning has plagioclase inclusions and cores of an altered mafic mineral, possibly pyroxene. Biotite occurs interstitially.

3. Hybrid rocks

The hybrid rocks are composed of small occurrences of homogeneous lithologies (biotite-tonalite to quartz-diorite), and heterogeneous lithologies, which consist of composite dikes, net-vein complexes and mafic pillow-shaped enclaves, within aplitic felsic matrix and a mafic component with gabbro and diorite composition.

Quartz-diorite and biotite-tonalite have a greenish gray color. Amphibole and rarely clinopyroxene appear only in the quartz-diorite. Subhedral plagioclase has a strong zoning at its border. Locally it has a well-defined calcic core and patchy zoning and presents irregular contacts with quartz. In the biotite-tonalite, plagioclase displays a strong oscillatory zoning, and has inclusions of clinopyroxene, elongated apatite and opaque minerals. Interstitial quartz includes apatite, zircon and opaque minerals. Subhedral to anhedral amphibole contains inclusions of apatite, plagioclase and opaque minerals and preserves clinopyroxene cores. Biotite contains inclusions of zircon, apatite and opaque minerals, and is locally intergrown with amphibole. Scarce pyroxene with irregular borders also occurs as elongated crystals in the groundmass. In the quartz-monzogabbro at La Iglesia de la Piedra, euhedral tabular plagioclase has a normal zoning.

Orthoclase occasionally forms an interesting graphic texture with quartz that occurs surrounded by crystals of plagioclase and amphibole (Fig. 3.2d). Amphibole has simple and lamellar twinning, contains apatite and opaque inclusions and presents zoning with darker borders. Apatite occurs as elongated and fractured crystals and zircon displays a skeletal habit. Euhedral ilmenite has acicular habits.

4. Synplutonic composite dikes

The synplutonic composite dikes are constituted of diabase enclaves in a leucocratic granite matrix.

The diabase enclaves have compositions of pyroxene- and hornblende-gabbro. There are few unaltered and unzoned phenocrysts of plagioclase (approximately 3 vol.%). Anhedral to subhedral amphibole has inclusions of ilmenite, which are aligned parallel. Subhedral clinopyroxene has simple twinning, small inclusions of opaque minerals.

Leucocratic granite matrix has rare orthoclase and plagioclase phenocrysts. Subhedral to anhedral orthoclase is spatially related to tourmaline and occasionally includes apatite, zircon and sphene. Euhedral to subhedral plagioclase sometimes has oscillatory zoning and includes quartz and opaque minerals. Euhedral to anhedral biotite has zircon and opaque mineral inclusions. Anhedral to euhedral quartz has rare inclusions of plagioclase, zircon, apatite, opaque minerals and semi-inclusions of amphibole. It is related in consertal texture with K-feldspar and other quartz crystals. Euhedral to anhedral amphibole is restricted to monzogranitic varieties and contains apatite and zircon inclusions. Smaller crystals of amphibole are euhedral and the larger ones have simple and multiple twinning. Apatite appears in long crystals with an aspect ratio of 1:8 disseminated in the groundmass. Relatively large crystals of zircon are abundant.

The presence of macroscopic and microscopic structures like synplutonic dikes, net vein complexes, pillowed mafic magma, quartz-feldspathic cores surrounded by amphibole crystals, rounded enclaves, resorption of the cores of plagioclase and elongated apatite clearly indicate interaction of chemically different magmas.

5. Postplutonic dikes

Porphyritic and glomeroporphyritic varieties of postplutonic diabase dikes have phenocrysts and glomerocrystals of plagioclase and clinopyroxene. The groundmass contains unoriented microliths of plagioclase and subhedral to euhedral pyroxene. Olivine at the matrix is totally replaced by pseudomorphs of serpentine, opaque minerals and sphene.

There are scarce postplutonic dikes with a granodioritic composition. In these, subhedral plagioclase has a marked zoning at the border and contains opaque minerals and apatite inclusions. Anhedral orthoclase has simple twinning. Quartz has undulatory extinction and consertal texture. Euhedral to subhedral amphibole has a simple twinning, is locally mantled by biotite and contains

clinopyroxene relicts. Opaque minerals, apatite, zircon and plagioclase occur as inclusion in orthoclase, quartz and amphibole.